Dissertation

submitted to the

Combined Faculty of Natural Sciences and Mathematics

of the Ruperto Carola University Heidelberg, Germany

for the degree of

Doctor of Natural Sciences

Presented by

M.Sc. Theresa Schmid

Born in Munich, Germany

Oral examination: 15th December 2021

BCAT1
is a novel target of MLL fusions and essential for leukemic stem cell transformation

Referees:

Prof. Dr. Ursula Klingmüller

Prof. Dr. Peter Lichter

Abstract

In cancer, the branched-chain amino acid (BCAA) metabolism is frequently activated through the increased uptake (second only to glutamine) of valine, leucine, and isoleucine (Jain et al., 2012), as well as the overexpression of branched-chain amino acid transaminase 1 (BCAT1), the cytoplasmic BCAA transaminase. We and others showed that proliferation, migration, and chemoresistance of a variety of cancer entities, such as glioblastoma, breast cancer, and myeloid leukemia, are heavily reliant on BCAT1 expression (Hattori et al., 2017; Raffel et al., 2017; Thewes et al., 2017; Tönjes et al., 2013).

Epigenetic gene regulation and metabolism are highly intertwined, as many histone and DNA modifiers rely on substrates and cofactors provided by various metabolic reactions. For example, in cancer, the upregulation of BCAT1 results in a decrease of α-KG and a reduced activity of α-KG dependent enzymes, such as EGLN1 (Raffel et al., 2017). Furthermore, DNA hypermethylation is observed upon BCAT1 suppression in acute myeloid leukemia (AML), suggesting an α-KG-dependent effect on the TET-family DNA demethylases (Raffel et al., 2017).

In an attempt to unravel the interdependencies of BCAT1 and chromatin-modifying enzymes, I discovered that the upregulation of BCAT1 in mammary carcinoma xenografts influences histone modifications in an α-KG-independent manner. Global upregulation of gene expression mediated by altered chromatin modifications in BCAT1 knockdown breast cancer xenografts led to a comparison between BCAT1 and histone modifiers in expression data sets of breast cancer and AML patients. H3K4 methyltransferase MLL was found to be the most significantly positively correlating modifier in both cancer entities. MLL has been extensively studied in leukemia in which recurring translocations lead to gain-of-function rearrangements, such as MLL-AF9 and MLL-ENL fusion. These oncogenic fusions are driver gene mutations, and I was able to identify BCAT1 as one of their targets regulating its expression. MLL-AF9 and MLL-ENL were able to transform hematopoietic stem and progenitor cells (HSPCs) into leukemic stem cells (LSCs). However, loss of Bcat1 or its transaminase activity results in loss of self-renewal and immortalization, making Bcat1 activity essential for MLL fusion-mediated tumor development. Further expression and histone modification profiling of transformed wildtype HSPCs, as well as Bcat1 knockout HSPCs and their rescues, revealed that the lack of Bcat1 initiates the inhibition of DNA replication and cell cycle arrest missing in Bcat1 wildtype cells.

BCAT1s limited expression in most healthy tissues makes it an interesting target for cancer therapy. Furthermore, this and other studies implicate that the inhibition of BCAT1's transaminase activity can eradicate LSCs and may prevent relapse. Additionally, controlling BCAT1 has the potential to reduce tumor development, relevant especially for patients harboring clonal hematopoiesis of intermediate potential (CHIP).

Zusammenfassung

Der Stoffwechsel verzweigtkettiger Aminosäuren (BCAA), Valin, Leucin, und Isoleucin, ist in Tumorzellen häufig verändert, um deren erhöhten Bedarf abzudecken. Besonders Tumorstammzellen und rezidivierende Tumore bewerkstelligen diese Anpassung unter anderem durch die Hochregulierung des metabolischen Enzyms Branched-Chain Amino Acid Transaminase 1 (BCAT1), welches den ersten Schritt im BCAA-Abbau katalysiert. Zusammen mit weiteren Studien konnten wir zeigen, dass bei einer Vielzahl unterschiedlicher Tumorarten, wie Brustkrebs oder akuter myeloischer Leukämie (AML), die Überexpression von BCAT1 im Zusammenhang mit Tumorwachstum, Migration und Chemoresistenz steht (Hattori et al., 2017; Raffel et al., 2017; Thewes et al., 2017; Tönjes et al., 2013).

Genexpression und Stoffwechsel sind durch epigenetische Regulation eng miteinander verknüpft, da viele Histon- und DNA modifizierende Enzyme auf die Substrate und Kofaktoren aus unterschiedlichsten Stoffwechselprozessen angewiesen sind. In Tumorzellen führt die Überexpression von BCAT1 zu einer Reduktion von α-KG, das wiederum die Aktivität von α-KG-abhängigen Enzymen wie EGLN1 (Raffel et al., 2017) limitiert. Darüber hinaus wurde DNA-Hypomethylierung bei Unterdrückung der BCAT1-Expression beobachtet, was wiederum einen α-KG-abhängigen Effekt auf DNA-Demethylasen der TET-Familie nahelegt. .

Bei dem Versuch die gegenseitigen Abhängigkeiten von BCAT1 und Histonmodifizierender Enzyme zu entschlüsseln, konnte ich feststellen, dass die Herunterregulierung von BCAT1 bei Mammakarzinom-Xenotransplantaten zu einer α-KG unabhängig Veränderung der Histonmodifikationen führte. Durch veränderte Chromatin-Modifikationen wurde in BCAT1-Knockdown Brustkrebs-Xenotransplantaten eine globale Hochregulierung in der Genexpression beobachtet und daraufhin wurde in RNA-Sequenzierungsdaten von Brustkrebs- und AML-Patienten die Expression von BCAT1 und Histon-modifizierender Enzyme verglichen. In beiden Tumorentitäten hatte die H3K4-Methyltransferase MLL die stärkste signifikante positive Korrelation. MLL wurde in Leukämien eingehend untersucht, bei denen wiederholt auftretender Translokationen zu Fusionsgenen mit einhergehendem Funktionsgewinn führen, wie z.B. MLL-AF9 und MLL-ENL. Ich konnte zeigen, dass diese onkogenen Fusionsproteine BCAT1-Regionen binden und so dessen Expression regulierten. Die Expression von MLL-AF9 und MLL-ENL führte zur Transformation von hämatopoetischer Stamm- und Vorläuferzellen (HSPCs) in leukämische Stammzellen (LSCs). Jedoch führte der Verlust von Bcat1 oder dessen Transaminaseaktivität zum Verlust von Selbsterneuerung und Immortalisierung. Dies zeigt, dass die Aktivität von Bcat1 essenziell für die Entstehung von AML durch MLL-Fusionsproteine ist. Die Charakterisierung der Expression und Histonmodifikationen von transformierten wildtyp- und Bcat1-Knockout HSPCs zeigte zusätzlich, dass das Fehlen von Bcat1 die DNA-Replikation hemmt und somit einen Zellzyklusarrest während der Tumorentwicklung bewirkt.

Die zumeist niedrige Expression von Bcat1 in gesundem Gewebe macht es zu einem interessanten Ziel für die Krebstherapie. Diese und weitere Studien zeigen, dass durch die Inhibition der

Transaminaseaktivität von Bcat1 leukämische Stammzellen beseitigt und dadurch möglicherweise ein Rückfall verhindert werden kann. Darüber hinaus kann durch präventive Kontrolle von BCAT1 die Tumorentwicklung minimiert werden, was insbesondere für Patienten mit klonaler Hämatopoese mit intermediärem Potenzial (CHIP) relevant ist.

Table of Contents

List of Abbreviations

a-KG	Alpha-Ketoglutarate (2-oxoglutarate)
ACT-seq	Antibody-guided chromatin tagmentation sequencing
AF4	AF4/FMR2 family member 4, AFF4
AF9	MLLT3 super elongation complex subunit, MLLT3
AF10	MLLT10 histone lysine methyltransferase DOT1L cofactor
AML	Acute myeloid leukemia
APCDD1L	APC down-regulated 1 like
APCDD1L-AS	APC down-regulated 1 like-antisense
ASH2L	ASH2 like histone lysine methyltransferase complex subunit
ASXL1 and 2	Additional sex combs like 1 and 2
AT-hooks	DNA binding domain, binds to the minor groove of adenine-thymine (AT) rich DNA
BCAA	Branched-chain amino acid
BCAT 1 and 2	Branched-chain aminotransferase 1 and isoenzyme 2
Bcat1$^{+/+}$	Murine Bcat1 wildtype, WT
Bcat1$^{-/-}$	Murine Bcat1 Knockout (KO)
Bcat1^{K222A}	Murine Bcat1 K222A mutant = catabolically dead
Bcat1^{SXXS}	Murine Bcat1 C335S and C338S mutant = redox insensitive
Bcat1^{WT}	Murine Bcat1 wildtype rescue
BCKA	Branched-chain keto acid
BCKDH	Branched-chain alpha-ketoacid dehydrogenase
CFU	Colony formation unit [assay]
CHIP	Clonal hematopoiesis of intermediate potential
ChIP	Chromatin immunoprecipitation
ChIP-seq	Chromatin immunoprecipitation sequencing
CMP	Common/Committed myeloid progenitor cell
CpG	5’ CG 3’, Cytosine Guanine sequence
CxxC	Cysteine-Xaa-Xaa-Cysteine sequence
DNMT1	DNA methyltransferase 1 (hemimethylation)
DNMT3A and B	DNA methyltransferase 3 alpha and beta (de novo methylation)
DNA	Deoxyribonucleic acid
DOT1L	DOT1 like histone lysine methyltransferase
Dox	Doxycycline
DPY30	Dpy-30 histone methyltransferase complex regulatory subunit
EED	Embryonic ectoderm development
EGLN1	Egl-9 family hypoxia-inducible factor 1
ENL	MLLT1 super elongation complex subunit, MLLT1
EPZ5676	DOT1L inhibitor, Pinometostat
EPZ004777	DOT1L inhibitor
EZH1 and 2	Enhancer of zeste 2 polycomb repressive complex 1 and 2 subunit
FACS	Fluorescence-activated cell sorting, Flowcytometry
FCS	Fetal calf serum
FYCR	phenylalanine/ tyrosine (FY)-rich domain C-terminal
FYRN	phenylalanine/ tyrosine (FY)-rich domain N-terminal
GFP	Green fluorescent protein
GMP	Granulocyte-macrophage progenitors
GPCF	Genomics & Proteomics Core Facility
H2A	Histone 2 A
H2B	Histone 2 B
H3	Histone 3

H3K4me1-3	Histone 3 lysine 4 mono-, di-, trimethylation
H3K9me3	Histone 3 lysine 9 trimethylation
H3K27me3	Histone 3 lysine 27 trimethylation
H3K36me3	Histone 3 lysine 36 trimethylation
H3K79me1-3	Histone 3 lysine 79 mono-, di-, trimethylation
H4	Histone 4
HIF1A	Hypoxia-inducible factor 1 alpha
HoxA	Homeobox A cluster
HOXA9	Homeobox A9
HSC	Hematopoietic stem cell
HSPCs	Hematopoietic stem and progenitor cells
IDH1 and 2	Isocitrate Dehydrogenase (NADP(+)) 1 and 2
KDM	Lysine demethylases (Fe (II) and α-KG dependent, JmJC family)
KMT	Lysine-N-methyltransferase family
KMT2A	Lysine-N-methyltransferase 2A, mixed-lineage leukemia, MLL, MLL1, ALL-1, HRX
LAD1	Ladinin 1
LEDGF	Lens epithelium-derived growth factor
LSC	Leukemic stem cell
LSR	Lipolysis stimulated lipoprotein receptor
MEIS1	Meis Homeobox 1
MEN1	Menin 1
miRNA	microRNA
MLL	Mixed-lineage leukemia, lysine-N-methyltransferase 2A, KMT2A, MLL1, ALL-1, HRX
MLL-AF4	KMT2A-AFF4, in-frame MLL fusion protein
MLL-AF9	KMT2A-MLLT3, in-frame MLL fusion protein
MLL-ENL	KMT2A-MLLT1, in-frame MLL fusion protein
MYC	MYC proto-oncogene, BHLH transcription factor, c-Myc
pATnP	Fusion of N-terminal Tn5 transposase to protein A
pATnPOme	Fusion of N-terminal Tn5 transposase to protein A loaded with oligo adapters
pATnPOme-Ab	Fusion of N-terminal Tn5 transposase to protein A loaded with oligo adapters and linked to the antibody of interest
pATnPOme-H2B	Fusion of N-terminal Tn5 transposase to protein A loaded with oligo adapters and linked to H2B (yeast) antibody
PLP	Pyridoxal 5-phosphate
PHD1-4	Plant homeotic domain 1-4 found in MLL
PRC1 and 2	Polycomp repressive complexes1 and 2
qPCR	Quantitative polymerase chain reaction
RBBP5	Retinoblastoma-binding protein 5
RNA	Ribonucleic acid
RNA-seq	RNA sequencing
SET	Su(var)3-9 enhancer-of-zeste trithorax, enzymatic domain
shBCAT1	Tet-inducible shRNA BCAT1 knockdown
shNT	Non-targeting
SH/shRNA	Short hairpin RNA
SUZ12	SUZ12 polycomb repressive complex 2 subunit
TCA	Tricarboxylic acid [cycle] (citric acid cycle)
TCGA	The Cancer Genome Atlas
TET	Ten-eleven translocation methylcytosine dioxygenase
Tet-inducible	Tetracycline-inducible
WDR5	WD repeat protein 5

List of Figures

List of Tables

1. Introduction

1.1. Hematopoiesis and its epigenetic regulation

Hematopoiesis is defined as the process in which the entire repertoire of blood cells is derived from a small pool of self-renewing hematopoietic stem and progenitor cells (HSPCs) in the hypoxic bone marrow niche of fetal and adult organisms (Y. Zhang et al., 2018). This complex process is highly regulated and relies on a multitude of synergistic factors. It is initiated on the one hand by genetically encoded differentiation programs enacted through epigenetic alterations and on the other hand by a multitude of cell-intrinsic and -extrinsic factors. For instance, signals from the niche microenvironment, activity of transcription factors, and changes in the cellular metabolic state play an essential role (Chambers et al., 2007; Rodrigues et al., 2021; Seita & Weissman, 2010; Trompouki et al., 2011; C. C. Zhang & Lodish, 2008).

In recent years, single-cell RNA-sequencing and *in vivo* lineage tracing defined the continuum model, which suggests a lineage bias of a heterogeneous population of hematopoietic stem cells (HSCs) (Busch et al., 2015; Carrelha et al., 2018; Pei et al., 2017; Rodriguez-Fraticelli et al., 2018; Velten et al., 2017; Weinreb et al., 2020). This lineage bias is assumed to be heavily dependent on epigenetic priming during hematopoiesis. The gradual reorganization of DNA methylation and alterations of the chromatin landscape are associated with lineage-specific differentiation programs (Lara-Astiaso et al., 2014; Rybtsov et al., 2014; V. W. C. Yu et al., 2017).

In his theory of epigenetic landscapes, Conrad Waddington describes in 1957 the process of cell fate determination and cellular decision-making during development (Figure 1) and hence hematopoiesis. For the first time, lineage regulators, such as epigenetic modifiers initiating a differentiation program during hematopoiesis, were proposed to alter a cell's expression pattern without changing the underlying genetic sequence. Over the last decades, the role of epigenetic landscapes and their regulators have been extensively studied in cell fate determination, differentiation, and diseases, such as cancer, revealing a vast epigenetic network of modifications (Avgustinova & Benitah, 2016; Goodell et al., 2015). This dynamic chromatin reorganization provides or abolishes DNA accessibility for binding a variety of transcription factors driving fate determination.

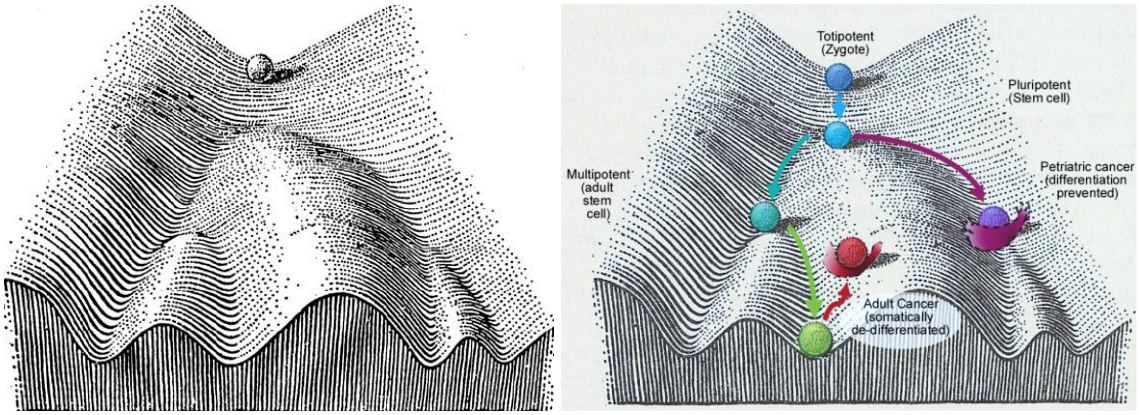

Figure 1- Epigenetic landscape during development proposed by C.H. Waddington and a simplified adaptation for cancer formation. In 1957 Conrad Waddington was the first to describe epigenetic patterns as the regulator for gene expression during development. He proposed a model of groves and vales (left), representing the process of cell fate and cellular decision-making during development (Waddington, 1957). In recent years this model has been adapted to various diseases, such as cancer, where cellular de-differentiation, as shown in the image on the right, is a crucial hallmark of cancer (Goel et al., 2021; Rossi et al., 2015)

Among the direct modifications are DNA methylations, histone modifications, and nucleosome remodeling. The epigenetic landscape is additionally altered indirectly through miRNA, long noncoding RNA, histone variants, and three dimensional chromatin conformation changes (Luo et al., 2015; Roden & Lu, 2016; Rodrigues et al., 2021). Together these factors form a highly interconnected and dynamic system to regulate gene expression.

1.1.1. DNA methylation

DNA methylation is a covalent modification at the 5’ position of the cytosine ring of a CpG dinucleotide. In this process, S-adenosyl methionine donates a methyl group, which is attached to the 5’ carbon of the ring. These modifications predominantly occur at CpG rich regions surrounding gene promoters, altering accessibility for transcription factors, such as methyl CpG-binding domain proteins. Methylated promoter regions are in general associated with reduced gene expression. DNA methyltransferase DNMT1, for instance, is associated with promoting self-renewal in HSCs by propagating hemimethylated DNA after cell replication (Cullen et al., 2014; Lyko, 2018; Schübeler, 2015). In contrast, DNMT3A and B elicit differentiation via *de novo* CpG methylation of crucial transcription factor binding sites (Challen et al., 2011, 2014; Izzo et al., 2020; Jeong et al., 2018). Prominent roles in the regulation of DNA methylation are also awarded to DNA demethylases ten-eleven translocation (TET), which oxidize 5mC to 5-hydroxy-

methylcytosine. TET2, in particular, functions as a regulator in HSCs (Izzo et al., 2020), resulting in a complex interplay between DNMTs and TET enzymes.

1.1.2. Histone modification

Adding to this complexity, histone modifications play an important role in gene regulation by influencing the highly ordered chromatin structure. Eukaryotic DNA is wrapped around an octamer of histone proteins, packaging it into a higher-order chromatin fiber. These octamers are formed by H2A, H2B, H3, and H4 core histone proteins, as shown in Figure 2. These histones undergo multiple posttranslational modifications, including acetylation and methylation at several amino acid positions in their N-terminal tails (Dillon, 2006). Combinations of these covalent modifications in specific genomic regions result in opened or closed chromatin structures associated with active or repressive gene transcription, respectively (Rodríguez-Paredes & Esteller, 2011). For example, acetylation of lysine residues such as lysine 27 of histone 3 (H3K27ac) or lysine 14 of histone 3 is associated with open chromatin structures and activation of gene transcription. This highly dynamic transcription regulation is tightly controlled by lysine acetyltransferases and histone deacetylases (Sheikh & Akhtar, 2019; Z. Wang et al., 2009).

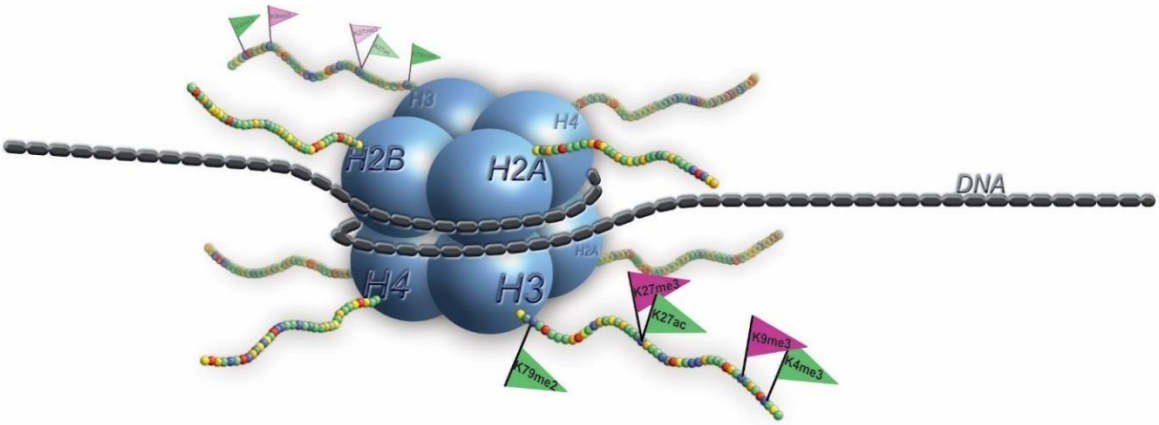

Figure 2 - Schematic representation of a nucleosome with a selection of modifications on the histone 3 tail. A nucleosome consists of a histone octamer wrapped by 146 to 147 base pairs. These octamers consist of double subunits H2A, H2B, H3, and H4. Histone modifications (indicated with flags for histone 3) on histone tails can influence this compacted DNA organization in the nucleus. For instance, activating histone modifications (green) such as H3K4me3, H3K27ac, and H3K79me2 result in open chromatin enabling transcription factor binding. In contrast, the repressive modifications H3K9me3 and H3K27me3 (pink) lead to tightly packed heterochromatin, associated with a lack of transcription.

In contrast, covalent lysine methylations vary in their functions. Monomethylation of lysine 4 on histone 3 (H3K4me1) identifies enhancers, while trimethylation of the same site (H3K4me3) is associated with promoter regions and active gene transcription. The two

activating modifications H3K4me3 and H3K27ac, are often observed in the same gene regions supporting gene expression. Di- or trimethylation of lysine 9 and 27 of histone 3 (H3K9me2, H3K9me3, H3K27me3) are examples of repressive marks. These histone tail modifications are commonly mediated by multi-subunit complexes containing enzymatic members such as the polycomb repressive complexes PRC1 and PRC2 directing H3K27me3 methylation. PRC1 has multiple variants, while PRC2 consists of three core subunits: SUZ12 polycomb repressive complex 2 subunit (SUZ12), embryonic ectoderm development (EED), and enhancer of zeste 2 polycomb repressive complex 1 subunit (EZH1) or 2 (EZH2). The putative polycomb-group proteins additional sex combs like 1 and 2 (ASXL1 and 2) are essential for accurate hematopoiesis (Bowman et al., 2018; Fujino & Kitamura, 2020).

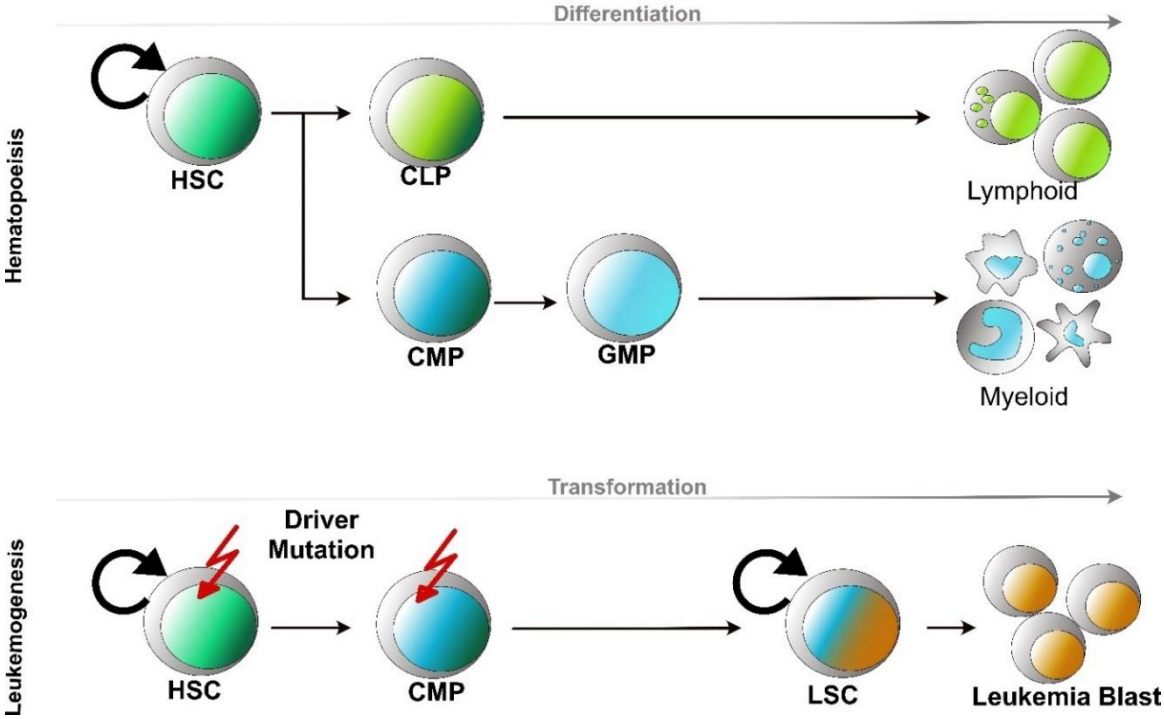

Figure 3 - Hematopoiesis and development of acute myeloid leukemia in direct comparison: The upper panel depicts the differentiation of self-renewing hematopoietic stem cells (HSCs) into fully functional lymphoid (natural killer cells, T lymphocytes, B lymphocytes) and myeloid cells (megakaryocytes, erythrocytes, mast cells, Basophils, neutrophils, eosinophils, macrophages). The differentiation program essential for accurate hematopoiesis is initiated and regulated by intricately balanced epigenetic processes. However, the bottom panel documents the transformation of HSCs to LSCs, which re-gain the potential for unlimited self-renewal and produce non-functioning leukemia blast cells. Driver mutations often observed in epigenetic regulators initiate this transformation process and occur either in HSCs or common myeloid progenitors (CMP). [HSC: hematopoietic stem cell; CLP: common lymphoid progenitor; CMP: common myeloid progenitors; GMP: granulocyte-monocyte progenitors; LSC: leukemic stem cell]

Epigenetic regulation plays a key role in initiating the differentiation program during hematopoiesis. Therefore, it is no surprise that chromatin deregulation largely contributes to impaired hematopoiesis and leukemia (Hu & Shilatifard, 2016; Ntziachristos et al., 2016). While genetic changes in epigenetic regulators are observed in most cancer entities, acute myeloid leukemia harbors particularly many mutations in respective genes.

1.2. Acute myeloid leukemia

Impaired hematopoiesis due to mutated driver genes, such as epigenetic regulators in HSCs or committed myeloid progenitor cells (CMPs), contributes to myeloid leukemia development as depicted in Figure 3 (Bereshchenko et al., 2009; Huntly et al., 2004; Andrei Krivtsov et al., 2006).

With nearly 120,000 cases per year worldwide, acute myeloid leukemia (AML) is the most common leukemia in adults and accounts for approximately 4% of all cancer-related deaths. This severe death rate results from a high number of relapses (about 50%) and a 5-year survival rate of only 30% (Medeiros et al., 2019). In the last two decades, advances in diagnostics and treatment have improved outcomes, especially for young patients (Yi et al., 2020). However, most AML patients are diagnosed at the age of 65 or older, which is associated with an even higher relapse probability (>65%) and thus a higher mortality rate (Ferrara et al., 2019; Yi et al., 2020). The current standard of care consists of harsh chemotherapy with a 7 + 3 regimen of cytarabine and anthracycline dating back to the 1970s (Dombret & Gardin, 2016; Heuser et al., 2020). Unfortunately, high-risk, older AML patients often have to be excluded from this treatment course due to their poor overall fitness. Another drawback of this approach is the escape of chemoresistant leukemic stem cells (LSCs), leading to relapse in many patients (Ferrara et al., 2019).

1.2.1. Characteristics of AML

AML is characterized by an overproduction of leukemic blasts originating from the myeloid lineage. These immature blast cells replace fully functional hematopoietic cells of all lineages, starting in the bone marrow, spreading to peripheral blood, and even infiltrating other organs (Prada-Arismendy et al., 2017). While most cancer therapies successfully eradicate these highly proliferative leukemic blast cells, quiescent LSCs evade elimination. LSCs, capable of limitless self-renewal, can regenerate AML blasts and constitute an AML long-term reservoir (Bonnet & Dick, 1997; Eppert et al., 2011; Lapidot et al., 1994; Somervaille & Cleary, 2006). This rare population of cells is necessary for cancer initiation

and maintenance, as demonstrated by serial engraftment models as well as relapsed patients after successful eradication of the leukemic blast.

Recently, transcription profiling revealed a gradual increase of somatic mutations in HSCs of healthy, elderly donors resulting in clonal hematopoiesis of intermediate potential (CHIP). The acquisition of additional driver mutations during hematopoiesis pushes these cells towards a LSC expression profile by which they gain the potential to promote leukemogenesis (Figure 1 and Figure 3) (Genovese et al., 2014; Hérault et al., 2017; Lee-Six et al., 2018; Shlush et al., 2014). Furthermore, it has been demonstrated that through this process, HSCs, as well as more mature myeloid progenitor cells, acquire immortalization and can serve as a cell of origin (Goardon et al., 2011; Kirstetter et al., 2008; Somervaille et al., 2009; Somervaille & Cleary, 2006).

1.2.2. AML and epigenetics

Epigenetic regulation is at the heart of cell identity and hematopoiesis. Therefore, it is no surprise that mutations in epigenetic regulators such as *DNTM3A*, *IDH2*, *TET1*, and *2* are among the earliest events conferring a survival advantage to CHIP and leukemic cells (Rao & Dou, 2015). Mutations of different epigenetic regulators often co-occur in AML, altering the global DNA methylation landscape and supporting the unique transcription pattern of LSCs (Charlton et al., 2020; Odejide et al., 2014; Quivoron et al., 2011; X. Zhang et al., 2016).

Oncogenic mutations in DNMT3 enzymes commonly observed in CHIP are viewed as cancer support, however, not tumor-initiating. In contrast, driver mutations such as translocations of H3K4 methyltransferase mixed-lineage leukemia (*MLL*) are able to drive tumor development by promoting self-renewal expression profiles through altered histone modifications.

1.3. Histone methyltransferase MLL and its fusions

The histone-lysine N methyltransferase 2 (KMT2) family shapes chromatin structure and DNA accessibility by methylating lysine 4 on the histone 3 tail (H3K4me1-3), which is associated with enhancers and active promoters (Rao & Dou, 2015). Advances in exome sequencing over the last decades revealed that the members of this family are commonly mutated in human cancers (Ding et al., 2008; Kandoth et al., 2013; Muzny et al., 2012). Mutations and rearrangements of lysine-N-methyltransferase 2A are among the most frequently detected alterations.

1.3.1. Structure and function of MLL

First described in 1992 (Y. Gu et al., 1992; Tkachuk et al., 1992), lysine-N-methyltransferase 2A (KMT2A) is well known as mixed-lineage leukemia (MLL, MLL1, ALL-1, HRX) named after its role in leukemia. The initial nomenclature “MLL” is still commonly accepted and hence, will be used in this thesis. The *MLL* gene on chromosome 11q23 encodes a 431 kDa protein, closely related to the *Drosophila melanogaster* protein trithorax. MLL protein levels are tightly controlled through degradation, dependent on its plant homeotic domain 2 (PHD2) domain's intrinsic E3 ubiquitin ligase activity (Liu et al., 2007; J. Wang, Muntean, & Hess, 2012; J. Wang, Muntean, Wu, et al., 2012). Hematopoietic cells, including stem and progenitors cells, ubiquitously express this large, multi-domain protein (Butler et al., 1997; Kawagoe et al., 1999). The full-length precursor, as shown in Figure 4, is cleaved by taspase 1, generating a 300 kDa N-terminal and 180 kDa C-terminal protein. The cleaved subunits reassemble at the FY-rich N-terminal (FYRN) and FYR C-terminal (FYRC) domains into a functional, non-covalently bound heterodimer (Hsieh et al., 2003; Yokoyama et al., 2002). This heterodimeric MLL is part of a large multi-component complex comprised of WD repeat protein (WDR5), retinoblastoma-binding protein 5 (RBBP5), lens epithelium-derived growth factor (LEDGF), ASH2 like histone lysine methyltransferase complex subunit (ASH2L), and Dpy-30 histone methyltransferase complex regulatory subunit (DPY30). The nuclear complex facilitates a change of MLL protein conformation, enabling the evolutionarily conserved SET domain at the C-terminus to methylate lysine 4 of the histone 3 tail, associated with active gene transcription. In addition to increased accessibility, MLL protects these sights from repressive DNA methylation (Deaton & Bird, 2011; Thomson et al., 2010). The CxxC domain of MLL recognizes and binds to unmethylated CpG islands commonly found in gene promoters resulting in mutually exclusive methylation of H3K4 and DNA (Ooi et al., 2007). The binding to DNA is further stabilized by AT-hooks, plant homeotic domain 3 (PHD3), and bromodomain, which can recognize activating histone modifications at the transcription start site (TSS). Zeleznik-Le and colleagues suggested that the DNA binding based on AT-hook motifs and the CxxC domain of MLL occurs in a sequence unspecific manner (Birke et al., 2002; Zeleznik-Le et al., 1994). Even though MLL harbors DNA binding domains, other complex interactions strongly influence their binding, i.e., the tumor-suppressor Menin (MEN1), which is essential for regulating MLL-mediated HoxA cluster gene expression (Yokoyama et al., 2005). While Hox genes are crucial targets of MLL during development, advances in chromatin immunoprecipitation (ChIP) have revealed more than 5400 genomic regions influenced by MLL. These studies showed that

90% of MLL-bound human promoters are occupied by RNA polymerase II suggesting a global regulatory role in transcription (Cierpicki et al., 2010; Guenther et al., 2005; Milne, Dou, et al., 2005).

1.3.2. MLL fusion regulated gene expression

Exome sequencing revealed a variety of mutations in *MLL* in a diverse set of cancers. Among the most common and best-studied *MLL* mutations are rearrangements that result in a gain of function fusion gene driving the development of acute leukemia. MLL rearrangements include translocations, tandem duplications, and amplifications. They are observed in about 10% of all acute leukemia cases and approximately 60% of AML infant leukemias (Ayton & Cleary, 2001; Hess, 2004) and are associated with a poor prognosis (Ayton & Cleary, 2001, 2003; Krivtsov & Armstrong, 2007; Liedtke & Cleary, 2009)

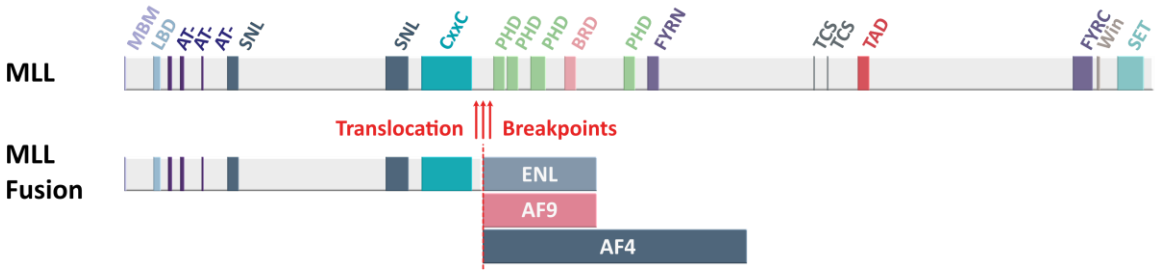

Figure 4 – Schematic architecture of MLL and the three most common MLL fusion proteins, including domain structures. The 3969 amino acid long human wildtype MLL contains various functional domains and active sites, drawn according to scale (Chan & Chen, 2019; Andrei V Krivtsov et al., 2007)**. A**s illustrated by red arrows, almost all translocation breakpoints occur in the region between the CxxC domain and PHDs domains. Balanced MLL rearrangements result in a gain of function fusion gene by maintaining the N-terminal MLL region and in-frame fusing to the partner. The three most common of the numerous observed fusion partners are depicted: MLL-ENL, MLL-AF9, MLL-AF4. [MLL: mixed lineage leukemia, lysine-N-methyltransferase 2A; MLL fusion: MLL-ENL, MLL-AF9, MLL-AF4; MBM: high-affinity Menin-binding motif; LBD: LEDGF-binding domain; AT-Hook: adenine-thymine rich DNA binding motif; SNL: nuclear-localization signal; CxxC: CxxC domain, C-rich DNA binding domain; PHD: plant homology domain; BRD: bromodomain; FYRN: FY-rich N-terminal domain; TCS: taspase 1 cleavage site; TAD: transactivator domain; FYRC: FY-rich C-terminal domain; Win: WDR5 interaction motif; SET: Su(Var)3-9, enhancer-of-zeste, trithorax domain].

MLL harbors an 8.3 kb breakpoint cluster region N-terminal of the PHD domains (exon 8-13, Figure 4). Multiple topoisomerase II cleavage sites, and nuclear attachment sequences in this region, contribute to the translocation mechanism (Strissel et al., 1998). Translocations always produce a chimeric fusion protein by combining the N-terminal *MLL* region (exon 8-13) in frame with a variable number of exons from the C-terminus of a fusion partner (Meyer et al., 2006, 2018). These oncogenic fusion proteins lack the proteolytic regulation and the enzymatic SET domain of MLL (Liu et al., 2010). The loss of

H3K4 methyltransferase activity suggests an oncogenic process mediated by its fusion partners.

While more than 50 known fusion partners provide a high heterogeneity (Tate et al., 2019), most fusion proteins are involved in transcriptional control and transcriptional elongation. The most frequent MLL rearrangements contain a C-terminal transcription activation domain and are recruited to the multi-component PAF1C and/or the disruptor of telomeric silencing 1-like DOT1L complex (Milne et al., 2010; Mueller et al., 2007; Muntean et al., 2010). Among those, MLLT3 super elongation complex subunit (*AF9*, *MLLT3*), MLLT1 super elongation complex subunit (*ENL*, *MLLT1*), AF4/FMR2 family member 4 (*AF4*, *AFF4*), and MLLT10 histone lysine methyltransferase DOT1L cofactor (*AF10*, *MLLT10*) contribute to more than two-thirds of all MLL fusion-associated leukemias (Meyer et al., 2018).

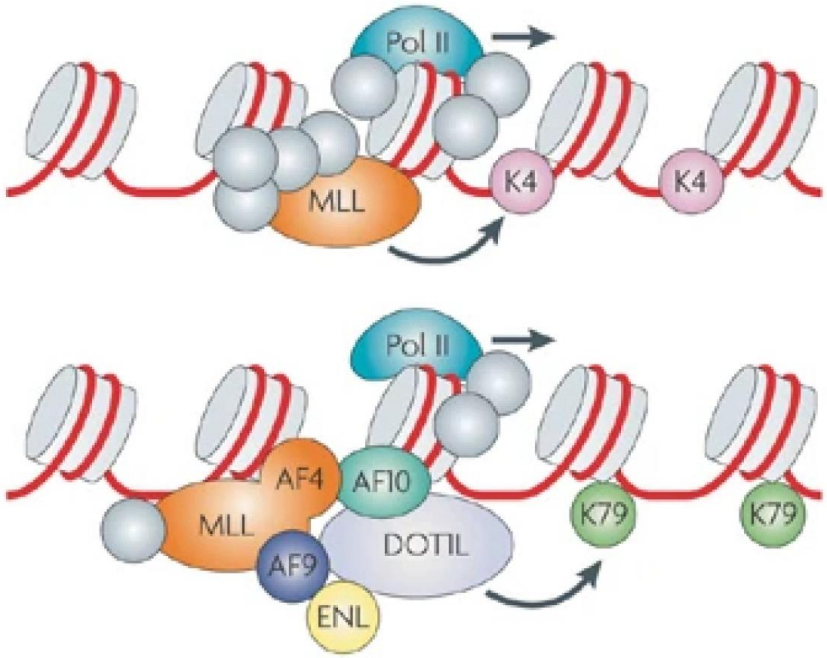

Figure 5 - Comparison between MLL and MLL fusion regulated gene expression. The upper panel shows gene activation through the binding of MLL (orange) and its interaction partners (grey). In a large multi-component complex, MLL acts as H3K4 (K4, red) histone methyltransferase in gene promoter regions, increasing accessibility for RNA polymerase II (Pol II). This mechanism results in gene activation. The most common MLL fusion genes (here: MLL-AF4, orange), however, form a different multi-component, as shown in the lower panel. This DOT1L complex (here: AF9, ENL, AF10, DOT1L) binds to DNA and mediates H3K79 (K79, green) methylation leading to aberrant gene expression. Modified from Krivtsov, A., and Armstrong, S,2007.

These balanced translocations lead to an in-frame gain of function oncoproteins which maintain their ability to interact with DOT1L complexes and a selection of MLL core

proteins as well as their DNA binding capabilities (Figure 5). For instance, the direct interaction of AF9 or ENL with the DOT1L complex results in its misguided recruitment to DNA by MLL-AF9 or MLL-ENL (Biswas et al., 2011; Mueller et al., 2007). The only known H3K79 methyltransferase DOT1L, in turn, di-methylates the activating histone mark H3K79 and cooperates with the histone acetyltransferase E1A binding protein P300 (EP300) and MYC proto-oncogene, BHLH transcription factor (MYC) to enhance further gene transcription (M.-H. Cho et al., 2015). In the context of MLL-AF9, these mechanisms are associated with mistargeted and inappropriate activation of gene expressions such as the MLL fusion targets *HOXA9* and *MEIS1* (Milne, Martin, et al., 2005). These MLL fusion protein-induced changes of the epigenetic landscape and transcription factor binding activated a leukemia stem cell-specific transcription program in hematopoietic stem and progenitor cells (Chen et al., 2008; Andrei Krivtsov et al., 2006).

1.3.3. Targeting MLL fusion mediated leukemia

One of the challenges that AML therapies face is the high clinical and intracellular heterogeneity of the tumor (The Cancer Genome Atlas Research Network, 2013). Heterogeneity is elicited by aberrant epigenetic regulation, making epigenetic driver mutations an emerging clinical target. In MLL-rearranged leukemias, loss of H3K79 methylation through downregulation of *DOT1L* or the administration of the DOT1L inhibitor EPZ5676 (Pinometostat) decreased leukemogenic potential and reduced AML relapse (Uckelmann et al., 2020; Yamashita et al., 2020). In contrast to MLL fusion proteins, however, most leukemia-associated mutations result in a loss of function. Therefore, novel therapeutic approaches aim to take advantage of the close interaction between epigenetic regulation and metabolism. By manipulating metabolic pathways, levels of essential substrates for epigenetic modifiers are affected, resulting in a restored differentiation capacity (Amatangelo et al., 2017; DiNardo et al., 2018).

The metabolic enzyme branched-chain amino acid transaminase 1 (BCAT1), which catalyzes the first step of branched-chain amino acid (BCAA) catabolism, constitutes a promising target for developing innovative AML therapies. *BCAT1* is upregulated in tumor stem cells and contributes to malignant growth and tumor aggressiveness (Z. Gu et al., 2019; Raffel et al., 2017; Thewes et al., 2017; Tönjes et al., 2013)

1.4. Cancer metabolism

Scientific advances in recent decades revealed many details on how reprogramming cellular energetics and metabolism accompany cancer development (Hanahan & Weinberg, 2011).

Within limits set by the cell of origin and its pre-oncogenic signaling, cancer cells need to adapt their metabolism to support increased cell proliferation and tumor growth (Birsoy et al., 2014; Palm et al., 2015; Yuneva et al., 2012). In many cancer entities, the most prevalent adaptation is the dysregulation of glucose metabolism by reducing aerobic glycolysis through the tricarboxylic acid cycle and electron transport chain and increasing less energy-efficient but fast and less error-prone anaerobic glycolysis (Koppenol et al., 2011; Warburg et al., 1927). In cancer, this so-called Warburg effect is implemented even in the presence of ample oxygen (Warburg, 1956). It satisfies tumor cells' elevated demand for energy and biomass while maintaining the cell's redox state (Sivanand & Vander Heiden, 2020). In addition, increased demand for essential and non-essential amino acids results in an elevated uptake of glutamate, and the BCAAs valine, leucine, and isoleucine that tumors can scavenge from the tumor environment as well as other sources (Jain et al., 2012; Mayers et al., 2016; L. S. Silva et al., 2017). These amino acids are repurposed to meet the increased demand of protein synthesis, energy production, glutamate, and nitrogen transfer, altering the BCAA metabolism in the process (Daikhin & Yudkoff, 2000; Finicle et al., 2018; Suryawan et al., 1998).

1.4.1. BCAA metabolism in cancer

In the first step of the BCAA metabolism, the essential amino acids valine, leucine, and isoleucine undergo transamination catalyzed by the highly compartment-specific and reversible enzymes branch chain amino acid transaminase 1 (BCAT1) and 2 (BCAT2).

The transfer of this α-amino group to α-ketoglutarate (α-KG) yields glutamate, and the respective branched chain-keto acids (BCKAs; α-ketoisovalerate [ketovaline]), α-keto-β-methyl valerate [ketoisoleucine], α-ketoisocaproate [ketoleucine], Branched-chain alpha-ketoacid dehydrogenase (BCKDH) irreversibly decarboxylates BCKAs further in a multistep reaction. Multiple degradation steps of these distinct branched-chain acyl-coenzyme A derivates result in succinyl-CoA and acetyl-CoA, respectively. These carbon precursors are either incorporated into the tricarboxylic (TCA) cycle as anaplerotic substrates or used for fatty acid synthesis.

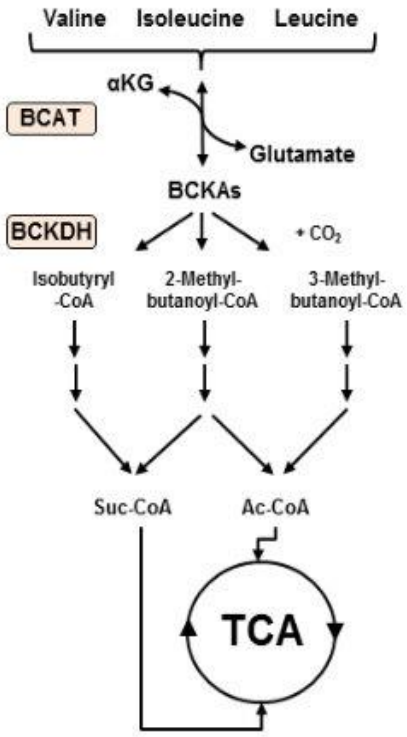

Figure 6- Schematic overview of the BCAA metabolism. BCAT1 mediates the first step of BCAA (valine, leucine, and isoleucine) degradation by transferring a nitrogen group to α-KG yielding glutamate and BCKA. Further steps involve decarboxylation, hydration, and carboxylation. The resulting succinyl-CoA and acetyl-CoA derivates are incorporated in the TCA cycle or fatty acid synthesis. This figure was adapted from Kneisel, 2017.

The inappropriate activation of BCAA metabolism is vital in many cancer entities for various reasons (Sullivan et al., 2019). Firstly, the breakdown of BCAAs frees carbons for the synthesis of other molecules, fueling the TCA and consequently providing energy. In addition to carbons, BCAA degradation supplies nitrogen for de novo nucleotides and secondly amino acid synthesis. Thirdly, levels of metabolites that act as catalytic cofactors are altered, potentially influencing numerous enzymes and the epigenetic landscape. Lastly, tightly regulated BCAA levels can affect protein synthesis as proteinogenic amino acids or indirectly by signaling amino acid availability and cell nutritional state (Ananieva & Wilkinson, 2018).

Affecting cell-intrinsic cancer properties and reflecting systematic changes in metabolism, altered BCAA metabolism, in the form of *BCAT1* overexpression, can serve as a marker for disease pathology associated with many cancer entities.

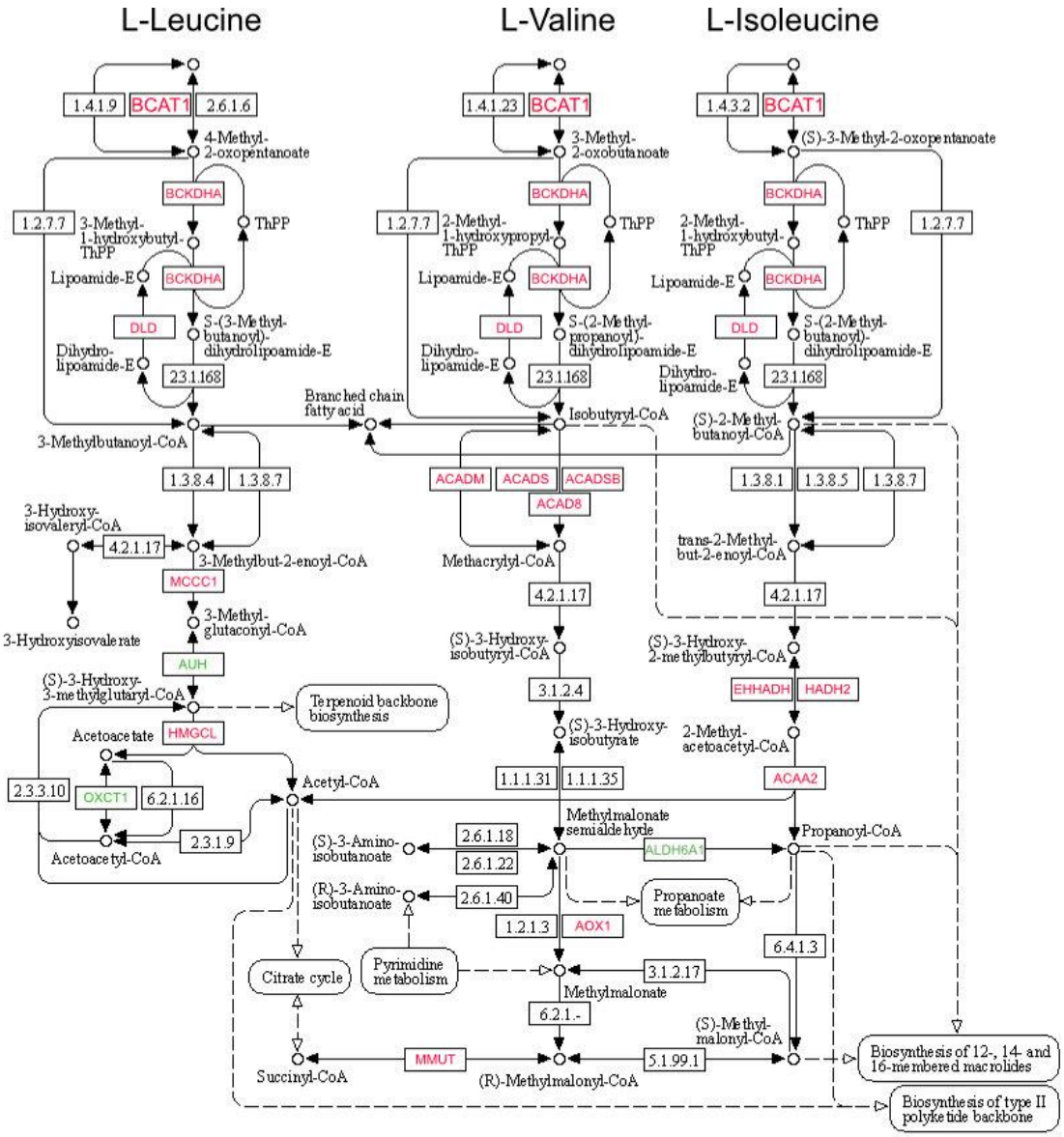

Figure 7 -Regulation of the BCAA degradation pathway in glioblastoma. Tönjes et al. (2013) demonstrated the alteration of BCAA metabolism in IDH wildtype glioma by identifying overexpressed (red) and downregulated (green) enzymes in this pathway. This modified KEGG pathway (hsa00280) shows human valine, leucine, and isoleucine degradation. Up- and down-regulation of RNA expression in IDHwt astrocytic gliomas relative to normal brain are indicated in red and green, respectively.

1.4.2. Branched-chain amino acid transaminase

Expression of cytosolic *BCAT1* is primarily limited to the nervous system and germinal tissues in healthy adults but has been demonstrated in many cancer entities (Ananieva & Wilkinson, 2018; Hutson et al., 2005; Vander Heiden, 2011). In contrast, most tissues express the mitochondrial isoenzyme *BCAT2*. Even though BCAT1 and BCAT2 share a highly conserved C-terminal amino acid sequence and an overall amino acid sequence homology of 58%, BCAT2 has been investigated in the context of cancer only recently

(Ananieva et al., 2018; Conway et al., 2016; Falcone & Maddocks, 2020; Lichti et al., 2015; Sweatt et al., 2004).

As mentioned above, BCAT1 catalyzes the breakdown of BCAAs by transferring the BCAA primary amino group to α-KG, forming glutamate and the corresponding BCKAs. This reaction is in principal reversible, but BCAA deamination is predominant under physiologic conditions (Hutson et al., 2005). During the transamination reaction, the cofactor (PLP) facilitates the proton transfer. This active form of vitamin B_6 covalently binds to the amino group of lysine 222 (K222) and is further stabilized by other residues at the active site of BCAT1 (Figure 8) (N. Yennawar et al., 2001). A single mutation at the active site (K222A) renders BCAT1 catalytically inactivate (François Martín del Campo, 2019; Kingsbury et al., 2015)

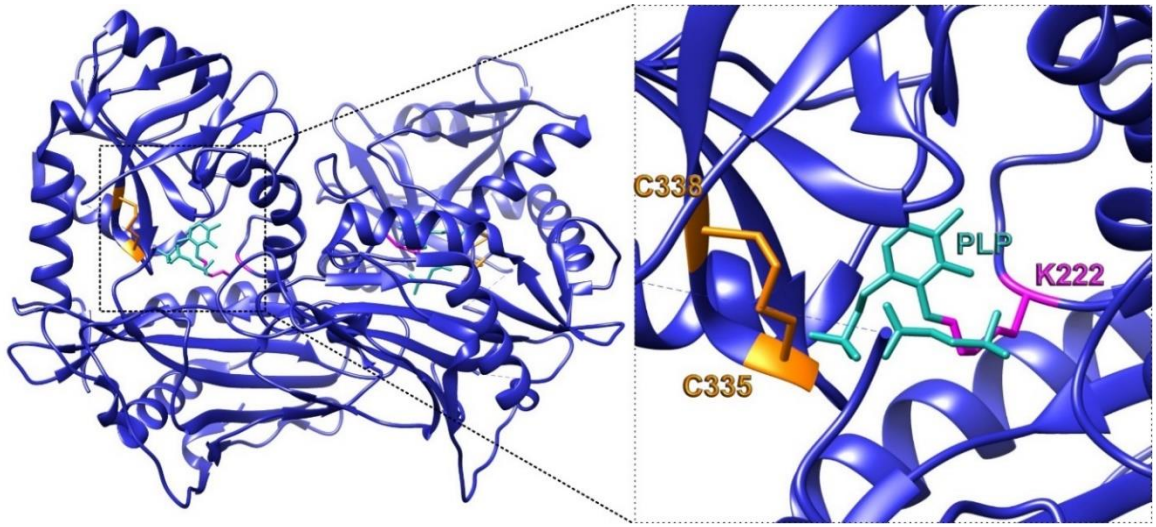

Figure 8 -3D structure of human BCAT1 homodimers and a detailed view of its active center. BCAT1 forms homodimers, as shown on the left side. Each subunit consists of a large and small domain, which together form the enzymatic pocket. The active center at the right side shows the bound cofactor PLP, stabilized by lysine 222 (K222). At the pocket entrance, cysteines 335 and 338 (C335, C338) form an intra-molecular disulfide bridge (highlighted in orange). I generated the graphic with UCSF Chimera 1.12rc based on the crystal structure 2COG (PDB) and Liliana François Martín del Campo,2019.

BCAT1 enzymatic activity is not only regulated by the availability of its cofactors and substrates but also by the formation of disulfide bonds between the thiols of the CxxC-motif surrounding the active site of these enzymes (Coles et al., 2012; François Martín del Campo, 2019; N. H. Yennawar et al., 2006). The presence of a potential redox switch suggests BCAT1 activity being sensitive to physiological reducing or oxidizing conditions within the cell.

1.4.3. BCAT1 and cancer

Reprogramming of BCAA metabolism is a common characteristic in many cancer entities, and high levels of cytosolic BCAT1 have been associated with tumor aggressiveness. While the first studies affiliating BCAT1 and cancer date back to 1977 (Goto et al., 1977), it took until the 1990s to discover BCAT1 as a direct target for MYC regulation in several MYC induced mouse tumors (Benvenisty et al., 1992). Soon after, BCAT1 overexpression was connected to a variety of human MYC-based tumors, such as mammary carcinomas, Burkitt's lymphomas, and subgroups of neuroblastomas (Ben-Yosef et al., 1996). In the following years, *BCAT1* overexpression was discovered in additional tumor types and was suggested as a biomarker for these entities (Yoshikawa et al., 2006). The clinical relevance of *BCAT1* was particularly emphasized as overexpression was correlated with tumor proliferation (Zhou et al., 2007), formation of metastasis (de Bont et al., 2008; Yoshikawa et al., 2006), and chemoresistance (Ju et al., 2009; Tönjes et al., 2013). More recently, our group was able to identify triple-negative breast cancer (Thewes et al., 2017) and myeloid leukemia (Hattori et al., 2017; Raffel et al., 2017) as particularly dependent on the overexpression of *BCAT1*. Furthermore, in AML, *BCAT1* expression was described as highly enriched in the chemoresistant LSCs and associated with an adverse prognosis (Raffel et al., 2017).

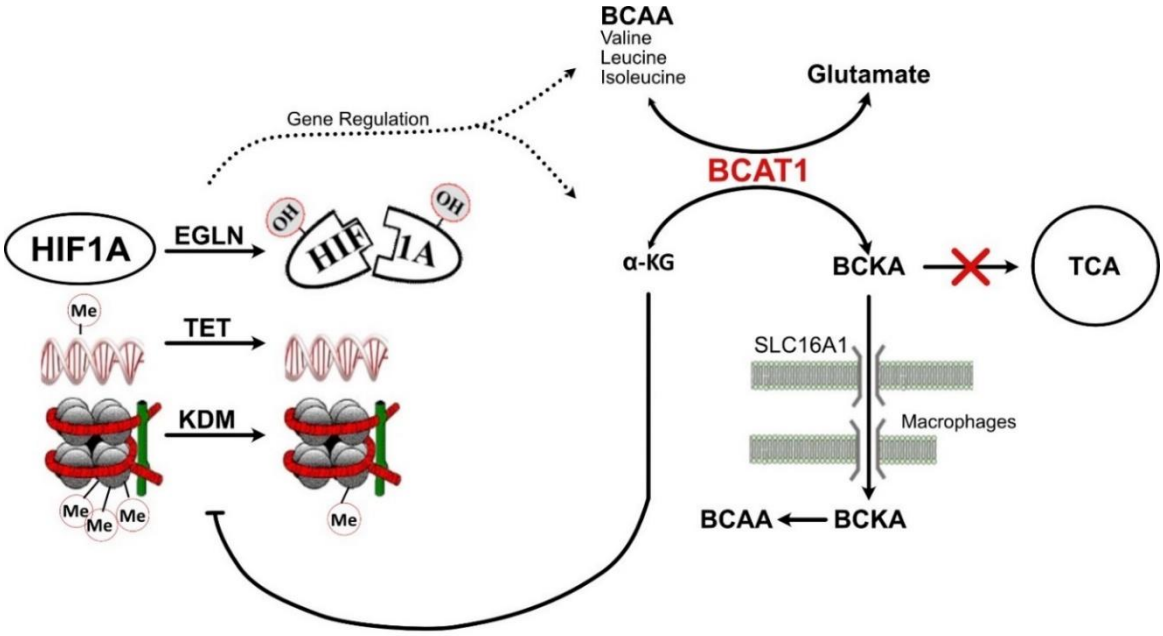

Figure 9 - Current view on the mode of action of BCAT1 in cancer. [EGLN: Egl-9 family hypoxia-inducible factor; TET: Ten-eleven translocation; KDM: Lysine demethylase; BCAA: Branched-chain amino acid; BCAT1: Branched-chain amino acid transaminase 1; BCKA: Branched-chain keto acid; α-KG: α-Ketoglutarate; TCA: tricarboxylic cycle; SLC16A1: Solute Carrier Family 16 Member 1] (*https://www.dkfz.de/en/genetics/pages/projects/Tumor-metabolism/Tumor_metabolism.html*, n.d.).

The precise role of glutamate and BCKAs, the BCAA transamination products, for these phenotypes is still unclear. Glioblastoma cells excrete most glutamate and BCKAs generated by BCAT1 (L. S. Silva et al., 2017; Tönjes et al., 2013), and BCAA carbon does not enter the tricarboxylic acid cycle in significant amounts in glioblastoma and AML (Raffel et al., 2017; L. Silva, 2017). Therefore, it seems unlikely that BCAT1 drives tumor growth by replenishing the tricarboxylic acid cycle and anaplerosis.

In collaboration with the group of Andreas Trumpp (DKFZ), we were able to show that BCAT1 controls cellular α-KG concentrations through the BCAA catabolism in AML. In these tumors, *BCAT1* overexpression and associated high BCAT1 activity resulted in the depletion of α-KG, influencing α-KG-dependent dioxygenases. Among these, Egl-9 family hypoxia-inducible factor 1 (EGLN1) activity was reduced, promoting the stabilization of the transcription factor hypoxia-inducible factor 1A (*HIF1A*) (Raffel et al., 2017). Furthermore, the reduced activity of α-KG-dependent TET family of DNA demethylases was suggested to be responsible for global DNA hypermethylation observed in leukemia (Raffel et al., 2017). These changes are associated with tumor proliferation, cell survival, and stem cell maintenance (Hattori et al., 2017; Raffel et al., 2017).

Even though other modes of action are suggested, in leukemia, BCAT1's central role seems to be linked to the BCAA metabolism. On the one hand, α-KG dependent metabolic and epigenetic programs are altered by BCAT1, and on the other hand, the tumor microenvironment is affected by produced BCKAs (Z. Gu et al., 2019).

2. Hypothesis and Aim

Epigenetic regulation and metabolism are tightly intertwined, as many histone and DNA modifiers rely on cofactors such as acetyl-CoA as a source for histone acetylation (S. L. Campbell & Wellen, 2018; Kaelin Jr. & McKnight, 2013; Schvartzman et al., 2018), or α-KG as the substrate for DNA and histone demethylation.

Our previous work showed that, in AML cells, depletion of α-KG by BCAT1 inactivated α-KG-dependent enzymes controlling HIF1A stability. Furthermore, suppression of *BCAT1* resulted in DNA-hypermethylation of AML cells, suggesting α-KG-dependent effects on TET-family DNA demethylases (Raffel et al., 2017).
Potential interdependencies between BCAT1 and other chromatin modifiers such as histone demethylases and histone methyltransferases and their effect on AML-cell transformation have not yet been addressed.

It is the aim of my thesis project to

- Identify interdependencies between BCAT1 and chromatin modifiers
- Determine whether BCAT1 is essential for AML-cell transformation

3. Materials and Methods

3.1. Materials

3.1.1. ACT-seq

Table 1 - Material and chemicals needed for ACT-seq experiments.

Material	
2x Complex Formation Buffer (2x CB)	100mM Tris (pH 8), 0.3M NaCl, 0.1% Triton X-100, 25% Glycerol
100x SYBRGreen	Provided by Dierter Weichenhan (C. Plass, DKFZ)
AmPure XP Beads	Beckman, Krefeld, Germany
AmPure Buffer	2.5M NaCl, 20% PEG 8000 (filter sterilized)
Load Adapter Mix Tn5ME-A+B	Provided by Dierter Weichenhan (C. Plass, DKFZ)
MinElute	Qiagen, Hilden, Germany
NEBNext High Fidelity 2X Mix	New England Biolabs, Massachusetts, United States
pATnp	Provided by Dierter Weichenhan (C. Plass, DKFZ)
pATnp transposome (pATnpOme)	Provided by Dierter Weichenhan (C. Plass, DKFZ)
Proteinase K (20mg/ml; 600 U/ml)	Thermo Fisher Scientific, Langenselbold, Germany
Tn5McP1n	Provided by Dierter Weichenhan (C. Plass, DKFZ)
Wash Buffer	50mM Tris (pH 8), 150mM NaCl, 0.05% Triton X-100
Yeast nuclei spike-in	Provided by Dierter Weichenhan (C. Plass, DKFZ)

3.1.2. Antibiotics and inhibitors

Table 2 - Antibiotics and inhibitors used.

Selection of antibiotics and inhibitors	Distributor
Ampicillin	Roche diagnostics, Mannheim, Germany
Geneticin Selective Antibiotic (G418 Sulfate)	Thermo Fisher Scientific, Langenselbold, Germany
Hygromycin B 100mg	MP Biomedicals
Kanamycin Solution	Sigma-Aldrich, Munich, Germany
Puromycin	Merck Millipore, Darmstadt, Germany

EPZ004777	Biomol, Hamburg, Germany
EPZ5657	Biomol, Hamburg, Germany

3.1.3. Antibodies

Table 3 - Antibodies used for ACT-seq, ChIP PCR, and western blot.

Antibody target	Specifications	Number	Distributor
ACT-seq			
Dot1l		A300-953A	Bethyl Laboratories, Montgomery, USA
DYKDDDK (Flag)	(D6W5B)	14793S	Cell Signaling Technology, Denver, USA
H2B (Yeast)		M30930	Boster Biological Technology, Pleastanton, USA
H3K4me3		Ab8580	Abcam, Cambridge, UK
H3K27ac		Ab4729	Abcam, Cambridge, UK
H3K79me2		AB177184	Abcam, Cambridge, UK
IgG		PP64B	Merck Millipore, Burlington, USA
MLL/HRX (NT) (N4.4)		05-764	Upstate, Merck, Darmstadt, Germany
MLL1		A300-087A	Bethyl Laboratories, Montgomery, USA
ChIP-PCR			
DOT1L		A300-953A	Bethyl Laboratories, Montgomery, USA
H3K4me3		Ab8580	Abcam, Cambridge, UK
H3K27ac		Ab4729	Abcam, Cambridge, UK
H3K79me2		AB177184	Abcam, Cambridge, UK
IgG		PP64B	Merck Millipore, Burlington, USA
MLL1		A300-087A	Bethyl Laboratories, Montgomery, USA
FACS			
Cd3ε (145-2C11)	Brilliant Violet V605	100351	BioLegend, San Diego, USA
Cd11b (M1/70)	PE/Cyanine7	101215	BioLegend, San Diego, USA
Cd45	PerCP/Cyanine	103132	BioLegend, San Diego, USA

Cd45R (B220) (RA3-6B2)	Alexa Fluor 700	56-0452-82	eBioscience, Thermo Fisher Scientific, Langenselbold, Germany
Cd115 (c-fms) (AFS98)	APC	14-1152-85	eBioscience, Thermo Fisher Scientific, Langenselbold, Germany
Cd117 (cKIT) (2B8)	PE	105807	BioLegend, San Diego, USA
Ly6A/E (Sca1) (D7)	APC/Cyanine7	108125	BioLegend, San Diego, USA
Ly-6G/Ly-G6C (RB-8C5)	eFluor450	48-5931-82	Thermo Fisher Scientific, Langenselbold, Germany

Western blot

BCAT1 (ECA39)		611271	BD Transduction Laboratories; BD Bioscience, Mississauga, USA
Bcat1		232700	Abcam, Cambridge, UK
FLAG (M2)		FI1804	Sigma-Aldrich, Munich Germany
H3K4me3		Ab8580	Abcam, Cambridge, UK
H3K27ac		Ab4729	Abcam, Cambridge, UK
H3K79me2		AB177184	Abcam, Cambridge, UK
H3 total		Ab201456	Abcam, Cambridge, UK
IgG		02-06102	Invitrogen, Thermo Fisher Scientific, Langenselbold, Germany
MLL/HRX (NT) (N4.4)		05-764	Upstate, Merck, Darmstadt, Germany
MLL1		A300-087A	Bethyl Laboratories, Montgomery, USA
Mouse IgG	HRP	7076S	Cell Signaling Technology, Denver, USA
Mouse kappa light chain IgG	HRP	Ab99617	Abcam, Cambridge, UK
Rabbit IgG	HRP	7074S	Cell Signaling Technology, Denver, USA

3.1.4. Biological material and cell culture

3.1.4.1. Cells lines and E.coli strains

Table 4 - Bacterial strains, human, and murine cell lines used.

Cells	Distributor
E.coli	
DH5α Competent Cells	Life Technologies, Thermo Fisher Scientific, Langenselbold, Germany
One Shot TOP10 Chemically Competent E.coli	Life Technologies, Thermo Fisher Scientific, Langenselbold, Germany
One Shot ™ Stbl3 ™ Chemically Competent E. coli	Life Technologies, Thermo Fisher Scientific, Langenselbold, Germany
Human Cell Lines	
293FT	Provided by Vector Core Facility, DKFZ
HEK293T	Provided by Dr. Liliana Francois Martín Del Campo (Prof. Dr. P.Lichter, DKFZ)
HL-60	Provided by Dr. Niclas Kneisel (P. Lichter, DKFZ)
MOLM-13	Provided by Dr. Niclas Kneisel (P. Lichter, DKFZ)
Phoenix-GP	Provided by Dr. Nikolas Dietlein (H.-R. Rodewald, DKFZ)
THP1	Provided by Pavle Boskovic (P.Lichter, DKFZ)
Murine Cell Lines	
NIH/3T3	Provided by Pavle Boskovic (P.Lichter, DKFZ)

3.1.4.2. Primary mouse cells

Table 5 - Primary mouse cells produced.

Mouse Strain	Cell Type Isolated
Bcat1$^{-/-}$ (B6-Bcat1m1.2Eaa; Background: C57BL/6N (CD45.2)) -	Bone marrow, isolated and enriched for cKIT+ progenitor cells
Bcat1$^{+/+}$ = C57BL/6N (CD45.2)	Bone marrow, isolated and enriched for cKIT+ progenitor cells

3.1.4.3. Modified cells

Table 6 - Primary cells and cell lines modified for experiments

Name	Modification	
HL-60 *shBCAT1*	Tet-inducible shRNA Knockdown of BCAT1	
HL-60 *shNT*	Tet-inducible shRNA Knockdown of NT	
MOLM-13 *shBCAT1*	Tet-inducible shRNA Knockdown of BCAT1	
MOLM-13 *shNT*	Tet-inducible shRNA Knockdown of NT	
Bcat1$^{-/-}$	Murine cKIT^{pos} BKO + MLL-AF9 + EV.puro	pMSCV.neo Flag MLL-AF9, pMSCV PIG empty
Bcat1^{WT}	Murine cKIT^{pos} BKO + MLL-AF9 + Bcat1^{WT}	pMSCV.neo Flag MLL-AF9, pMSCV PIG mBcat1^{WT}
Bcat1^{SXXS}	Murine cKIT^{pos} BKO + MLL-AF9 + Bcat1^{SXXS}	pMSCV.neo Flag MLL-AF9, pMSCV PIG mBcat1^{SXXS}
Bcat1^{K222A}	Murine cKIT^{pos} BKO + MLL-AF9 + Bcat1^{K222A}	pMSCV.neo Flag MLL-AF9, pMSCV PIG mBcat1^{K222A}
Bcat1$^{+/+}$	Murine cKIT^{pos} BWT +MLL-AF9+ EV.puro	pMSCV.neo Flag MLL-AF9, pMSCV PIG empty

3.1.4.4. Mouse strains used

Table 7 - Mouse strains used in these experiments

Mouse Strain	Function
Bcat1$^{-/-}$ (B6-Bcat1m1.2Eaa; Background: C57BL/6N (CD45.2)) -	Donor of fetal liver cells
Bcat1$^{+/+}$= C57BL/6N (CD45.2)	Donor of fetal liver cells, syngraft recipient
Bcat1$^{+/+}$= C57BL/6-Ly5.1 (B6.SJL-Ptprc(a)Pepc(b)BoyJ (Cd45.1))	Syngraft recipient

3.1.4.5. Cell culture buffer and medium

Table 8 - General cell culture buffers and medium

Medium	Supplements added	Used for
Dulbecco's Modified Eagle's Medium (DMEM) high Glucose	10% FCS, 1x Pen/Strep, 0.5 mM L-Glutamine	NIH/3T3
Hematopoietic Stem Cell (HSC) Medium	40% DMEM, 40% IMDM, 20% FCS, 1x Pen/Strep (100 U/ml), 0.05 mM 2-Mercaptoethanol, 20 ng/ml SCF, 2 ng/ml IL-3, 2 ng/ml IL-6	Primary murine bone marrow cells, Primary murine fetal liver cells

Iscove's Modified Dulbecco's Medium (IMDM)	10% FCS, 1x Pen/Strep, 0.5 mM L-Glutamine	HEK293T
Fetal Liver dissociation buffer (FLDB)	2% FCS, 2.5 mM EDTA, 10 mM Glucose, in PBS	HSPCs Isloation
MethoCult GF M3534	Antibiotics (G418, Hygro, or Puro)	CFU
OptiMEM		Thermo Fischer Scientific, Langenselbold, Germany
Phoenix-GP Growth Medium	10% FCS, 1x Pen/Strep (100 U/ml), 1x GlutaMax, 10 mM HEPES, 1 mM NaOH	Phoenix-GP
RPMI-1640 high Glucose	10% FCS, 1% Pen/Strep, 0.5 mM L-Glutamine	THP1, MOLM-13
StemSpan SFEM	20 ng/ml SCF, 2 ng/ml IL-3, and 2 ng/ml IL-6	StemCell Technologies, Cologne, Germany

3.1.4.6. Cell culture material

Table 9 - Cell culture materials used.

Name	Distributor
3cc syringes	StemCell Technologies, Cologne, Germany
18G 1 ½ inch blunt end needle	BD biosciences, Heidelberg, Germany
35mm culture dishes	StemCell Technologies, Cologne, Germany
96 well plate white	Greiner Bio-One International, Kremsmünster, Austria
Calcium phosphate-Transfection Kit	Thermo Fisher Scientific, Langenselbold, Germany
Cell culture flasks and multi-well plates	Tritech Research, Los Angeles, USA
Chloroquine diphosphate salt	Merk, Darmstadt, Germany
Corning 60mm Gridded Scoring Dish	StemCell Technologies, Cologne, Germany
Dimethyl sulphoxide (DMSO)	Sigma-Aldrich, Munich, Germany
Einweg-Zählkammer C-Chip	Biochrom, Berlin, Germany
EasySep™ Mouse CD117 (cKIT) Positive Selection Kit	StemCell Technologies, Cologne, Germany
Fetal Calf serum (FCS)	Merck Millipore, Darmstadt, Germany
L-Glutamine (100x)	Thermo Fischer Scientific, Langenselbold, Germany
Penicillin/Streptomycin (10000 U/ml, 100 µg/ml)	Thermo Fischer Scientific, Langenselbold, Germany

Polyethylenimine	Polysciences Europe, Hirschenberg an der Bergstraße, Germany
Spinner flask	Weaton DWK LifeSciences, Wertheim, Germany
Tet System Approved FBS	Takara Bio Europe, Saint-Germain-en-Laye, France
TransIT®-LT1 Transfection Reagent	Mirus Bio, VWR, Madison, USA
Trypsin EDTA solution (0.5 %)	Sigma-Aldrich, Munich, Germany

3.1.5. Chemicals, kits, and reagents

Table 10 - General chemicals, kits, and reagents used.

Reagents	Distributor
16 % Formaldehyde solution (w/v), methanol-free	Pierce, Thermo Fisher Scientific, Rockford, USA
CellTiter-GloR	Promega, Madison, USA
Direct-zol RNA MicroPrep	Zymo Research Corporation, Irvine, USA
cOmplete™, Mini, EDTA-free Protease Inhibitor Cocktail	Sigma-Aldrich, Munich, Germany
EDTA (≥99 %)	Carl Roth, Karlsruhe, Germany
Ethanol (≥99.8%)	Sigma-Aldrich, Munich, Germany
Glycine	Sigma-Aldrich, Munich, Germany
Isopropanol (≥99.8%)	Sigma-Aldrich, Munich, Germany
Magnesium chloride, powder	Sigma-Aldrich, Munich, Germany
Methanol (≥99.8%)	Sigma-Aldrich, Munich, Germany
Maxwell RSC simplyRNA Cells kit	Promega, Madison, USA
SDS Pellets (≥99 %)	Carl Roth, Karlsruhe, Germany
Sodium chloride (≥99.5%)	Guangzhou Fischer Chemical Co., Ltd., Waltham, USA
Triton X-100 Solution	Sigma-Aldrich, Munich, Germany

3.1.6. ChIP-PCR

Table 11 - Materials and chemicals needed for ChIP-seq experiments

Material	
ChIP Elution Buffer	10 mM Tris (pH 8), 0.1 mM EDTA, 1% SDS
Covaris microTube (130µl)	Covaris Inc., Woburn, MA, US
Dynabeads™ Protein G for Immunoprecipitation	Thermo Fisher Scientific, Langenselbold, Germany
Farnham Lysis Buffer	5 mM HEPES (pH 8), 85 mM KCL, 0.5% NP-40

High Salt Wash Buffer	20 mM HEPES-KOH (pH 7.9), 200 mM NaCl, 2mM EDTA, 0.1% SDS, 1% Triton X-100
LiCl Wash Buffer.	100 mM Tris (pH 7.5), 0.5 mM LiCl, 1% NP-40, 1% Sodium deoxycholate
Low Salt Wash Buffer	20 mM HEPES-KOH (pH 7.9), 150 mM NaCl, 2mM EDTA, 0.1% SDS, 1% Triton X-100
Proteinase K (20mg/ml; 600 U/ml)	Thermo Fisher Scientific, Langenselbold, Germany
QIAquick PCR Purification	Qiagen, Hilden, Germany
RNase A (100 mg/ml)	Qiagen, Hilden, Germany
Shearing Buffer (low SDS buffer)	10 mM Tris (pH 8.1), 1 mM EDTA, 0.1% SDS
TE Buffer	10 mM Tris (pH 8), 0.1 mM EDTA
Wash Buffer	10 mM Tris (pH 8.1), 200 mM NaCl, 1 mM EDTA (pH 8), 0.5 mM EGTA (pH 8)

3.1.7. Cloning material

Table 12 - Material used for cloning

Material	Distributor
LB (Luria Bertani) medium	0.5 % (w/v) NaCl, 1 % (w/v) Tryptone, 0.5 % (w/v) Yeast extract
LB Agar	0.5 % (w/v) NaCl, 1 % (w/v) Tryptone, 0.5 % (w/v) Yeast extract, 1.6% (w/v) Agarose
PCR nucleotide mix	Roche Diagnostics, Mannheim, Germany
Precisor High-Fidelity DNA Polymerase	BioCat GmbH, Heidelberg, Germany
QIAGEN Plasmid Maxi Kit	Qiagen, Hilden, Germany
QIAGEN Plasmid Mini Kit	Qiagen, Hilden, Germany
QIAquick Gel Extractions Kit	Qiagen, Hilden, Germany
Quick Ligation Kit	New England Biolabs, Massachusetts, United States
QuickChange II XL site-directed mutagenesis kit	Agilent, Waldbronn, Germany
QuikChange Lightning Site-directed mutagenesis Kit	Agilent, Waldbronn, Germany
T4 DNA Ligase	New England Biolabs, Massachusetts, United States
BamHI	Thermo Fischer Scientific, Langenselbold, Germany
XhoI	Thermo Fischer Scientific, Langenselbold, Germany

3.1.8. Equipment

Table 13 - Equipment used in experiments.

Equipment	Company
Agarose gel electrophoresis	Biozym, Hamburg, Germany
Airfuge ultracentrifuge	Beckman Coulter GmbH, Krefeld, Germany
BD FACSCanto™ II	BD biosciences, Heidelberg, Germany
BD LSRFortessa™	BD biosciences, Heidelberg, Germany
Bioanalyser	Agilent, Waldbronn, Germany
Cell Observer	Carl Zeiss, Oberkochen, Germany
CO2 incubator ThermoForma	Thermo Fischer Scientific, Langenselbold, Germany
ECL Chemostar	INTAS Science Imaging Instruments GmbH, Göttingen, Germany
GloMax® Discover	Promega, Madison, USA
Heraeus Biofuge fresco	Thermo Fischer Scientific, Langenselbold, Germany
LightCycler480	Hoffmann-La Roche, Basel, Switzerland
Mastercycler epGradient S	Eppendorf, Hamburg, Germany
Mithras LB 940 plate reader	Berthold Technologies, Bad Wilbad, Germany
NanoDrop® ND-2000C spectrometer	NanoDrop, Wilmington, USA
QuantStudio 5 Real-Time PCR System	Thermo Fischer Scientific, Langenselbold, Germany
Qubit™	Thermo Fischer Scientific, Langenselbold, Germany
Shaker DRS-12	neoLab Migge GmbH
Sterile bench HERA safe	Thermo Scientific, Langenselbold, Germany
TapeStation 4150	Agilent, Waldbronn, Germany
Thermal cycler PTC-200	MJ resear, BioRad, Hercules, USA
Vi-CELL XR 2.03	Beckman Coulter GmbH, Krefeld, Germany
Zeiss Axio Vert.A1	Carl Zeiss, Germany

3.1.9. Primers

Table 14 - Primers used for ACT-seq, ChIP PCR, and qPCR.

Name	Sequence
ACT-seq	
Complementary oligo: Tn5MErev*	5'-[phos]CTGTCTCTTATACACATCT-3'
Top oligo 1 Tn5ME-A*	5'-TCGTCGGCAGCGTCAGATGTGTATAAGAGACAG-3'
Top oligo 2 Tn5ME-B*	5'-GTCTCGTGGGCTCGGAGATGTGTATAAGAGACAG-3’
Tn5mCP1n*	5'-AATGATACGGCGACCACCGAGATCTACACTCGTCGGCAGCGTC-3’

Tn5mCBar_n1*	5'-CAAGCAGAAGACGGCATACGAGATGGATGTTCTGTCTCGTGGGCTCGG-3'
Tn5mCBar_n2*	5'-CAAGCAGAAGACGGCATACGAGATCTTATCCAGGTCTCGTGGGCTCGG-3'
Tn5mCBar_n3*	5'-CAAGCAGAAGACGGCATACGAGATGTAAGTCACGTCTCGTGGGCTCGG-3'
Tn5mCBar_n4*	5'-CAAGCAGAAGACGGCATACGAGATTTCAGTGAGGTCTCGTGGGCTCGG-3'
Tn5mCBar_n5*	5'-CAAGCAGAAGACGGCATACGAGATCTCGTAATGGTCTCGTGGGCTCGG-3'
Tn5mCBar_n6*	5'-CAAGCAGAAGACGGCATACGAGATCATGTCTCAGTCTCGTGGGCTCGG-3'
Tn5mCBar_n7*	5'-CAAGCAGAAGACGGCATACGAGATAATCGTGGAGTCTCGTGGGCTCGG-3'
Tn5mCBar_n8*	5'-CAAGCAGAAGACGGCATACGAGATGTATCAGTCGTCTCGTGGGCTCGG-3'
Tn5mCBar9*	5'-CAAGCAGAAGACGGCATACGAGATTCGCCTTAGTCTCGTGGGCTCGG-3'
Tn5mCBar10*	5'-CAAGCAGAAGACGGCATACGAGATCTAGTACGGTCTCGTGGGCTCGG-3'
Tn5mCBar11*	5'-CAAGCAGAAGACGGCATACGAGATTTCTGCCTGTCTCGTGGGCTCGG-3'
Tn5mCBar12*	5'-CAAGCAGAAGACGGCATACGAGATGCTCAGGAGTCTCGTGGGCTCGG-3'
Tn5mCBar13*	5'-CAAGCAGAAGACGGCATACGAGATAGGAGTCCGTCTCGTGGGCTCGG-3'
Tn5mCBar14*	5'-CAAGCAGAAGACGGCATACGAGATCATGCCTAGTCTCGTGGGCTCGG-3'
Tn5mCBar15*	5'-CAAGCAGAAGACGGCATACGAGATGTAGAGAGGTCTCGTGGGCTCGG-3'
Tn5mCBar16*	5'-CAAGCAGAAGACGGCATACGAGATCCTCTCTGGTCTCGTGGGCTCGG-3'
Tn5mCBar17*	5'-CAAGCAGAAGACGGCATACGAGATAGCGTAGCGTCTCGTGGGCTCGG-3'
Tn5mCBar18*	5'-CAAGCAGAAGACGGCATACGAGATCAGCCTCGGTCTCGTGGGCTCGG-3'
Tn5mCBar19*	5'-CAAGCAGAAGACGGCATACGAGATTGCCTCTTGTCTCGTGGGCTCGG-3'
Tn5mCBar20*	5'-CAAGCAGAAGACGGCATACGAGATTCCTCTACGTCTCGTGGGCTCGG-3'

ChIP-PCR

BCAT1_A_Fw**	5'-ATGGGGCAAGAACTCAGGAA-3'
BCAT1_A_Rev**	5'-CCTCTCCCTCAATGCAGGAT-3'
BCAT1_B_Fw**	5'-CAGGAGCCAGTGATGACGGA-3'
BCAT1_B_Rev**	5'-AGAGGTGCCAGTGTTGCAAGC-3'
BCAT1_C_Fw**	5'-TGTACTCTTGAGCCCAGTGG-3'
BCAT1_C_Rev**	5'-TCCCCAGTTCCACCTTTCCAGG-3'
BCAT1_D_Fw**	5'-GAAGAGGTGAGTGGTGGGCCAT-3'
BCAT1_D_Rev**	5'-TGAGCTGACAAGAGGTGGAGTTC-3'
BCAT1_E_Fw**	5'-TGGGCTTTGATTCTTTTCCAAAA-3'
BCAT1_E_Rev**	5'-AGATCACCAATTAAAAGCCCCC-3'

HOXA9_ex1_Fw	5'-CTCCGATGGCTGTGACAATG-3’
HOXA9_ex1_Rev	5'-GAGAGAGGAGAGGATGTGCC-3’
HOXA9_ex2_Fw	5'-GCGGTGCCCCTATACAAAAC-3’
HOXA9_ex2_rev	5'-ACCAGATCTTGACCTGCCTC-3’
MEIS1_ex1_Fw	5'-GCAAAGAGGGAGAGAGAGGG-3’
MEIS1_ex1_Rev	5'-TCCGCTCTGTCTTCTTCTGG-3’
MEIS1_ex2_Fw	5'-GGCATGGATGGAGTAGGCAT-3’
MEIS1_ex2_Rev	5'-CATGGCGTTGGTATGAGCTG-3’
TBP_Fw (neg. control)**	5'-CAGTTCTGGGAAAATGGTGTG-3’
TBP_Rev (neg. control)**	5'-GCATATTTTCTTGCTGCCAGTC-3’

qPCR

ARF Fwd (Housekeeper)	5'-ATGGGGAACATCTTCGCCAAC-3’
ARF Rev (Housekeeper)	5’- GTGGTCACGATCTCACCCAG-3’
DCTN2 Fwd (Housekeeper)	5’- ATGGCGGACCCTAAATACGC-3’
DCTN2 Rev (Housekeeper)	5’- TCAGGTAGGTCGCTAGTTTCATA-3’
DOT1L Fwd (TS_94)	5’- AATCCCGGATCTCAAGCTCG-3’
DOT1L Rev (TS_95)	5’- AATCCCGGATCTCAAGCTCG-3’
MLL-AF9 Fwd (TS_110)	5’-CCGCCCAAGTATCCCTGTAA-3’
MLL-AF9 Rev (TS_107)	5’-CTGGCAGGACTGGGTTGTT-3’
HOXA9 Fwd (TS_96)	5'-TACGTGGACTCGTTCCTGCT-3’
HOXA9 Rev (TS_97)	5'-CGTCGCCTTGGACTGGAAG-3’
MEIS1 Fwd (TS_100)	5'-GGGCATGGATGGAGTAGGC-3’
MEIS1 Rev (TS_101)	5'-GGGTACTGATGCGAGTGCAG-3’
MYC Fwd (TS_98)	5'-TCCCTCCACTCGGAAGGAC-3’
MYC Rev (TS_99)	5'-CTGCGTAGTTGTGCTGATGT-3’
TBP Fwd (Housekeeper)	5'-CCACTCACAGACTCTCACAAC-3’
TBP Rev (Housekeeper)	5'-CTGCGGTACAATCCCAGAACT-3’
Dot1l Fwd (TS_78)	5'-GAGGCTCAAGTCGCCTGTG-3’
Dot1l Rev (TS_79)	5'-GACCCACCGGATAGTCTCAAT-3’
Gapdh Fwd (Housekeeper)	5'-AGGTCGGTGTGAACGGATTTG-3’
Gapdh Rev (Housekeeper)	5'-GGGGTCGTTGATGGCAACA-3’
HoxA9 Fwd (TS_80)	5'-CCCCGACTTCAGTCCTTGC-3’
HoxA9 Rev (TS_81)	5'-GATGCACGTAGGGGTGGTG-3’
Meis1 Fwd (TS_84)	5'-GCCCATGATAGACCAGTCCAA-3’
Meis1 Rev (TS_85)	5'-ACCGTCCATTACAAAACCTCC-3’
Myc Fwd (TS_82)	5'-CCCTATTTCATCTGCGACGAG-3’
Myc r Rev (TS_83)	5'-GAGAAGGACGTAGCGACCG-3’

* Provided by Dierter Weichenhan (C. Plass, DKFZ)

** (Oktyabri et al., 2016)

3.1.10. Protein preparation material

Table 15 - Chemicals and materials used for western blot analysis.

Material	Company
1x Transfer buffer	25 mM Tris, 200 mM glycine, 20 % methanol, pH 8.8
1x TRIS buffered saline (TBS)	150 mM NaCl, 10 mM Tris, pH 7.5
1x TBS-T	TBS 1X, 1:1000 (v/v) Tween 20
20xMOPS buffer	Life Technologies, Darmstadt, Germany
20xMES buffer	Life Technologies, Darmstadt, Germany
Blocking buffer (WB)	5% milk or albumin in TBS-0.1% Tween20
cOmplete Mini, Edta free	Sigma-Aldrich, Munich Germany
GelCode Blue Stain Reagent	Thermo Fischer Scientific, Langenselbold, Germany
Immobilion-P Transfer Membrane	Merck Millipore, Darmstadt, Germany
NuPAGE 4xLDS sample buffer	Life Technologies, Darmstadt, Germany
NuPAGE 4-12% Bis-Tris Protein Gels, 1.0 mm, 12well/15well	Life Technologies, Darmstadt, Germany
NuPAGE 4-12% Bis-Tris Protein Gels, 1.5 mm, 15well	Life Technologies, Darmstadt, Germany
NuPage Novex 12% Bis-Tris Protein Gels, 1.0 mm, 15 well	Life Technologies, Darmstadt, Germany
NuPAGE Sample Reducing Agent (10X)-10 ml	Life Technologies GmbH
Pierce ECL Western Blotting Substrate	Thermo Fischer Scientific, Langenselbold, Germany
Pierce BCA Protein Assay	Thermo Fischer Scientific, Langenselbold, Germany
Pierce® IP Lysis Buffer	Thermo Fischer Scientific, Langenselbold, Germany
RIPA Buffer	Sigma-Aldrich, Munich Germany

3.1.11. Plasmids

Table 16 - Plasmids used in the following experiments and their origin.

Name	Provider
Commercial Plasmids	
pMIG MLL-AF9 (#71443)	Addgene, Cambridge, USA
pMSCV-FlagMLL-pl-ENL (#20873)	Addgene, Cambridge, USA
pMSCV PIG empty (#21654)	Addgene, Cambridge, USA

Generated Plasmids	
pMSCV.neo Flag MLL-AF9	Based on pMIG MLL-AF9 and pMSCV.neo Flag empty
pMSCV PIG mBcat1^{WT}	Based on pMSCV PIG empty and pLVX HygR mBcat1
pMSCV PIG mBcat1^{SXXS}	Based on pMSCV PIG empty and pLVX HygR mBcat1
pMSCV PIG mBcat1^{K222A}	Based on pMSCV PIG empty and pLVX HygR mBcat1
Provided Plasmids	
K73	Provided by Dr. Nikolas Dietlein (Prof. Dr. H.-R. Rodewald, DKFZ)
M57DAW	Provided by Dr. Nikolas Dietlein (Prof. Dr. H.-R. Rodewald, DKFZ)
pLVX HygR mBcat1	Provided by Pavle Boskovic (Prof. Dr. P.Lichter, DKFZ)
pLentiCRISPRv2 BCAT1 E3g1-sgRNA (clone 4)	Provided by Dr. Liliana Francois Martín Del Campo (Prof. Dr. P.Lichter, DKFZ)
pLentiCRISPRv2 NT-sgRNA	Provided by Dr. Liliana Francois Martín Del Campo (Prof. Dr. P.Lichter, DKFZ)
pMSCV.neo Flag empty	Provided by Prof. Dr. C. Scholl, DKFZ

3.1.12. Software

Table 17 - Software used for experimental setup, measurements, and analysis.

Software	Version	Distributor
Basic Local Alignment Search Tool (BLAST)		NCBI, Bethesda, USA
Fiji, ImageJ	1.52p	ImageJ, NIH, Bethesda, USA
Flowjo	V10	Flowjo, LLC, Ashland, USA
GraphPad Prism	6.01	GraphPad, San Diego, USA
Ingenuity Pathway Analysis (IPA)		QIAGEN, Hilden, Germany
Leica LAS-X Life Science		Leica Mycrosystems, Wetzlar, Germany
Mendeley	1.19.4	Mendeley Ltd., London, UK
Microsoft Office 365		Microsoft Corporation, Redmond, USA
QuantStudio Design & Analysis Software		Thermo Fischer Scientific, Langenselbold, Germany
UCSF Chimera	1.12rc	The Regents of the University of California, California, USA
SnapGene View		GDL Biotech LLC, San Diego, USA
R		
ChIPseeker	1.28.3	Bioconductor; (G. Yu et al., 2015)

clusterProfiler	4.0.5	Bioconductor; (G. Yu et al., 2012)
DiffBind	3.2.6	Bioconductor; (Ross-Innes et al., 2012)
edgeR	3.34.1	Bioconductor; (McCarthy et al., 2012; Robinson et al., 2010)
R	4.0.1	Free Software Foundation, GNU project
R	4.1.0	Free Software Foundation, GNU project
R Studio	1.4.1717	RStudio, PBC

3.2. Methods

3.2.1. ACT-seq

3.2.1.1. Sample preparation

In brief, antibody-guided chromatin tagmentation (ACT) combined with sequencing (seq) enables efficient mapping of histone modifications and chromatin-binding proteins in samples with low cell numbers. The Tn5 transposase – Protein A fusion (pATnP) is guided towards chromatin modifications by an associated antibody, leading to the insertion of sequence tags at the site of the bound fusion (Carter et al., 2019). These labeled fragments are amplified by real-time PCR and sequenced.

Based on Carter et al., 2019, my collaborator, Dieter Weichenhan, established and modified ACT-seq in the laboratories of Christoph Plass, DKFZ. I performed the assay as follows.

The purified fusion protein pATnP was generated from the expression vector pET15bpATnp, and its activity was empirically tested by Dieter Weichenhan. 50 µM Tn5ME-A and Tn5ME-B were annealed with the adapter-primer Tn5MErev by a slow cooling renaturation process in a PCR cycler. The adapter was bound to pATnP during a 10min incubation at room temperature. This loaded pATnpOme complex was linked to the antibody of interest by incubating 1 µl pATnpOme with 0.8 µl antibody of interest for 30min at room temperature, forming the pATnpOme-Ab complex.

Table 18 – Specifications for antibodies used in ACT-seq experiment

ACT-seq target	Cat. No.	Species	Concentration	Amount of Ab	Cells used for target Ab
DYKDDDK (Flag)	14793S	Rabbit		0.8 ug	2 x 10^5
H2B (Yeast)	M30930				
H3K4me3	Ab8580	Rabbit	1 mg/ml	0.8 ug	0.5 x 10^5
H3K27ac	Ab4729	Rabbit	1 mg/ml	0.8 ug	0.5 x 10^5
H3K79me2	Ab177184	Rabbit	0.38 mg/ml	0.8 ug	2 x 10^5
IgG	02-6102	Rabbit	5 mg/ml	0.8 ug	2 x 10^5
Total cell number per condition					7 x 10^5

In addition to the targets of interest listed in Table 18, I used antibodies against IgG as control and H2B (yeast) as spike-in.

About 100,000 cells were permeabilized with 25 µl 1x Complex Formation Buffer (CB) for 10min on ice for each investigated histone modification. Respectively, per transcription factor target, 200,000 cells were lysed in 50 µl CB. The cells were permeabilized in bulk and aliquoted. Before the targeting reaction, 25 µl 1xCB was added to all histone aliquots to reach a final volume of 50 µl in each sample. H3K79me2 is less abundant than other histone modifications and was treated as a transcription factor rather than a histone modification in all following steps. In parallel to the cell lysis, about 100,000 yeast spheroplasts were permeabilized in 50 µl 1x CB and later used as spike-in.

To target the chromatin modifications, I added 50 µl of lysed cells to the pATnpOme-Ab solution. Then, respectively, permeabilized yeast nuclei were added to the pATnpOme-H2B antibody complex.

After 60min incubation at room temperature, 2 µl of yeast nuclei-pATnpOme-H2B was added to each permeabilized cell-pATnpOme-Ab reaction. Before continuing, I performed multiple washing steps, using the wash buffer described in Table 1.

The transposition reaction was initiated by adding 1 µl of 1 M $MgCl_2$. The tagmentation proceeded for 60min at 37°C, until it was stopped by 4 µl 0.5M EDTA (pH 8), 2 µl 10% SDS, and 1 µl proteinase K (20 mg/ml stock). The reaction was further incubated for 60min at 55°C.

Afterward, DNA was purified using MinElute columns according to standard protocol. The final elution was performed with 2*10 µl 55°C-warmed EB buffer.

3.2.1.2. Library preparation and sequencing

The sequencing library was prepared by real-time PCR in a 50 µl reaction volume using the complete DNA eluted in the previous step. NEBNext Fidelity 2x Mastermix, 100x SYBRGreen, Tn5mCP1n Primer, and barcode primer were used for the reaction. After 5min at 72°C for gap repair, initial melting occurred at 98°C for 10sec. Each cycle consisted of 10sec denaturation at 98°C, 10sec annealing at 63°C, and 10sec elongation at 72°C. The reaction was stopped after a minimum difference of 5 FU was reached between the lowest and final FU. This difference was usually achieved at cycles 12-18 for histone modification and cycles 16-22 for transcription factors and IgG.

After amplification, I conducted single-phase AmPure XP bead purification. All fragment sizes were recovered for transcription factors and IgG, while a biphasic AmPure XP bead purification was performed for histone modifications. In biphasic purification, particular short fragments, typical for most histone modifications, were recovered.

For the single-phase purification, 10 µl beads were diluted with 60 µl AmPure Buffer and mixed with 50 µl PCR product (1.4:1 ratio). After DNA fragments were bound to paramagnetic beads, a magnet was used to separate beads and contaminants. Next, I washed the beads twice with 70% ethanol before the supernatant was removed entirely and beads were slightly dried. Finally, 12 µl EB was used to eluate DNA from beads.

In the biphasic purification, long fragments were bound to AmPure beads by diluting 10 µl beads with 30 µl AmPure buffer and adding 50 µl PCR reaction (0.8:1 ratio). After the large fragments were bound, beads were collected with a magnet, and the supernatant was transferred to a new 200 µl tube. This supernatant was further purified by adding 10 µl AmPure XP beads diluted with 20 µl AmPure buffer (1.4:1 ratio). Both purifications were washed twice with 70% ethanol. Then, ethanol was removed, and beads were slightly dried. Finally, I eluted the DNA in 12 µl EB.

The concentrations of all eluates were measured by Qubit, and fragments size was determined with Bioanalyzer or TapeStation.

Libraries were multiplexed, with up to 6 samples for common targets such as histone marks and up to 9-plex for periodic modifications or TFs such as transcription factors and the IgG control. This multiplexing resulted in pooled libraries of approximately 10 nM genomic DNA in a final volume of 30 µl.

Sequencing was performed by the DKFZ Genomics and Proteomics core facility using the ACT-seq application with NextSeq 550 Mid Output (104 M reads) Illumina sequencer and NextSeq 550 Paired-End 75bp Mid-Output.

3.2.1.3. ACT-seq data analysis

The data analysis was conducted in collaboration with Kersten Breuer and Pavlo Lutsik, DKFZ. First, alignments and quality controls were performed as shown in the CW workflow in Figure 10 (*Workflow: ACTseq_spike_in.cwl*, 2021). Within this analysis, the normalization was conducted with the yeast spike-in. Next, the Galaxy server (DKFZ) was used for peak calling (MACS2), and further research was performed with ChIPseeker and DiffBind.

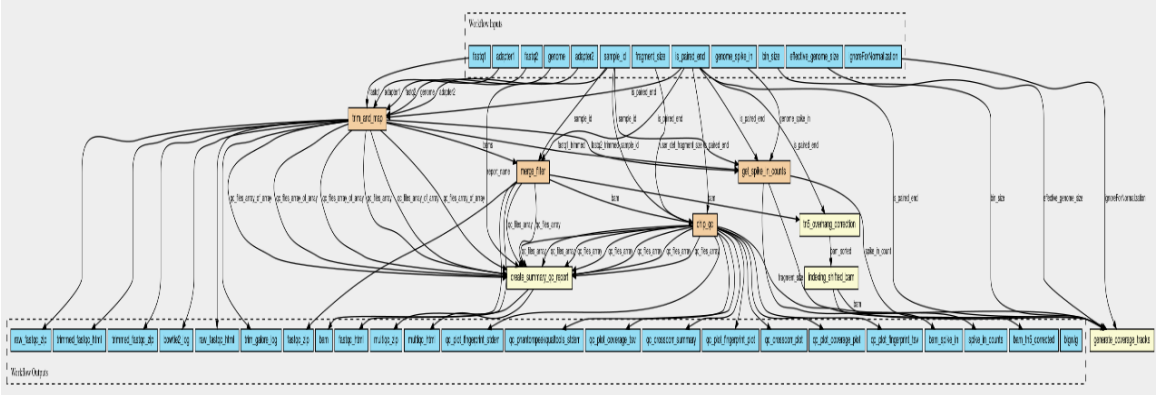

Figure 10 - Graphical representation of workflow: ACTseq_spike_in.cwl;

3.2.2. AML-Syngraft model

For this AML model, fetal liver cells of Bcat1$^{+/+}$ and Bcat1$^{-/-}$ mice were isolated, transfected with MLL-AF9, and transplanted in irradiated mice (animal number G-175/20).

3.2.2.1. Preparation of pre-tumor cells

Pregnant Bcat1$^{+/+}$ and Bcat1$^{-/-}$ mice (E11.5-E13.5) were euthanized with CO_2 or cervical dislocations. The abdomen and peritoneum were opened, which reveals the uterus with separate embryos. The uterus was isolated by introducing cuts on both uterine horns and the blood vessel connecting the uterus to the vagina. The uterus was carefully placed into ice-cold PBS and transferred into sterile conditions.

Individual fetuses were isolated by removing the uterine wall and peeling the yolk sac. Each fetus was placed in a well of a 6-well plate containing ice-cold fetal liver dissociation buffer (FLDB, Table 8). The red liver was visible in the pale fetus enabling careful removal of the connective tissue in a sterile hood. The fetal liver was mechanically dissociated using a P1000 pipette, and erythrocytes were lysed with Ammonium-Chloride-Potassium (ACK) buffer for 1 min at room temperature. Fetal liver cells were washed with PBS +2% FCS and homogenized before filtering them through a 70 µM strainer. Cells were resuspended in HSC-medium and incubated for 48 h at 37°C and 5% CO_2, enriching hematopoietic stem and progenitor cells (HSPCs).

After 48h, I collected and counted HSPCs. Spinfection with pMIG MLL-AF9 was used to increase the transduction efficiency of HSPCs. The retrovirus pMIG MLL-AF9 was

produced as described below (*3.2.10 Retrovirus production*). The protocol for spinfection is detailed in *3.2.11 Spinfection*.

After integrating the construct and recovering for 48 h, cells were collected and sorted for transduced cells (GFP^+). GFP^+ HSPCs were washed twice with PBS before $Bcat1^{+/+,}$ and $Bcat1^{-/-}$ HSPCs were adjusted to the same concentration. The transduced HSPCs which were not needed for transplantation were used to verify high cell viability. Samples were additionally tested for contaminations before transplantation.

3.2.2.2. Irradiation and transplantation

Lethal and sublethal irradiation protocols were tested with C57BL/6-Ly5.1 (Cd45.1) as well as C57BL/6N (CD45.2). All mice were irradiated by Barrier D (DKFZ) members, and antibiotic follow-up treatment was performed by caretakers of the mouse facility ATV1.108, DKFZ, following the SOP guidelines “08_ Bestrahlung von Versuchsnagern”. In brief, 24 recipient mice (7 weeks old, SOPF) were ordered from Janvier Labs, and bone marrow was irradicated or reduced by irradiation (137Caesium) after a week of recovery. Lethal whole-body irradiation was conducted by applying two doses of 500 cGy with a break of approximately 4 h in between to minimize morbidity and mortality of the treatment. Sublethal whole-body irradiation was performed with a single treatment of 550 cGy. Mice were allowed to recover for approximately 4 h before transduced pre-tumor cells and reconstitution cells were transplanted.

Per mouse, 0.2 µl PBS containing 3500 transduced HSPCs ($Bcat1^{+/+}$ or $Bcat1^{-/-}$ background) and $1*10^6$ HSPCs ($Bcat1^{+/+}$) for bone marrow reconstitution were transplanted via tail vein injection.

For the following 3 weeks, mice were treated with broad-spectrum antibiotics (Cotrim K Ratiopharm Saft, 90-100 mg/kg), and the state of health was examined at least twice a day. Additionally, I weighed the animals regularly to monitor weight loss.

3.2.2.3. Tumor load and survival

Blood was collected at regular intervals via the vena facialis to track tumor development and tumor load. Whole blood samples were collected in EDTA-coated tubes, and 25 µl whole blood were lysed with ACK buffer for 5 min. After washing twice with PBS, each sample was constituted with FACS counting beads (eBioScience). GFP^+ tumor cells were measured on BD FACS Canto.

Mice were euthanized as soon as termination criteria were reached, including but not limited to blood or weight loss, overall health, and tumor load per µl.

3.2.3. Bone marrow harvest and isolation (Murine)

Mice were sacrificed by CO_2 asphyxiation, and I harvested femurs as well as tibias. The isolated bones were placed in ice-cold PBS supplemented with 2% FCS on ice. The ends of each bone were cut, and the bone was carefully flushed with about 10 ml ice-cold PBS containing 2% FCS. A 10cc syringe was used with a 25G needle for the femur and a 23G needle for the tibia. Cells were homogenized by passing through the 23G needle 2-3 times and centrifuged at 1500 rpm for 5 min at 4°C. Cells were resuspended in cold ACK lysing buffer to remove all red blood cells. After approximately 1 min at room temperature, 4 ml PBS +2% FCS was added, and cell solution was passed through a 70 µm cell restrainer. Cells were centrifuged, and the pellet was resuspended in 5 ml PBS +2% FCS. After an additional wash step, cells were diluted to $6*10^7$ cells/ml for FACS stainings or $1*10^8$ cells/ml for hematopoietic progenitor enrichment via the EasySep system. Cells kept in culture were diluted to 3*106 cells/ml in HSC Medium or StemSpan medium supplemented with 20 ng/ml SCF, 2 ng/ml IL-3, and 2 ng/ml IL-6. Both media were favoring a hematopoietic stem and progenitor growth.

3.2.4. ChIP-PCR

The human AML cell lines MOLM-13 *shNT* and *shBCAT1*, as well as HL-60 *shNT* and *shBCAT1*, were seeded at a suspension of $0.5*10^6$ cells/ml. A 96h treatment of doxycycline was used to activate *BCAT1* knockdown (*shBCAT1#2*) and a non-targeted control (*shNT*) through short hairpin RNAs previously established (Raffel et al., 2017; Thewes et al., 2017; Tönjes et al., 2013). I verified the successful knockdown by qPCR and western blot.

For ChIP, DNA was cross-linked in 1 % methanol-free formaldehyde solution for 10min at room temperature. The reaction was quenched with 0.125M glycine for 5min. Subsequently, cells were lysed on ice using Farnham Lysis Buffer for 10min, and the remaining nuclei pellet was washed multiple times with wash buffer as well as a shearing buffer to remove high salt concentrations.

A nuclei pellet of approximately $1*10^7$ cells was diluted in 130 µl shearing buffer, and chromatin was sheared using the settings described in Table 19 with a Covaris S220 Focused-ultrasonicator.

Table 19 - Cell line-specific settings for chromatin shearing with Covaris S220 Focused-ultrasonicator

	MOLM-13	HL-60
Time	4 min	4 min
Duty cycle	5%	5%
Intensity	4	4
Cycle per Burst	200	200
Power mode Frequency	Sweeping	Sweeping
Degassing Mode	Continuous	Continuous
AFA intensifier	No intensifier	No intensifier
Water level	(S2 sonicator)	(S2 sonicator)
Bath Temperature Limit	7	7

I added 1% Triton-X-100 and 150 mM NaCl to sheared and cross-linked DNA before taking an aliquot as input control.

For immunoprecipitation, target antibodies or IgG from the same species were added to sheared and cross-linked DNA and incubated overnight at 4°C. The amount of antibodies and cells number used is listed in Table 20.

Table 20 - Specifications for antibodies and immunoprecipitation used in this ChIP PCR experiment

ChIP Target	Cat. No.	Species	Concentration	Amount of Ab	Cells used Ab	Dynabeads ™ Protein G used
H3K4me3	Ab8580	Rabbit	1 mg/ml	2.5 µg [6]	$5*10^6$	25 µl
H3K27ac	Ab4729	Rabbit	1 mg/ml	2.5 µg	$5*10^6$	25 µl
H3K79me2	Ab177184	Rabbit	0.38 mg/ml	3.8 µg	$10*10^6$	40 µl
DOT1L	A300955A	Rabbit	1 mg/ml	5 µg	$10*10^6$	50 µl
MLL	A300-085	Rabbit		10µl	$10*10^6$	40 µl
IgG	02-6102	Rabbit	5 mg/ml	10 µg	$10*10^6$	50 µl
Total cell number per cell line					$50*10^6$	

Dynabeads™ Protein G for immunoprecipitation were added to each sample in the lowest possible concentration, as shown in the table above. After 1.5h incubation at 4°C, the bound fragments were washed multiple times with low salt wash buffer, high salt wash

buffer, LiCl wash buffer, and TE. Next, DNA was eluted by adding 200 µl ChIP Elution Buffer and shaking the immunoprecipitation at 65°C for 30min.

Cross-linking was reversed by incubating the samples overnight at 65°C with 0.2 M NaCl and 1 µl RNase A (100 mg/ml). 2 µl Proteinase K was added and incubated at 50°C for 2h. DNA samples were purified with QIAquick PCR purification columns following the manufacturer's protocol.

Primer for *BCAT1*, *HOXA9*, and *MEIS1* (as listed in Table 14) were used for qPCR with 5 ng purified DNA per reaction. Results were normalized to the input and IgG sample. *TBP* primer were used as a negative control.

3.2.5. Cell culture

HEK293, HEK293T, and NIH 3T3 were cultured in DMEM high glucose with 10% FCS, 1x penicillin-streptomycin (Pen/strep), and 0.5 mM L-glutamine. The retrovirus-producer cell line Phoenix-GP was cultured in DMEM supplemented with 10% FCS, 1x Pen/Strep (100 U/ml), 1x GlutaMax, 10 mM HEPES, and 1 mM NaOH. THP1, MOLM-13, and HL-60 were cultured in RPMI-1640 supplemented with 10% FCS, 1x penicillin-streptomycin (Pen/strep), and 0.5 mM L-glutamine. The cell lines modified with a Tet-ON shRNA knockdown system, such as MOLM-13 *shNT* and *shBCAT1*, were cultured in the same medium composition, except Tet-free FCS was used.

Primary murine bone marrow cells as well as fetal liver cells were cultured in supplemented StemSpan or HSC Medium, consisting of 40% DMEM, 40% IMDM, 20% FCS, 1x Pen/Strep (100 U/ml), 0.05 mM 2-Mercaptoethanol, 20 ng/ml SCF, 2 ng/ml IL-3, and 2 ng/ml IL-6.

Cell lines were maintained in an incubator at 37°C and 5% CO_2

3.2.6. Colony formation unit assays

Methylcellulose MethoCult GF M3534 was slowly thawed overnight at 4°C and warmed to 37°C before aliquoting 3 ml using a sterile 3cc syringe with a G18 blunt end needle. Aliquots were frozen at -20°C and thawed only once, as MethoCult GF M3534 contains cytokines.

I diluted cells to $1.5*10^5$ cells/ml and added 200 µl of this cell suspension to one pre-warmed 3 ml methylcellulose aliquot. Antibiotics such as Pen/Strep, G418 (0.25 µg/µl),

and Puromycine (0.25 µg/ml) were added in a final volume of 100 µl to each methylcellulose aliquot. The cell methylcellulose mix was vortexed for 20sec and placed into the water bath for 5min until all bubbles were settled.

I transferred 1.1 ml cell methylcellulose mix into a 35 mm cell culture dish using a sterile 3cc syringe with a G18 blunt end needle and equally distributed it within the plate. Each cell condition was seeded in duplicates. The 35 mm cell culture dishes were placed into a 15 cm cell culture dish containing two 35 mm cell culture dishes and one 50 mm cell culture dish filled with sterile PBS to form a humidified chamber. This chamber was placed in a 37°C incubator with 5% CO_2 for 7 days.

After 7 days, colony number and colony types were determined manually using a gridded dish and the Zeiss Axio Vert.A1. Additionally, the cells were documented using the automated tile scanning function of the Cell Observer (2.5x Objective), and the recorded images were stitched.

On the following day, cells were re-plated. 1 ml pre-warmed medium was added to each 35 mm cell culture dish and placed in the incubator for several minutes to soften methylcellulose. I dissolved the methylcellulose by carefully pipetting up and down with 1 ml pipette. The dishes were washed three times with medium to collect all cells. The duplicates of the same cell type were combined, and cells were washed twice with medium before counting them.

Cells were diluted as previously described, and $3*10^4$ cells and antibiotics were added to 3 ml methylcellulose. The cells were seeded and placed in the humidified chamber before incubating for 7 days, as described above.

Colonies were counted every 7 days and re-plated every 8 days for about 4 to 8 re-platings.

Cells not used for re-plating were stained and analyzed via FACS. Cell lines were established after the 3rd plating with cells not needed for re-platings.

3.2.7. Dose-response and killing curves using CellTiter Glo

Dose-response curve analyses were conducted with MOLM-13 *shNT* and *shBCAT1* as well as HL-60 *shNT* and *shBCAT1* to verify IC_{50} values of DOT1L inhibitor EPZ5676 and EPZ04777. Furthermore, a killing curve analysis was performed to optimize the selection of HSPCs after spinfection.

I seeded the cells in a 96 well white clear-bottom plate with a density ideal for logarithmic growth of the investigated cells. Therefore, $0.5*10^6$ cells/ml were used for HL-60, and

correspondingly $1*10^6$ cells/ml for MOLM-13. For the slow-growing HSPCs, $2*10^6$ cells/ml were seeded.

A dilution series ranging from 0 to 10 µM EPZ5676 or EPZ04777 was prepared for the dose-response curve with the solvent DMSO. New inhibitors and medium were added every 2-3 days, and cell activity was measured after 7 days of treatment using CellTiter Glo. CellTiter Glo Buffer was dissolved in CellTiter-Glo substrate as recommended by the manufacture and added to each well, doubling the volume. After orbital shaking for 10 min in the dark, luminescence was measured using Mithras LB 940 plate reader.

In the CFU assay, HSPCs were strongly selected for 2 days using high concentrations of puromycin, followed by 8 days using lower concentrations within methylcellulose. Hence, killing curves for 2- and 8-day selections were generated with a range from 0 to 5 µg/µl G418 and 0 to 20 µg/ml puromycin. Treatment was applied only once, mimicking later conditions. Measurements were performed as described for dose-response curves.

3.2.8. DOT1L inhibition treatment using EPZ5676 and EPZ004777

The human AML cell lines MOLM-13 *shNT* and *shBCAT1*, as well as HL-60 *shNT* and shBCAT1, were treated with DOT1L inhibitors for 7 days. In addition to human cell lines, the primary murine $Bcat1^{+/+}$ cell line transformed by MLL-AF9 (CFU) was treated in an identical manner.

For each concentration and inhibitor $0.5*10^6$ cells/ml were seeded in RPMI medium supplemented with TET-free 10%FCS, 1x penicillin-streptomycin (Pen/strep), and 0.5 mM L-glutamine. The murine cell line was cultured in supplemented HSC Medium. Cell lines were diluted every 48h and maintained in an incubator at 37°C and 5% CO_2 throughout the treatment.

Doxycycline activated short hairpin RNAs resulting in BCAT1 knockdown (*shBCAT1#2*) and non-targeted control (*shNT*) (Raffel et al., 2017; Thewes et al., 2017; Tönjes et al., 2013). A successful knockdown was verified by qPCR and western blot.

Both inhibitors were dissolved in DMSO at a concentration of 10 mM, and aliquots were stored at -20°C. The treatment and doxycycline were renewed every 48 to 72h with a freshly prepared dilution series. Each cell line was treated with 7 different concentrations of the inhibitor (10 µM, 1 µM, 0.25 µM, 0.0625 µM, 0.031 µM, 0.008 µM, 0.004 µM) as well as a control treatment with 0.1% DMSO equal to the treatment's DMSO concentration.

3.2.9. Real-time qPCR

3.2.9.1. RNA isolation

The Maxwell RSC simplyRNA Cells kit was used to purify total RNA from fresh or frozen cell pellets. The cell pellet was dispersed with chilled 1-Thioglycerol/Homogenization solution and lysed with the same volume of lysis buffer following the manufacturer's protocol. Blue DNase I solution was added to each sample. The Maxwell RSC simplyRNA cartridge was prepared by positioning the cartridge in the deck tray and the plunger in the 8th well. Empty elution tubes were placed in the tray, and 50 µl H_2O was added.

The entire lysate was transferred into the prepared cartridge's first well, and the deck tray was inserted in the Maxwell instrument platform. Then, the simplyRNA Tissue method was selected, and the extraction was started. After the extraction process, eluted RNA concentrations and quality were measured using the Nanodrop system.

3.2.9.2. Reverse transcription and qPCR reaction

The reverse transcription (NEB #M0368) denatured 1 µg eluate RNA, a random primer mix, and a 10 mM dNTP mix at 65°C for 5min to synthesize the first-strand cDNA. 5x ProtoScript II Buffer, 0.1 M DTT, ProtoScript II RT, and RNase inhibitor were added following the manufacturer's protocol. The reaction was incubated at 25°C for 5min before cDNA was synthesized at 42°C for 1h. The reverse transcriptase was inactivated at 65°C for 20min. The cDNA concentration amounted to approximately 10 ng/µl

For each qPCR reaction, 2 µl cDNA, 5 µl CyperGreen mix containing the passive reference dye ROX, 0.2 µl forward and reverse Primer (10 µM) were mixed. 2.6 µl H_2O was used to fill up the reaction to a final volume of 10 µl. Each reaction was measured in technical triplicates. The temperature profile of 50°C for 2min, 95°C for 15min, [95°C for 15sec, 60°C for 1min]x40 cycles, 95°C for 15sec, and 60°C for 15sec was run on a QuantStudio5 with a 384-well block.

3.2.9.3. qPCR normalization and analysis

ROX was used as a passive reference, and the recorded melting curve was verified for each reaction. Expression changes were analyzed by the comparative C_t (threshold cycle) method and relative quantification.

The mean C_t value of technical triplicates with a low standard deviation was determined for all samples. Next, the mean of all housekeeper reactions for each sample was formed

and subtracted from the individual mean C_t values, normalizing each reaction. The resulting ΔCT value was put into perspective by removing the ΔC_t value of the control sample (i.e., DMSO) from each sample (i.e., treated with 10 µM EPZ5676). Finally, to determine expression fold change, the formula $2^{-\Delta\Delta Ct}$ was applied.

3.2.10. Retrovirus production

I produced retrovirus for the CFU assay as well as the syngraft mouse model. Therefore, the retrovirus-producer cell line Phoenix-GP, a highly transfectable cell line constitutively expressing Gag/Pol, was used with a calcium phosphate transfection kit.

For each virus, one T175 flask of 70-80% confluent Phoenix-GP cells was used. These cells were cultured in DMEM supplemented with 10% FCS, 1x Pen/Strep (100 U/ml), 1x GlutaMax, 10 mM HEPES, 1 mM NaOH. 40 µg plasmid of interest was mixed with 50 µg Gag/Pol plasmid (M75DAW), 15 µg envelope plasmid (K73), 180 µl 2 M $CaCl_2$, and filled up to a final volume of 750 µl with sterile H_2O. An equal amount of 2x HBS provided with the kit was added to the transfection mix. Air was bubbled into the solution for 1 min to ensure proper mixing. After 45min incubation at room temperature, 1.5 ml medium with 25 µM chloroquine was added to the transfection mix. The medium of each flask was changed to 10 ml supplemented medium containing 25 µM chloroquine. The transfection mix was added to each flask and distributed without disturbing the cell layer.

After 24h, I exchanged the medium with 12 ml supplemented medium. The cells were incubated for an additional 24h to allow virus production. Virus containing supernatant was collected and replaced by 12 ml fresh medium without disturbing the cell layer allowing for additional virus production. The collected supernatant was filtered into ultraclear SW41 centrifuge tubes using 0.45 µm syringe filters. Tubes were placed into buckets, and the contents were well balanced. Samples were ultracentrifuged using an SW41 rotor at 25000 rpm for 90min at 4°C. I carefully removed most of the supernatant, closed the tubes with parafilm, and stored them overnight at 4°C.

After 24h, new and filtered supernatant was added to the corresponding centrifuge tube, and the ultracentrifugation was repeated as described above. The supernatant was carefully decanted, and all leftover liquid was removed with a paper towel. Finally, I resuspended the virus in 90 µl OptiMEM and aliquoted it in 10 µl volumes.

The virus titration was conducted with NIH 3T3 cells cultured in DMEM high glucose with 10% FCS, 1x Pen/strep, and 0.5 mM L-glutamine. $5*10^4$ highly transfectable NIH 3T3 cells were seeded per well of a 12-well plate and incubated overnight at 37°C. I prepare a

dilution series of a fluorophore containing virus and transduced cells in a final volume of 500 µl medium containing 25 µM chloroquine to increase efficiency. After 24h, medium was replaced with 1 ml fresh medium without chloroquine. The transduction efficiency was measured by FACS, and the virus titer was calculated in order to determine the ideal virus concentration for further experiments.

3.2.11. Spinfection

As hematopoietic and fetal liver stem and progenitor cells are tough to transfect, transduction was performed in the form of a double Spinfection, increasing efficiency.

Therefore, wells of untreated cell culture plates were coated with an appropriate volume of 20 µg/ml RetroNectin and incubated overnight at 4°C. Subsequently, RetronNectin was removed, and all wells were washed twice with PBS. Virus was added to each well with HSC medium or StemSpan in a previously determined concentration. To bind the virus to the coated RetroNectin surface, I centrifuged the coated plate containing the virus at 2000 rpm for 20min at 32°C. Next, cells were added to the virus and centrifuged at 1800 rpm for 45min at 32°C. After an incubation of 24h, the new virus was added to corresponding wells, and the spinfection was repeated.

After 24h incubation at 37°C, the cells were carefully flushed off the well surface and re-plated in a fresh untreated cell culture plate with HSC or StemSpan medium. To enrich HSCPs, I cultured the cells with 20 ng/ml SCF, 2 ng/ml IL-3, and 2 ng/ml IL-6 for 48h. For the CFU assay, a harsh selection (2 µg/µl G418, 0.001 µg/µl Puromycine) was performed during this culturing period.

Cells used for the syngraft model or in the RNA-seq analysis were sorted for GFP^+ with the FACSAria Sorter Fusion.

3.2.12. Ultra-low RNA-seq

3.2.12.1. Sample preparation

To get an understanding of expression changes between the conditions of the CFU, I performed RNA sequencing analysis. Samples from the CFU experiment at the first seeding and before the third plating were used. The methods for cell isolation, spinfection, and CFU were described in chapters *3.2.3*, *3.2.6,* and *3.2.11.* As the transduction efficiency and the viability after the selection was low, samples were sorted for GFP^+ cells

using the FACSAria Sorter Fusion. Following the manufacturer's instructions, RNA was extracted using the Direct-zol RNA MicroPrep.

3.2.12.2. Library preparation and sequencing

As only a minimal number of cells could be collected for specific samples, the Genomic and Proteomics core facility (GPCF, DKFZ) performed the ultra-low RNA-seq protocol. After passing the quality control standards, libraries were prepared and sequenced on a HiSeq 4000 (4-Color patterned/235 M reads) with single reads (50bp sequencing length).

3.2.12.3. Differential expression

The measured reads were aligned to the mouse genome Mm10 by the Omics IT and Data management core facility (ODCF, DKFZ), and I further analyzed the data using the R package edgeR.

A table of read counts (Rsubread) was produced, and genes with very low counts (min.count = 10; min.total = 15) in all samples were filtered out (edgeR) based on count-per-million (CPM). The effective library size was calculated by normalizing the original library size with a scale factor of the trimmed mean of M-values (TMM) between each pair of samples. EdgeR uses the Cox-Reid profile adjusted likelihood (CR) method in estimating dispersions. It can adapt to multiple factors by fitting generalized linear models (GLM) with a design matrix. After dispersion estimates were obtained and negative binomial generalized linear models were fitted, procedures for determining differential expression were tested using quasi-likelihood (QL)-F-test. A contrast matrix was created to compare the different biological parameters, such as differences over time or between $Bcat1^{+/+}$ and $Bcat1^{-/-}$ at the same time point, which was used to call upon a variety of factors.

The differentially expressed genes were plotted and clustered (unsupervised) as a heatmap (ggplot::heatmap.2; based on the top 500 most differential genes) or plotted as Venn diagrams (ggplot::venn; logFC=+/-4, FDR=0.01).

The differential expression output was additionally used for further analysis, such as the gene set enrichment analysis (GSEA, clusterProfiler).

3.2.12.4. Gene set enrichment analysis

GSEA determines whether a pre-defined set of genes, which belong to either a specific gene ontology (GO) term or KEGG pathway, exhibits significant differences between two conditions or over time. In R, this computation method was performed with ClusterProfiler (3.13, (Yu et al., 2012)).

To interpret the previously identified differentially expressed genes between two biological states, I used gseGO and gseKEGG with stringent cutoff values: A minimum of 10 genes had to be in a gene set in order to be considered, and a p-value of 0.01 was selected. 10,000 permutations were chosen to ensure accurate results.

The comparison between GO term results and KEGG pathways was performed manually for the most significantly enriched pathways.

I presented the analyzed output as dot plot (DOSE::dotplot), enrichment map (clusterProfiler::emapplot), GSEA plot (clusterProfiler::gseaplot), and KEGG pathway (pathview::pathview)

3.2.13. Western blot

Cell pellets were lysed with RIPA buffer containing a proteinase inhibitor cocktail for approximately 15min on ice. After centrifuging, the protein concentration of the supernatant was determined by Pierce™ BCA Protein Assay following the manufacturer's instructions and was quantified with 560 nm absorbance at Mithras LB 940 plate reader. A dilution series of bovine serum albumin standards were prepared and measured as a reference.

The NuPAGE® electrophoresis system was used as described by the manufacturer. In brief, an appropriate amount of LDS (Lithium dodecyl sulfate) sample buffer and Reducing agent was added to each sample before boiling it at 95°C for 5 min. Samples were loaded on a pre-casted NuPAGE® 4-12% Bis-Tris Protein gel. Protein separation was conducted in MES or MOPS buffer supplemented with NuPAGE® Antioxidant at 250 V and 170 mA for approximately 50min. Depending on the abundance of proteins investigated, 10 to 15 µg protein was loaded per well. After electrophoreses, a wet transfer onto methanol-activated Immobilon-P transfer membrane was gradually performed by stepwise increasing the current every 10min by 50 mA (300 V, 150 W, 200 - 500 mA).

After blocking the membrane in 5% milk dissolved in TBS-T buffer, the primary antibody was incubated overnight at 4°C. Next, the membrane was washed in multiple steps with

fresh TBS-T and incubated for 1.5h at room temperature with an HRP-linked secondary antibody.

Pierce™ ECL Western Blotting Substrate was used for detection according to the manufacturer, and blots were imaged with Intas ChemoStar.

The resulting images were analyzed with ImageJ's gel function, and proteins of interest were normalized to the housekeeping genes (GAPDH, TUBA)

4. Results

4.1. Molecular characterization of orthotopic mammary carcinoma xenograft tumors

Many cancer entities rely on the inappropriate activation of the BCAA metabolism (Sullivan et al., 2019). This activation can be achieved by upregulating *BCAT1* expression und with it, increasing the degradation of valine, leucine, and isoleucine (Tönjes et al., 2013). The resulting α-KG reduction in tumor cells, such as MDA-MB231 mammary carcinoma and AML cell lines, is tightly linked to BCAT1 expression (Raffel et al., 2017).

To identify potential mechanistic interdependencies between BCAT1 and α-KG-dependent chromatin modifiers, such as histone demethylases, I performed RNA and ChIP-seq analysis of BCAT1 knockdown and control cells. For this purpose, I used material from mammary carcinoma xenograft tumors from previous work of our group that had demonstrated a potent reduction of tumor growth as a result of BCAT1 suppression (Thewes et al., 2017). This experimental approach allowed me to evaluate the link between BCAT1 and chromatin modifiers in an *in vivo* model system with the relevant molecular and phenotypic properties.

ChIP-seq libraries of the xenograft tumors were generated in collaboration with Frank Westermann. I analyzed activating lysine modifications in enhancer (H3K4me1) and promoter regions (H3K4me3 and H3K27ac), as well as the repressive marks H3K9me2, H3K9me3, and H3K27me3. The analysis was performed in triplicates (*shNT*) and duplicates (*shBCAT1*), as one replicate of *shBCAT1* tumors had to be excluded due to the overall poor quality of the sample.

The histone modifications directly associated with transcription activation, such as H3K4me3 and H3K27ac at promoter regions, greatly increased upon *BCAT1* knockdown (Figure 11). Specifically, the histone mark H3K4me3 showed a strong bias with modifications significantly increased in 283 promoter regions and only 80 promoters demethylated by inducing *BCAT1* knockdown. While not as strongly, H3K27ac exhibited the same tendencies: 253 promoter regions gained acetylation, and 130 sites lost these modifications.

I additionally analyzed differentially modified enhancer regions using the histone mark H3K4 monomethylation (H3K4me1). Genomic regions equally gained (45) and lost (45) the less common H3K4me1 modification upon *BCAT1* silencing in these orthotopic

mammary carcinoma xenografts. Neither global changes nor a one-sided gain or loss of this mark was observed.

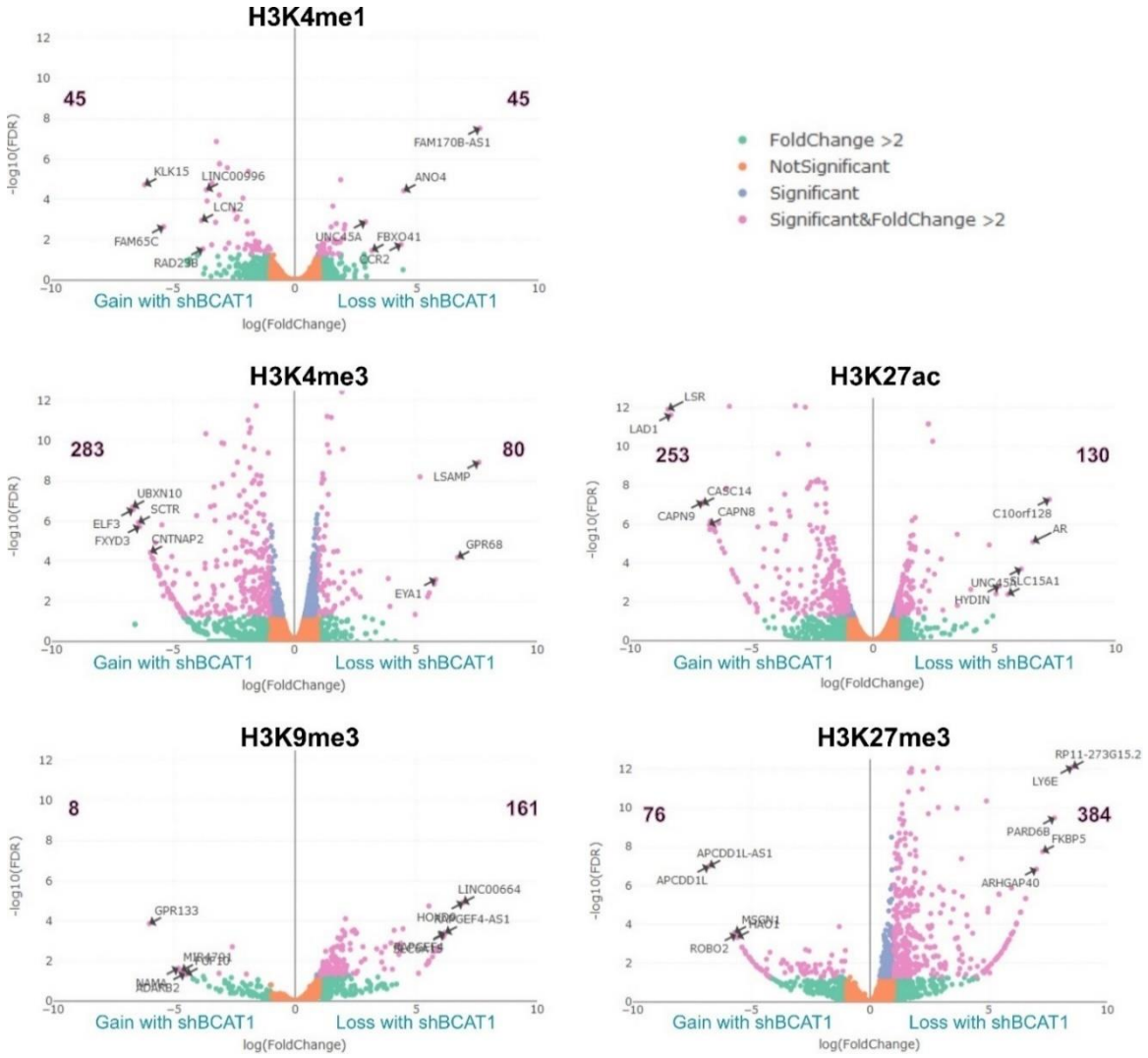

Figure 11 – Global changes in differentially modified promoter regions in orthotopic MDA-MB231 xenografts due to inducing BCAT1 knockdown. Epigenetic regulation of *shNT* and *shBCAT1* knockdown tumors was investigated using the most common histone marks (H3K4me1, H3K4me3, H3K9me3, H3K27ac, and H3K27me3). The volcano blots show differentially modified regions in the human genome for each modification. Each dot represents one region, while the colors indicate the significance and fold change (green: fold change > 2; orange: not significant (P > 0,01), blue: significant (P ≤ 0,01), pink: significant (P ≤ 0,01) and fold change > 2). Each blot's left side shows regions that gained modifications upon silencing *BCAT1*, while the right side highlights areas with lost histone marks due to *BCAT1* reduction. The top 5 most upregulated and downregulated regions were labeled by the closest gene. The total number of significant regions with a fold change greater than 2 or lower than -2 are shown in the graph. (N_{NT}=3, N_{SH}=2)

In contrast to gene activating marks, the broad and repressive histone modifications were mainly removed during BCAT1 silencing: H3K9me3 was absent in 161 promoters and significantly gained in only 8 regions. Furthermore, 76 areas reduced H3K27me3 and obtained the modification in 384 gene regions. In addition, the histone mark H3K9me2 was

measured and analyzed, however, no significant differences were detected between control and *BCAT1* knockdown (not shown).

The gain of gene-activating and reduction of repressive histone modifications suggests a global increase in gene transcription upon silencing *BCAT1*. To verify the effect of these histone modification changes on transcription, I performed RNA-seq analysis of mammary carcinoma xenograft tumors.

Independent clustering of the RNA expression data resulted in the clear separation of control and *BCAT1* silenced xenografts (Figure S1). The expression profiles of these tumors revealed the global expression increase in *BCAT1* knockdown tumors (Figure S2) already indicated by the histone modifications described above. Only a limited number of genes were downregulated, among which *BCAT1* was identified, verifying the successful knockdown.

The changes in RNA expression correlated with previously identified differentially modified regions. For instance, acetylation of H3K27 at the promoter region of lipolysis-stimulated lipoprotein receptor (*LSR*) and Ladinin 1 (*LAD1*) correlated with a substantial expression increase, making them two of the most upregulated expressed genes. In contrast, the gain of H3K27me3 was associated with repressed RNA transcription of APC down-regulated 1 like (*APCDD1L*) and antisense (*APCDD1L-AS*) upon *BCAT1* knockdown.

In summary, I analyzed the effects of *BCAT1* suppression on gene activating and inactivating histone modifications by performing ChIP-seq analysis of *BCAT1* knockdown and control mammary carcinoma xenograft tumors. The analysis showed an increase of activation and a decrease of suppression marks, consistent with a state of global gene activation determined by RNA-seq analysis.

These findings appear inconsistent with the hypothesis of BCAT1-dependent α-KG depletion inhibiting the activity of α-KG-dependent dioxygenases (Raffel et al., 2017), like most histone demethylases. According to this hypothesis, BCAT1 knockdown would be expected to globally reduce chromatin modifications due to the activation of histone demethylases by increased α-KG availability. However, these data suggest cellular α-KG does not primarily regulate the activity of α-KG-dependent histone demethylases in AML. Instead, a more complex mechanism of regulation must exist that nevertheless appears to be strongly affected by BCAT1 downregulation.

4.2. Linking BCAT1 to histone modifiers in breast cancer and leukemia tumors

As described above, RNA and ChIP-seq analysis of the mammary carcinoma xenograft tumors indicated mechanistic interdependence between BCAT1 expression and the activity of histone modifiers independent of α-KG.

Therefore, I extended my examination by correlating the RNA expression of BCAT1 and chromatin modifiers in publicly available patient datasets. For this analysis, I used whole-transcriptome profiling of triple-negative breast tumors in 226 African American women (GSE142102) as well as expression data of 172 acute myeloid leukemia patients available in TCGA. Both tumor entities were chosen based on previously observed dependencies on BCAT1 expression. Graphical representations of the correlation between BCAT1 expression and a selection of histone modifiers are shown in Figure 12. The complete list of over 40 analyzed chromatin modifiers in both tumor entities can be found in the supplements (Table S1).

The RNA expression of three enzymes was found to be significantly correlated with *BCAT1* expression in both cancer entities: The lysine demethylases *JMJD1C* and *KDM1A*, and H3K4 methyltransferase *MLL*; *BCAT1,* which showed the highest significance in the mammary carcinoma and AML patient cohorts (Breast cancer: $R=0.24$, $p=2.61*10^{-4}$; AML: $R=0.57$, $p=4.73*10^{-16}$).

As described above, *MLL* additionally stands out for its many implications in cancer and its numerous mutations in different tumor entities. The catalog of somatic mutations in cancer COSMIC lists a total of 2697 coding mutations and 666 fusion events throughout 33 cancer entities involving the human *MLL* gene (Tate et al., 2019). These rearrangements gain functions by generating new chimeric proteins containing the N-terminus of MLL fused in-frame with one of many potential partner proteins (Ayton & Cleary, 2001). Fusion genes, including fusions with *AF9* and *ENL*, enable binding and misguided recruitment of the only known H3K79 methyltransferase DOT1L, initiating a leukemic expression profile.

To summarize, I investigated potential epigenetic regulation of *BCAT1* by correlating the RNA expression of *BCAT1* and modifiers of activation and repression chromatin marks. Of over 40 analyzed chromatin modifiers, the expression of the H3K4 methyltransferase *MLL* and *BCAT1* positively correlated with the highest significance in mammary carcinoma and AML patient cohorts. The most common MLL fusion genes can initiate unique leukemic expression patterns through mistargeted DOT1L complex-mediated H3K79me2 modification in acute leukemias.

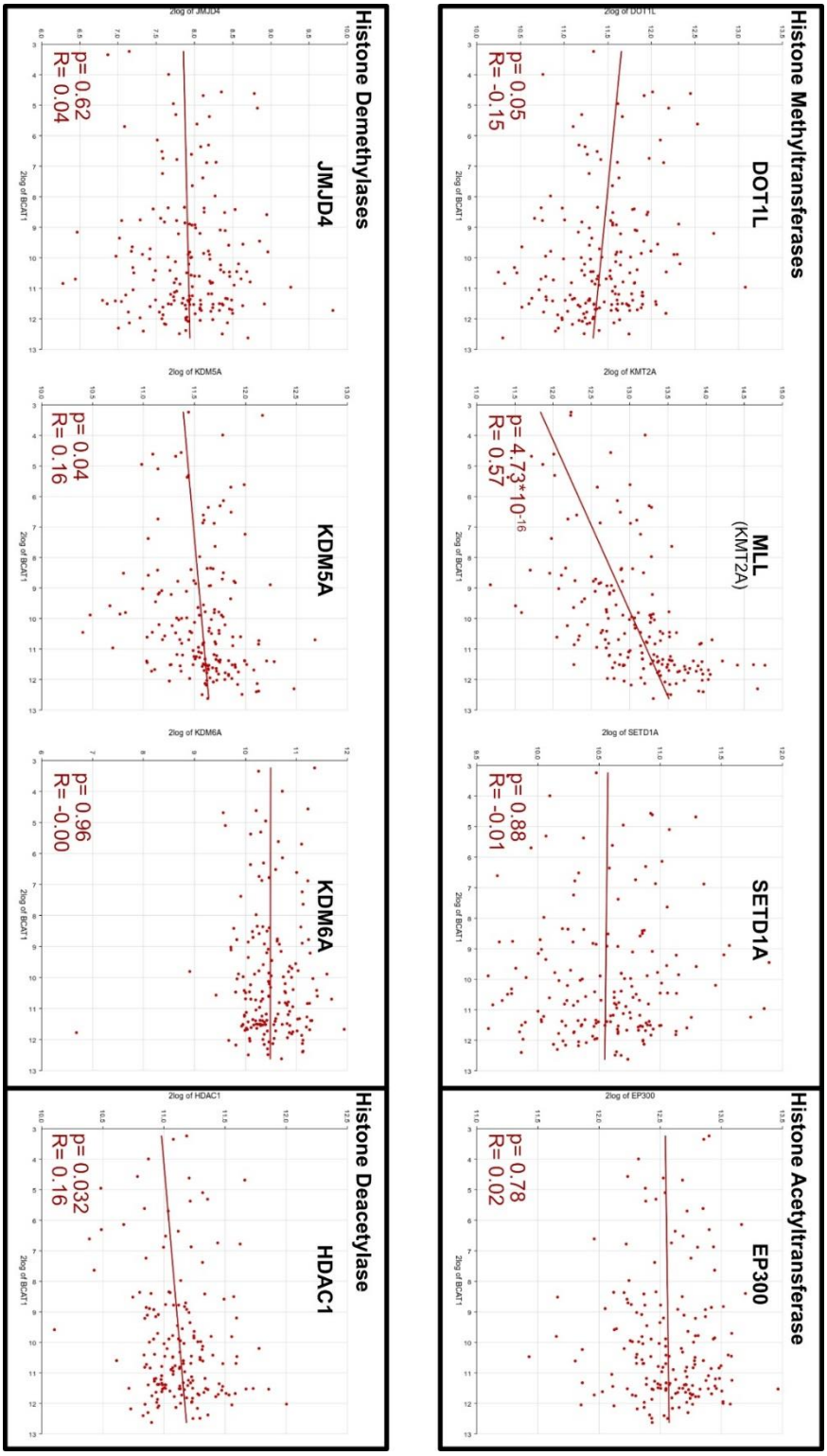

Figure 12 – Visualization of correlations between *BCAT1* expression and selected epigenetic histone modifiers in expression profiling data of 172 acute myeloid leukemia patients (TCGA LAML) using R2 (Koster & Versteeg, 2008)**.** Each dot represents the log2 transformed expression in a patient with *BCAT1* expression indicated on the x-axis and the investigated gene on the y-axis. A red line shows the linear fit, and significance (p), as well as correlation (R), are outlined in the lower-left corner of each graph. Histone lysine methyltransferases and demethylases, as well as the histone acetyltransferase and deacetylase, are visually separated. Exhibiting a highly significant correlation with *BCAT1* in both cancer entities identifies histone lysine methyltransferase *MLL* as a critical epigenetic regulator. A complete list of correlations between *BCAT1* and all relevant histone modifiers in acute myeloid leukemia and triple-negative breast cancer is found in the supplements (Table S1).

4.3. BCAT1 as a direct target of MLL fusion genes in AML

The most frequent MLL fusion proteins in AML are able to recruit the only known H3K79 methyltransferase DOT1L through direct interactions with fusion partners such as ENL or AF9 (Biswas et al., 2011; Mueller et al., 2007). This recruitment is associated with a mistargeted upregulation of H3K79me2, as well as RNA Pol II and MYC binding. All three adaptations are followed by inappropriate activation of gene expression (Kerry et al., 2017; Krivtsov & Armstrong, 2007; Liedtke & Cleary, 2009). As shown in Figure 13, this mechanism enables MLL fusion proteins to initiate a leukemic stem cell expression pattern and, thus, the transformation of hematopoietic stem cells. Among the fusion targets, the developmental genes homeobox A9 (*HOXA9*) and Meis homeobox 1 (*MEIS1*) are the most studied genes based on their role in self-renewal (Rice & Licht, 2007; B. D. Yu et al., 1995).

In order to investigate the interdependencies between MLL fusion proteins and *BCAT1*, I performed all experiments in this chapter with the human AML cell line MOLM-13 harboring a balanced *MLL-AF9* fusion and the non-fusion human AML cell line HL-60. In addition, selected experiments were performed in primary mouse AML cells transformed by MLL-AF9 and the human non-fusion cancer cell lines MDA-MB231 and U87.

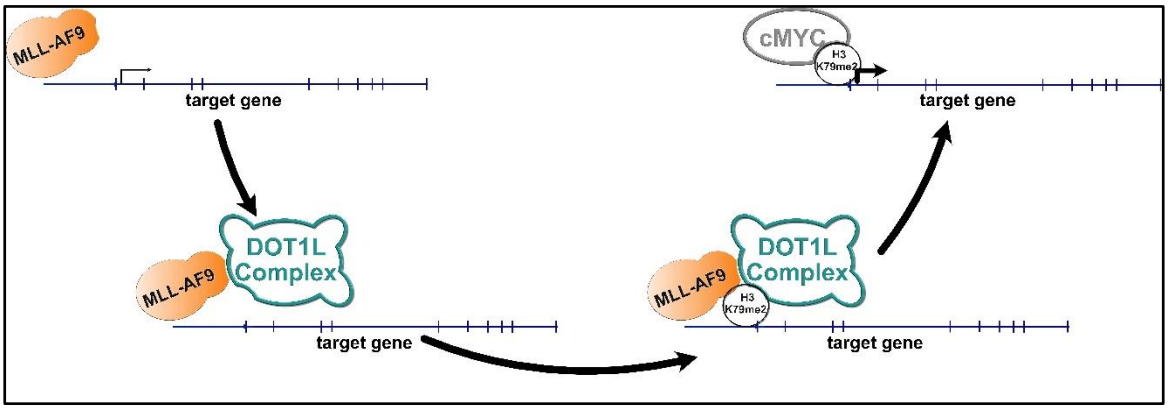

Figure 13 - Initiation of leukemogenic expression profile during MLL fusion-driven transformation of leukemic stem cells. I hypothesized that MLL fusion proteins, such as MLL-AF9, are directly responsible for *BCAT1* upregulation in leukemic stem cells (LSCs) by recruiting the methyltransferase DOT1L. DOT1L, in turn, upregulates the activating histone modification H3K79me2, enabling MYC binding and hence *BCAT1* expression. Furthermore, I assume that BCAT1 plays a vital role during already established leukemia and is essential during tumor development.

4.3.1. Epigenetic regulation of BCAT1 through DOT1L in MLL-AF9 AML cell line

Based on the observed correlation between patient-tumor *BCAT1* and *MLL* expression, I hypothesized that *BCAT1* is an MLL fusion-protein target activated by DOT1L-dependent H3K79me tagging (Figure 13). In line with this, inhibition of DOT1L should be accompanied by reduced H3K79 dimethylation and thus diminished expression of MLL-AF9 target genes, including *BCAT1*. To test my hypothesis, I treated the *MLL-AF9* fusion cell line MOLM13 and the non-fusion cell line HL-60 with increasing concentrations of two different DOT1L inhibitors ranging from 2nM to 10µM. In addition, I analyzed the expression patterns of *BCAT1* and the well-known fusion targets *HOXA9* and *MEIS1* using real-time quantitative PCR (qPCR). EPZ5676 (Pinometostat) and EPZ00477 are both highly potent and selective amino nucleoside inhibitors of DOT1L (C. T. Campbell et al., 2017; Daigle et al., 2011, 2013; Kühn et al., 2015). The long half-life of H3K79 methylation (Barth & Imhof, 2010; Chory et al., 2019) made a treatment course of 7 days necessary.

While MLL-AF9 and DOT1L expression in MOLM-13 was unaffected by DOT1L inhibition and H3K79 loss, the expression of the known MLL-AF9 target genes *HOXA9* and *MEIS1* inversely correlated with increasing concentration of DOT1L inhibitor (Figure 14). The expression of both genes continuously declined until a reduction of 85% and 95%, respectively, at 10 µM EPZ5676. Mirroring the expression pattern of well-established MLL fusion target genes, *BCAT1* expression continuously dropped to a final expression reduction of 78% at 10 µM EPZ5676 treatment in MOLM-13 cells. Using a second DOT1L inhibitor (EPZ004777), I measured comparable expression changes; the transcription of *BCAT1* decreased continuously until reaching 76% upon 7-day treatment of MOLM-13 with 10 µM EPZ004777, while *MLL-AF9* and *DOT1L* expression was not affected. The expression of both *HOXA9* and *MEIS1* was reduced to 85% at the highest concentration used.

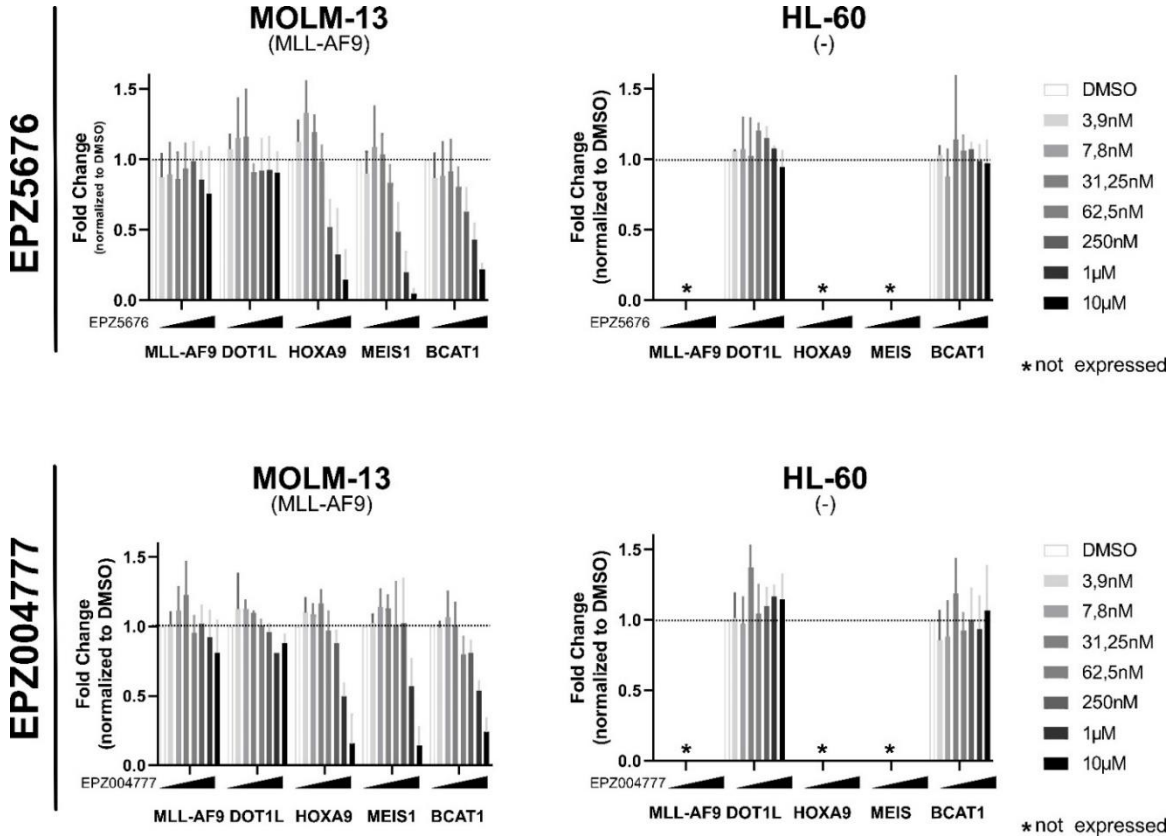

Figure 14 – Reduced *BCAT1* expression is detected with qPCR upon DOT1L inhibition in MOLM-13 cell line harboring an *MLL-AF9* fusion. EPZ5676 (upper panel) and EPZ004777 (lower panel) inhibit the only known H3K79 methyltransferase DOT1L. The resulting reduction of H3K79 methylation at MLL-AF9 target genes leads to reduced expression, which can be detected via real-time quantitative PCR. *BCAT1* expression shows an explicit dependency on DOT1L activity in MOLM-13 but not in HL-60, a human AML cell line without an *MLL* fusion gene. A gradual decrease of up to ~78% *BCAT1* expression inverse correlates with increasing concentration with either of the two DOT1L inhibitors in MOLM-13. These changes are analog to the expression differences measured in the known MLL-AF9 target genes *HOXA9* (~85%) and *MEIS*1 (95%; 86%). The inhibition of DOT1L did not influence the expression of *MLL-AF9* and *DOT1*L. The cell line HL-60 did not express *MLL-AF9* and only deficient levels of *HOXA9* and *MEIS1*, which are highlighted by *. ($N_{MOLM-13}$=3, N_{HL-60}=3)

As expected, no *MLL-AF9* transcripts could be detected in the fusion-free cell line HL-60. Furthermore, MLL-AF9 target genes *HOXA9* and *MEIS1* were hardly expressed in this cell line, excluding them from this analysis. In accordance with these data, *BCAT1* is expressed less in HL-60 than in the *MLL*-fusion cell line MOLM-13. Nevertheless, expression levels were sufficient to confirm that DOT1l inhibition did not reduce *BCAT1* expression in HL-60.

To exclude regulation through protein degradation or stabilization, I additionally verified my findings on protein level. Using the same cell lines treated with two different DOT1L inhibitors, I observed a continuing reduction of BCAT1 with increasing DOT1L inhibitor concentrations in the *MLL-AF9* cell line MOLM-13 (Figure 15). As anticipated, no changes in BCAT1 were observed in HL-60, independent of the DOT1L inhibitor used. The

quantification of BCAT1 protein levels was conducted relative to GAPDH loading control (shown in Figure 6) and ponceau staining. Both normalization variants highlighted the similarity between the previously observed reduction of proliferation and mRNA levels following DOT1L inhibition.

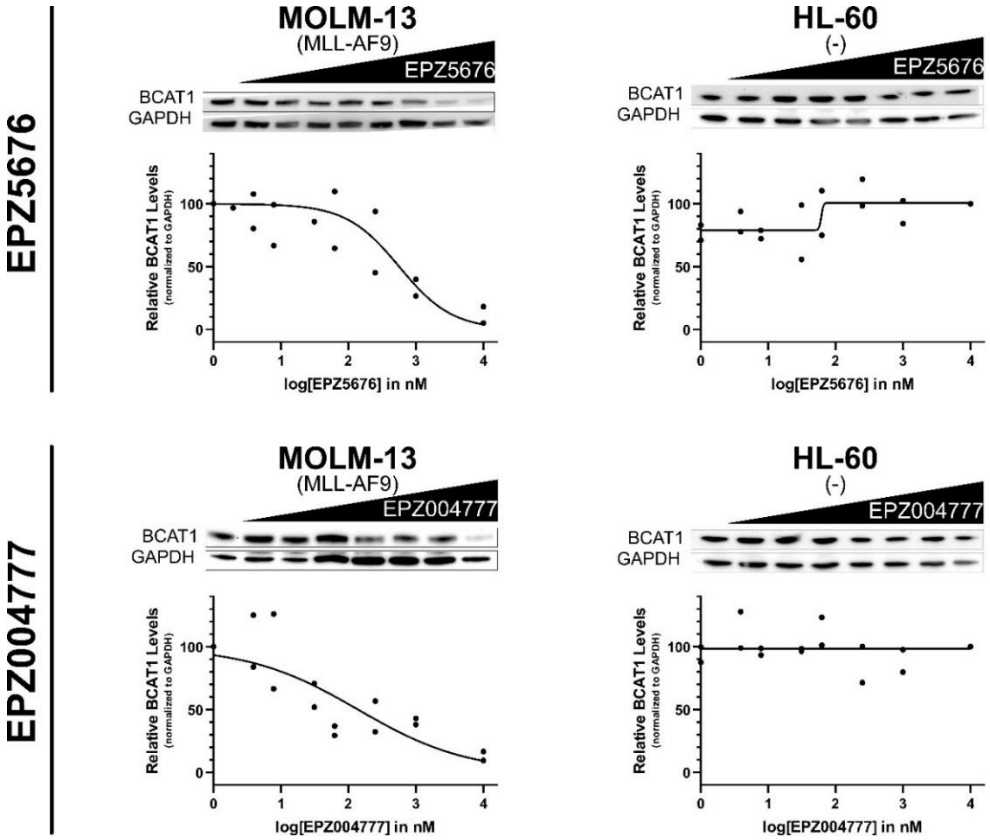

Figure 15 – DOT1L inhibition reduces protein levels of BCAT1 in *MLL*-fusion cell line MOLM-13 identified by Western blot analysis. As observed with mRNA expression, BCAT1 protein levels were reduced with increasing DOT1L inhibitor treatment in MOLM-13 but not HL-60. Representative western blots show a striking reduction of BCAT1 with EPZ5676 and EPZ004777 inhibitors, while barely any changes were observed in the non-fusion cell line HL-60. The values of independent western blots were quantified below the representative blots by normalization to GAPDH. In parallel to my previous results, I observed a higher sensitivity with the DOT1L inhibitor EPZ5676 than EPZ004777. ($N_{MOLM-13}$=2, N_{HL-60}=2)

4.3.2. Methyltransferase DOT1L drives proliferation in a BCAT1 dependent manner

To investigate the dependency of AML tumor proliferation on the MLL fusion-DOT1L-BCAT1 axis, I treated cell lines harboring the oncogenic *MLL-AF9* fusion as well as non-fusion cell lines with increasing concentrations of the DOT1L inhibitors EPZ5676 and EPZ004777. After the treatment, I used CellTiter-Glo® Luminescent Cell Viability Assay to measure the effects of DOT1L inhibition on cell viability and proliferation. In parallel, I identified cell viability with trypan blue to be similar in all measured samples. This allowed

me to determine the differences in CellTiter-Glo® Luminescent Cell Viability Assay exclusively to changes in proliferation. As a result, I could show that MOLM-13 was sensitive to both DOT1L inhibitors (EPZ5676 IC50=170.6 nM; EPZ00477 IC50=1.7 µM) while HL-60 showed resistance to DOT1L inhibition (Figure 16).

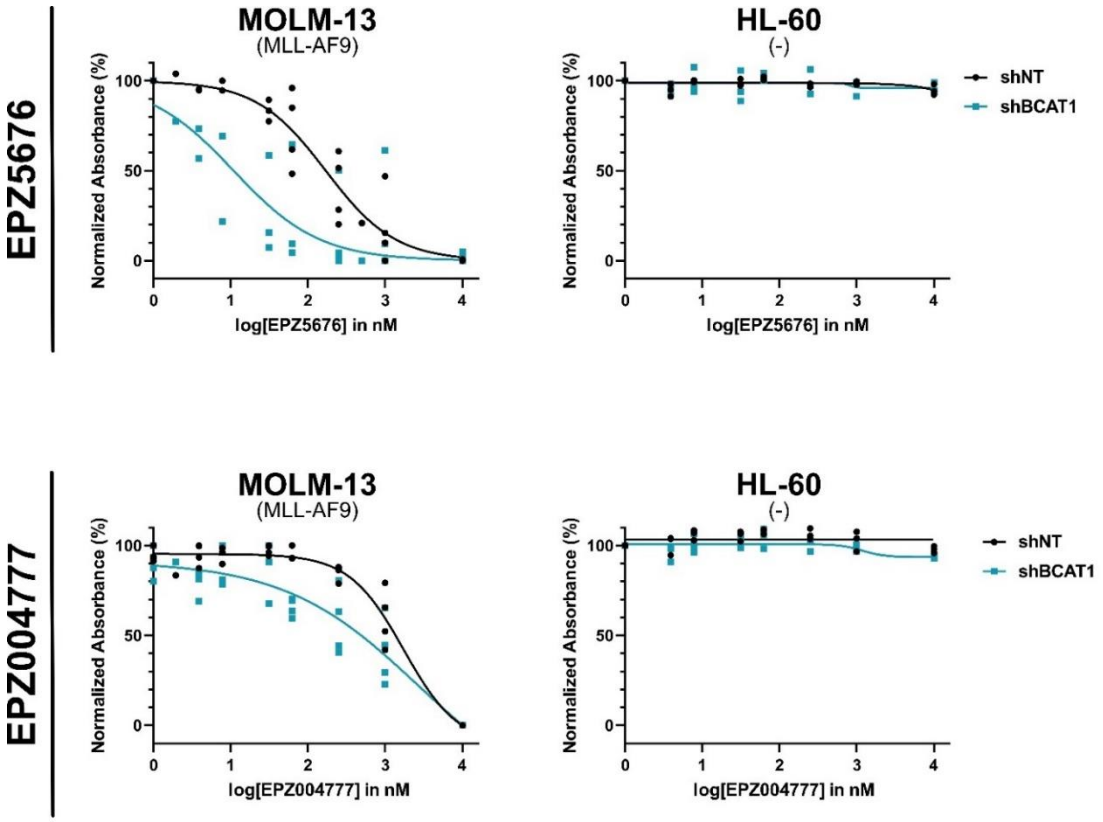

Figure 16 - DOT1L inhibition of the *MLL-AF9* cell line reduces proliferation in *BCAT1* dependent manner. Both DOT1L inhibitor treatments reduce proliferation in MLL-AF9 fusion cell line MOLM-13 *shNT* measured with CellTiter-Glo® (EPZ5676 IC50=170.6 nM; EPZ00477 IC50=1.7 µM) MOLM-13 *shBCAT1* cells show an even higher sensitivity to DOT1L inhibition (EPZ5676 IC50=11 nM; EPZ00477 IC50=1.0 µM). The human *MLL* wildtype cell line HL-60 is resistant to EPZ5676 or EPZ004777 treatment independent of *BCAT1* expression. ($N_{MOLM-13}$=3, N_{HL-60}=3)

These findings were further verified in cell lines (MDA-MB231 and U87) of other cancer entities free of *MLL* mutations (not shown). In addition to these well-established human cell lines, I treated a primary mouse AML cell line harboring an *MLL-AF9* fusion mutation resulting in even higher sensitivity (EPZ5676 IC50=70 nM) to DOT1L inhibitor EPZ5676 (Figure S7).

Remarkably, I detected an even higher sensitivity to DOT1L inhibition (EPZ5676 IC50=11 nM; EPZ00477 IC50=1.0 µM) in MOLM-13 carrying doxycycline induced *BCAT1* knockdown (*shBCAT1*) in comparison to the non-targeted control (*shNT*). The *shBCAT1-2* RNA diminished BCAT1 immensely; however, trace amounts of BCAT1 are still present in

these cells 7 days after activation with doxycycline. Furthermore, I could show that increasing concentrations of either of the DOT1L inhibitors reduced BCAT1 protein levels even further (Figure S6), giving an additional indication that epigenetic regulation of BCAT1 through DOT1L is vital for tumor proliferation in *MLL*-fusion cell lines.

4.3.3. Epigenetic regulation of BCAT1 is MLL-AF9 dependent in human AML cell lines

I demonstrated that *BCAT1* expression and proliferation of *MLL-AF9* fusion cell lines is dependent on DOT1L activity. Next, I performed ChIP-PCR targeting the activating histone marks H3K4me3 and H3K27ac, as well as DOT1L-dependent H3K79me2, and the transcription factor MLL. Target enrichments were quantified in five different *BCAT1* regions, and regions of *HOXA9* and *MEIS1* served as positive controls.

Figure 17 displays the fold change of normalized enrichment of each corresponding mark in one representative region of the respective gene. Normalization was performed to the input and an IgG control to exclude unspecific binding and detect enrichment. All analyzed *BCAT1* regions were strongly enriched in pulldown of H3K4me3 and H3K27ac exclusively in the *MLL-AF9* fusion gene cell line MOLM-13 and not HL-60. These enrichments mirrored the positive controls *HOXA9* and *MEIS1*. Furthermore, I measured an increase of H3K4me3 and H3K27ac modifications upon doxycycline-induced *shBCAT1* in *BCAT1* and *MEIS1* regions of MOLM-13. The histone modification H3K79me2 exclusively mediated by DOT1L was uniquely enriched in MOLM-13, supporting the hypothesis of misguided MLL-AF9-mediated DOT1L recruitment to *BCAT1* analogous to known MLL fusion target genes *HOXA9* and *MEIS1*. The reduced binding of H3K79me2 in *shBCAT1* MOLM-13 cells indicates a potential feedback loop, which needs further investigation. The antibody targeting N-terminal MLL cannot differentiate between endogenous MLL and the fusion gene MLL-AF9; nonetheless, the difference between MLL-AF9 carrying MOLM-13 cell line and HL-60 is an indication for fusion specific binding at these sites.

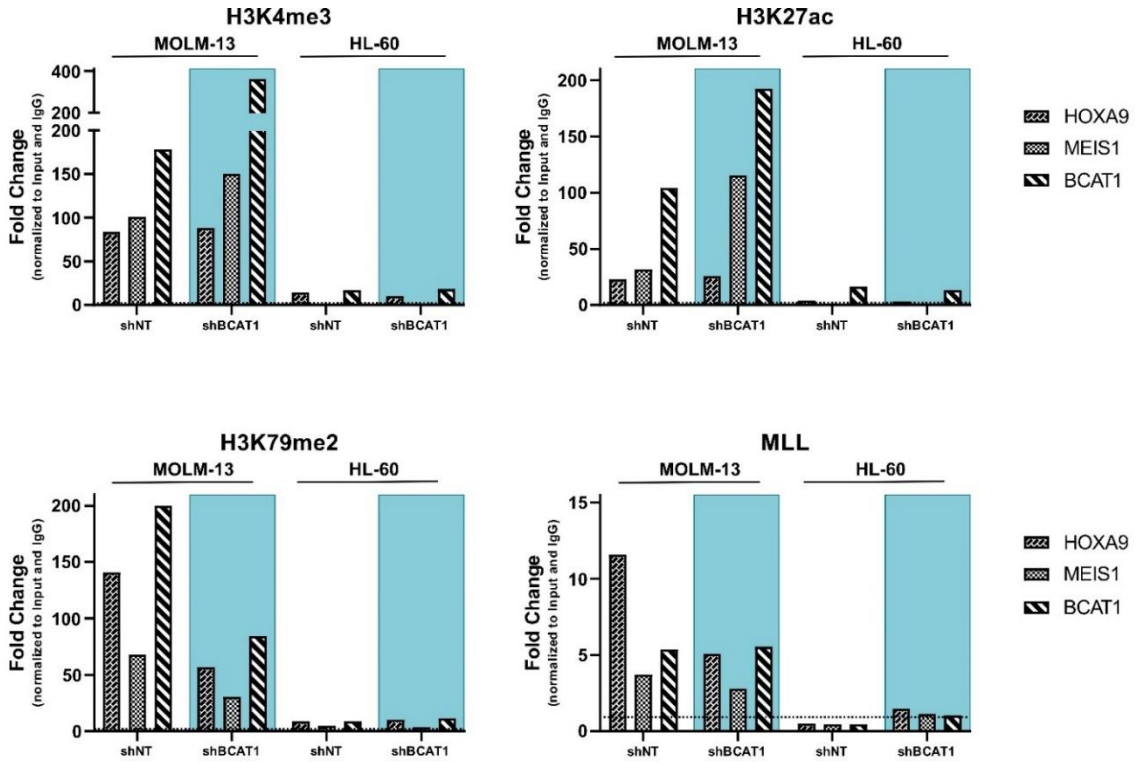

Figure 17 – ChIP-PCR verifies binding of epigenetic regulators and increase of activation marks to human *BCAT1* DNA regions comparably to well-known MLL-AF9 target *HOXA9* and *MEIS1*. The activating chromatin modifications H3K4me3 and H3K27ac are particularly enriched in promoter regions of *BCAT1*, *HOXA9*, and *MEIS1* of MOLM-13 but not in HL-60. This epigenetic regulation is accompanied by translational upregulation of these genes. Both marks seem to be specifically prominent in the first exons of *BCAT1* in the MLL-AF9 cell line MOLM-13 with doxycycline-induced *shBCAT1* knockdown (*shBCAT1*; turquoise background), potentially indicating an epigenetic feedback loop. The less common activating histone mark H3K79me2 and the transcription factor MLL/MLL-AF9 are mainly observed at *BCAT1*, *HOXA9*, and *MEIS1* gene regions in MOLM-13 but nearly absent in HL-60. Interestingly, H3K79me2 modifications drop in promoter regions of all investigated genes in MOLM-13 BCAT1 knockdown cells compared to MOLM-13 *shNT*. All measurements were normalized to the input amount of sample and IgG negative control (dashed line) and therefore represented as fold change. (N= 1, multiple sites per gene)

To summarize, I showed that *BCAT1* is an MLL-AF9 target gene regulated by the H3K79 methyltransferase DOT1L. Pharmacologic inhibition of DOT1L resulted in the transcriptional suppression of *BCAT1* and known MLL-AF9 target genes and subsequent reduction of BCAT1 protein expression and cell proliferation, specifically in an *MLL*-fusion cell line; a control cell line without MLL fusion did not show comparable effects. Thus, even in already established tumor cell lines, I could show that the proliferation of *MLL* fusion-driven AML strongly depends on *BCAT1*. ChIP-PCR verified the binding of the oncogene MLL-AF9 at *BCAT1* regions and the accompanying demethylation of H3K79 by histone methyltransferase DOT1L. In addition, known MLL-AF9 target genes showed an identical enrichment. Combining these findings, I conclude that *BCAT1* indeed is activated by the MLL fusion-DOT1L-axis in *MLL*-fusion gene-driven AML.

4.4. *Bcat1* is essential for the development of MLL fusion-driven leukemia

4.4.1. Establishment of *in vitro* model for AML development

I identified *BCAT1* as a novel target of the oncogenic gain of function *MLL* fusion gene in human AML cell lines; however, its role in *MLL* fusion-dependent AML is still unclear.

The immortalization of *MLL*-fusion cell lines permanently changes the epigenetic landscape and expression pattern, making it a lacking model for direct and indirect effects of MLL fusion proteins. Therefore, I took advantage of a murine *in vitro* tumor development model to explore the function of BCAT1 during tumorigenesis. I established a colony formation unit (CFU) assay with hematopoietic stem and progenitor cells (HSPCs) isolated from bone marrow of *Bcat1* WT and *Bcat1* KO mice. Hereafter these genotypes will be referred to as Bcat1$^{+/+}$ and Bcat1$^{-/-}$, respectively.

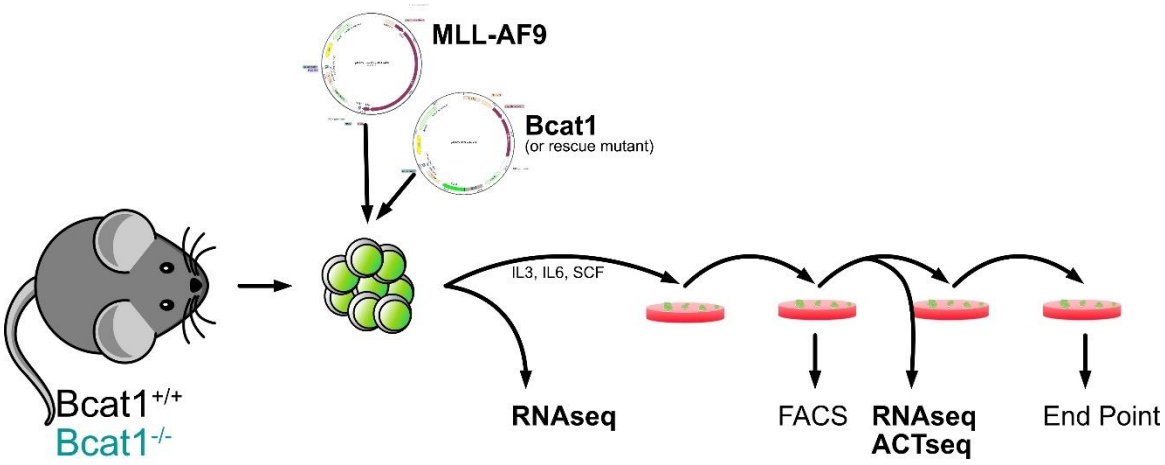

Figure 18 – Graphical representation of experimental setup for colony formation unit (CFU) assay and further downstream analysis. Hematopoietic stem and progenitor cells (HSPCs) from *Bcat1* WT (Bcat1$^{+/+}$) and KO (Bcat1$^{-/-}$) mice were transduced with either the oncogenic driver fusion MLL-AF9 or MLL-ENL. *Bcat1*$^{-/-}$ HSPCs were further transfected with Bcat1^{WT} or *Bcat1* mutant. As a control, an empty vector was added to Bcat1$^{+/+}$ and Bcat1$^{-/-}$ cells without rescue constructs. A colony formation assay was conducted with samples collected for RNA-seq and ACT-seq before and during transformation. A total of four platings were performed, and surfaces markers were analyzed with FACS at each stage.

As shown in Figure 18, HSPCs were transduced with either *MLL-AF9* or *MLL-ENL* fusion gene and an empty vector or a *Bcat1* rescue construct. These constructs carried antibiotic resistance genes for constant low selection and a fluorophore (GFP) to monitor expression. The cells were serially replated *in vitro* four times, and the colony formation potential was determined by counting colony numbers. Tumor development was tracked

by surface marker staining and FACS analysis throughout the assay. The differences between Bcat1$^{+/+}$ and Bcat1$^{-/-}$ HSPCs during tumor development were further characterized by RNA-seq and ACT-seq at the beginning and the midpoint of the CFU assay.

4.4.2. Bcat1$^{-/-}$ HSPCs are incapable of transforming into LSCs through *MLL* fusion genes

The CFU assay is based on the ability of a single *MLL* rearrangement such as *MLL-AF9* or *MLL-ENL* to induce leukemic transformation in hematopoietic stem and progenitor cells (HSPCs) by upregulating selected target genes and triggering stem-cell-like properties (Krivtsov & Armstrong, 2007; Liedtke & Cleary, 2009). It enabled me to investigate the importance of BCAT1 during the development of MLL fusion-driven murine AML.

As anticipated, Bcat1$^{+/+}$ HSPCs transduced with either of the oncogenic drivers *MLL-AF9* or *MLL-ENL* formed numerous dense and compact colonies as shown in Figure 19 (upper panels). This compressed colony type has been associated with tumor transformation (Somervaille & Cleary, 2006), and its potential to divide unlimited is a hallmark of cancer (Somervaille et al., 2009). In contrast, only single cells or loose and differentiated CFU-GM-like (granulocyte, macrophage) colonies were found in cells lacking Bcat1, resulting in a low number of colonies observed with either the *MLL-AF9* or *MLL-ENL* transduced Bcat1$^{-/-}$ HSPCs.

To better understand the cells comprising these colonies, I established a broad range panel of surface markers for FACS analysis. This panel included markers for stem and progenitor cells (SCA1, cKIT1), the hematopoietic lineage (CD45), macrophages (MAC1/CD11b), granulocytes (Gr1), monocytes (CD115), T cells (CD3), and B cells (B220). In addition, gating for GFP^{+} cells enabled me to successfully track transduced cells with a constant expression of the oncogenes under the same promoter.

Already at an early time point (2nd plating), FACS analysis of transduced Bcat1$^{+/+}$ HSPCs showed a majority of cells transformed into leukemic stem cells (LSCs; GFP^{+}, CD45^{+}, Lin^{-}, cKIT^{+}, Sca1^{+}) highlighting their tumorigenesis (Figure 19). This subpopulation represents about 53% of MLL-AF9 and about 72% of MLL-ENL Bcat1$^{+/+}$ cells. In contrast, only a small subpopulation (19% and 11%) of Bcat1$^{-/-}$ HSPCs expressing either one of the *MLL* fusion genes are stem-cell-like at the same time point, emphasizing the importance of Bcat1 in MLL fusion-driven tumor development.

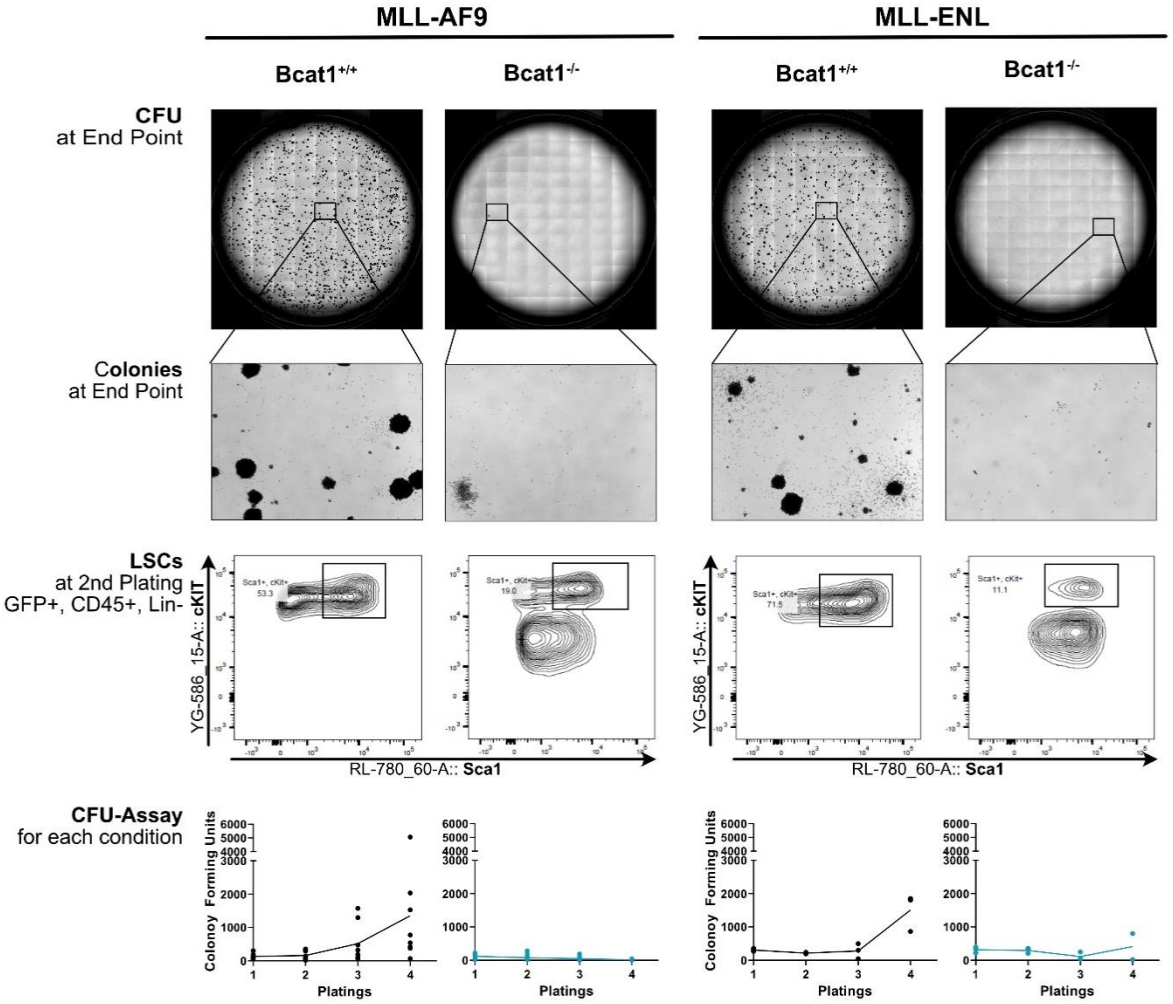

Figure 19 – Transformation of Bcat1$^{+/+}$ HSPCs to leukemic stem cells in a colony formation unit assay. Representative images of CFU colonies at the endpoint (4th Plating) are shown as an overview (128 tails for full 3 cm dish) and in detail (2.5× / 0.075 PlnN objective, Zeiss Cell Observer (Motorized Widefield Microscope)). Numerous dense colonies verify that the transduction of Bcat1$^{+/+}$ HSPCs with *MLL* fusion genes transforms them into tumor cells. Furthermore, FACS analysis of surface markers identifies most of these cells as LSCs (GFP$^+$, CD45$^+$, Lin$^-$, cKIT$^+$, Sca$^+$) after the 2nd plating. In contrast, barely any to no colonies can be observed when transducing Bcat1$^{-/-}$ HSPCs with *MLL* fusion genes. No transformation occurs with Bcat1$^{-/-}$ cells, and only a few LSCs can be identified at the 2nd plating. The last row gives a detailed view of the colony-forming potential during the CFU assay for each condition. ($N_{MLL\text{-}AF9}$= 8; $N_{MLL\text{-}ENL}$= 3)

At the 3rd plating, a vast number of colonies were counted with an average of 460 (*MLL-AF9*) and 280 (*MLL-ENL*) colonies, as illustrated in the bottom panels of Figure 19 and Figure 20. Bcat1$^{-/-}$ HSPCs were not immortalized as shown in and therefore showed lower colony-forming potential (Figure 20). An average of 52 (*MLL-AF9*) and 112 (*MLL-ENL*) Bcat1$^{-/-}$ colonies were counted at the 3rd plating.

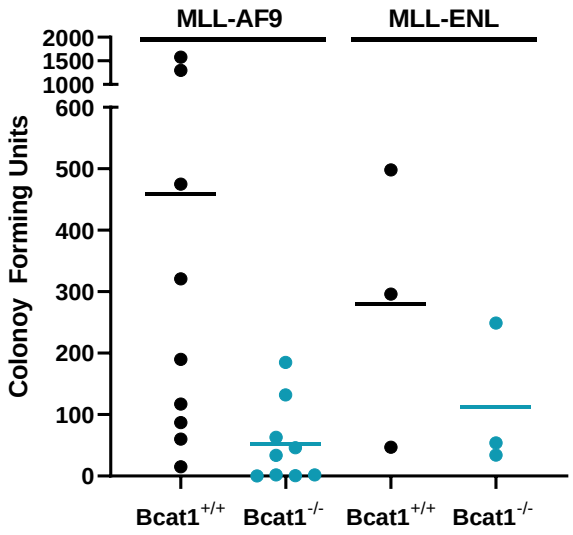

Figure 20 – *Bcat1* is essential for *MLL* fusion-driven tumor development. Already after the 3rd plating, the vast difference in colony numbers was observed, as shown here. Both fusion genes *MLL-AF9* and *MLL-ENL* confer the ability to form unlimited colonies in Bcat1$^{+/+}$ HSPCs (black). Strongly reduced or even complete loss of this oncogenic potential was observed in Bcat1$^{-/-}$ HSPCs (turquoise), highlighting the pivotal role BCAT1 plays in AML development. The mean of each sample is indicated by the bar. ($N_{MLL\text{-}AF9}$= 9; $N_{MLL\text{-}ENL}$= 3; 3rd Plating)

4.4.3. Transformation potential is rescued by wildtype but not metabolic mutant Bcat1

I demonstrated that BCAT1 is essential for the MLL fusion-driven transformation of leukemic stem cells. Next, I used *Bcat1* rescue constructs from a collaboration with Liliana François Martín del Campo and Pavle Boskovic within our lab. The rescues included *Bcat1* wildtype (Bcat1^{WT}), a redox dead (Bcat1^{SXXS}), and a metabolic dead *Bcat1* mutant (Bcat1^{K222A}) to rescue the loss of unlimited self-renewal in the Bcat1$^{-/-}$ CFU assay. Liliana François Martín del Campo (2019) was able to show that BCAT1^{WT}, as well as BCAT1^{SXXS} mutant constructs, were translated into metabolic functional proteins, while the point mutation of K222A resulted in a catalytically inactive protein. However, mutation of the BCAT1 CXXC motive of BCAT1 to SXXS could no longer function in maintaining cellular redox homeostasis (François Martín del Campo, 2019).

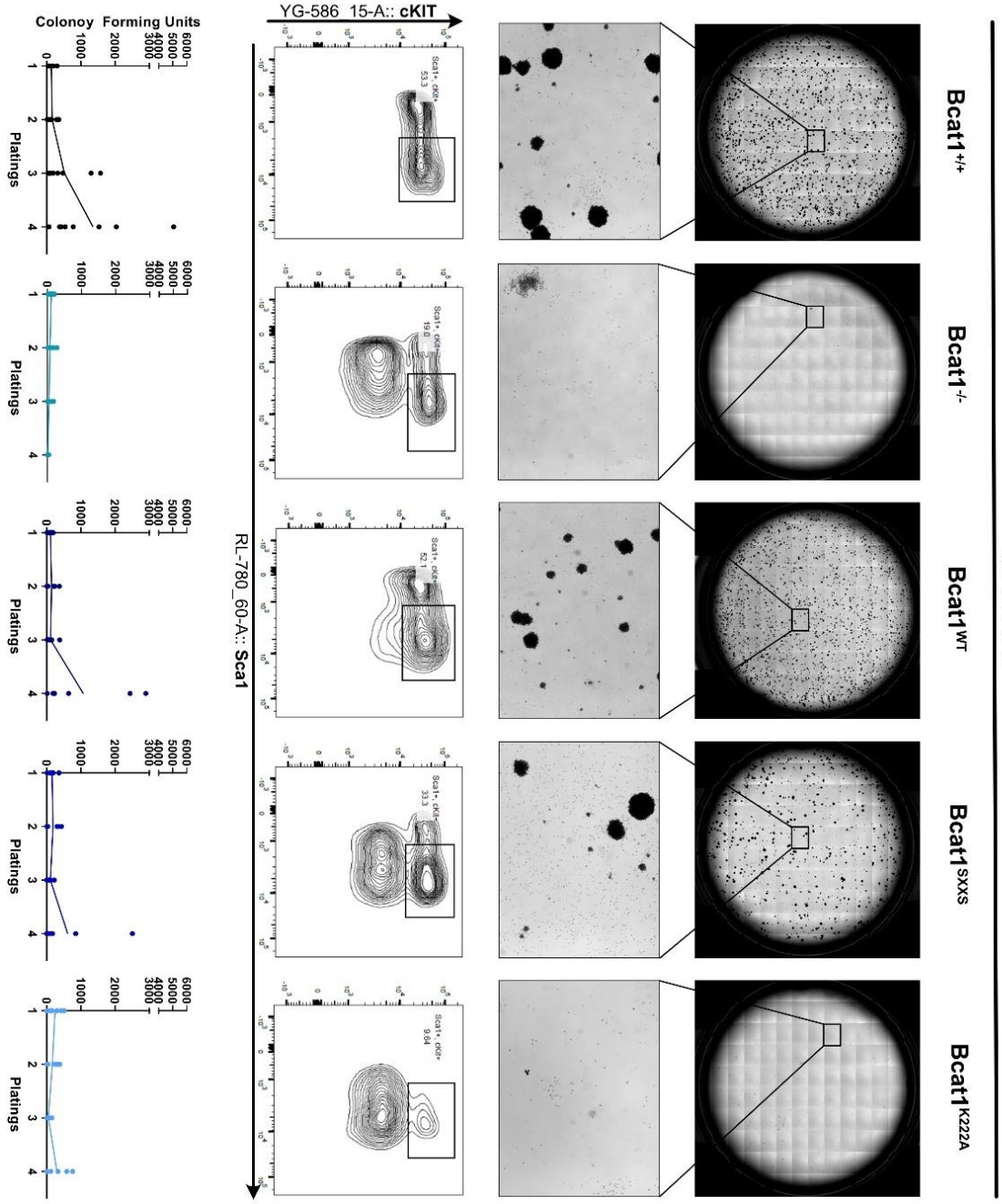

Figure 21 – Tumorigenic potential of Bcat1$^{-/-}$ HSPCs with *MLL-AF9* can be rescued by adding Bcat1^{WT} but not with the metabolic dead mutant. Representative images of colonies at the endpoint (4th plating) of the CFU show that Bcat1$^{+/+}$ HSPCs as well as Bcat1$^{-/-}$ HSPCs rescued with Bcat1^{WT} construct or redox dead Bcat1^{SXXS} mutant form dense colonies when transduced with *MLL-AF9*. FACS analysis simultaneously verified the LSC population's rescue (GFP^{+}, CD45^{+}, Lin^{-}, cKIT^{+}, Sca1^{+}) for these cells. Bcat1$^{-/-}$ HSPCs transduced with *MLL-AF9* and metabolic dead Bcat1 mutant (Bcat1^{K222A}) barely show any to no colonies. Furthermore, only a few LSCs (GFP^{+}, CD45^{+}, Lin^{-}, cKIT^{+}, Sca1^{+}) can be observed at the 2nd plating of these cells. The last row shows the full CFU assay in detail for all rescues. ($N_{WT/KO}$= 8; $N_{Rescues}$= 6)

The Bcat1^{SXXS} mutant construct showed a delayed rescue capability (Figure 22), potentially due to this mutant's slightly reduced metabolic activity compared to Bcat1$^{+/+}$ (François Martín del Campo, 2019). This delay was also seen using surface markers to analyze the cell types via FACS, as many but not the majority of cells were LSCs at the 2nd Plating (Figure 21).

Strikingly, the metabolic dead Bcat1^{K222A} did not possess the capability to rescue the transformation phenotype, resulting in mainly single cells and loose CFU-GM colonies similar to Bcat1$^{-/-}$ cells (Figure 21 and Figure 22). Furthermore, barely any LSCs could be detected following Bcat1^{K222A} rescue, verifying the importance of Bcat1 metabolic activity during *MLL* fusion-driven tumor development.

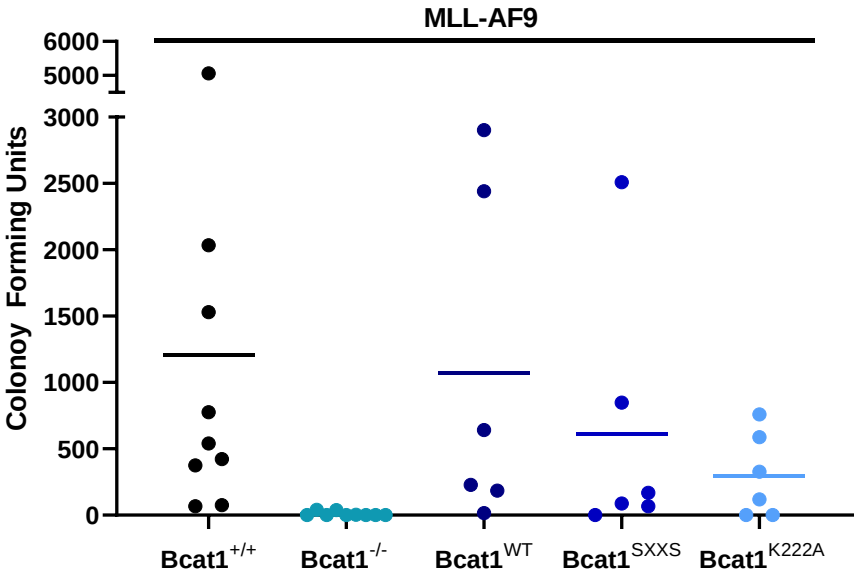

Figure 22 – Rescue of colony-forming potential using *Bcat1* WT, redox dead SXXS, and metabolic dead K222A mutant constructs in Bcat1$^{-/-}$ HSPC transduced with *MLL-AF9* fusion. After transduction with the *MLL-AF9* fusion gene, Bcat1$^{+/+}$ HSPCs gain an unlimited colony-forming potential. The lack of this transformation of Bcat1$^{-/-}$ HSPCs in a CFU can be rescued by introducing a Bcat1^{WT} construct. The rescue effect is slightly delayed when adding a redox mutant (Bcat1^{SXXS}) to Bcat1$^{-/-}$ HSPCs and completely diminished when using a metabolic mutant of *Bcat1* (Bcat1^{K222A}). At the 4th plating, Bcat1$^{+/+}$ HSPCs form on average 1209 colonies, while 9 Bcat1$^{-/-}$ colonies were observed. Bcat1$^{-/-}$ HSPCs transduced with MLL-AF9 and a Bcat1^{WT} construct almost fully rescue the colony-forming ability with an average of 1069 colonies. The redox mutated Bcat1^{SXXS} shows a delayed rescue potential (614 colonies) and metabolic dead Bcat1^{K222A} with minimal rescue capabilities (299 colonies). ($N_{WT/KO}$= 9; $N_{Rescues}$= 6; 4th Plating)

In summary, these CFU assays identified BCAT1 as essential for MLL fusion-driven transformation, and rescue mutants showed the importance of its enzymatic transaminase activity, indicating a mechanistic role during leukemogenesis.

4.5. Bcat1$^{-/-}$ drives HSPCs towards cell cycle arrest

4.5.1. RNA-seq analysis identifies differentially expressed genes

To better understand the role Bcat1 plays in oncogenic transformation, I performed ultra-low RNA-seq of Bcat1$^{+/+}$ HSPCs and Bcat1$^{-/-}$ HSPCs at the beginning as well as during the CFU assay. In this analysis, I included Bcat1$^{-/-}$ transduced with rescue Bcat1^{WT} construct in order to exclude any expression differences unrelated to BCAT1. I conducted the analysis in biological duplicates.

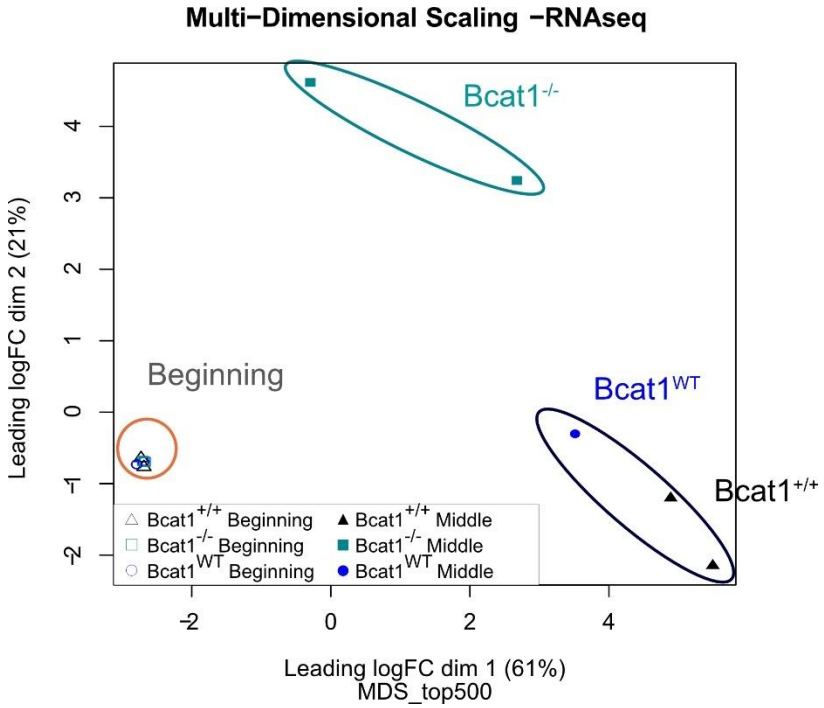

Figure 23 – Multi-dimension plot reveals clustering of CFU samples based on their *Bcat1* status. Phenotypic differences are supported by differential expression profiles identified by ultra-low RNAseq. HSPCs cluster tightly together at the beginning of the CFU, independent of their *Bcat1* status or sample's origin. Over time, Bcat1$^{+/+,}$ as well as the Bcat1^{WT}-rescue expression profiles drift apart from Bcat1$^{-/-}$ and the original HSPCs. Bcat1$^{-/-}$ expression programs show the highest differences to the self-renewing HSPCs at the beginning. This multi-dimension scaling was performed based on the 500 most differentially expressed genes.

At the beginning of the CFU, Bcat1$^{+/+}$, Bcat1$^{-/-}$, and Bcat1^{WT} HSPCs exhibited an almost indistinguishable expression profile, even though the cells originated from different donor animals. Multi-dimensional scaling (Figure 23), and differential gene expression analysis (Figure 24), highlight these similarities based on the 500 most differentially expressed genes. Furthermore, in supervised clustering analysis, these samples cluster primarily according to time points and secondarily to their *Bcat1* status (Figure S11). Strikingly, the only significant differentially expressed gene at the beginning is *Bcat1* (logFC=-4.3 and

false discovery rate (FDR)=1.8*10^{-12}), verifying a successful knockout as well as a very homogeneous starting point for this assay (Figure 24).

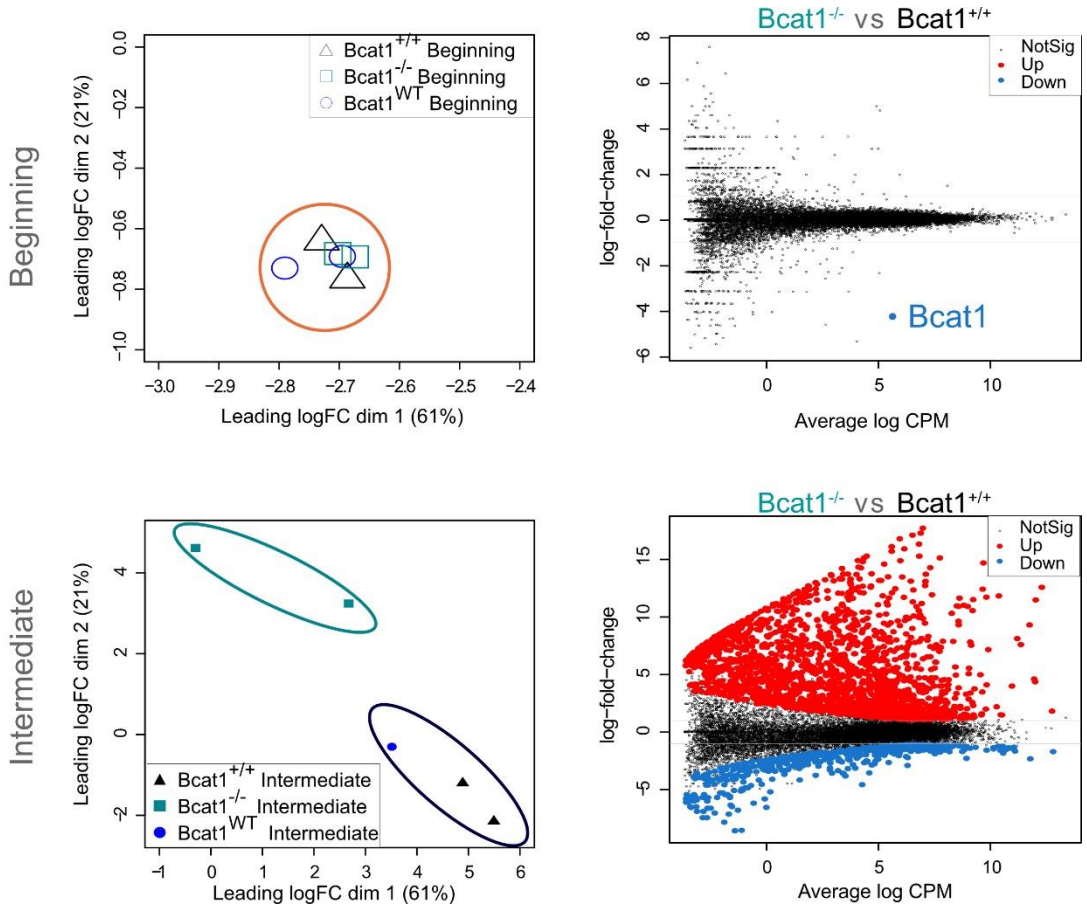

Figure 24 –Bcat1$^{+/+}$ and Bcat1$^{-/-}$ show vastly altered expression profiles. At the beginning of the CFU, all samples cluster tightly together in a multi-dimension analysis based on the 500 differentially expressed genes. Analysis of all expressed genes reveals *Bcat1* (logFC= -4.3; FDR=1.8*10^{-12}) as the only significantly reduced transcript within all HSPC samples independent of their origin (mean-difference plot of log-intensity ratios in upper panel). The lower panel highlights the vast differences in expression between transformed Bcat1$^{+/+}$ and non-transformed Bcat1$^{-/-}$ at an intermediate time point. With 2082 significantly upregulated (red) and only 518 significantly downregulated transcripts, Bcat1$^{-/-}$ exhibits a global expression increase. Not significantly expressed genes are shown in black (right side) with a cutoff value logFC=1 and FDR=0.05.

Over time Bcat1+/+ and Bcat1-/- expression profiles drifted apart, resulting in a vastly different transcription program. As observed in the multi-dimensional analysis (Figure 23), duplicates group together while the different conditions of the intermediate time point show an altered expression profile. While Bcat1-/- cells did not transform in the CFU assay, a global upregulation of gene transcription was observed, as highlighted in the mean-difference plot of Figure 24 (lower panel).

Unfortunately, one replicate of Bcat1$^{-/-}$ transduced with rescue Bcat1^{WT} construct lost the Bcat1^{WT} rescue expression over time and exhibited an expression profile identical to Bcat1$^{-/-}$ samples at the intermediate time point. Therefore, this replicate was excluded from further analysis. However, the rescue sample expressing Bcat1^{WT} exhibited an expression profile very similar to Bcat1$^{+/+}$ samples verifying that BCAT1 is the key to these transcriptional changes.

	Significant **Up**	Significant **Down**
Bcat1$^{+/+}$	776	1242
Bcat1$^{-/-}$	799	436
Bcat1^{WT}	849	676

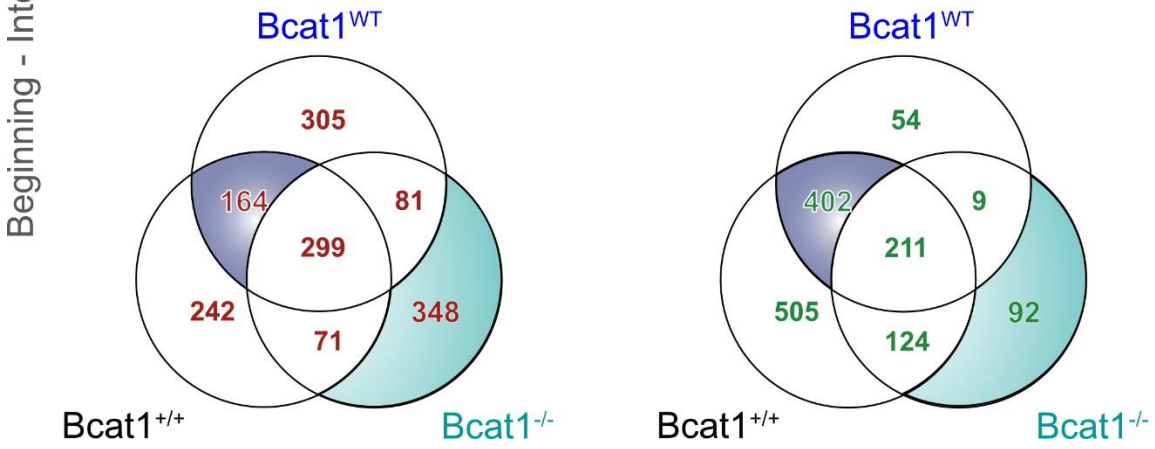

Figure 25 – Expression profile differences over time: individually and in comparison to other conditions. The table on top shows the number of highly significant differentially expressed genes in the intermediate samples. Very stringent cutoffs were applied for this data: logFC= +/-4, FDR=0.01. Genes are separated in up and down-regulated expression in individual conditions. For instance, the expression of 776 genes increased in the intermediate Bcat1$^{+/+}$ sample, while the expression of 1242 genes was reduced. In Bcat1$^{-/-}$, I observed the opposite tendencies: 799 genes were upregulated at the intermediate time point, while 436 genes were downregulated. The Venn diagrams on the bottom of the figure compare the previously identified differentially expressed genes with the other conditions. The upregulated genes are plotted on the left side in red, and the downregulated ones are on the right in green. The colored fields are particularly relevant in this setting: The dark blue area shows all genes that overlap between Bcat1$^{+/+}$ and Bcat1^{WT} rescue but is not found in Bcat1$^{-/-}$. Turquoise highlights the genes exclusively up or downregulated in Bcat1$^{-/-}$ at the intermediate time point.

In the next step, I compared the expression profiles over time within and between conditions. As shown in Figure 25, even with stringent cutoff criteria (logFC ≥ +/-4, FDR ≤ 0.01), a variety of genes were found up and down-regulated. While the library sizes of all samples were similar and normalization was performed, the number of differentially

expressed genes deviated between the conditions. At the intermediate time point of the CFU assay, downregulation of genes seemed to be more pronounced in Bcat1$^{+/+}$ than Bcat1$^{-/-}$ with 776 significantly upregulated and 1242 significantly downregulated genes. Bcat1$^{-/-}$ exhibited about the same number of upregulated genes but a reduced number of downregulated genes. The number of downregulated genes in the intermediate Bcat1^{WT} rescue was in-between the two other conditions.

These highly differentially expressed genes were further compared between all conditions. In total, 510 genes were equally regulated over time, independent of the Bcat1 status. Particularly interesting are the 566 genes (164 up, 402 down; Table S2) that were significantly differentially expressed in both Bcat1$^{+/+}$ and Bcat1^{WT} conditions but were not altered in Bcat1$^{-/-}$. The 440 genes (348 up, 92 down; Table S3) differentially expressed exclusively in Bcat1$^{-/-}$ were investigated further.

4.5.2. GSEA indicates repression of DNA replication and cell cycle pathways during tumor development

I performed a gene set enrichment analysis (GSEA) to identify the relevant changes within a condition over time and between Bcat1$^{+/+}$ and Bcat1$^{-/-}$ during tumor development. When comparing expression profiles of HSPCs at different time points, pathways associated with virus transfection or immune response exhibited genes with highly differentially expression (Figure S12, Figure S14, Figure S16). Among other pathways, COVID-19, Hepatitis C, and viral protein interactions were activated in the early samples due to viral transfections of *MLL-AF9* and Bcat1^{WT} constructs. Therefore, they were excluded from further consideration.

Interestingly, almost all significantly regulated pathways in the intermediate-time point Bcat1$^{-/-}$ were repressed, despite the observed global activation of transcription. The most significantly altered KEGG pathways exclusively found upon comparing Bcat1$^{-/-}$ over time showed DNA replication (mmu03030) and cell cycle (mmu04110) pathways reduced. Gene ontology (GO) gene set enrichment analysis highlighted identical terms.

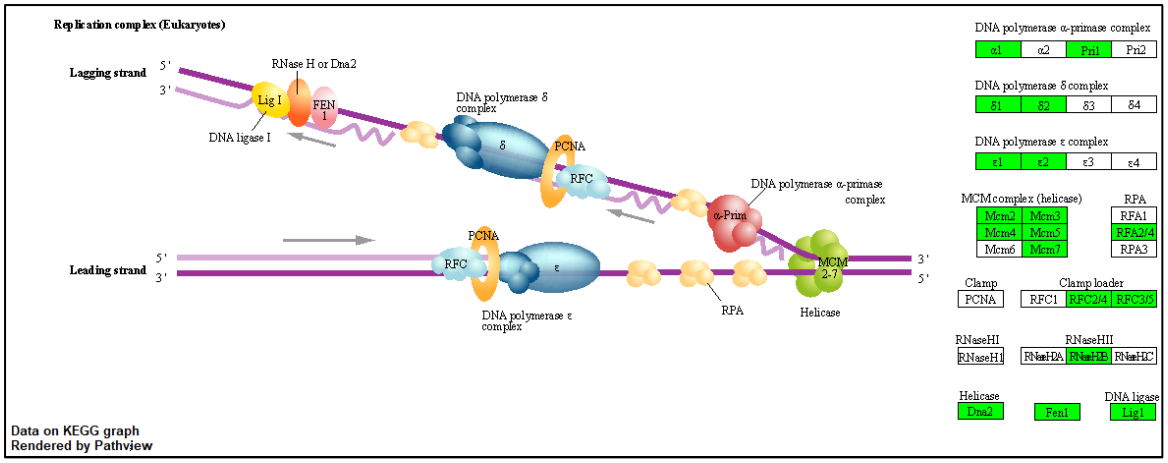

Figure 26 – Gene expression of Bcat1$^{-/-}$ over time in the eukaryotic DNA replication, sectioned from the KEGG DNA replication pathway (mmu03030). The multistep DNA replication process entails a complex network of interacting proteins. At the DNA replication fork, the DNA helicase (MCM complex) supported by the RPA unwinds the duplex parental DNA. The DNA synthesis machinery forms a permanent complex with a DNA polymerase as well as the clamp PCNA and clamp loader RFC. FEN1 and RNase H2 remove the RNA on the lagging strand, and DNA ligase joins the Okazaki fragments (Stillman, 1994). The comparison between early and intermediate time points of Bcat1$^{-/-}$ showed almost every complex downregulated (green) over time. Each of the three known polymerase complexes showed the repression of two components. Additionally, almost all *MCM* complex components were downregulated. Subunits of RPA and the clamp loader RFC are reduced. In the formation of the lagging strand RNAaseHII, helicase DNA2, FEN1, and DNA ligase are affected. Bcat1$^{-/-}$ resulted in a global suppression of this pathway over time. The complete mmu03030 pathway is shown in the supplements (Figure S13) [Dna2: DNA Replication Helicase/Nuclease 2; Fen1: Flap Structure-Specific Endonuclease 1; Lig1: DNA Ligase1; MCM: Minichromosome Maintenance; RFC: Replication Factor C; RPA: Replication Protein A]

As DNA replication is a vital part of the cell cycle, both pathways, as shown in Figure 27 and Figure 26, contain the minichromosome maintenance (MCM) complex, which consists of various downregulated subunits. This hexameric protein complex regulates the helicase activity of the pre-replication complex. In addition to MCM complex components (*Mcm*2-5 and 7), the expression of a variety of DNA polymerase complex components was also reduced. Downregulation, as observed in the intermediate Bcat1$^{-/-}$ samples, resulted in the suppression of DNA replication and hence, cell proliferation. The inhibition of cell proliferation matches the observed phenotype in Bcat1$^{-/-}$, which loses colony formation capability over time.

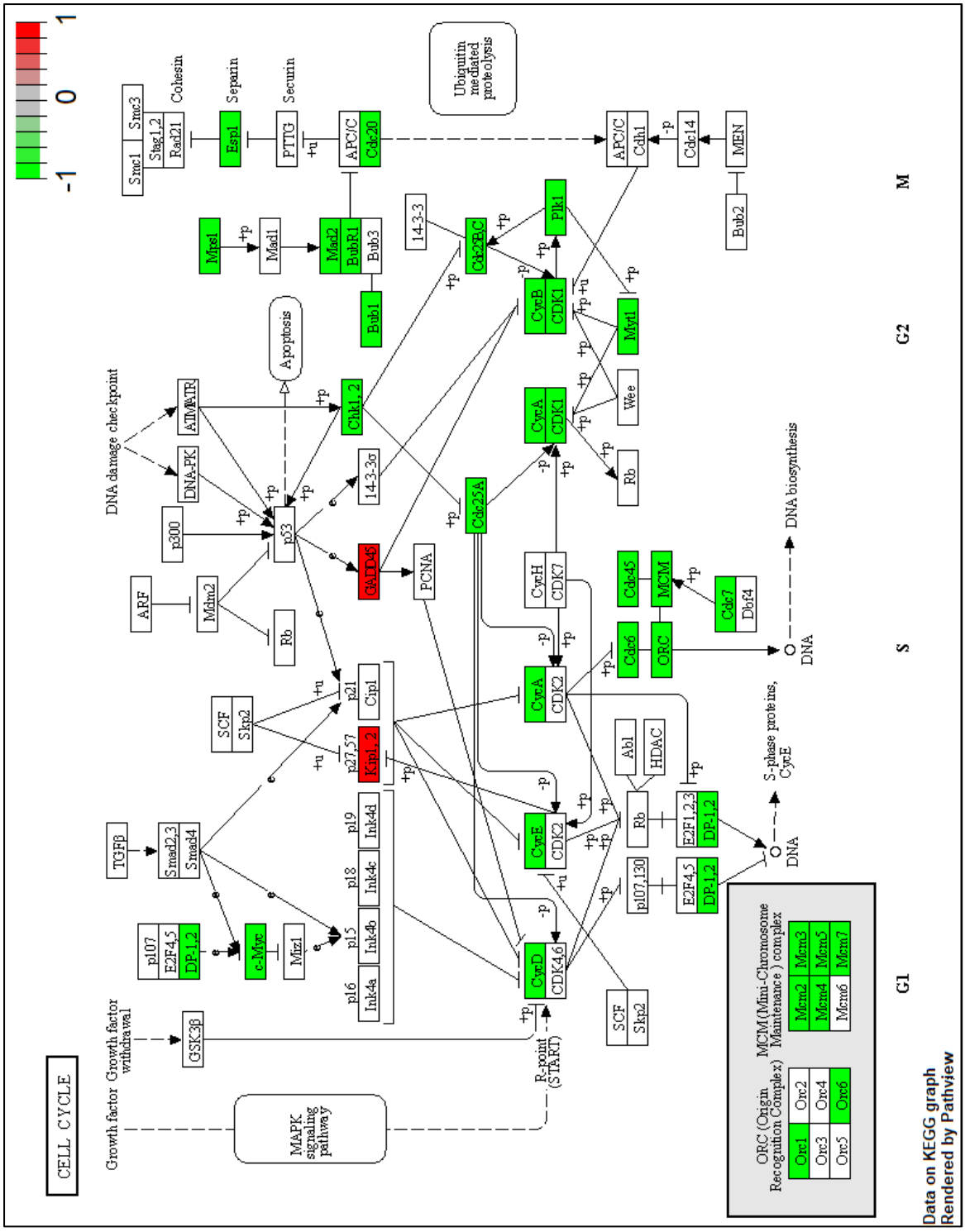

Figure 27 – Gene expression of Bcat1$^{-/-}$ over time in the KEGG pathway cell cycle (mmu04110) The mitotic cell cycle progression is defined by S-phase (DNA replication) and M-phase (mitosis) separated by G1 and G2-phases (gaps). The cell cycle pathway consists of a highly complex sequence of reactions, interactions, and protein modifications. For instance, cyclin-dependent kinases, such as the CDK1, are key regulator enzymes mediating the process through the cell cycle by the availability of substrates. On the other hand, CDK inhibitors are involved in the negative regulation of the cell cycle. For instance, CDKN1c (KIP1) reduces the activity of CDK2, altering the cell's procession. Furthermore, a variety of enzymes in this pathway, such a checkpoint kinases CHK1 and 2, are able to sense DNA damage and respond accordingly. In this pathway, the expression of numerous genes is altered in Bcat1$^{-/-}$ over time. Most downregulated genes are positive regulators, while at least one of the two upregulated genes is a negative one. All differentially expressed genes and their functions are listed in Table S4.

The global downregulation of expression in genes associated with various stages of the cell cycle, as shown in the KEGG pathway mmu04110, is more complex to interpret: The cell cycle pathway contains a variety of checkpoint proteins, which in parts harbor dosage-dependent functions or play multiple roles throughout the cell cycle. A detailed list of genes altered in Bcat1$^{-/-}$ over time and their functions are shown in Table S4.

Remarkably, almost all downregulated genes, such as cell division cycle genes and cyclin-dependent kinases, are associated with regulatory functions, essential for cell cycle progression. In contrast, the only two upregulated genes in this pathway, cyclin-dependent kinase inhibitor 1 (*Cdkn1*, *Kip1*) and growth arrest and DNA damage-inducible gamma (*Gadd45g*), are connected to cell cycle inhibition and growth arrest.

Comparing Bcat1$^{+/+}$ over time does not reveal a significant expression difference of genes involved in the DNA replication machinery or cell cycle processes. However, KEGG pathway hematopoietic cell lineage (mmu04640, Figure S15) was significantly suppressed. This pathway highlights that particular surface markers associated with cell differentiation were downregulated. For instance, the macrophage marker *Cd11b* (*Itgam*), monocyte lineage marker *Cd115* (*Csf1r*), and the granulocyte-macrophage marker *Cd116* (*Csf2ra*) were found to be downregulated in the intermediate Bcat1$^{+/+}$ samples. The lack of differentiation marker expression in the intermediate Bcat1$^{+/+}$ samples represents the LSC expression profile.

These pathway analyses suggest that HSPCs expressing *Bcat1* developed into tumorigenic LSCs in the presence of oncogenic fusion MLL-AF9. In contrast, the cell cycle of HSPCs lacking *Bcat1* is inhibited instead of proceeding with transformation and tumor development. The knockout of *Bcat1* seems to come into effect only in cancerogenic cell cycle progression during tumor development but not in HSPC upkeep.

4.6. Activating histone modifications and MLL fusion binding

The expression profile analysis of Bcat1$^{+/+}$ and Bcat1$^{-/-}$ at the beginning and during the CFU identified DNA replication and the cell cycle as the major differentially suppressed pathways. This implicates the lack of Bcat1 as relevant for cell cycle arrest.

To support the RNAseq analysis' conclusions and identify possible BCAT1-to-MLL fusion feedback, I investigated activating histone modifications and MLL fusion binding in Bcat1$^{+/+}$, Bcat1$^{-/-}$, and Bcat1^{WT} at the intermediate time point. As the CFU yielded a limited amount of cells, antibody-guided chromatin tagmentation (ACT-seq) for low cell numbers

was used (Carter et al., 2019) to analyze changes in histone modifications H3K4me3, H3K27ac, and H3K79me2 as well as the Flag-tagged oncogene MLL-AF9.
In brief, a purified fusion complex consisting of transposase Tn5 and protein A carries the transposon, a DNA adapter (Figure 28). The antibody of interest is bound by the protein A subunit and directs the complex to the relevant antigen defining the target DNA. Here the transposon is inserted and can be amplified without inefficient pulldown methods.

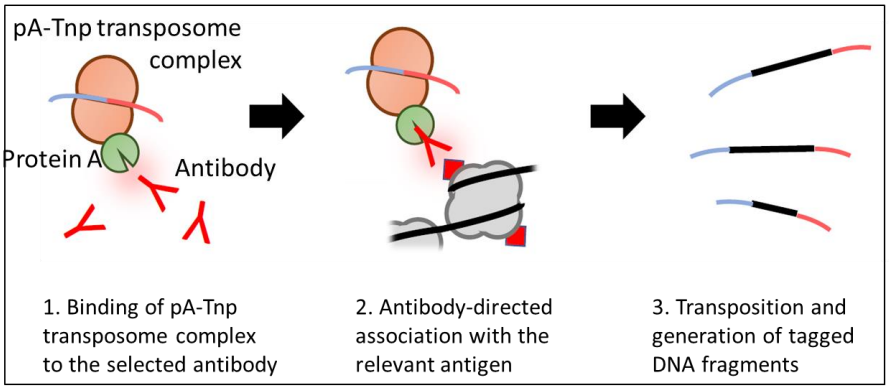

Figure 28 – Schematic of antibody-guided chromatin tagmentation method (ACT-seq). A synthetic fusion protein consisting of the transposase Tn5 and protein A binds transposons. This pA-TnP is able to attach to the antibody of interest, which in turn guides the complex to its antigen. At this site, the enzyme cuts the DNA and inserts the transposon, which can be directly amplified. [pA= Protein A; TnP= transposase Tn5]

Because of the low peak heights provided by this method, data analysis of ACT-seq turned out to be very complex. Nonetheless, I was able to associate histone modifications with the expressional differences previously observed in most DNA replication and cell cycle pathway genes. For instance, the promoter region of *Gadd45g*, a direct target of the tumor suppressor TP53, exhibited exclusive modification of H3K27ac in the intermediate Bcat1$^{-/-}$ (Figure S17). This histone modification is associated with open chromatin, enabling transcription factor binding and the observed upregulation of this gene. In contrast, the H3K27ac of the *Mcm* components were similar in all samples. However, Bcat1$^{+/+}$ and Bcat1^{WT} showed binding of MLL-AF9 and/or its associated H3K79me2 in almost all *Mcm* genomic regions (Figure S17). The lack of MLL-AF9 binding and H3K79me2 at the *Mcm* genomic regions in the intermediate Bcat1$^{-/-}$ could explain the lack of *Mcm2-5* and *Mcm 7* expressions.

Even though difficult to interpret, ACT-seq data does support the general findings previously described with RNA-seq data.

4.7. A mouse model for Bcat1-dependent leukemogenesis

I was able to show that BCAT1 is essential for *MLL* fusion-driven leukemogenesis *in vitro*. Bcat1$^{-/-}$ HSPCs lack the LSC forming potential provided by *MLL* fusion genes observed in Bcat1$^{+/+}$. Ultra-low RNA sequencing showed minimal differences at the onset of this experiment but profound expression changes at the intermediate time point. Gene set enrichment analysis of the most differentially expressed genes suggested cell cycle arrest initiated by the lack of Bcat1. To further support my *in vitro* findings, I have been testing my hypothesis in an AML mouse model.

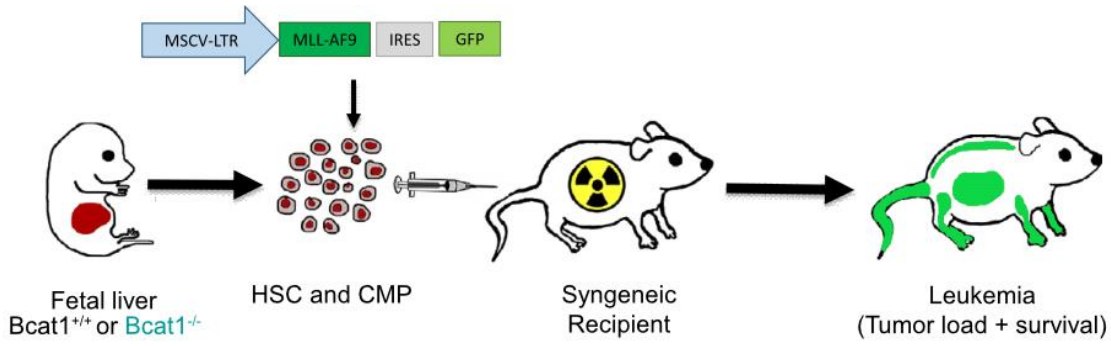

Figure 29 – Schematic representation of ongoing mouse model investigating the dependency of AML development on Bcat1 *in vivo*. Fetal liver stem and progenitor cells harvested from Bcat1$^{+/+}$ and Bcat1$^{-/-}$ mice were transduced with *MLL-AF9*. These cells were transplanted in sublethally irradiated wildtype mice, and tumor development was measured.

In this pilot experiment, I isolated the liver of Bcat1$^{+/+}$ and Bcat1$^{-/-}$ E12.5 fetuses to harvest HSPCs. These HSPCs were transfected with MLL-AF9 fusion genes and transplanted into sublethal and lethal irradiated wildtype recipient mice. Additionally, Bcat1$^{+/+}$ HSPCs were used for the reconstitution of bone marrow in all conditions. I am following tumor development by FACs analysis of GFP and perform survival analysis.

Interestingly, lethally irradiated mice transplanted with Bcat1$^{-/-}$ pre-tumor cells and reconstituting Bcat1$^{+/+}$ HSPCs did not recover from the irradiation. In contrast, almost all lethally irradiated recipients transduced with Bcat1$^{+/+}$ pre-tumor cells and reconstituting Bcat1$^{+/+}$ HSPCs fully recovered and developed tumor symptoms approximately 77 days after transplantation, as expected. However, this was a pilot experiment with a limited number of mice; therefore, I cannot draw conclusions regarding technical errors or potential biological effects at this point.

Sublethal irradiation of recipient mice reduces toxicity but opens limited space in the bone marrow resulting in a decreased engraftment in this niche (Flomerfelt & Gress, 2016).

Hence, tumor development is delayed, and termination criteria are reached later (Almosailleakh & Schwaller, 2019; Andrade et al., 2011; Frasca et al., 2000). In compliance with this, all mice recovered from sublethal irradiation independent of the condition. 143 days after transplanting Bcat1$^{-/-}$ pre-tumor cells, the first mouse showed symptoms of leukemia, with a spleen weight of 0.55 g, almost 6 times the weight observed in healthy mice. Bcat1$^{+/+}$ leukemia caused symptoms in a mouse after 170 days, and a spleen of 1.0 g was measured. At this point in the pilot experiment, 10 recipient mice (5 vs. 5) have not reached terminal criteria. As the *in vivo* verification is ongoing, no biological or technical conclusion can be drawn at this time.

5. Discussion

In cancer, BCAA metabolism is frequently activated through the increased uptake (second only to glutamine) of valine, leucine, and isoleucine (Jain et al., 2012), as well as the overexpression of *BCAT1*, the cytoplasmic BCAA transaminase. We and others showed that proliferation, migration, and chemoresistance of a variety of cancer entities, such as glioblastoma, breast cancer, and myeloid leukemia, are heavily reliant on *BCAT1* expression (Hattori et al., 2017; Raffel et al., 2017; Thewes et al., 2017; Tönjes et al., 2013).

Epigenetic gene regulation and metabolism are interdependent, as many cellular enzymes and processes require substrates and cofactors provided by metabolic reactions. For example, in cancer, the upregulation of *BCAT1* depletes its substrate α-KG and results in the reduced activity of α-KG-dependent enzyme EGLN1, a prolyl-hydroxylase that regulates HIF1A stability (Raffel et al., 2017). Furthermore, DNA hypermethylation is observed upon *BCAT1* suppression of AML, suggesting an α-KG-dependent effect on the TET-family DNA demethylases (Raffel et al., 2017). However, the connection to other epigenetic regulators such as histone demethylases and histone methyltransferases and their effect on AML-cell transformation has not been addressed.

With this thesis, I aimed to unravel the interdependencies of BCAT1 and chromatin modifiers, as well as to discover the role of Bcat1 during the development of MLL fusion-mediated leukemia.

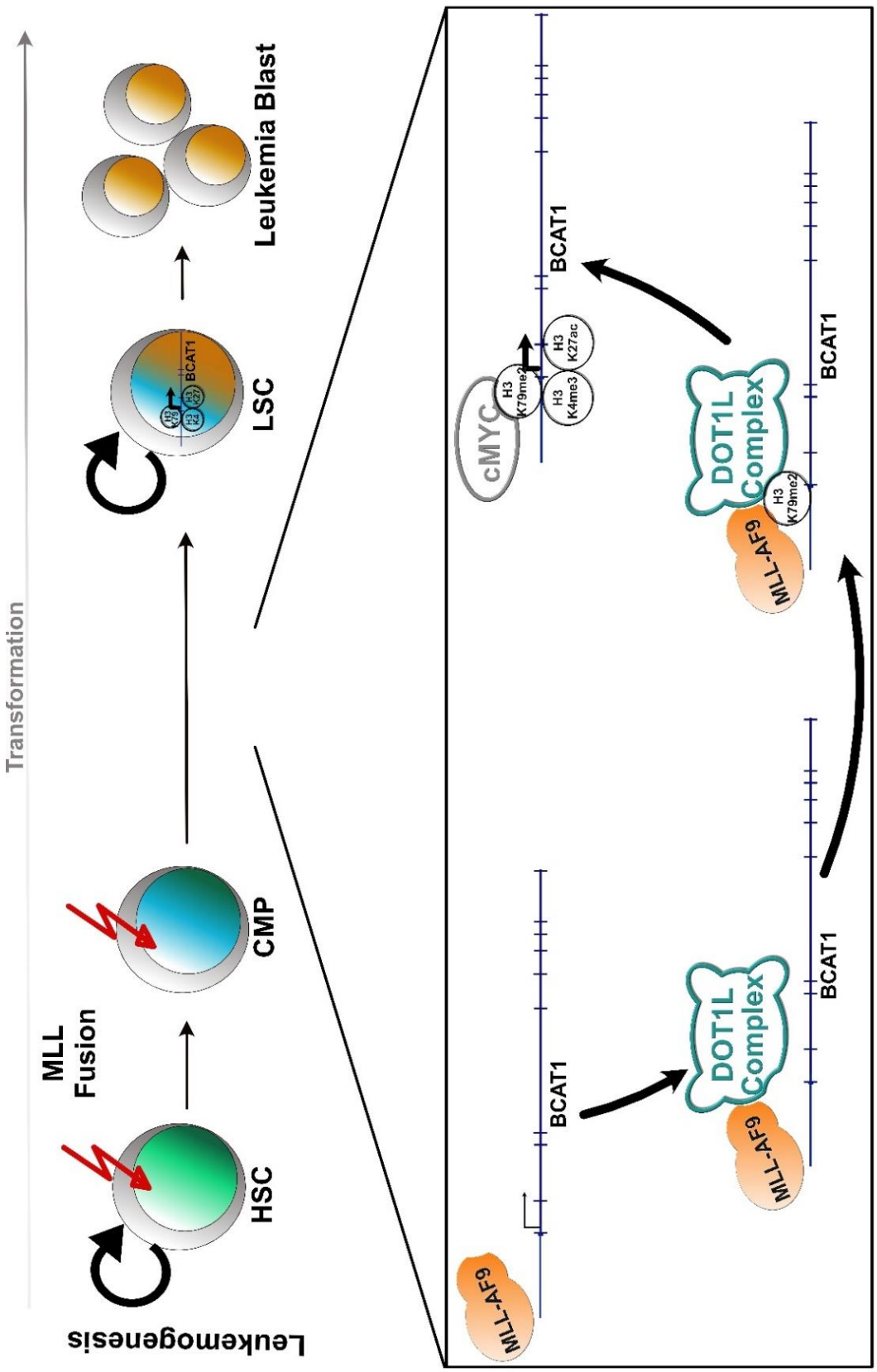

Figure 30 – Graphical summary of the findings in this thesis. Translocations of *MLL* generate oncogenic fusion proteins capable of transforming HSCs or CMPs into LSCs. Fusion proteins such as MLL-AF9 recruit the DOT1L complex to gene regions causing misguided gene regulation. I showed that *BCAT1* is a novel MLL fusion target and that its oncogenic upregulation by DOT1L mediated histone modifications. This upregulation of *BCAT1* and its transaminase activity is essential for the transformation of HSCPs into LSCs, and AML development. The lack of *Bcat1* results in the inhibition of DNA replication and cell cycle arrest**.**

5.1. Differential effects of *BCAT1* suppression on histone modifications

Epigenetic gene regulation and metabolism are extensively interconnected, as the activities of many chromatin modifiers are partially regulated by the concentrations of their essential metabolic substrates or cofactors (Lu & Thompson, 2012). For instance, the TET family of DNA demethylases and the Jumonji-C domain-containing histone demethylase family relies on α-KG, oxygen, and Fe (II) (Klose & Zhang, 2007; Shinsuke et al., 2011; Yu-Fei et al., 2011).

α-KG is a metabolite of the TCA cycle and a substrate of transaminase reactions in the catabolism of BCAAs and other amino acids (Chowdhury et al., 2011; Ichihara & Koyama, 1966; Taylor & Jenkins, 1966; Thirstrup et al., 2011). Tumor-associated mutations in metabolic enzymes highlight the importance of α-KG in cancer. Isocitrate dehydrogenase 1 (*IDH1*) and *IDH2* are two frequently mutated enzymes in low-grade gliomas (Yan et al., 2009), adult *de novo* AML (Mardis et al., 2009; Ward et al., 2010), and other cancer entities (Amary et al., 2011; Cairns et al., 2012). These mutations result in the production of 2-hydroxyglutarate (2HG), a structural analog of α-KG (Dang et al., 2009; Ward et al., 2010). Tumors harboring IDH mutations exhibit patterns of global DNA hypermethylation (Figueroa et al., 2010; Noushmehr et al., 2010). due to inhibition of TET methylcytosine dioxygenase 2 (TET2) by 2HG (Turcan et al., 2012)

Furthermore, 2HG has the potential to competitively inhibit the activity of more than 60 α-KG-dependent human enzymes (Chowdhury et al., 2011; Loenarz & Schofield, 2008). Thus, the inhibition of several histone demethylases *in vitro* (Chowdhury et al., 2011; Xu et al., 2011) was associated with increased repressive histone modifications H3K9me3 and H3K27me3 (Lu et al., 2012; Turcan et al., 2012). The resulting failure to differentiate is solely driven by these histone modifications in IDH-mutated cells and not DNA hypermethylation (Lu et al., 2012; Ohm et al., 2007; Widschwendter et al., 2007).

In AML without IDH or TET mutations but high BCAT1 expression, global DNA hypermethylation also has been proposed to result from BCAT1-mediated α-KG depletion and consequential inactivation of DNA demethylases (Raffel et al., 2017). Based on these findings, I hypothesized that BCAT1/α-KG-dependent regulation extends to histone demethylases. To investigate this connection between *BCAT1* and histone-modifying enzymes, I performed RNA and ChIP-seq analysis of a mammary carcinoma xenograft model.

I purposefully chose an *in vivo* model to test my hypothesis since epigenetic modifications are highly dynamic and easily influenced by the technical limitations of classical cell culture. For instance, it has been reported that cells in traditional culture exhibit considerably altered epigenetic and expression profiles compared to cells culture in three-dimensional conditions (G. N. Li et al., 2007). Furthermore, cells are dependent on their cellular microenvironment, which includes the secretome, availability of nutrients, cell-cell interactions, and niche specificities, such as hypoxic effects (Begley & Ioannidis, 2015; Bissell & Labarge, 2005; Iyer et al., 1998).

To best possibly account for these confounding effects, I used BCAT1 knockdown and control mammary carcinoma xenograft tumors from our lab's previous work (Thewes et al., 2017). These knockdown tumors exhibited the same severe proliferation phenotype as AML and glioblastoma models. Furthermore, BCAT1 suppression resulted in a significant depletion of cellular α-KG in the transplanted MDA-MB-231 mammary carcinoma cell line in vitro, comparable to our findings in AML and glioblastoma cell lines (Raffel et al., 2017; L. S. Silva et al., 2017). These data support the use of the mammary xenograft material to analyze BCAT1-dependent effects on histone methylation.

ChIP-seq analysis of these tumors revealed differential, histone mark-specific effects upon silencing *BCAT1*. Activating histone marks, such as H3K4me3 and H3K27ac, were enriched, while the repressive modifications H3K9me3 and H3K27me3 were reduced in shBCAT1 tumors. These findings were corroborated by a global rise in RNA transcription in the slow-growing *shBCAT1* tumors.

This histone mark-specific rather than global regulation suggests a complex interdependency of BCAT1 and chromatin modifiers. Hence, I investigated the expression profiles of histone regulators and *BCAT1* in triple-negative breast cancer (GSE142102) and AML patients (TCGA). Both cancer entities' proliferation, migration, and chemoresistance are highly dependent on *BCAT1* (Raffel et al., 2017; Thewes et al., 2017; L. Zhang & Han, 2017). The most apparent correlation in both tumors was found with the histone methyltransferase *MLL*. This relatively unspecific H3K4 methyltransferase is associated with over 5000 human promoter regions playing a pivotal role in gene regulation during development and stem cell maintenance (Cierpicki et al., 2010; Guenther et al., 2005). The catalog of somatic mutations in cancer COSMIC lists a total of 2697 coding mutations and 666 translocation events throughout 33 cancer entities involving the human *MLL* gene (Tate et al., 2019). In my analysis, I found *BCAT1* exceptionally high in AML patients with DNA aberrations, suggesting a connection between the reoccurring *MLL* translocations and *BCAT1* expression in AML.

5.2. *BCAT1* is a novel target of MLL fusion proteins

MLL translocations are found in about 10% of acute leukemia patients (Ayton & Cleary, 2001; Hess, 2004). The chimeric fusion proteins combine the N-terminal MLL protein with one of over 53 known fusion partners (Tate et al., 2019). This recombination results in an in-frame gain of function fusion, which loses the enzymatic activity of MLL (Thiel et al., 2010). The most common *MLL* rearrangements in acute leukemia are *MLL-AF9*, *MLL-ENL*, and *MLL-AF4*. The corresponding fusion proteins drive tumorigenesis by recruiting the DOT1L complex to previously unmodified chromatin regions (Milne et al., 2010; Mueller et al., 2007; Muntean et al., 2010). DOT1L, the only known H3K79 methyltransferase, shapes the chromatin through di-methylation of H3K79, stimulating RNA Pol II (Krivtsov & Armstrong, 2007) and MYC interactions (M. H. Cho et al., 2015), resulting in the misguided activation of self-renewal and stem cell genes (Daigle et al., 2013; Nguyen & Zhang, 2011; Okada et al., 2005; Yamashita et al., 2020).

The heterogeneity of MLL fusion proteins poses a challenge to the development of effective therapies. Hence, targeting MLL fusion protein-dependent pathways through small molecular inhibitors against MLL fusion-interacting proteins or fusion target genes, such as CDK6, has been investigated in recent years (Rao & Dou, 2015; Tsakaneli & Williams, 2021). For instance, *in vivo* and *in vitro* experiments showed that the reduction of H3K79 methylation either by silencing DOT1L or inhibiting its activity by administration of EPZ5676 (Pinometostat) decreased tumorigenic potential in MLL fusion leukemias (C. T. Campbell et al., 2017; Oktyabri et al., 2016; Yamashita et al., 2020; Yang et al., 2019). Even though EPZ5676 is a highly potent and selective amino nucleoside inhibitor of DOT1L (C. T. Campbell et al., 2017; Daigle et al., 2011, 2013), a phase I trial (ClinicalTrials.gov Identifier: NCT02141828) was not able to identify a clinical effect (Shukla et al., 2016). EPZ5676 is currently tested as a combination treatment with Azacytidine (ClinicalTrials.gov Identifier: NCT03701295) and chemotherapy (ClinicalTrials.gov Identifier: NCT03724084). In order to circumvent the shortcomings of EPZ5676 in clinical settings, novel DOT1L inhibitors, such as EPZ004777, were developed and are currently under investigation.

Epigenetic regulation of *BCAT1* was previously demonstrated in the context of gene silencing by IDH mutation-dependent DNA hypermethylation in glioblastoma and AML (Ananieva & Wilkinson, 2018; Mayers et al., 2016; Raffel et al., 2017; Tönjes et al., 2013). However, for breast cancer, an epigenetic mechanism of *BCAT1* activation has been proposed, in which the MLL-DOT1L-complex maintains open chromatin and recruits MYC at the *BCAT1* locus (Oktyabri et al., 2016).

I hypothesized that *BCAT1* expression is activated through *MLL* fusion-mediated DOT1L recruitment and H3K79 methylation. Therefore, I treated two *MLL-AF9* harboring AML cell lines and multiple non-fusion cell lines with two different DOT1L inhibitors (EPZ5676, EPZ004777). *BCAT1* expression continuously decreased with increasing concentrations of each DOT1L inhibitor, identical to established MLL-AF9 target genes HOXA9 and MEIS1 in MLL fusion-harboring cells. In contrast, even with the highest DOT1L inhibitor concentration, the RNA expression of BCAT1 was not altered in the non-fusion cell lines. The findings were verified using Western blot analysis of BCAT1 protein levels.

Strong suppression of proliferation by shBCAT1 knockdown has been demonstrated for several cancers (Hattori et al., 2017; Oktyabri et al., 2016; Raffel et al., 2017; Thewes et al., 2017; Tönjes et al., 2013). Based on our hypothesis of the MLL fusion-DOT1L-BCAT1 axis, we expect a proliferation reduction only in the *MLL-AF9*-mediated AML cell lines treated with DOT1L inhibitors. Both inhibitors resulted in a similar decrease of proliferation upon increasing DOT1L treatment of the *MLL*-fusion cell lines but not the non-fusion counterparts. Interestingly, *shBCAT1* knockdown of MOLM-13, the *MLL-AF9* harboring cell line, was even more sensitive to DOT1L inhibitors. The analysis of BCAT1 in these cells showed that the induced knockdown reduces BCAT1 but does not abolish it entirely. The DOT1L inhibitor treatment of *shBCAT1* MOLM-13 cells results in an additive effect, reducing BCAT1 even further. The non-fusion cell line is neither affected by the *BCAT1* knockdown nor by the combination of knockdown and DOT1L inhibition.

To verify that these phenotypes are directly connected to MLL-AF9 binding and H3K79 methylation, I performed ChIP-PCR. N-terminal MLL (including MLL-AF9) binding and H3K79me2 modifications are exclusively enriched at *HOXA9*, *MEIS1*, and *BCAT1* gene regions in *MLL* fusion mediated AML cell lines. However, the AML cell line without fusion did not show any enrichment.

These data indicate BCAT1 as a new target of the DOT1L complex mediated by MLL-AF9 in MLL fusion leukemias.

5.3. BCAT1 is essential for *MLL* fusion mediated AML development

I was able to elucidate that in leukemias, driven by *MLL* rearrangements, the fusion proteins recruit DOT1L to *BCAT1* gene regions. H3K79me2 alters the chromatin structure at these sites, enabling RNA pol II and MYC to activate gene transcription. As *MLL* translocations in HSPCs initiate tumor development, the gene targets of MLL fusions are

associated with a LCS transcription profile. For instance, the MLL fusion binding to homeobox gene *HOXA9* and *MEIS1* results in gene overexpression directly linked to maintaining self-renewal and immortalization (Chen et al., 2008; Andrei Krivtsov et al., 2006; Placke et al., 2014). Both of these genes, as well as other MLL fusion target genes, are essential transcription factors regulating early differentiation and respectively leukemia development (Cierpicki et al., 2010; Luo et al., 2015; Roden & Lu, 2016). Therefore, I tested the hypothesis that the newly identified MLL target gene BCAT1 is essential for MLL-dependent leukemic transformation.

A colony formation unit (CFU) assay enabled me to track leukemia development mediated by MLL fusions over time. I showed that *MLL-AF9* and *MLL-ENL* could transform HSPCs into myeloid leukemia cells, concordant with previous studies (Hattori et al., 2017; Somervaille & Cleary, 2006; Stavropoulou et al., 2016). In contrast, neither fusion gene could maintain the immortalization of HSPCs harvested from a *Bcat1* knockout (Bcat1$^{-/-}$) mouse in this serial replating experiment. A similar but less extreme phenotype was observed in chronic myeloid leukemia (CML) by others, in which Bcat1 knockdown or inhibition of Bcat1 by Gabapentin treatment resulted in smaller colonies and 40-60% reduction in colony-forming ability (Hattori et al., 2017).

Further analysis revealed that both MLL-AF9 and MLL-ENL in *Bcat1*-expressing (Bcat1$^{+/+}$) HSPCs produced mostly LSCs. Interestingly, previous reports have described *BCAT1* to predominantly be overexpressed in these chemoresistant LSCs as well as relapse tumors (Hattori et al., 2017; Raffel et al., 2017), supporting my findings. Besides a minimal overall cell number, Bcat1$^{-/-}$ exhibited only a very small subpopulation of LSC-like cells after the second plating. This was visible in the colony morphology –dense and compact for Bcat1$^{+/+}$ and loose granulocyte-macrophage (GM)-like colonies with Bcat1$^{-/-}$– as well as in surface marker stainings with flow cytometry.

The high variance between replicates observed in this assay might be explained by the cells of origin. *In vivo* observations could show that AML derived from progenitor cells is less aggressive than its stem cell-derived counterpart (George et al., 2016; A V Krivtsov et al., 2013; Uckelmann et al., 2020). In this, as well as the following assays, hematopoietic stem and progenitor cells were transduced with MLL-fusion genes, resulting in varying aggressive colony growth. Nonetheless, a clear difference in *Bcat1*-dependent leukemogenesis was observed.

I repeated the CFU as a rescue experiment that included a *Bcat1* wildtype (Bcat1^{WT}) construct, a redox-dead *Bcat1* mutant (Bcat1^{SXXS}), and a metabolic dead *Bcat1* mutant (Bcat1^{K222A}). As previously stated, Bcat1$^{+/+}$ HSPCs transfected with *MLL-AF9* transformed

into tightly clumped LSC colonies, while Bcat1$^{-/-}$ HSPCs did not maintain immortality. The Bcat1^{WT} rescue protein ultimately recovered this phenotype in *Bcat1* knockout HSPCs. Colony numbers, colony type, and cell surface markers were equal to Bcat1$^{+/+}$.

The redox-dead Bcat1^{SXXS} construct did not fully rescue the knockout phenotype. My colleague Liliana François was able to show that the redox-dead Bcat1^{SXXS} construct lost all its redox activity. However, as the CXXC guards the entrance to the metabolic pocket of Bcat1, a reduction of enzymatic activity accompanied the mutations from cysteine (335, 338) to serine (Coles et al., 2012; François Martín del Campo, 2019; N. H. Yennawar et al., 2006). The findings of the CFU support the idea that this educed enzymatic activity might explain the slower growth of Bcat1^{SXXS} cells and I speculate that two more platings could have achieved the complete transformation towards LSCs.

The Bcat1^{K222A} mutant cannot bind the necessary cofactor PIP, and therefore, no metabolic activity was measured (François Martín del Campo, 2019; Kingsbury et al., 2015). The lack of transaminase activity is enough to render the rescue inefficient. This metabolic-dead rescue protein produced only small, loose colonies with barely any LSC-like cells, very similar to Bcat1$^{-/-}$.

While these findings clearly show that *Bcat1* expression and its transaminase activity are essential for *MLL* fusion-mediated AML development, the CFU assay harbors limitations. On the one hand, high variances between biological replicates complicate interpretation, and on the other hand, a low cell number in certain conditions restricts further analysis. Furthermore, multiple studies were able to show that *in vivo* settings do not always align with *in vitro* experiments. All three shortcomings are tackled in the ongoing pilot study of an AML development mouse model.

5.4. CFU reveals expression differences driven by BCAT1

To better understand the mechanistic processes that make BCAT1 essential for MLL fusion-driven AML development, I characterized Bcat1$^{+/+}$ and Bcat1$^{-/-}$ HSPCs at the beginning and towards the middle of the experiment by gene expression and chromatin modification analysis. In order to reduce the general effects of *Bcat1* knockout, the Bcat1^{WT} rescue was included in this analysis. One of the challenges in characterizing these samples was that Bcat1$^{-/-}$ HSPCs did not attain immortality resulting in small loose colonies and a deficient overall cell number. To accommodate the low material input, I performed ultra-low RNA-seq and ACT-seq, a technique using a tagmentation method to identify

transcription factor binding and chromatin modifications of interest in a minimum of cells (Carter et al., 2019). Additional to these specific methods, the latest possible time point was after the second plating, as not enough Bcat1$^{-/-}$ cells proliferated until the endpoint of the experiment.

The multidimensional analysis of ultra-low RNA-seq revealed a tight clustering and hence a high homology of all samples at the beginning of the assay. Remarkably, *Bcat1* was the sole significantly differentially expressed gene in HSPCs transduced with *MLL-AF9*, and an empty vector or a Bcat1^{WT} rescue construct independent of the murine origins. At the intermediate time point, the RNA profiles of the different conditions diverged from each other while Bcat1^{WT} rescue gene expression clusters with Bcat1$^{+/+}$ rather than Bcat1$^{-/-}$, its original genotype.

Over time, the expression of the Bcat1^{WT} rescue construct was lost in one replicate, while it prevailed in the other. The replicate without Bcat1^{WT} expression at the second time point exhibited a colony formation phenotype as well as an expression profile highly similar to Bcat1$^{-/-}$. In contrast, the replicate which expressed Bcat1^{WT} throughout the assay showed an almost identical colony formation pattern and expression profile to Bcat1$^{+/+}$. This indicates that in the presence of the MLL fusion protein, BCAT1 determines the LSC expression profile.

Comparison of the expression profiles at the intermediate time point showed a global gene expression increase in Bcat1$^{-/-}$. I hypothesized that the lack of gene expression in transformed Bcat1$^{+/+}$ is connected to the almost quiescent stemness phenotype of LSCs with only a very limited number of highly expressed genes (Gal et al., 2006; Gentles et al., 2010; Sadovnik et al., 2016).

In addition to the global changes, the expression of MLL-AF9 target genes, such as the homeobox genes *Hoxa9* and *Meis1*, was not diminished in Bcat1$^{-/-}$ over time. This suggests that there is no feedback loop from *Bcat1* towards these genes and once more highlights Bcat1 as a critical element of MLL fusion-driven tumor development. Surprisingly, the homeobox cluster A (HoxA) was not expressed in Bcat1$^{+/+}$ and Bcat1^{WT} rescue at the intermediate time point. A possible explanation could be that endogenous *MLL*, which is upregulated exclusively in these two conditions, is competitively displacing the MLL-AF9 fusion protein at these regions. In contrast to MLL-AF9, MLL bound to the HoxA cluster is associated with tightly regulated gene expression by recruiting Menin1 to this region (Yokoyama et al., 2005). MEN1 can, in turn, act as an oncogene or as a tumor suppressor depending on its surroundings. Unfortunately, my ACT-seq analysis did not

enable me to definitively conclude or discard this hypothesis. Further optimizations are needed to overcome the technical limitations.

Another possible explanation could be altered DNA methylation. Previous studies showed that suppression of *Bcat1* resulted in global DNA hypomethylation (Raffel et al., 2017). The loss of DNA methylation at the HoxA site would permit MLL-AF9 binding and enable the upregulation of gene expression. A DNA methylation analysis, such as bisulfite sequencing, would give further information and insights into the complex interplay between DNA and histone modifications (Y. Li et al., 2021).

Despite the lacking HoxA cluster expression, almost all HoxA target genes are expressed equally in Bcat1$^{+/+}$, Bcat1$^{-/-}$, and Bcat1^{WT}. For instance, HoxA9 downstream target genes *Pim1*, *Id2*, *Pbx3*, *Meis1*, *Cdk6*, and others are similarly expressed in all conditions (Alharbi et al., 2013). Exclusively *Cybb*, *HoxA7*, *HoxA10*, and *Camk2d* mirror the *HoxA9* expression pattern. This suggests an additional mechanism of regulation independent of the HoxA cluster in this specific setting.

5.5. *Bcat1* knockout inhibits DNA replication and cell cycle progression

To identify the mechanism underlying the striking phenotypical differences, I performed a GO and KEGG gene set enrichment analysis of differentially expressed genes in each condition at the two time points. The first time point was collected two days after transfection. Hence numerous pathways related to virus transfection were significantly downregulated at the intermediate relative to the early time point in both Bcat1$^{+/+}$ and Bcat1$^{-/-}$. After excluding these, hematopoietic cell lineage was found among the most downregulated pathways in Bcat1$^{+/+}$. The suppression of hematopoietic cell lineage genes may seem counter-intuitive for cancer stem cells. However, the immunophenotype and global expression profiles of LSCs are analog to normal granulocyte-macrophage progenitors (GMPs) with only a small subset of genes expressed in HSCs, reactivated in LSCs (Eppert et al., 2011; Andrei Krivtsov et al., 2006; Ng et al., 2016; Rao & Dou, 2015). Hence, the downregulation of surface markers associated with cell differentiation, as well as the downregulation of genes related to omnipotent stem cells, are consistent with the literature (Meyer et al., 2006, 2018).

Remarkably, however, was the gene set enrichment analysis comparing Bcat1 knockout cells over time. DNA replication and the cell cycle are the two most significantly altered pathways in the intermediate Bcat1$^{-/-}$ condition.

The initiation of DNA replication is guided by the stepwise assembly of the pre-replicative complex on the DNA helix (Machida et al., 2005; Méchali, 2010; Remus & Diffley, 2009): During late mitosis and G1-phase, the heterohexameric origin recognition complex relocates to the chromatin, where it binds CDC6 and CDT1 proteins (Blow et al., 2011; Siddiqui et al., 2013)—followed by the CDT1-dependent recruitment of MCM2-7, which are critical components of the hexametric helicase (Blow et al., 2011; Evrin et al., 2009; Remus & Diffley, 2009). Next, the replication start is initiated by CDKs and CDC7 in the S-phase, which results in MYC-mediated binding of CDC45 and Go-Ichi-Ni-San (GINS) tetramer to the MCM complex (Costa et al., 2011; Ilves et al., 2010; Moir et al., 1982; Nepon-Sixt et al., 2019; Riera et al., 2017). Finally, the formed CDC45-MCM2-7-GINS (CMG) helicase complex unwinds the DNA (Fu et al., 2011; Gambus et al., 2006; Ilves et al., 2010; Pacek et al., 2006) and supports the binding of DNA polymerase-α, initiating DNA synthesis (Heller et al., 2011; Labib, 2010).

This mechanism is essential for various DNA processes, including replication, repair, recombination, and telomere maintenance to preserve genome integrity (Brosh, 2013; Croteau et al., 2014). Hence, overexpression or activating mutations of genes in this pathway are associated with cancer promotion. For instance, the upregulation of *MCM* subunits strongly correlates with poor survival in breast cancer patients (Kwok et al., 2014) and relapse in AML (Lee et al., 2017). Overexpression of *CDC45* is, among others, observed in leukemia (Pollok et al., 2007). Even the proto-oncogene MYC, a well-known regulator of cell growth and cell cycle progression (Armelin et al., 1984; Kelly et al., 1983), plays a critical role in this process (Fernandez et al., 2003; Patel et al., 2004): DNA replication is impaired in the absence of MYC, identical to CDC45, and GINS loss (Srinivasan et al., 2013)

Interestingly, almost all genes involved in this pathway are downregulated in the intermediate time point Bcat1$^{-/-}$. For instance, the highly conserved *Mcm2-5* and *7*, *Cdc6* and *Cdc7*, *Cdk1*, *Cdc45*, and *Myc* were reduced at the intermediate time point. I was able to associate the low expression of these genes with alterations in histone modifications or MLL-AF9 binding. Cyclin-dependent kinases (CDKs), such as CDK6 or CDK9, have been previously described as direct target genes of MLL fusion proteins, highlighting the importance of these pathways in AML (Garcia-Cuellar et al., 2014; Placke et al., 2014; Richter et al., 2021). The suppression of DNA replication and hence, the cell cycle explains the lack of proliferation observed in Bcat1$^{-/-}$ cells.

Furthermore, no effects were observed in healthy tissues upon limiting MCMs (Ibarra et al., 2008; Lei et al., 1996). However, limited *MCM*s expression or reduced activity became

highly relevant during replication stress commonly observed in cancer and resulted in tumor growth inhibition (Ge et al., 2007; Neves & Kwok, 2017; Woodward et al., 2006). This increased dependency on DNA replication proteins during replicative stress could be one explanation for the drastic differences between early and intermediate time points: RNA expression of HSPCs was not affected by *Bcat1* knockdown at the beginning, resulting in a highly homogeneous grouping, while large differences were observed in $Bcat1^{+/+}$ and $Bcat1^{-/-}$ at the intermediate time point.

Unfortunately, I could not investigate the mechanistic link between BCAT1 and DNA replication within the scope of this thesis. One potential mechanism is based on targeted epigenetic changes, altering the chromatin and specifically suppressing the transcription of DNA replication and cell cycle genes. This hypothesis is supported by previous observations that loss of DOT1L function causes cell cycle arrest during G0/G1 transition in MLL fusion-driven AML (Daigle et al., 2013; Nguyen & Zhang, 2011; Okada et al., 2005; Yang et al., 2019). Terminal differentiation is another possible explanation for stopping replication and cell cycle progression in $Bcat1^{-/-}$. Previous studies suggested that *BCAT1* knockdown or inhibition of its enzymatic activity results in the initiation of hematopoietic differentiation (Z. Gu et al., 2019; Hattori et al., 2017; Raffel et al., 2017), which could lead to terminal differentiation, suppression of DNA replication, and tumor prevention. Furthermore, this mechanism supports the idea of BCAT1 overexpression mirroring the effect of DH mutations in cancer, as described above (Raffel et al., 2017). IDH mutations are associated with blocking cell differentiation by increasing repressive histone modifications through inhibition of α-KG-dependent chromatin-modifying enzymes (Lu et al., 2012).

Further investigations have to be made in order to determine the Bcat1-dependent process responsible for the inhibition of DNA replication and cell cycle progression.

5.6. Relevance of this study

More than 10% of all acute leukemia patients and 60% of infant AML harbor an MLL fusion gene (Ayton & Cleary, 2001; El Chaer et al., 2020; Hess, 2004; Meyer et al., 2013). The already unfavorable survival rate of AML is even worse for patients with MLL fusion tumors. Most AML patients are excluded from the harsh chemotherapy because of an overall lack of fitness. In addition, this therapy approach is not able to eliminate the chemoresistant LSCs (Dombret & Gardin, 2016; Heuser et al., 2020). Unfortunately, this results in a

relapse of 60% of patients in the favorable category and even 85% of patients in the adverse risk category (Ferrara et al., 2019).

Therefore, recent efforts have focused on developing novel therapies targeting a range of aspects, such as epigenetic deregulation, microenvironmental alterations, proteasomal activity, immunophenotypic markers, and many more. The most promising is a combination treatment of Venetoclax, a B cell lymphoma 2 BCL-2 inhibitor, and Azacytidine, a DNA methylation inhibitor that is successful in treating de-novo AML in older patients unsuitable for chemotherapy (Pollyea et al., 2018). Others, such as Midostaurin, Enasidenib, or Ivosidenib, target genes commonly found mutated in AML (Amatangelo et al., 2017; DiNardo et al., 2018; Stein et al., 2017; Weisberg et al., 2002). However, all these novel therapies still fail to successfully eradicate LSCs in a clinical setting facilitating relapses (Culp-Hill et al., 2021; Vetrie et al., 2020).

Quiescent LSCs with self-renewal capacity remain therapeutical resistant by utilizing alternative pathways (Bonnet & Dick, 1997; Eppert et al., 2011; Lapidot et al., 1994; Somervaille & Cleary, 2006). This study explored the role of BCAT1 in *MLL* fusion-driven AML and was able to show that the loss of transaminase activity of BCAT1 inhibited AML development. Thus, the suppression of BCAA catabolism through the inhibition of BCAT1 could provide a novel therapeutic approach to improve patient outcomes.

6. Conclusion

In this work, the intricate dynamics between epigenetic gene regulations and BCAA metabolism have been investigated. Contrary to my initial working hypothesis, BCAT1-dependent α-KG levels did not uniformly increase histone modifications. However, using publicly available patient data I connected *BCAT1* expression to the lysine methyltransferase *MLL*. Epigenetic dysregulation through MLL fusion proteins in HSPCs results in AML development. The upregulation of *Bcat1*, a novel MLL fusion target, is essential for these cells to transform into cancer. Conversely, the loss of *Bcat1* repressed DNA replication and cell cycle progression in the context of MLL fusions, preventing tumor transformation *in vitro*. This work identified BCAT1 as a potential new target gene of MLL-fusion proteins that is essential for leukemic transformation.

7. References

Alharbi, R. A., Pettengell, R., Pandha, H. S., & Morgan, R. (2013). The role of HOX genes in normal hematopoiesis and acute leukemia. *Leukemia*, *27*(5), 1000–1008. https://doi.org/10.1038/leu.2012.356

Almosailleakh, M., & Schwaller, J. (2019). Murine Models of Acute Myeloid Leukaemia. In *International Journal of Molecular Sciences* (Vol. 20, Issue 2). https://doi.org/10.3390/ijms20020453

Amary, M. F., Bacsi, K., Maggiani, F., Damato, S., Halai, D., Berisha, F., Pollock, R., O'Donnell, P., Grigoriadis, A., Diss, T., Eskandarpour, M., Presneau, N., Hogendoorn, P. C. W., Futreal, A., Tirabosco, R., & Flanagan, A. M. (2011). IDH1 and IDH2 mutations are frequent events in central chondrosarcoma and central and periosteal chondromas but not in other mesenchymal tumours. *The Journal of Pathology*, *224*(3), 334–343. https://doi.org/https://doi.org/10.1002/path.2913

Amatangelo, M. D., Quek, L., Shih, A., Stein, E. M., Roshal, M., David, M. D., Marteyn, B., Farnoud, N. R., de Botton, S., Bernard, O. A., Wu, B., Yen, K. E., Tallman, M. S., Papaemmanuil, E., Penard-Lacronique, V., Thakurta, A., Vyas, P., & Levine, R. L. (2017). Enasidenib induces acute myeloid leukemia cell differentiation to promote clinical response. *Blood*, *130*(6), 732–741. https://doi.org/10.1182/blood-2017-04-779447

Ananieva, E. A., Bostic, J. N., Torres, A. A., Glanz, H. R., McNitt, S. M., Brenner, M. K., Boyer, M. P., Addington, A. K., & Hutson, S. M. (2018). Mice deficient in the mitochondrial branched-chain aminotransferase (BCATm) respond with delayed tumour growth to a challenge with EL-4 lymphoma. *British Journal of Cancer*, *119*(8), 1009–1017. https://doi.org/10.1038/s41416-018-0283-7

Ananieva, E. A., & Wilkinson, A. C. (2018). Branched-chain amino acid metabolism in cancer. *Current Opinion in Clinical Nutrition and Metabolic Care*, *21*(1), 64–70. https://doi.org/10.1097/MCO.0000000000000430

Andrade, J., Ge, S., Symbatyan, G., Rosol, M. S., Olch, A. J., & Crooks, G. M. (2011). Effects of Sublethal Irradiation on Patterns of Engraftment after Murine Bone Marrow Transplantation. *Biology of Blood and Marrow Transplantation*, *17*(5), 608–619. https://doi.org/https://doi.org/10.1016/j.bbmt.2010.12.697

Armelin, H. A., Armelin, M. C. S., Kelly, K., Stewart, T., Leder, P., Cochran, B. H., & Stiles, C. D. (1984). Functional role for c-myc in mitogenic response to platelet-derived growth factor. *Nature*, *310*(5979), 655–660. https://doi.org/10.1038/310655a0

Avgustinova, A., & Benitah, S. A. (2016). Epigenetic control of adult stem cell function. *Nature Reviews Molecular Cell Biology*, *17*(10), 643–658. https://doi.org/10.1038/nrm.2016.76

Ayton, P. M., & Cleary, M. L. (2001). Molecular mechanisms of leukemogenesis mediated by MLL fusion proteins. *Oncogene*, *20*(40), 5695–5707. https://doi.org/10.1038/sj.onc.1204639

Ayton, P. M., & Cleary, M. L. (2003). Transformation of myeloid progenitors by MLL oncoproteins is dependent on Hoxa7 and Hoxa9. *Genes and Development*, *17*(18), 2298–2307. https://doi.org/10.1101/gad.1111603

Barth, T. K., & Imhof, A. (2010). Fast signals and slow marks: the dynamics of histone modifications. *Trends in Biochemical Sciences*, *35*(11), 618–626. https://doi.org/10.1016/j.tibs.2010.05.006

Begley, C. G., & Ioannidis, J. P. A. (2015). Reproducibility in Science. *Circulation Research*, *116*(1), 116–126. https://doi.org/10.1161/CIRCRESAHA.114.303819

Ben-Yosef, T., Yanuka, O., & Benvenisty, N. (1996). ECA39 is regulated by c-Myc in human and by a Jun/Fos homolog, Gcn4, in yeast. *Oncogene*, *13*(9), 1859–1866. http://europepmc.org/abstract/MED/8934531

Benvenisty, N., Leder, A., Kuo, A., & Leder, P. (1992). An embryonically expressed gene is a target for c-Myc regulation via the c-Myc-binding sequence. *Genes & Development*, *6*(12B), 2513–2523. https://doi.org/10.1101/gad.6.12b.2513

Bereshchenko, O., Mancini, E., Moore, S., Bilbao, D., Månsson, R., Luc, S., Grover, A., Jacobsen, S. E. W., Bryder, D., & Nerlov, C. (2009). Hematopoietic Stem Cell Expansion Precedes the Generation of Committed Myeloid Leukemia-Initiating Cells in C/EBPα Mutant AML. *Cancer Cell*, *16*(5), 390–400. https://doi.org/https://doi.org/10.1016/j.ccr.2009.09.036

Birke, M., Schreiner, S., García-Cuéllar, M.-P., Mahr, K., Titgemeyer, F., & Slany, R. K. (2002). The MT domain of the proto-oncoprotein MLL binds to CpG-containing DNA and discriminates against methylation. *Nucleic Acids Research*, *30*(4), 958–965. https://doi.org/10.1093/nar/30.4.958

Birsoy, K., Possemato, R., Lorbeer, F. K., Bayraktar, E. C., Thiru, P., Yucel, B., Wang, T., Chen, W. W., Clish, C. B., & Sabatini, D. M. (2014). Metabolic determinants of cancer cell sensitivity to glucose limitation and biguanides. *Nature*, *508*(7494), 108–112. https://doi.org/10.1038/nature13110

Bissell, M. J., & Labarge, M. A. (2005). Context, tissue plasticity, and cancer: are tumor stem cells also regulated by the microenvironment? *Cancer Cell*, *7*(1), 17–23. https://doi.org/10.1016/j.ccr.2004.12.013

Biswas, D., Milne, T. A., Basrur, V., Kim, J., Elenitoba-Johnson, K. S. J., Allis, C. D., & Roeder, R. G. (2011). Function of leukemogenic mixed lineage leukemia 1 (MLL) fusion proteins through distinct partner protein complexes. *Proceedings of the National Academy of Sciences*, *108*(38), 15751 LP – 15756. https://doi.org/10.1073/pnas.1111498108

Blow, J. J., Ge, X. Q., & Jackson, D. A. (2011). How dormant origins promote complete genome replication. *Trends in Biochemical Sciences*, *36*(8), 405–414. https://doi.org/https://doi.org/10.1016/j.tibs.2011.05.002

Bonnet, D., & Dick, J. E. (1997). Human acute myeloid leukemia is organized as a hierarchy that originates from a primitive hematopoietic cell. *Nature Medicine*, *3*(7), 730–737. https://doi.org/10.1038/nm0797-730

Bowman, R. L., Busque, L., & Levine, R. L. (2018). Clonal Hematopoiesis and Evolution to Hematopoietic Malignancies. *Cell Stem Cell*, *22*(2), 157–170. https://doi.org/https://doi.org/10.1016/j.stem.2018.01.011

Brosh, R. M. (2013). DNA helicases involved in DNA repair and their roles in cancer. *Nature Reviews Cancer*, *13*(8), 542–558. https://doi.org/10.1038/nrc3560

Busch, K., Klapproth, K., Barile, M., Flossdorf, M., Holland-Letz, T., Schlenner, S. M., Reth, M., Höfer, T., & Rodewald, H.-R. (2015). Fundamental properties of unperturbed haematopoiesis from stem cells in vivo. *Nature*, *518*(7540), 542–546. https://doi.org/10.1038/nature14242

Butler, L. H., Slany, R., Cui, X., Cleary, M. L., & Mason, D. Y. (1997). The HRX Proto-oncogene Product Is Widely Expressed in Human Tissues and Localizes to Nuclear Structures. *Blood*, *89*(9), 3361–3370. https://doi.org/https://doi.org/10.1182/blood.V89.9.3361

Cairns, R. A., Iqbal, J., Lemonnier, F., Kucuk, C., de Leval, L., Jais, J.-P., Parrens, M., Martin, A., Xerri, L., Brousset, P., Chan, L. C., Chan, W.-C., Gaulard, P., & Mak, T. W. (2012). IDH2 mutations are frequent in angioimmunoblastic T-cell lymphoma. *Blood*, *119*(8), 1901–1903. https://doi.org/10.1182/blood-2011-11-391748

Campbell, C. T., Haladyna, J. N., Drubin, D. A., Thomson, T. M., Maria, M. J., Yamauchi, T., Waters, N. J., Olhava, E. J., Pollock, R. M., Smith, J. J., Copeland, R. A., Blakemore, S. J., Bernt, K. M., & Daigle, S. R. (2017). Mechanisms of Pinometostat (EPZ-5676) Treatment–Emergent Resistance in MLL-Rearranged Leukemia. *Molecular Cancer Therapeutics*, *16*(8), 1669 LP – 1679. https://doi.org/10.1158/1535-7163.MCT-16-0693

Campbell, S. L., & Wellen, K. E. (2018). Metabolic Signaling to the Nucleus in Cancer. *Molecular Cell*, *71*(3), 398–408. https://doi.org/https://doi.org/10.1016/j.molcel.2018.07.015

Carrelha, J., Meng, Y., Kettyle, L. M., Luis, T. C., Norfo, R., Alcolea, V., Boukarabila, H., Grasso, F., Gambardella, A., Grover, A., Högstrand, K., Lord, A. M., Sanjuan-Pla, A., Woll, P. S., Nerlov, C., & Jacobsen, S. E. W. (2018). Hierarchically related lineage-restricted fates of multipotent haematopoietic stem cells. *Nature*, *554*(7690), 106–111. https://doi.org/10.1038/nature25455

Carter, B., Ku, W. L., Kang, J. Y., Hu, G., Perrie, J., Tang, Q., & Zhao, K. (2019). Mapping histone modifications in low cell number and single cells using antibody-guided chromatin tagmentation (ACT-seq). *Nature Communications*, *10*(1), 3747. https://doi.org/10.1038/s41467-019-11559-1

Challen, G. A., Sun, D., Jeong, M., Luo, M., Jelinek, J., Vasanthakumar, A., Meissner, A., Issa, J.-P., Godley, L., Li, W., & Goodell, M. A. (2011). Dnmt3a Is Essential for Hematopoietic Stem Cell Differentiation. *Blood*, *118*(21), 386. https://doi.org/10.1182/blood.V118.21.386.386

Challen, G. A., Sun, D., Mayle, A., Jeong, M., Luo, M., Rodriguez, B., Mallaney, C., Celik, H., Yang, L., Xia, Z., Cullen, S., Berg, J., Zheng, Y., Darlington, G. J., Li, W., & Goodell, M. A. (2014). Dnmt3a and Dnmt3b Have Overlapping and Distinct Functions in Hematopoietic Stem Cells. *Cell Stem Cell*, *15*(3), 350–364. https://doi.org/https://doi.org/10.1016/j.stem.2014.06.018

Chambers, S. M., Boles, N. C., Lin, K.-Y. K., Tierney, M. P., Bowman, T. V, Bradfute, S. B., Chen, A. J., Merchant, A. A., Sirin, O., Weksberg, D. C., Merchant, M. G., Fisk, C. J., Shaw, C. A., & Goodell, M. A. (2007). Hematopoietic Fingerprints: An Expression Database of Stem Cells and Their Progeny. *Cell Stem Cell*, *1*(5), 578–591. https://doi.org/10.1016/j.stem.2007.10.003

Chan, A. K. N., & Chen, C.-W. (2019). Rewiring the Epigenetic Networks in MLL-Rearranged Leukemias: Epigenetic Dysregulation and Pharmacological Interventions . In *Frontiers in Cell and Developmental Biology* (Vol. 7, p. 81). https://www.frontiersin.org/article/10.3389/fcell.2019.00081

Charlton, J., Jung, E. J., Mattei, A. L., Bailly, N., Liao, J., Martin, E. J., Giesselmann, P., Brändl, B., Stamenova, E. K., Müller, F.-J., Kiskinis, E., Gnirke, A., Smith, Z. D., & Meissner, A. (2020). TETs compete with DNMT3 activity in pluripotent cells at thousands of methylated somatic enhancers. *Nature Genetics*, *52*(8), 819–827. https://doi.org/10.1038/s41588-020-0639-9

Chen, W., Kumar, A. R., Hudson, W. A., Li, Q., Wu, B., Staggs, R. A., Lund, E. A., Sam, T. N., & Kersey, J. H. (2008). Malignant Transformation Initiated by Mll-AF9: Gene Dosage and Critical Target Cells. *Cancer Cell*, *13*(5), 432–440. https://doi.org/https://doi.org/10.1016/j.ccr.2008.03.005

Cho, M.-H., Park, J.-H., Choi, H.-J., Park, M.-K., Won, H.-Y., Park, Y.-J., Lee, C. H., Oh, S.-H., Song, Y.-S., Kim, H. S., Oh, Y.-H., Lee, J.-Y., & Kong, G. (2015). DOT1L cooperates with the c-Myc-p300 complex to epigenetically derepress CDH1 transcription factors in breast cancer progression. *Nature Communications*, *6*(1), 7821. https://doi.org/10.1038/ncomms8821

Cho, M. H., Park, J. H., Choi, H. J., Park, M. K., Won, H. Y., Park, Y. J., Lee, C. H., Oh, S. H., Song, Y. S., Kim, H. S., Oh, Y. H., Lee, J. Y., & Kong, G. (2015). DOT1L cooperates with the c-Myc-p300 complex to epigenetically derepress CDH1 transcription factors in breast cancer progression. *Nature Communications*, *6*, 1–14. https://doi.org/10.1038/ncomms8821

Chory, E. J., Calarco, J. P., Hathaway, N. A., Bell, O., Neel, D. S., & Crabtree, G. R. (2019). Nucleosome Turnover Regulates Histone Methylation Patterns over the Genome. *Molecular Cell*, *73*(1), 61-72.e3. https://doi.org/https://doi.org/10.1016/j.molcel.2018.10.028

Chowdhury, R., Yeoh, K. K., Tian, Y.-M., Hillringhaus, L., Bagg, E. A., Rose, N. R., Leung, I. K. H., Li, X. S., Woon, E. C. Y., Yang, M., McDonough, M. A., King, O. N., Clifton, I. J., Klose, R. J., Claridge, T. D. W., Ratcliffe, P. J., Schofield, C. J., & Kawamura, A. (2011). The oncometabolite 2-hydroxyglutarate inhibits histone lysine demethylases. *EMBO Reports*, *12*(5), 463–469. https://doi.org/https://doi.org/10.1038/embor.2011.43

Cierpicki, T., Risner, L. E., Grembecka, J., Lukasik, S. M., Popovic, R., Omonkowska, M., Shultis, D. D., Zeleznik-Le, N. J., & Bushweller, J. H. (2010). Structure of the MLL CXXC domain–DNA complex and its functional role in MLL-AF9 leukemia. *Nature Structural and Molecular Biology*, *17*(1), 62–68. https://doi.org/10.1038/nsmb.1714

Coles, S. J., Hancock, J. T., & Conway, M. E. (2012). Differential redox potential between the human cytosolic and mitochondrial branched-chain aminotransferase. *Acta Biochimica et Biophysica Sinica*, *44*(2), 172–176. https://doi.org/10.1093/abbs/gmr103

Conway, M. E., Hull, J., El Hindy, M., Taylor, S. C., El Amraoui, F., Paton-Thomas, C., White, P., Williams, M., Ellis, H. P., Bertoni, A., Radlwimmer, B., Hutson, S. M., & Kurian, K. M. (2016). Decreased expression of the mitochondrial BCAT protein correlates with improved patient survival in IDH-WT gliomas. *Brain Pathology (Zurich, Switzerland)*, *26*(6), 789–791. https://doi.org/10.1111/bpa.12385

Costa, A., Ilves, I., Tamberg, N., Petojevic, T., Nogales, E., Botchan, M. R., & Berger, J. M. (2011). The structural basis for MCM2–7 helicase activation by GINS and Cdc45. *Nature Structural & Molecular Biology*, *18*(4), 471–477. https://doi.org/10.1038/nsmb.2004

Croteau, D. L., Popuri, V., Opresko, P. L., & Bohr, V. A. (2014). Human RecQ Helicases in DNA Repair, Recombination, and Replication. *Annual Review of Biochemistry*, *83*(1), 519–552. https://doi.org/10.1146/annurev-biochem-060713-035428

Cullen, S. M., Mayle, A., Rossi, L., & Goodell, M. A. (2014). Chapter Two - Hematopoietic Stem Cell Development: An Epigenetic Journey. In M. B. T.-C. T. in D. B. Rendl (Ed.), *Stem Cells in Development and Disease* (Vol. 107, pp. 39–75). Academic Press. https://doi.org/https://doi.org/10.1016/B978-0-12-416022-4.00002-0

Culp-Hill, R., D'Alessandro, A., & Pietras, E. M. (2021). Extinguishing the Embers: Targeting AML Metabolism. *Trends in Molecular Medicine*. https://doi.org/10.1016/j.molmed.2020.10.001

Daigle, S. R., Olhava, E. J., Therkelsen, C. A., Basavapathruni, A., Jin, L., Boriack-Sjodin, P. A., Allain, C. J., Klaus, C. R., Raimondi, A., Scott, M. P., Waters, N. J., Chesworth, R., Moyer, M. P., Copeland, R. A., Richon, V. M., & Pollock, R. M. (2013). Potent inhibition of DOT1L as treatment of MLL-fusion leukemia. *Blood*, *122*(6), 1017–1025. https://doi.org/10.1182/blood-2013-04-497644

Daigle, S. R., Olhava, E. J., Therkelsen, C. A., Majer, C. R., Sneeringer, C. J., Song, J., Johnston, L. D., Scott, M. P., Smith, J. J., Xiao, Y., Jin, L., Kuntz, K. W., Chesworth, R., Moyer, M. P., Bernt, K. M., Tseng, J.-

C., Kung, A. L., Armstrong, S. A., Copeland, R. A., … Pollock, R. M. (2011). Selective Killing of Mixed Lineage Leukemia Cells by a Potent Small-Molecule DOT1L Inhibitor. *Cancer Cell*, *20*(1), 53–65. https://doi.org/https://doi.org/10.1016/j.ccr.2011.06.009

Daikhin, Y., & Yudkoff, M. (2000). Compartmentation of Brain Glutamate Metabolism in Neurons and Glia. *The Journal of Nutrition*, *130*(4), 1026S-1031S. https://doi.org/10.1093/jn/130.4.1026S

Dang, L., White, D. W., Gross, S., Bennett, B. D., Bittinger, M. A., Driggers, E. M., Fantin, V. R., Jang, H. G., Jin, S., Keenan, M. C., Marks, K. M., Prins, R. M., Ward, P. S., Yen, K. E., Liau, L. M., Rabinowitz, J. D., Cantley, L. C., Thompson, C. B., Vander Heiden, M. G., & Su, S. M. (2009). Cancer-associated IDH1 mutations produce 2-hydroxyglutarate. *Nature*, *462*(7274), 739–744. https://doi.org/10.1038/nature08617

de Bont, J. M., Kros, J. M., Passier, M. M. C. J., Reddingius, R. E., Smitt, P. A. E. S., Luider, T. M., Boer, M. L. den, & Pieters, R. (2008). Differential expression and prognostic significance of SOX genes in pediatric medulloblastoma and ependymoma identified by microarray analysis. *Neuro-Oncology*, *10*(5), 648–660. https://doi.org/10.1215/15228517-2008-032

Deaton, A. M., & Bird, A. (2011). CpG islands and the regulation of transcription. *Genes & Development* , *25*(10), 1010–1022. https://doi.org/10.1101/gad.2037511

Dillon, N. (2006). Gene regulation and large-scale chromatin organization in the nucleus. *Chromosome Research*, *14*(1), 117–126. https://doi.org/10.1007/s10577-006-1027-8

DiNardo, C. D., Stein, E. M., de Botton, S., Roboz, G. J., Altman, J. K., Mims, A. S., Swords, R., Collins, R. H., Mannis, G. N., Pollyea, D. A., Donnellan, W., Fathi, A. T., Pigneux, A., Erba, H. P., Prince, G. T., Stein, A. S., Uy, G. L., Foran, J. M., Traer, E., … Kantarjian, H. M. (2018). Durable Remissions with Ivosidenib in IDH1-Mutated Relapsed or Refractory AML. *New England Journal of Medicine*, *378*(25), 2386–2398. https://doi.org/10.1056/NEJMoa1716984

Ding, L., Getz, G., Wheeler, D. A., Mardis, E. R., McLellan, M. D., Cibulskis, K., Sougnez, C., Greulich, H., Muzny, D. M., Morgan, M. B., Fulton, L., Fulton, R. S., Zhang, Q., Wendl, M. C., Lawrence, M. S., Larson, D. E., Chen, K., Dooling, D. J., Sabo, A., … Wilson, R. K. (2008). Somatic mutations affect key pathways in lung adenocarcinoma. *Nature*, *455*(7216), 1069–1075. https://doi.org/10.1038/nature07423

Dombret, H., & Gardin, C. (2016). An update of current treatments for adult acute myeloid leukemia. *Blood*, *127*(1), 53–61. https://doi.org/10.1182/blood-2015-08-604520

El Chaer, F., Keng, M., & Ballen, K. K. (2020). MLL-Rearranged Acute Lymphoblastic Leukemia. *Current Hematologic Malignancy Reports*, *15*(2), 83–89. https://doi.org/10.1007/s11899-020-00582-5

Eppert, K., Takenaka, K., Lechman, E. R., Waldron, L., Nilsson, B., van Galen, P., Metzeler, K. H., Poeppl, A., Ling, V., Beyene, J., Canty, A. J., Danska, J. S., Bohlander, S. K., Buske, C., Minden, M. D., Golub, T. R., Jurisica, I., Ebert, B. L., & Dick, J. E. (2011). Stem cell gene expression programs influence clinical outcome in human leukemia. *Nature Medicine*, *17*(9), 1086–1093. https://doi.org/10.1038/nm.2415

Evrin, C., Clarke, P., Zech, J., Lurz, R., Sun, J., Uhle, S., Li, H., Stillman, B., & Speck, C. (2009). A double-hexameric MCM2-7 complex is loaded onto origin DNA during licensing of eukaryotic DNA replication. *Proceedings of the National Academy of Sciences*, *106*(48), 20240 LP – 20245. https://doi.org/10.1073/pnas.0911500106

Falcone, M., & Maddocks, O. D. K. (2020). The KRAS-BCAA-BCAT2 axis in PDAC development. *Nature Cell Biology*, *22*(2), 139–140. https://doi.org/10.1038/s41556-020-0467-2

Fernandez, P. C., Frank, S. R., Wang, L., Schroeder, M., Liu, S., Greene, J., Cocito, A., & Amati, B. (2003). Genomic targets of the human c-Myc protein. *Genes & Development* , *17*(9), 1115–1129. https://doi.org/10.1101/gad.1067003

Ferrara, F., Lessi, F., Vitagliano, O., Birkenghi, E., & Rossi, G. (2019). Current Therapeutic Results and Treatment Options for Older Patients with Relapsed Acute Myeloid Leukemia. In *Cancers* (Vol. 11, Issue 2). https://doi.org/10.3390/cancers11020224

Figueroa, M. E., Abdel-Wahab, O., Lu, C., Ward, P. S., Patel, J., Shih, A., Li, Y., Bhagwat, N., Vasanthakumar, A., Fernandez, H. F., Tallman, M. S., Sun, Z., Wolniak, K., Peeters, J. K., Liu, W., Choe, S. E., Fantin, V. R., Paietta, E., Löwenberg, B., … Melnick, A. (2010). Leukemic IDH1 and IDH2 Mutations Result in a Hypermethylation Phenotype, Disrupt TET2 Function, and Impair Hematopoietic Differentiation. *Cancer Cell*, *18*(6), 553–567. https://doi.org/10.1016/j.ccr.2010.11.015

Finicle, B. T., Jayashankar, V., & Edinger, A. L. (2018). Nutrient scavenging in cancer. *Nature Reviews Cancer*, *18*(10), 619–633. https://doi.org/10.1038/s41568-018-0048-x

Flomerfelt, F. A., & Gress, R. E. (2016). *Bone Marrow and Fetal Liver Radiation Chimeras BT - T-Cell Development: Methods and Protocols* (R. Bosselut & M. S. Vacchio (Eds.); pp. 109–115). Springer New York. https://doi.org/10.1007/978-1-4939-2809-5_9

François Martín del Campo, L. (2019). *Novel mode of action of the branched-chain amino acid transaminase BCAT1 in glioblastoma* (Issue December).

Frasca, D., Guidi, F., Arbitrio, M., Pioli, C., Poccia, F., Cicconi, R., & Doria, G. (2000). Hematopoietic reconstitution after lethal irradiation and bone marrow transplantation: effects of different hematopoietic cytokines on the recovery of thymus, spleen and blood cells. *Bone Marrow Transplantation*, *25*(4), 427–433. https://doi.org/10.1038/sj.bmt.1702169

Fu, Y. V., Yardimci, H., Long, D. T., Guainazzi, A., Bermudez, V. P., Hurwitz, J., van Oijen, A., Schärer, O. D., & Walter, J. C. (2011). Selective Bypass of a Lagging Strand Roadblock by the Eukaryotic Replicative DNA Helicase. *Cell*, *146*(6), 931–941. https://doi.org/https://doi.org/10.1016/j.cell.2011.07.045

Fujino, T., & Kitamura, T. (2020). ASXL1 mutation in clonal hematopoiesis. *Experimental Hematology*, *83*, 74–84. https://doi.org/https://doi.org/10.1016/j.exphem.2020.01.002

Gal, H., Amariglio, N., Trakhtenbrot, L., Jacob-Hirsh, J., Margalit, O., Avigdor, A., Nagler, A., Tavor, S., Ein-Dor, L., Lapidot, T., Domany, E., Rechavi, G., & Givol, D. (2006). Gene expression profiles of AML derived stem cells; similarity to hematopoietic stem cells. *Leukemia*, *20*(12), 2147–2154. https://doi.org/10.1038/sj.leu.2404401

Gambus, A., Jones, R. C., Sanchez-Diaz, A., Kanemaki, M., van Deursen, F., Edmondson, R. D., & Labib, K. (2006). GINS maintains association of Cdc45 with MCM in replisome progression complexes at eukaryotic DNA replication forks. *Nature Cell Biology*, *8*(4), 358–366. https://doi.org/10.1038/ncb1382

Garcia-Cuellar, M.-P., Füller, E., Mäthner, E., Breitinger, C., Hetzner, K., Zeitlmann, L., Borkhardt, A., & Slany, R. K. (2014). Efficacy of cyclin-dependent-kinase 9 inhibitors in a murine model of mixed-lineage leukemia. *Leukemia*, *28*(7), 1427–1435. https://doi.org/10.1038/leu.2014.40

Ge, X. Q., Jackson, D. A., & Blow, J. J. (2007). Dormant origins licensed by excess Mcm2–7 are required for human cells to survive replicative stress. *Genes & Development* , *21*(24), 3331–3341. https://doi.org/10.1101/gad.457807

Genovese, G., Kähler, A. K., Handsaker, R. E., Lindberg, J., Rose, S. A., Bakhoum, S. F., Chambert, K., Mick, E., Neale, B. M., Fromer, M., Purcell, S. M., Svantesson, O., Landén, M., Höglund, M., Lehmann, S., Gabriel, S. B., Moran, J. L., Lander, E. S., Sullivan, P. F., … McCarroll, S. A. (2014). Clonal Hematopoiesis and Blood-Cancer Risk Inferred from Blood DNA Sequence. *New England Journal of Medicine*, *371*(26), 2477–2487. https://doi.org/10.1056/NEJMoa1409405

Gentles, A. J., Plevritis, S. K., Majeti, R., & Alizadeh, A. A. (2010). Association of a Leukemic Stem Cell Gene Expression Signature With Clinical Outcomes in Acute Myeloid Leukemia. *JAMA*, *304*(24), 2706–2715. https://doi.org/10.1001/jama.2010.1862

George, J., Uyar, A., Young, K., Kuffler, L., Waldron-Francis, K., Marquez, E., Ucar, D., & Trowbridge, J. J. (2016). Leukaemia cell of origin identified by chromatin landscape of bulk tumour cells. *Nature Communications*, *7*(1), 12166. https://doi.org/10.1038/ncomms12166

Goardon, N., Marchi, E., Atzberger, A., Quek, L., Schuh, A., Soneji, S., Woll, P., Mead, A., Alford, K. A., Rout, R., Chaudhury, S., Gilkes, A., Knapper, S., Beldjord, K., Begum, S., Rose, S., Geddes, N., Griffiths, M., Standen, G., … Vyas, P. (2011). Coexistence of LMPP-like and GMP-like Leukemia Stem Cells in Acute Myeloid Leukemia. *Cancer Cell*, *19*(1), 138–152. https://doi.org/https://doi.org/10.1016/j.ccr.2010.12.012

Goel, S., Bhatia, V., Biswas, T., & Ateeq, B. (2021). Epigenetic reprogramming during prostate cancer progression: A perspective from development. *Seminars in Cancer Biology*. https://doi.org/https://doi.org/10.1016/j.semcancer.2021.01.009

Goodell, M. A., Nguyen, H., & Shroyer, N. (2015). Somatic stem cell heterogeneity: diversity in the blood, skin and intestinal stem cell compartments. *Nature Reviews Molecular Cell Biology*, *16*(5), 299–309. https://doi.org/10.1038/nrm3980

Goto, M., Shinno, H., & Ichihara, A. (1977). Isozyme patterns of branched-chain amino acid transaminase in human tissues and tumors. *Gann Japanese Journal of Cancer Research*, *68*(5), 663–667. https://doi.org/10.20772/cancersci1959.68.5_663

Gu, Y., Nakamura, T., Alder, H., Prasad, R., Canaani, O., Cimino, G., Croce, C. M., & Canaani, E. (1992). The t(4;11) chromosome translocation of human acute leukemias fuses the ALL-1 gene, related to Drosophila trithorax, to the AF-4 gene. *Cell*, *71*(4), 701–708. https://doi.org/https://doi.org/10.1016/0092-

8674(92)90603-A

Gu, Z., Liu, Y., Cai, F., Patrick, M., Zmajkovic, J., Cao, H., Zhang, Y., Tasdogan, A., Chen, M., Qi, L., Liu, X., Li, K., Lyu, J., Dickerson, K. E., Chen, W., Ni, M., Merritt, M. E., Morrison, S. J., Skoda, R. C., … Xu, J. (2019). Loss of EZH2 reprograms BCAA metabolism to drive leukemic transformation. *Cancer Discovery*, *9*(9), 1228–1247. https://doi.org/10.1158/2159-8290.CD-19-0152

Guenther, M. G., Jenner, R. G., Chevalier, B., Nakamura, T., Croce, C. M., Canaani, E., & Young, R. A. (2005). Global and Hox-specific roles for the MLL1 methyltransferase. *Proceedings of the National Academy of Sciences of the United States of America*, *102*(24), 8603 LP – 8608. https://doi.org/10.1073/pnas.0503072102

Hanahan, D., & Weinberg, R. A. (2011). Hallmarks of Cancer: The Next Generation. *Cell*, *144*(5), 646–674. https://doi.org/https://doi.org/10.1016/j.cell.2011.02.013

Hattori, A., Tsunoda, M., Konuma, T., Kobayashi, M., Nagy, T., Glushka, J., Tayyari, F., McSkimming, D., Kannan, N., Tojo, A., Edison, A. S., & Ito, T. (2017). Cancer progression by reprogrammed BCAA metabolism in myeloid leukaemia. *Nature*, *545*(7655), 500–504. https://doi.org/10.1038/nature22314

Heller, R. C., Kang, S., Lam, W. M., Chen, S., Chan, C. S., & Bell, S. P. (2011). Eukaryotic Origin-Dependent DNA Replication In Vitro Reveals Sequential Action of DDK and S-CDK Kinases. *Cell*, *146*(1), 80–91. https://doi.org/https://doi.org/10.1016/j.cell.2011.06.012

Hérault, A., Binnewies, M., Leong, S., Calero-Nieto, F. J., Zhang, S. Y., Kang, Y.-A., Wang, X., Pietras, E. M., Chu, S. H., Barry-Holson, K., Armstrong, S., Göttgens, B., & Passegué, E. (2017). Myeloid progenitor cluster formation drives emergency and leukaemic myelopoiesis. *Nature*, *544*(7648), 53–58. https://doi.org/10.1038/nature21693

Hess, J. L. (2004). MLL: a histone methyltransferase disrupted in leukemia. *Trends in Molecular Medicine*, *10*(10), 500–507. https://doi.org/10.1016/j.molmed.2004.08.005

Heuser, M., Ofran, Y., Boissel, N., Brunet Mauri, S., Craddock, C., Janssen, J., Wierzbowska, A., & Buske, C. (2020). Acute myeloid leukaemia in adult patients: ESMO Clinical Practice Guidelines for diagnosis, treatment and follow-up††Approved by the ESMO Guidelines Committee: August 2002, last update January 2020. This publication supersedes the previously published ver. *Annals of Oncology*, *31*(6), 697–712. https://doi.org/https://doi.org/10.1016/j.annonc.2020.02.018

Hsieh, J. J.-D., Cheng, E. H.-Y., & Korsmeyer, S. J. (2003). Taspase1: A Threonine Aspartase Required for Cleavage of MLL and Proper HOX Gene Expression. *Cell*, *115*(3), 293–303. https://doi.org/https://doi.org/10.1016/S0092-8674(03)00816-X

https://www.dkfz.de/en/genetics/pages/projects/Tumor-metabolism/Tumor_metabolism.html. (n.d.). https://www.dkfz.de/en/genetics/pages/projects/Tumor-metabolism/Tumor_metabolism.html

Hu, D., & Shilatifard, A. (2016). Epigenetics of hematopoiesis and hematological malignancies. *Genes & Development* , *30*(18), 2021–2041. https://doi.org/10.1101/gad.284109.116

Huntly, B. J. P., Shigematsu, H., Deguchi, K., Lee, B. H., Mizuno, S., Duclos, N., Rowan, R., Amaral, S., Curley, D., Williams, I. R., Akashi, K., & Gilliland, D. G. (2004). MOZ-TIF2, but not BCR-ABL, confers properties of leukemic stem cells to committed murine hematopoietic progenitors. *Cancer Cell*, *6*(6), 587–596. https://doi.org/https://doi.org/10.1016/j.ccr.2004.10.015

Hutson, S. M., Sweatt, A. J., & LaNoue, K. F. (2005). Branched-Chain Amino Acid Metabolism: Implications for Establishing Safe Intakes. *The Journal of Nutrition*, *135*(6), 1557S-1564S. https://doi.org/10.1093/jn/135.6.1557S

Ibarra, A., Schwob, E., & Méndez, J. (2008). Excess MCM proteins protect human cells from replicative stress by licensing backup origins of replication. *Proceedings of the National Academy of Sciences*, *105*(26), 8956 LP – 8961. https://doi.org/10.1073/pnas.0803978105

Ichihara, A., & Koyama, E. (1966). Transaminase of Branched Chain Amino Acids: I. Branched Chain Amino Acids-α-Ketoglutarate Transaminase. *The Journal of Biochemistry*, *59*(2), 160–169. https://doi.org/10.1093/oxfordjournals.jbchem.a128277

Ilves, I., Petojevic, T., Pesavento, J. J., & Botchan, M. R. (2010). Activation of the MCM2-7 Helicase by Association with Cdc45 and GINS Proteins. *Molecular Cell*, *37*(2), 247–258. https://doi.org/https://doi.org/10.1016/j.molcel.2009.12.030

Iyer, N. V, Kotch, L. E., Agani, F., Leung, S. W., Laughner, E., Wenger, R. H., Gassmann, M., Gearhart, J. D., Lawler, A. M., Yu, A. Y., & Semenza, G. L. (1998). Cellular and developmental control of O2 homeostasis by hypoxia-inducible factor 1α. *Genes & Development* , *12*(2), 149–162.

https://doi.org/10.1101/gad.12.2.149

Izzo, F., Lee, S. C., Poran, A., Chaligne, R., Gaiti, F., Gross, B., Murali, R. R., Deochand, S. D., Ang, C., Jones, P. W., Nam, A. S., Kim, K.-T., Kothen-Hill, S., Schulman, R. C., Ki, M., Lhoumaud, P., Skok, J. A., Viny, A. D., Levine, R. L., … Landau, D. A. (2020). DNA methylation disruption reshapes the hematopoietic differentiation landscape. *Nature Genetics*, *52*(4), 378–387. https://doi.org/10.1038/s41588-020-0595-4

Jain, M., Nilsson, R., Sharma, S., Madhusudhan, N., Kitami, T., Souza, A. L., Kafri, R., Kirschner, M. W., Clish, C. B., & Mootha, V. K. (2012). Metabolite profiling identifies a key role for glycine in rapid cancer cell proliferation. *Science*, *336*(6084), 1040–1044. https://doi.org/10.1126/science.1218595

Jeong, M., Park, H. J., Celik, H., Ostrander, E. L., Reyes, J. M., Guzman, A., Rodriguez, B., Lei, Y., Lee, Y., Ding, L., Guryanova, O. A., Li, W., Goodell, M. A., & Challen, G. A. (2018). Loss of Dnmt3a Immortalizes Hematopoietic Stem Cells In Vivo. *Cell Reports*, *23*(1), 1–10. https://doi.org/https://doi.org/10.1016/j.celrep.2018.03.025

Ju, W., Yoo, B. C., Kim, I.-J., Kim, J. W., Kim, S. C., & Lee, H. P. (2009). Identification of genes with differential expression in chemoresistant epithelial ovarian cancer using high-density oligonucleotide microarrays. *Oncology Research*, *18*(2–3), 47–56. https://doi.org/10.3727/096504009789954672

Kaelin Jr., W. G., & McKnight, S. L. (2013). Influence of Metabolism on Epigenetics and Disease. *Cell*, *153*(1), 56–69. https://doi.org/10.1016/j.cell.2013.03.004

Kandoth, C., McLellan, M. D., Vandin, F., Ye, K., Niu, B., Lu, C., Xie, M., Zhang, Q., McMichael, J. F., Wyczalkowski, M. A., Leiserson, M. D. M., Miller, C. A., Welch, J. S., Walter, M. J., Wendl, M. C., Ley, T. J., Wilson, R. K., Raphael, B. J., & Ding, L. (2013). Mutational landscape and significance across 12 major cancer types. *Nature*, *502*(7471), 333–339. https://doi.org/10.1038/nature12634

Kawagoe, H., Humphries, R. K., Blair, A., Sutherland, H. J., & Hogge, D. E. (1999). Expression of HOX genes, HOX cofactors, and MLL in phenotypically and functionally defined subpopulations of leukemic and normal human hematopoietic cells. *Leukemia*, *13*(5), 687–698. https://doi.org/10.1038/sj.leu.2401410

Kelly, K., Cochran, B. H., Stiles, C. D., & Leder, P. (1983). Cell-specific regulation of the c-myc gene by lymphocyte mitogens and platelet-derived growth factor. *Cell*, *35*(3, Part 2), 603–610. https://doi.org/https://doi.org/10.1016/0092-8674(83)90092-2

Kerry, J., Godfrey, L., Repapi, E., Tapia, M., Blackledge, N. P., Ma, H., Ballabio, E., O'Byrne, S., Ponthan, F., Heidenreich, O., Roy, A., Roberts, I., Konopleva, M., Klose, R. J., Geng, H., & Milne, T. A. (2017). MLL-AF4 Spreading Identifies Binding Sites that Are Distinct from Super-Enhancers and that Govern Sensitivity to DOT1L Inhibition in Leukemia. *Cell Reports*, *18*(2), 482–495. https://doi.org/10.1016/j.celrep.2016.12.054

Kingsbury, J. M., Sen, N. D., & Cardenas, M. E. (2015). Branched-Chain Aminotransferases Control TORC1 Signaling in Saccharomyces cerevisiae. *PLoS Genetics*, *11*(12). https://doi.org/10.1371/journal.pgen.1005714

Kirstetter, P., Schuster, M. B., Bereshchenko, O., Moore, S., Dvinge, H., Kurz, E., Theilgaard-Mönch, K., Månsson, R., Pedersen, T. Å., Pabst, T., Schrock, E., Porse, B. T., Jacobsen, S. E. W., Bertone, P., Tenen, D. G., & Nerlov, C. (2008). Modeling of C/EBPα Mutant Acute Myeloid Leukemia Reveals a Common Expression Signature of Committed Myeloid Leukemia-Initiating Cells. *Cancer Cell*, *13*(4), 299–310. https://doi.org/https://doi.org/10.1016/j.ccr.2008.02.008

Klose, R. J., & Zhang, Y. (2007). Regulation of histone methylation by demethylimination and demethylation. *Nature Reviews Molecular Cell Biology*, *8*(4), 307–318. https://doi.org/10.1038/nrm2143

Koppenol, W. H., Bounds, P. L., & Dang, C. V. (2011). Otto Warburg's contributions to current concepts of cancer metabolism. *Nature Reviews Cancer*, *11*(5), 325–337. https://doi.org/10.1038/nrc3038

Koster, J., & Versteeg, R. (2008). *R2: Genomics analysis and visualization platform*. Available at R2. Amc. Nl. Accessed January. https://hgserver1.amc.nl/cgi-bin/r2/main.cgi

Krivtsov, Andrei, Twomey, D., Feng, Z., Stubbs, M. C., Wang, Y., Faber, J., Levine, J. E., Wang, J., Hahn, W. C., Gilliland, D. G., Golub, T. R., & Armstrong, S. A. (2006). Transformation from committed progenitor to leukaemia stem cell initiated by MLL-AF9. *Nature*, *442*(7104), 818–822. https://doi.org/10.1038/nature04980

Krivtsov, & Armstrong. (2007). MLL translocations, histone modifications and leukaemia stem-cell development. *Nature Reviews Cancer*, *7*(11), 823–833. https://doi.org/10.1038/nrc2253

Krivtsov, A V, Figueroa, M. E., Sinha, A. U., Stubbs, M. C., Feng, Z., Valk, P. J. M., Delwel, R., Döhner, K., Bullinger, L., Kung, A. L., Melnick, A. M., & Armstrong, S. A. (2013). Cell of origin determines clinically

relevant subtypes of MLL-rearranged AML. *Leukemia*, *27*(4), 852–860. https://doi.org/10.1038/leu.2012.363

Krivtsov, Andrei V, Feng, Z., Lemieux, M., Faber, J., Xia, X., Kung, A. L., & Armstrong, S. A. (2007). Global Increase in H3K79 Dimethylation in Murine and Human MLL-AF4 Lymphoblastic Leukemias. *Blood*, *110*(11), 344. https://doi.org/10.1182/blood.V110.11.344.344

Kühn, M. W. M., Hadler, M. J., Daigle, S. R., Koche, R. P., Krivtsov, A. V., Olhava, E. J., Caligiuri, M. A., Huang, G., Bradner, J. E., Pollock, R. M., Armstrong, S. A., Michael W.M. Kühn, Michael J. Hadler, Scott R. Daigle, Richard P. Koche, Andrei V. Krivtsov, Edward J. Olhava, Michael A. Caligiuri, Gang Huang, … Scott A. Armstrong. (2015). MLL partial tandem duplication leukemia cells are sensitive to small molecule DOT1L inhibition. *Haematologica*, *100*(5 SE-Online Only Articles), e190–e193. https://doi.org/10.3324/haematol.2014.115337

Kwok, H. F., Zhang, S.-D., McCrudden, C. M., Yuen, H.-F., Ting, K.-P., Wen, Q., Khoo, U.-S., & Chan, K. Y.-K. (2014). Prognostic significance of minichromosome maintenance proteins in breast cancer. *American Journal of Cancer Research*, *5*(1), 52–71. https://pubmed.ncbi.nlm.nih.gov/25628920

Labib, K. (2010). How do Cdc7 and cyclin-dependent kinases trigger the initiation of chromosome replication in eukaryotic cells? *Genes & Development* , *24*(12), 1208–1219. https://doi.org/10.1101/gad.1933010

Lapidot, T., Sirard, C., Vormoor, J., Murdoch, B., Hoang, T., Caceres-Cortes, J., Minden, M., Paterson, B., Caligiuri, M. A., & Dick, J. E. (1994). A cell initiating human acute myeloid leukaemia after transplantation into SCID mice. *Nature*, *367*(6464), 645–648. https://doi.org/10.1038/367645a0

Lara-Astiaso, D., Weiner, A., Lorenzo-Vivas, E., Zaretsky, I., Jaitin, D. A., David, E., Keren-Shaul, H., Mildner, A., Winter, D., Jung, S., Friedman, N., & Amit, I. (2014). Chromatin state dynamics during blood formation. *Science*, *345*(6199), 943 LP – 949. https://doi.org/10.1126/science.1256271

Lee-Six, H., Øbro, N. F., Shepherd, M. S., Grossmann, S., Dawson, K., Belmonte, M., Osborne, R. J., Huntly, B. J. P., Martincorena, I., Anderson, E., O'Neill, L., Stratton, M. R., Laurenti, E., Green, A. R., Kent, D. G., & Campbell, P. J. (2018). Population dynamics of normal human blood inferred from somatic mutations. *Nature*, *561*(7724), 473–478. https://doi.org/10.1038/s41586-018-0497-0

Lee, J. S., Cheong, H. S., Koh, Y., Ahn, K.-S., Shin, H. D., & Yoon, S.-S. (2017). MCM7 polymorphisms associated with the AML relapse and overall survival. *Annals of Hematology*, *96*(1), 93–98. https://doi.org/10.1007/s00277-016-2844-2

Lei, M., Kawasaki, Y., & Tye, B. K. (1996). Physical interactions among Mcm proteins and effects of Mcm dosage on DNA replication in Saccharomyces cerevisiae. *Molecular and Cellular Biology*, *16*(9), 5081–5090. https://doi.org/10.1128/MCB.16.9.5081

Li, G. N., Livi, L. L., Gourd, C. M., Deweerd, E. S., & Hoffman-Kim, D. (2007). Genomic and Morphological Changes of Neuroblastoma Cells in Response to Three-Dimensional Matrices. *Tissue Engineering*, *13*(5), 1035–1047. https://doi.org/10.1089/ten.2006.0251

Li, Y., Chen, X., & Lu, C. (2021). The interplay between DNA and histone methylation: molecular mechanisms and disease implications. *EMBO Reports*, *22*(5), e51803. https://doi.org/https://doi.org/10.15252/embr.202051803

Lichti, C. F., Mostovenko, E., Wadsworth, P. A., Lynch, G. C., Pettitt, B. M., Sulman, E. P., Wang, Q., Lang, F. F., Rezeli, M., Marko-Varga, G., Végvári, Á., & Nilsson, C. L. (2015). Systematic Identification of Single Amino Acid Variants in Glioma Stem-Cell-Derived Chromosome 19 Proteins. *Journal of Proteome Research*, *14*(2), 778–786. https://doi.org/10.1021/pr500810g

Liedtke, M., & Cleary, M. L. (2009). Therapeutic targeting of MLL. *Blood*, *113*(24), 6061–6068. https://doi.org/10.1182/blood-2008-12-197061

Liu, H., Cheng, E. H.-Y., & Hsieh, J. J.-D. (2007). Bimodal degradation of MLL by SCFSkp2 and APCCdc20 assures cell cycle execution: a critical regulatory circuit lost in leukemogenic MLL fusions. *Genes & Development*, *21*(19), 2385–2398. https://doi.org/10.1101/gad.1574507

Liu, H., Takeda, S., Kumar, R., Westergard, T. D., Brown, E. J., Pandita, T. K., Cheng, E. H.-Y., & Hsieh, J. J.-D. (2010). Phosphorylation of MLL by ATR is required for execution of mammalian S-phase checkpoint. *Nature*, *467*(7313), 343–346. https://doi.org/10.1038/nature09350

Loenarz, C., & Schofield, C. J. (2008). Expanding chemical biology of 2-oxoglutarate oxygenases. *Nature Chemical Biology*, *4*(3), 152–156. https://doi.org/10.1038/nchembio0308-152

Lu, C., & Thompson, C. B. B. (2012). Metabolic Regulation of Epigenetics. *Cell Metabolism*, *16*(1), 9–17. https://doi.org/10.1016/j.cmet.2012.06.001

Lu, C., Ward, P. S., Kapoor, G. S., Rohle, D., Turcan, S., Abdel-Wahab, O., Edwards, C. R., Khanin, R., Figueroa, M. E., Melnick, A., Wellen, K. E., O'Rourke, D. M., Berger, S. L., Chan, T. A., Levine, R. L., Mellinghoff, I. K., Thompson, C. B., Oğrourke, D. M., Berger, S. L., … Thompson, C. B. (2012). IDH mutation impairs histone demethylation and results in a block to cell differentiation. *Nature*, *483*(7390), 474–478. https://doi.org/10.1038/nature10860

Luo, M., Jeong, M., Sun, D., Park, H. J., Rodriguez, B. A. T., Xia, Z., Yang, L., Zhang, X., Sheng, K., Darlington, G. J., Li, W., & Goodell, M. A. (2015). Long Non-Coding RNAs Control Hematopoietic Stem Cell Function. *Cell Stem Cell*, *16*(4), 426–438. https://doi.org/https://doi.org/10.1016/j.stem.2015.02.002

Lyko, F. (2018). The DNA methyltransferase family: a versatile toolkit for epigenetic regulation. *Nature Reviews Genetics*, *19*(2), 81–92. https://doi.org/10.1038/nrg.2017.80

Machida, Y. J., Hamlin, J. L., & Dutta, A. (2005). Right Place, Right Time, and Only Once: Replication Initiation in Metazoans. *Cell*, *123*(1), 13–24. https://doi.org/https://doi.org/10.1016/j.cell.2005.09.019

Mardis, E. R., Ding, L., Dooling, D. J., Larson, D. E., McLellan, M. D., Chen, K., Koboldt, D. C., Fulton, R. S., Delehaunty, K. D., McGrath, S. D., Fulton, L. A., Locke, D. P., Magrini, V. J., Abbott, R. M., Vickery, T. L., Reed, J. S., Robinson, J. S., Wylie, T., Smith, S. M., … Ley, T. J. (2009). Recurring Mutations Found by Sequencing an Acute Myeloid Leukemia Genome. *New England Journal of Medicine*, *361*(11), 1058–1066. https://doi.org/10.1056/NEJMoa0903840

Mayers, J. R., Torrence, M. E., Danai, L. V., Papagiannakopoulos, T., Davidson, S. M., Bauer, M. R., Lau, A. N., Ji, B. W., Dixit, P. D., Hosios, A. M., Muir, A., Chin, C. R., Freinkman, E., Jacks, T., Wolpin, B. M., Vitkup, D., & Vander Heiden, M. G. (2016). Tissue of origin dictates branched-chain amino acid metabolism in mutant Kras-driven cancers. *Science*, *353*(6304), 1161–1165. https://doi.org/10.1126/science.aaf5171

McCarthy, D. J., Chen, Y., & Smyth, G. K. (2012). Differential expression analysis of multifactor RNA-Seq experiments with respect to biological variation. *Nucleic Acids Research*, *40*(10), 4288–4297. https://doi.org/10.1093/nar/gks042

Méchali, M. (2010). Eukaryotic DNA replication origins: many choices for appropriate answers. *Nature Reviews Molecular Cell Biology*, *11*(10), 728–738. https://doi.org/10.1038/nrm2976

Medeiros, B. C., Chan, S. M., Daver, N. G., Jonas, B. A., & Pollyea, D. A. (2019). Optimizing survival outcomes with post-remission therapy in acute myeloid leukemia. *American Journal of Hematology*, *94*(7), 803–811. https://doi.org/10.1002/ajh.25484

Meyer, C., Burmeister, T., Gröger, D., Tsaur, G., Fechina, L., Renneville, A., Sutton, R., Venn, N. C., Emerenciano, M., Pombo-De-Oliveira, M. S., Barbieri Blunck, C., Almeida Lopes, B., Zuna, J., Trka, J., Ballerini, P., Lapillonne, H., De Braekeleer, M., Cazzaniga, G., Corral Abascal, L., … Marschalek, R. (2018). The MLL recombinome of acute leukemias in 2017. *Leukemia*, *32*(2), 273–284. https://doi.org/10.1038/leu.2017.213

Meyer, C., Hofmann, J., Burmeister, T., Gröger, D., Park, T. S., Emerenciano, M., Pombo De Oliveira, M., Renneville, A., Villarese, P., MacIntyre, E., Cavé, H., Clappier, E., Mass-Malo, K., Zuna, J., Trka, J., De Braekeleer, E., De Braekeleer, M., Oh, S. H., Tsaur, G., … Marschalek, R. (2013). The MLL recombinome of acute leukemias in 2013. *Leukemia*, *27*(11), 2165–2176. https://doi.org/10.1038/leu.2013.135

Meyer, C., Schneider, B., Jakob, S., Strehl, S., Attarbaschi, A., Schnittger, S., Schoch, C., Jansen, M. W. J. C., van Dongen, J. J. M., den Boer, M. L., Pieters, R., Ennas, M.-G., Angelucci, E., Koehl, U., Greil, J., Griesinger, F., zur Stadt, U., Eckert, C., Szczepański, T., … Marschalek, R. (2006). The MLL recombinome of acute leukemias. *Leukemia*, *20*(5), 777–784. https://doi.org/10.1038/sj.leu.2404150

Milne, T. A., Dou, Y., Martin, M. E., Brock, H. W., Roeder, R. G., & Hess, J. L. (2005). MLL associates specifically with a subset of transcriptionally active target genes. *Proceedings of the National Academy of Sciences of the United States of America*, *102*(41), 14765 LP – 14770. https://doi.org/10.1073/pnas.0503630102

Milne, T. A., Kim, J., Wang, G. G., Stadler, S. C., Basrur, V., Whitcomb, S. J., Wang, Z., Ruthenburg, A. J., Elenitoba-Johnson, K. S. J., Roeder, R. G., & Allis, C. D. (2010). Multiple Interactions Recruit MLL1 and MLL1 Fusion Proteins to the HOXA9 Locus in Leukemogenesis. *Molecular Cell*, *38*(6), 853–863. https://doi.org/https://doi.org/10.1016/j.molcel.2010.05.011

Milne, T. A., Martin, M. E., Brock, H. W., Slany, R. K., & Hess, J. L. (2005). Leukemogenic MLL Fusion Proteins Bind across a Broad Region of the Hox a9 Locus, Promoting Transcription and Multiple Histone Modifications. *Cancer Research*, *65*(24), 11367 LP – 11374. https://doi.org/10.1158/0008-5472.CAN-05-1041

Moir, D., Stewart, S. E., Osmond, B. C., & Botstein, D. (1982). COLD-SENSITIVE CELL-DIVISION-CYCLE MUTANTS OF YEAST: ISOLATION, PROPERTIES, AND PSEUDOREVERSION STUDIES. *Genetics*, *100*(4), 547–563. https://doi.org/10.1093/genetics/100.4.547

Mueller, D., Bach, C., Zeisig, D., Garcia-Cuellar, M.-P., Monroe, S., Sreekumar, A., Zhou, R., Nesvizhskii, A., Chinnaiyan, A., Hess, J. L., & Slany, R. K. (2007). A role for the MLL fusion partner ENL in transcriptional elongation and chromatin modification. *Blood*, *110*(13), 4445–4454. https://doi.org/10.1182/blood-2007-05-090514

Muntean, A. G., Tan, J., Sitwala, K., Huang, Y., Bronstein, J., Connelly, J. A., Basrur, V., Elenitoba-Johnson, K. S. J., & Hess, J. L. (2010). The PAF Complex Synergizes with MLL Fusion Proteins at HOX Loci to Promote Leukemogenesis. *Cancer Cell*, *17*(6), 609–621. https://doi.org/10.1016/J.CCR.2010.04.012

Muzny, D. M., Bainbridge, M. N., Chang, K., Dinh, H. H., Drummond, J. A., Fowler, G., Kovar, C. L., Lewis, L. R., Morgan, M. B., Newsham, I. F., Reid, J. G., Santibanez, J., Shinbrot, E., Trevino, L. R., Wu, Y.-Q., Wang, M., Gunaratne, P., Donehower, L. A., Creighton, C. J., … group, T. source sites and disease working. (2012). Comprehensive molecular characterization of human colon and rectal cancer. *Nature*, *487*(7407), 330–337. https://doi.org/10.1038/nature11252

Nepon-Sixt, B. S., Bryant, V. L., & Alexandrow, M. G. (2019). Myc-driven chromatin accessibility regulates Cdc45 assembly into CMG helicases. *Communications Biology*, *2*(1), 110. https://doi.org/10.1038/s42003-019-0353-2

Neves, H., & Kwok, H. F. (2017). In sickness and in health: The many roles of the minichromosome maintenance proteins. *Biochimica et Biophysica Acta (BBA) - Reviews on Cancer*, *1868*(1), 295–308. https://doi.org/https://doi.org/10.1016/j.bbcan.2017.06.001

Ng, S. W. K., Mitchell, A., Kennedy, J. A., Chen, W. C., McLeod, J., Ibrahimova, N., Arruda, A., Popescu, A., Gupta, V., Schimmer, A. D., Schuh, A. C., Yee, K. W., Bullinger, L., Herold, T., Görlich, D., Büchner, T., Hiddemann, W., Berdel, W. E., Wörmann, B., … Wang, J. C. Y. (2016). A 17-gene stemness score for rapid determination of risk in acute leukaemia. *Nature*, *540*(7633), 433–437. https://doi.org/10.1038/nature20598

Nguyen, A. T., & Zhang, Y. (2011). The diverse functions of Dot1 and H3K79 methylation. [Genes Dev. 2011] - PubMed - NCBI. *Genes and Development*, *3*(13), 1345–1358. https://doi.org/10.1101/gad.2057811.ute

Noushmehr, H., Weisenberger, D. J., Diefes, K., Phillips, H. S., Pujara, K., Berman, B. P., Pan, F., Pelloski, C. E., Sulman, E. P., Bhat, K. P., Verhaak, R. G. W., Hoadley, K. A., Hayes, D. N., Perou, C. M., Schmidt, H. K., Ding, L., Wilson, R. K., Van Den Berg, D., Shen, H., … Aldape, K. (2010). Identification of a CpG Island Methylator Phenotype that Defines a Distinct Subgroup of Glioma. *Cancer Cell*, *17*(5), 510–522. https://doi.org/10.1016/j.ccr.2010.03.017

Ntziachristos, P., Abdel-Wahab, O., & Aifantis, I. (2016). Emerging concepts of epigenetic dysregulation in hematological malignancies. *Nature Immunology*, *17*(9), 1016–1024. https://doi.org/10.1038/ni.3517

Odejide, O., Weigert, O., Lane, A. A., Toscano, D., Lunning, M. A., Kopp, N., Kim, S., van Bodegom, D., Bolla, S., Schatz, J. H., Teruya-Feldstein, J., Hochberg, E., Louissaint, A., Dorfman, D., Stevenson, K., Rodig, S. J., Piccaluga, P. P., Jacobsen, E., Pileri, S. A., … Weinstock, D. M. (2014). A targeted mutational landscape of angioimmunoblastic T-cell lymphoma. *Blood*, *123*(9), 1293–1296. https://doi.org/10.1182/blood-2013-10-531509

Ohm, J. E., McGarvey, K. M., Yu, X., Cheng, L., Schuebel, K. E., Cope, L., Mohammad, H. P., Chen, W., Daniel, V. C., Yu, W., Berman, D. M., Jenuwein, T., Pruitt, K., Sharkis, S. J., Watkins, D. N., Herman, J. G., & Baylin, S. B. (2007). A stem cell–like chromatin pattern may predispose tumor suppressor genes to DNA hypermethylation and heritable silencing. *Nature Genetics*, *39*(2), 237–242. https://doi.org/10.1038/ng1972

Okada, Y., Feng, Q., Lin, Y., Jiang, Q., Li, Y., Coffield, V. M., Su, L., Xu, G., & Zhang, Y. (2005). hDOT1L Links Histone Methylation to Leukemogenesis. *Cell*, *121*(2), 167–178. https://doi.org/10.1016/j.cell.2005.02.020

Oktyabri, D., Ishimura, A., Tange, S., Terashima, M., & Suzuki, T. (2016). DOT1L histone methyltransferase regulates the expression of BCAT1 and is involved in sphere formation and cell migration of breast cancer cell lines. *Biochimie*. https://doi.org/10.1016/j.biochi.2016.01.005

Ooi, S. K. T., Qiu, C., Bernstein, E., Li, K., Jia, D., Yang, Z., Erdjument-Bromage, H., Tempst, P., Lin, S.-P., Allis, C. D., Cheng, X., & Bestor, T. H. (2007). DNMT3L connects unmethylated lysine 4 of histone H3 to de novo methylation of DNA. *Nature*, *448*(7154), 714–717. https://doi.org/10.1038/nature05987

Pacek, M., Tutter, A. V, Kubota, Y., Takisawa, H., & Walter, J. C. (2006). Localization of MCM2-7, Cdc45, and

GINS to the Site of DNA Unwinding during Eukaryotic DNA Replication. *Molecular Cell*, *21*(4), 581–587. https://doi.org/https://doi.org/10.1016/j.molcel.2006.01.030

Palm, W., Park, Y., Wright, K., Pavlova, N. N., Tuveson, D. A., & Thompson, C. B. (2015). The Utilization of Extracellular Proteins as Nutrients Is Suppressed by mTORC1. *Cell*, *162*(2), 259–270. https://doi.org/https://doi.org/10.1016/j.cell.2015.06.017

Patel, J. H., Loboda, A. P., Showe, M. K., Showe, L. C., & McMahon, S. B. (2004). Analysis of genomic targets reveals complex functions of MYC. *Nature Reviews Cancer*, *4*(7), 562–568. https://doi.org/10.1038/nrc1393

Pei, W., Feyerabend, T. B., Rössler, J., Wang, X., Postrach, D., Busch, K., Rode, I., Klapproth, K., Dietlein, N., Quedenau, C., Chen, W., Sauer, S., Wolf, S., Höfer, T., & Rodewald, H.-R. (2017). Polylox barcoding reveals haematopoietic stem cell fates realized in vivo. *Nature*, *548*(7668), 456–460. https://doi.org/10.1038/nature23653

Placke, T., Faber, K., Nonami, A., Putwain, S. L., Salih, H. R., Heidel, F. H., Krämer, A., Root, D. E., Barbie, D. A., Krivtsov, A. V., Armstrong, S. A., Hahn, W. C., Huntly, B. J., Sykes, S. M., Milsom, M. D., Scholl, C., & Fröhling, S. (2014). Requirement for CDK6 in MLL-rearranged acute myeloid leukemia. *Blood*, *124*(1), 13–23. https://doi.org/10.1182/blood-2014-02-558114

Pollok, S., Bauerschmidt, C., Sänger, J., Nasheuer, H.-P., & Grosse, F. (2007). Human Cdc45 is a proliferation-associated antigen. *The FEBS Journal*, *274*(14), 3669–3684. https://doi.org/https://doi.org/10.1111/j.1742-4658.2007.05900.x

Pollyea, D. A., Stevens, B. M., Jones, C. L., Winters, A., Pei, S., Minhajuddin, M., D'Alessandro, A., Culp-Hill, R., Riemondy, K. A., Gillen, A. E., Hesselberth, J. R., Abbott, D., Schatz, D., Gutman, J. A., Purev, E., Smith, C., & Jordan, C. T. (2018). Venetoclax with azacitidine disrupts energy metabolism and targets leukemia stem cells in patients with acute myeloid leukemia. *Nature Medicine*, *24*(12), 1859–1866. https://doi.org/10.1038/s41591-018-0233-1

Prada-Arismendy, J., Arroyave, J. C., & Röthlisberger, S. (2017). Molecular biomarkers in acute myeloid leukemia. *Blood Reviews*, *31*(1), 63–76. https://doi.org/https://doi.org/10.1016/j.blre.2016.08.005

Quivoron, C., Couronné, L., Della Valle, V., Lopez, C. K., Plo, I., Wagner-Ballon, O., Do Cruzeiro, M., Delhommeau, F., Arnulf, B., Stern, M.-H., Godley, L., Opolon, P., Tilly, H., Solary, E., Duffourd, Y., Dessen, P., Merle-Beral, H., Nguyen-Khac, F., Fontenay, M., … Bernard, O. A. (2011). TET2 Inactivation Results in Pleiotropic Hematopoietic Abnormalities in Mouse and Is a Recurrent Event during Human Lymphomagenesis. *Cancer Cell*, *20*(1), 25–38. https://doi.org/https://doi.org/10.1016/j.ccr.2011.06.003

Raffel, S., Falcone, M., Kneisel, N., Hansson, J., Wang, W., Lutz, C., Bullinger, L., Poschet, G., Nonnenmacher, Y., Barnert, A., Bahr, C., Zeisberger, P., Przybylla, A., Sohn, M., Tönjes, M., Erez, A., Adler, L., Jensen, P., Scholl, C., … Trumpp, A. (2017). BCAT1 restricts αkG levels in AML stem cells leading to IDHmut-like DNA hypermethylation. *Nature*, *551*(7680), 384–388. https://doi.org/10.1038/nature24294

Rao, R. C., & Dou, Y. (2015). Hijacked in cancer: the KMT2 (MLL) family of methyltransferases. *Nature Reviews Cancer*, *15*(6), 334–346. https://doi.org/10.1038/nrc3929

Remus, D., & Diffley, J. F. X. (2009). Eukaryotic DNA replication control: Lock and load, then fire. *Current Opinion in Cell Biology*, *21*(6), 771–777. https://doi.org/https://doi.org/10.1016/j.ceb.2009.08.002

Rice, K. L., & Licht, J. D. (2007). HOX deregulation in acute myeloid leukemia. *The Journal of Clinical Investigation*, *117*(4), 865–868. https://doi.org/10.1172/JCI31861

Richter, A., Schoenwaelder, N., Sender, S., Junghanss, C., & Maletzki, C. (2021). Cyclin-Dependent Kinase Inhibitors in Hematological Malignancies—Current Understanding, (Pre-)Clinical Application and Promising Approaches. In *Cancers* (Vol. 13, Issue 10). https://doi.org/10.3390/cancers13102497

Riera, A., Barbon, M., Noguchi, Y., Reuter, L. M., Schneider, S., & Speck, C. (2017). From structure to mechanism—understanding initiation of DNA replication. *Genes & Development* , *31*(11), 1073–1088. http://genesdev.cshlp.org/content/31/11/1073.abstract

Robinson, M. D., McCarthy, D. J., & Smyth, G. K. (2010). edgeR: a Bioconductor package for differential expression analysis of digital gene expression data. *Bioinformatics*, *26*(1), 139–140. https://doi.org/10.1093/bioinformatics/btp616

Roden, C., & Lu, J. (2016). MicroRNAs in Control of Stem Cells in Normal and Malignant Hematopoiesis. *Current Stem Cell Reports*, *2*(3), 183–196. https://doi.org/10.1007/s40778-016-0057-1

Rodrigues, C. P., Shvedunova, M., & Akhtar, A. (2021). Epigenetic Regulators as the Gatekeepers of

Hematopoiesis. *Trends in Genetics*, *37*(2), 125–142. https://doi.org/10.1016/j.tig.2020.09.015

Rodriguez-Fraticelli, A. E., Wolock, S. L., Weinreb, C. S., Panero, R., Patel, S. H., Jankovic, M., Sun, J., Calogero, R. A., Klein, A. M., & Camargo, F. D. (2018). Clonal analysis of lineage fate in native haematopoiesis. *Nature*, *553*(7687), 212–216. https://doi.org/10.1038/nature25168

Rodríguez-Paredes, M., & Esteller, M. (2011). Cancer epigenetics reaches mainstream oncology. *Nature Medicine*, *17*(3), 330–339. https://doi.org/10.1038/nm.2305

Ross-Innes, C. S., Stark, R., Teschendorff, A. E., Holmes, K. A., Ali, H. R., Dunning, M. J., Brown, G. D., Gojis, O., Ellis, I. O., Green, A. R., Ali, S., Chin, S.-F., Palmieri, C., Caldas, C., & Carroll, J. S. (2012). Differential oestrogen receptor binding is associated with clinical outcome in breast cancer. *Nature*, *481*(7381), 389–393. https://doi.org/10.1038/nature10730

Rossi, C., Madl, P., Foletti, A., & Mocenni, C. (2015). *Fields of the Cell, Chapter 4* (D. Fels, M. Cifra, & F. Scholkmann (Eds.)).

Rybtsov, S., Batsivari, A., Bilotkach, K., Paruzina, D., Senserrich, J., Nerushev, O., & Medvinsky, A. (2014). Tracing the Origin of the HSC Hierarchy Reveals an SCF-Dependent, IL-3-Independent CD43− Embryonic Precursor. *Stem Cell Reports*, *3*(3), 489–501. https://doi.org/10.1016/j.stemcr.2014.07.009

Sadovnik, I., Herrmann, H., Blatt, K., Eisenwort, G., Mueller, N., Stefanzl, G., Hoermann, G., Herndlhofer, S., Bauer, K., Peter, B., Gaupmann, R., Schulenburg, A., Sperr, W. R., & Valent, P. (2016). Evaluation of Cell Surface Markers and Targets in Leukemic Stem Cells (LSC) Reveals Distinct Expression Profiles, Unique Drug Effects, and Specific Checkpoint Regulation in AML LSC and CML LSC. *Blood*, *128*(22), 4234. https://doi.org/10.1182/blood.V128.22.4234.4234

Schübeler, D. (2015). Function and information content of DNA methylation. *Nature*, *517*(7534), 321–326. https://doi.org/10.1038/nature14192

Schvartzman, J. M., Thompson, C. B., & Finley, L. W. S. (2018). Metabolic regulation of chromatin modifications and gene expression. *Journal of Cell Biology*, *217*(7), 2247–2259. https://doi.org/10.1083/jcb.201803061

Seita, J., & Weissman, I. L. (2010). Hematopoietic stem cell: self-renewal versus differentiation. *Wiley Interdisciplinary Reviews. Systems Biology and Medicine*, *2*(6), 640–653. https://doi.org/10.1002/wsbm.86

Sheikh, B. N., & Akhtar, A. (2019). The many lives of KATs — detectors, integrators and modulators of the cellular environment. *Nature Reviews Genetics*, *20*(1), 7–23. https://doi.org/10.1038/s41576-018-0072-4

Shinsuke, I., Li, S., Qing, D., C., W. S., B., C. L., A., S. J., Chuan, H., & Yi, Z. (2011). Tet Proteins Can Convert 5-Methylcytosine to 5-Formylcytosine and 5-Carboxylcytosine. *Science*, *333*(6047), 1300–1303. https://doi.org/10.1126/science.1210597

Shlush, L. I., Zandi, S., Mitchell, A., Chen, W. C., Brandwein, J. M., Gupta, V., Kennedy, J. A., Schimmer, A. D., Schuh, A. C., Yee, K. W., McLeod, J. L., Doedens, M., Medeiros, J. J. F., Marke, R., Kim, H. J., Lee, K., McPherson, J. D., Hudson, T. J., Pan-Leukemia Gene Panel Consortium, T. H., … Dick, J. E. (2014). Identification of pre-leukaemic haematopoietic stem cells in acute leukaemia. *Nature*, *506*(7488), 328–333. https://doi.org/10.1038/nature13038

Shukla, N., Wetmore, C., O'Brien, M. M., Silverman, L. B., Brown, P., Cooper, T. M., Thomson, B., Blakemore, S. J., Daigle, S., Suttle, B., Waters, N. J., Krivstov, A. V, Armstrong, S. A., Ho, P. T., & Gore, L. (2016). Final Report of Phase 1 Study of the DOT1L Inhibitor, Pinometostat (EPZ-5676), in Children with Relapsed or Refractory MLL-r Acute Leukemia. *Blood*, *128*(22), 2780. https://doi.org/10.1182/blood.V128.22.2780.2780

Siddiqui, K., On, K. F., & Diffley, J. F. X. (2013). Regulating DNA Replication in Eukarya. *Cold Spring Harbor Perspectives in Biology* , *5*(9). https://doi.org/10.1101/cshperspect.a012930

Silva, L. (2017). *Branched-chain amino acid metabolism in the tumor microenvironment interaction*.

Silva, L. S., Poschet, G., Nonnenmacher, Y., Becker, H. M., Sapcariu, S., Gaupel, A.-C., Schlotter, M., Wu, Y., Kneisel, N., Seiffert, M., Hell, R., Hiller, K., Lichter, P., & Radlwimmer, B. (2017). Branched-chain ketoacids secreted by glioblastoma cells via MCT1 modulate macrophage phenotype. *EMBO Reports*, *18*(12), 2172–2185. https://doi.org/https://doi.org/10.15252/embr.201744154

Sivanand, S., & Vander Heiden, M. G. (2020). Emerging Roles for Branched-Chain Amino Acid Metabolism in Cancer. *Cancer Cell*, *37*(2), 147–156. https://doi.org/https://doi.org/10.1016/j.ccell.2019.12.011

Somervaille, T. C. P., & Cleary, M. L. (2006). Identification and characterization of leukemia stem cells in murine MLL-AF9 acute myeloid leukemia. *Cancer Cell*, *10*(4), 257–268. https://doi.org/https://doi.org/10.1016/j.ccr.2006.08.020

Somervaille, T. C. P., Matheny, C. J., Spencer, G. J., Iwasaki, M., Rinn, J. L., Witten, D. M., Chang, H. Y., Shurtleff, S. A., Downing, J. R., & Cleary, M. L. (2009). Hierarchical maintenance of MLL myeloid leukemia stem cells employs a transcriptional program shared with embryonic rather than adult stem cells. *Cell Stem Cell*, *4*(2), 129–140. https://doi.org/10.1016/j.stem.2008.11.015

Srinivasan, S. V., Dominguez-Sola, D., Wang, L. C., Hyrien, O., & Gautier, J. (2013). Cdc45 Is a Critical Effector of Myc-Dependent DNA Replication Stress. *Cell Reports*, *3*(5), 1629–1639. https://doi.org/https://doi.org/10.1016/j.celrep.2013.04.002

Stavropoulou, V., Kaspar, S., Brault, L., Sanders, M. A., Juge, S., Morettini, S., Tzankov, A., Iacovino, M., Lau, I. J., Milne, T. A., Royo, H., Kyba, M., Valk, P. J. M., Peters, A. H. F. M., & Schwaller, J. (2016). MLL-AF9 Expression in Hematopoietic Stem Cells Drives a Highly Invasive AML Expressing EMT-Related Genes Linked to Poor Outcome. *Cancer Cell*, *30*(1), 43–58. https://doi.org/10.1016/j.ccell.2016.05.011

Stein, E. M., DiNardo, C. D., Pollyea, D. A., Fathi, A. T., Roboz, G. J., Altman, J. K., Stone, R. M., DeAngelo, D. J., Levine, R. L., Flinn, I. W., Kantarjian, H. M., Collins, R., Patel, M. R., Frankel, A. E., Stein, A., Sekeres, M. A., Swords, R. T., Medeiros, B. C., Willekens, C., … Tallman, M. S. (2017). Enasidenib in mutant IDH2 relapsed or refractory acute myeloid leukemia. *Blood*, *130*(6), 722–731. https://doi.org/10.1182/blood-2017-04-779405

Stillman, B. (1994). Smart machines at the DNA replication fork. *Cell*, *78*(5), 725–728. https://doi.org/https://doi.org/10.1016/S0092-8674(94)90362-X

Strissel, P. L., Strick, R., Rowley, J. D., & Zeleznik-Le, N. J. (1998). An In Vivo Topoisomerase II Cleavage Site and a DNase I Hypersensitive Site Colocalize Near Exon 9 in the MLLBreakpoint Cluster Region. *Blood*, *92*(10), 3793–3803. https://doi.org/https://doi.org/10.1182/blood.V92.10.3793

Sullivan, M. R., Danai, L. V, Lewis, C. A., Chan, S. H., Gui, D. Y., Kunchok, T., Dennstedt, E. A., Vander Heiden, M. G., & Muir, A. (2019). Quantification of microenvironmental metabolites in murine cancers reveals determinants of tumor nutrient availability. *ELife*, *8*, e44235. https://doi.org/10.7554/eLife.44235

Suryawan, A., Hawes, J. W., Harris, R. A., Shimomura, Y., Jenkins, A. E., & Hutson, S. M. (1998). A molecular model of human branched-chain amino acid metabolism. *The American Journal of Clinical Nutrition*, *68*(1), 72–81. https://doi.org/10.1093/ajcn/68.1.72

Sweatt, A. J., Wood, M., Suryawan, A., Wallin, R., Willingham, M. C., & Hutson, S. M. (2004). Branched-chain amino acid catabolism: unique segregation of pathway enzymes in organ systems and peripheral nerves. *American Journal of Physiology-Endocrinology and Metabolism*, *286*(1), E64–E76. https://doi.org/10.1152/ajpendo.00276.2003

Tate, J. G., Bamford, S., Jubb, H. C., Sondka, Z., Beare, D. M., Bindal, N., Boutselakis, H., Cole, C. G., Creatore, C., Dawson, E., Fish, P., Harsha, B., Hathaway, C., Jupe, S. C., Kok, C. Y., Noble, K., Ponting, L., Ramshaw, C. C., Rye, C. E., … Forbes, S. A. (2019, January 8). *COSMIC: The Catalogue Of Somatic Mutations In Cancer*. Nucleic Acids Research. https://doi.org/10.1093/nar/gky1015

Taylor, R. T., & Jenkins, W. T. (1966). Leucine Aminotransferase: II. PURIFICATION AND CHARACTERIZATION. *Journal of Biological Chemistry*, *241*(19), 4396–4405. https://doi.org/https://doi.org/10.1016/S0021-9258(18)99734-6

Thewes, V., Simon, R., Hlevnjak, M., Schlotter, M., Schroeter, P., Schmidt, K., Wu, Y., Anzeneder, T., Wang, W., Windisch, P., Kirchgäßner, M., Melling, N., Kneisel, N., Büttner, R., Deuschle, U., Sinn, H. P., Schneeweiss, A., Heck, S., Kaulfuss, S., … Tönjes, M. (2017). The branched-chain amino acid transaminase 1 sustains growth of antiestrogen-resistant and ERα-negative breast cancer. *Oncogene*, *36*(29), 4124–4134. https://doi.org/10.1038/onc.2017.32

Thiel, A. T., Blessington, P., Zou, T., Feather, D., Wu, X., Yan, J., Zhang, H., Liu, Z., Ernst, P., Koretzky, G. A., & Hua, X. (2010). MLL-AF9-Induced Leukemogenesis Requires Coexpression of the Wild-Type Mll Allele. *Cancer Cell*, *17*(2), 148–159. https://doi.org/https://doi.org/10.1016/j.ccr.2009.12.034

Thirstrup, K., Christensen, S., Møller, H. A., Ritzén, A., Bergström, A.-L., Sager, T. N., & Jensen, H. S. (2011). Endogenous 2-oxoglutarate levels impact potencies of competitive HIF prolyl hydroxylase inhibitors. *Pharmacological Research*, *64*(3), 268–273. https://doi.org/https://doi.org/10.1016/j.phrs.2011.03.017

Thomson, J. P., Skene, P. J., Selfridge, J., Clouaire, T., Guy, J., Webb, S., Kerr, A. R. W., Deaton, A., Andrews, R., James, K. D., Turner, D. J., Illingworth, R., & Bird, A. (2010). CpG islands influence chromatin structure via the CpG-binding protein Cfp1. *Nature*, *464*(7291), 1082–1086.

https://doi.org/10.1038/nature08924

Tkachuk, D. C., Kohler, S., & Cleary, M. L. (1992). Involvement of a homolog of Drosophila trithorax by 11q23 chromosomal translocations in acute leukemias. *Cell*, *71*(4), 691–700. https://doi.org/10.1016/0092-8674(92)90602-9

Tönjes, M., Barbus, S., Park, Y. J., Wang, W., Schlotter, M., Lindroth, A. M., Pleier, S. V., Bai, A. H. C. C., Karra, D., Piro, R. M., Felsberg, J., Addington, A., Lemke, D., Weibrecht, I., Hovestadt, V., Rolli, C. G., Campos, B., Turcan, S., Sturm, D., … Radlwimmer, B. (2013). BCAT1 promotes cell proliferation through amino acid catabolism in gliomas carrying wild-type IDH1. *Nature Medicine*, *19*(7), 901–908. https://doi.org/10.1038/nm.3217

Trompouki, E., Bowman, T. V., Lawton, L. N., Fan, Z. P., Wu, D.-C., DiBiase, A., Martin, C. S., Cech, J. N., Sessa, A. K., Leblanc, J. L., Li, P., Durand, E. M., Mosimann, C., Heffner, G. C., Daley, G. Q., Paulson, R. F., Young, R. A., & Zon, L. I. (2011). Lineage Regulators Direct BMP and Wnt Pathways to Cell-Specific Programs during Differentiation and Regeneration. *Cell*, *147*(3), 577–589. https://doi.org/10.1016/j.cell.2011.09.044

Tsakaneli, A., & Williams, O. (2021). Drug Repurposing for Targeting Acute Leukemia With KMT2A (MLL)—Gene Rearrangements . In *Frontiers in Pharmacology* (Vol. 12, p. 2513). https://www.frontiersin.org/article/10.3389/fphar.2021.741413

Turcan, S., Rohle, D., Goenka, A., Walsh, L. A., Fang, F., Yilmaz, E., Campos, C., Fabius, A. W. M., Lu, C., Ward, P. S., Thompson, C. B., Kaufman, A., Guryanova, O., Levine, R., Heguy, A., Viale, A., Morris, L. G. T., Huse, J. T., Mellinghoff, I. K., & Chan, T. A. (2012). IDH1 mutation is sufficient to establish the glioma hypermethylator phenotype. *Nature*, *483*(7390), 479–483. https://doi.org/10.1038/nature10866

Uckelmann, H. J., Kim, S. M., Wong, E. M., Hatton, C., Giovinazzo, H., Gadrey, J. Y., Krivtsov, A. V, Rücker, F. G., Döhner, K., McGeehan, G. M., Levine, R. L., Bullinger, L., Vassiliou, G. S., & Armstrong, S. A. (2020). Therapeutic targeting of preleukemia cells in a mouse model of NPM1 mutant acute myeloid leukemia. *Science*, *367*(6477), 586 LP – 590. https://doi.org/10.1126/science.aax5863

Vander Heiden, M. G. (2011). Targeting cancer metabolism: a therapeutic window opens. *Nature Reviews Drug Discovery*, *10*(9), 671–684. https://doi.org/10.1038/nrd3504

Velten, L., Haas, S. F., Raffel, S., Blaszkiewicz, S., Islam, S., Hennig, B. P., Hirche, C., Lutz, C., Buss, E. C., Nowak, D., Boch, T., Hofmann, W.-K., Ho, A. D., Huber, W., Trumpp, A., Essers, M. A. G., & Steinmetz, L. M. (2017). Human haematopoietic stem cell lineage commitment is a continuous process. *Nature Cell Biology*, *19*(4), 271–281. https://doi.org/10.1038/ncb3493

Vetrie, D., Vignir Helgason, G., Copland, M., Helgason, G. V., & Copland, M. (2020). The leukaemia stem cell: similarities, differences and clinical prospects in CML and AML. *Nature Reviews Cancer*, *20*(3), 158–173. https://doi.org/10.1038/s41568-019-0230-9

Waddington, C. H. (1957). The Strategy of the Genes. In *The Strategy of the Genes*. https://doi.org/10.4324/9781315765471

Wang, J., Muntean, A. G., & Hess, J. L. (2012). ECSASB2 mediates MLL degradation during hematopoietic differentiation. *Blood*, *119*(5), 1151–1161. https://doi.org/10.1182/blood-2011-06-362079

Wang, J., Muntean, A. G., Wu, L., & Hess, J. L. (2012). A subset of mixed lineage leukemia proteins has plant homeodomain (PHD)-mediated E3 ligase activity. *The Journal of Biological Chemistry*, *287*(52), 43410–43416. https://doi.org/10.1074/jbc.M112.423855

Wang, Z., Zang, C., Cui, K., Schones, D. E., Barski, A., Peng, W., & Zhao, K. (2009). Genome-wide Mapping of HATs and HDACs Reveals Distinct Functions in Active and Inactive Genes. *Cell*, *138*(5), 1019–1031. https://doi.org/10.1016/j.cell.2009.06.049

Warburg, O. (1956). On the origin of cancer cells. *Science*, *123*(3191), 309–314. https://doi.org/10.1126/science.123.3191.309

Warburg, O., Wind, F., & Negelein, E. (1927). THE METABOLISM OF TUMORS IN THE BODY . *Journal of General Physiology*, *8*(6), 519–530. https://doi.org/10.1085/jgp.8.6.519

Ward, P. S., Patel, J., Wise, D. R., Abdel-Wahab, O., Bennett, B. D., Coller, H. A., Cross, J. R., Fantin, V. R., Hedvat, C. V., Perl, A. E., Rabinowitz, J. D., Carroll, M., Su, S. M., Sharp, K. A., Levine, R. L., & Thompson, C. B. (2010). The Common Feature of Leukemia-Associated IDH1 and IDH2 Mutations Is a Neomorphic Enzyme Activity Converting α-Ketoglutarate to 2-Hydroxyglutarate. *Cancer Cell*, *17*(3), 225–234. https://doi.org/10.1016/j.ccr.2010.01.020

Weinreb, C., Rodriguez-Fraticelli, A., Camargo, F. D., & Klein, A. M. (2020). Lineage tracing on transcriptional landscapes links state to fate during differentiation. *Science*, *367*(6479), eaaw3381. https://doi.org/10.1126/science.aaw3381

Weisberg, E., Boulton, C., Kelly, L. M., Manley, P., Fabbro, D., Meyer, T., Gilliland, D. G., & Griffin, J. D. (2002). Inhibition of mutant FLT3 receptors in leukemia cells by the small molecule tyrosine kinase inhibitor PKC412. *Cancer Cell*, *1*(5), 433–443. https://doi.org/https://doi.org/10.1016/S1535-6108(02)00069-7

Widschwendter, M., Fiegl, H., Egle, D., Mueller-Holzner, E., Spizzo, G., Marth, C., Weisenberger, D. J., Campan, M., Young, J., Jacobs, I., & Laird, P. W. (2007). Epigenetic stem cell signature in cancer. *Nature Genetics*, *39*(2), 157–158. https://doi.org/10.1038/ng1941

Woodward, A. M., Göhler, T., Luciani, M. G., Oehlmann, M., Ge, X., Gartner, A., Jackson, D. A., & Blow, J. J. (2006). Excess Mcm2–7 license dormant origins of replication that can be used under conditions of replicative stress . *Journal of Cell Biology*, *173*(5), 673–683. https://doi.org/10.1083/jcb.200602108

Workflow: ACTseq_spike_in.cwl. (2021). https://doi.org/https://doi.org/10.7490/f1000research.1114375.1

Xu, W., Yang, H., Liu, Y., Yang, Y., Wang, P., Kim, S.-H., Ito, S., Yang, C., Wang, P., Xiao, M.-T., Liu, L., Jiang, W., Liu, J., Zhang, J., Wang, B., Frye, S., Zhang, Y., Xu, Y., Lei, Q., … Xiong, Y. (2011). Oncometabolite 2-Hydroxyglutarate Is a Competitive Inhibitor of α-Ketoglutarate-Dependent Dioxygenases. *Cancer Cell*, *19*(1), 17–30. https://doi.org/10.1016/j.ccr.2010.12.014

Yamashita, M., Dellorusso, P. V, Olson, O. C., & Passegué, E. (2020). Dysregulated haematopoietic stem cell behaviour in myeloid leukaemogenesis. *Nature Reviews Cancer*, *20*(7), 365–382. https://doi.org/10.1038/s41568-020-0260-3

Yan, H., Parsons, D. W., Jin, G., McLendon, R., Rasheed, B. A., Yuan, W., Kos, I., Batinic-Haberle, I., Jones, S., Riggins, G. J., Friedman, H., Friedman, A., Reardon, D., Herndon, J., Kinzler, K. W., Velculescu, V. E., Vogelstein, B., & Bigner, D. D. (2009). IDH1 and IDH2 Mutations in Gliomas. *New England Journal of Medicine*, *360*(8), 765–773. https://doi.org/10.1056/NEJMoa0808710

Yang, L., Lei, Q., Li, L., Yang, J., Dong, Z., & Cui, H. (2019). Silencing or inhibition of H3K79 methyltransferase DOT1L induces cell cycle arrest by epigenetically modulating c-Myc expression in colorectal cancer. *Clinical Epigenetics*, *11*(1), 199. https://doi.org/10.1186/s13148-019-0778-y

Yennawar, N., Dunbar, J., Conway, M., Hutson, S., & Farber, G. (2001). The structure of human mitochondrial {\-}branched-{\-}chain aminotransferase. *Acta Crystallographica Section D*, *57*(4), 506–515. https://doi.org/10.1107/S0907444901001925

Yennawar, N. H., Islam, M. M., Conway, M., Wallin, R., & Hutson, S. M. (2006). Human Mitochondrial Branched Chain Aminotransferase Isozyme: STRUCTURAL ROLE OF THE CXXC CENTER IN CATALYSIS *. *Journal of Biological Chemistry*, *281*(51), 39660–39671. https://doi.org/10.1074/jbc.M607552200

Yi, M., Li, A., Zhou, L., Chu, Q., Song, Y., & Wu, K. (2020). The global burden and attributable risk factor analysis of acute myeloid leukemia in 195 countries and territories from 1990 to 2017: estimates based on the global burden of disease study 2017. *Journal of Hematology & Oncology*, *13*(1), 72. https://doi.org/10.1186/s13045-020-00908-z

Yokoyama, A., Kitabayashi, I., Ayton, P. M., Cleary, M. L., & Ohki, M. (2002). Leukemia proto-oncoprotein MLL is proteolytically processed into 2 fragments with opposite transcriptional properties. *Blood*, *100*(10), 3710–3718. https://doi.org/10.1182/blood-2002-04-1015

Yokoyama, A., Somervaille, T. C. P., Smith, K. S., Rozenblatt-Rosen, O., Meyerson, M., & Cleary, M. L. (2005). The Menin Tumor Suppressor Protein Is an Essential Oncogenic Cofactor for MLL-Associated Leukemogenesis. *Cell*, *123*(2), 207–218. https://doi.org/10.1016/j.cell.2005.09.025

Yoshikawa, R., Yanagi, H., Shen, C.-S., Fujiwara, Y., Noda, M., Yagyu, T., Gega, M., Oshima, T., Yamamura, T., Okamura, H., Nakano, Y., Morinaga, T., & Hashimoto-Tamaoki, T. (2006). ECA39 is a novel distant metastasis-related biomarker in colorectal cancer. *World Journal of Gastroenterology*, *12*(36), 5884–5889. https://doi.org/10.3748/wjg.v12.i36.5884

Yu-Fei, H., Bin-Zhong, L., Zheng, L., Peng, L., Yang, W., Qingyu, T., Jianping, D., Yingying, J., Zhangcheng, C., Lin, L., Yan, S., Xiuxue, L., Qing, D., Chun-Xiao, S., Kangling, Z., Chuan, H., & Guo-Liang, X. (2011). Tet-Mediated Formation of 5-Carboxylcytosine and Its Excision by TDG in Mammalian DNA. *Science*, *333*(6047), 1303–1307. https://doi.org/10.1126/science.1210944

Yu, B. D., Hess, J. L., Horning, S. E., Brown, G. A. J., & Korsmeyer, S. J. (1995). Altered Hox expression and segmental identity in Mll-mutant mice. *Nature*, *378*(6556), 505–508. https://doi.org/10.1038/378505a0

Yu, G., Wang, L.-G., Han, Y., & He, Q.-Y. (2012). clusterProfiler: an R Package for Comparing Biological

Themes Among Gene Clusters. *OMICS: A Journal of Integrative Biology*, *16*(5), 284–287. https://doi.org/10.1089/omi.2011.0118

Yu, G., Wang, L.-G., & He, Q.-Y. (2015). ChIPseeker: an R/Bioconductor package for ChIP peak annotation, comparison and visualization. *Bioinformatics*, *31*(14), 2382–2383. https://doi.org/10.1093/bioinformatics/btv145

Yu, V. W. C., Yusuf, R. Z., Oki, T., Wu, J., Saez, B., Wang, X., Cook, C., Baryawno, N., Ziller, M. J., Lee, E., Gu, H., Meissner, A., Lin, C. P., Kharchenko, P. V, & Scadden, D. T. (2017). Epigenetic Memory Underlies Cell-Autonomous Heterogeneous Behavior of Hematopoietic Stem Cells. *Cell*, *168*(5), 944–945. https://doi.org/https://doi.org/10.1016/j.cell.2017.02.010

Yuneva, M. O., Fan, T. W. M., Allen, T. D., Higashi, R. M., Ferraris, D. V., Tsukamoto, T., Matés, J. M., Alonso, F. J., Wang, C., Seo, Y., Chen, X., & Bishop, J. M. (2012). The Metabolic Profile of Tumors Depends on Both the Responsible Genetic Lesion and Tissue Type. *Cell Metabolism*, *15*(2), 157–170. https://doi.org/https://doi.org/10.1016/j.cmet.2011.12.015

Zeleznik-Le, N. J., Harden, A. M., & Rowley, J. D. (1994). 11q23 translocations split the “AT-hook” cruciform DNA-binding region and the transcriptional repression domain from the activation domain of the mixed-lineage leukemia (MLL) gene. *Proceedings of the National Academy of Sciences of the United States of America*, *91*(22), 10610 LP – 10614. https://doi.org/10.1073/pnas.91.22.10610

Zhang, C. C., & Lodish, H. F. (2008). Cytokines regulating hematopoietic stem cell function. *Current Opinion in Hematology*, *15*(4), 307–311. https://doi.org/10.1097/MOH.0b013e3283007db5

Zhang, L., & Han, J. (2017). Branched-chain amino acid transaminase 1 (BCAT1) promotes the growth of breast cancer cells through improving mTOR-mediated mitochondrial biogenesis and function. *Biochemical and Biophysical Research Communications*, *486*(2), 224–231. https://doi.org/10.1016/j.bbrc.2017.02.101

Zhang, X., Su, J., Jeong, M., Ko, M., Huang, Y., Park, H. J., Guzman, A., Lei, Y., Huang, Y.-H., Rao, A., Li, W., & Goodell, M. A. (2016). DNMT3A and TET2 compete and cooperate to repress lineage-specific transcription factors in hematopoietic stem cells. *Nature Genetics*, *48*(9), 1014–1023. https://doi.org/10.1038/ng.3610

Zhang, Y., Gao, S., Xia, J., & Liu, F. (2018). Hematopoietic Hierarchy – An Updated Roadmap. *Trends in Cell Biology*, *28*(12), 976–986. https://doi.org/https://doi.org/10.1016/j.tcb.2018.06.001

Zhou, W., Feng, X., Li, H., Li, H., Zhu, B., Zhang, H., Yao, K., & Ren, C. (2007). Functional Evidence for a Nasopharyngeal Carcinoma-Related Gene BCAT1 Located at 12p12. *Oncology Research*, *16*, 405–413. https://doi.org/10.3727/000000007783980873

8. Supplements

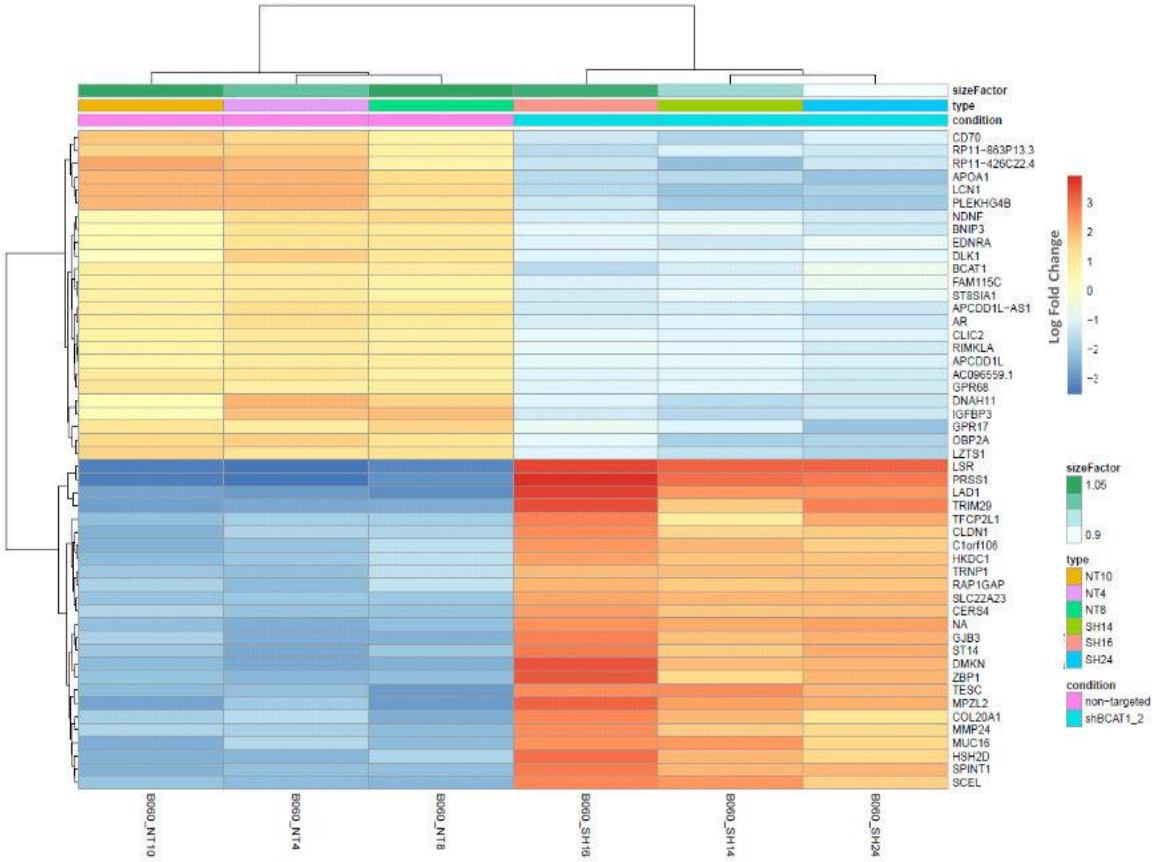

Figure S1 - Unsupervised clustering of RNA-seq data obtained from orthotopic mammary carcinoma xenografts with and without BCAT1. RNA-seq analysis was conducted after excluding any mouse RNA fragments, and unsupervised clustering was based on the entire data set. The resulting hierarchy correlates with the conditions of these xenografts: non-targeted control (*NT*) and BCAT1 knockdown with short hairpin RNA (*shBCAT1_2*, SH). Here the top 25 most downregulated genes upon doxycycline induced BCAT1 knockdown (SH) such as CD70, BCAT1, and APCDD1L are depicted in the upper half of the heatmap, while the 25 most upregulated gene transcripts in Bcat1 knockdown tumors such as LSR and ZBP1 are shown in the bottom half. (N_{NT}=3, N_{SH}=3)

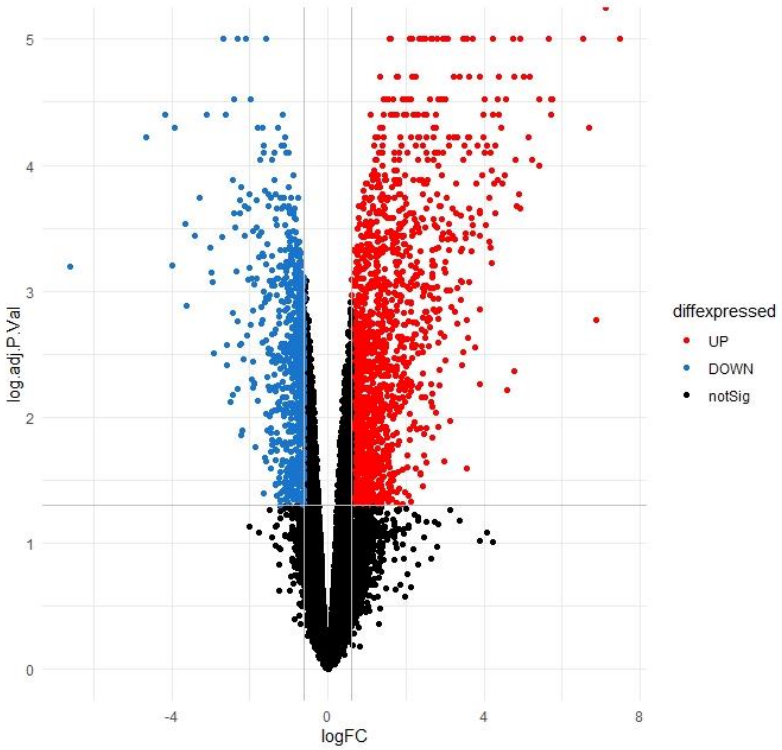

Figure S2 - Volcano Plot of MDA-MB231 RNA-seq data highlights global upregulation observed in shBCAT1 knockdown xenografts. Significantly upregulated genes (red) in shBCAT1 knockdown MDA-MB231 xenografts are on the right and significantly downregulated genes are depicted in blue. I observed 1555genes significantly upregulated and 787 genes were found significantly downregulated. (N_{NT}=3, N_{SH}=3)

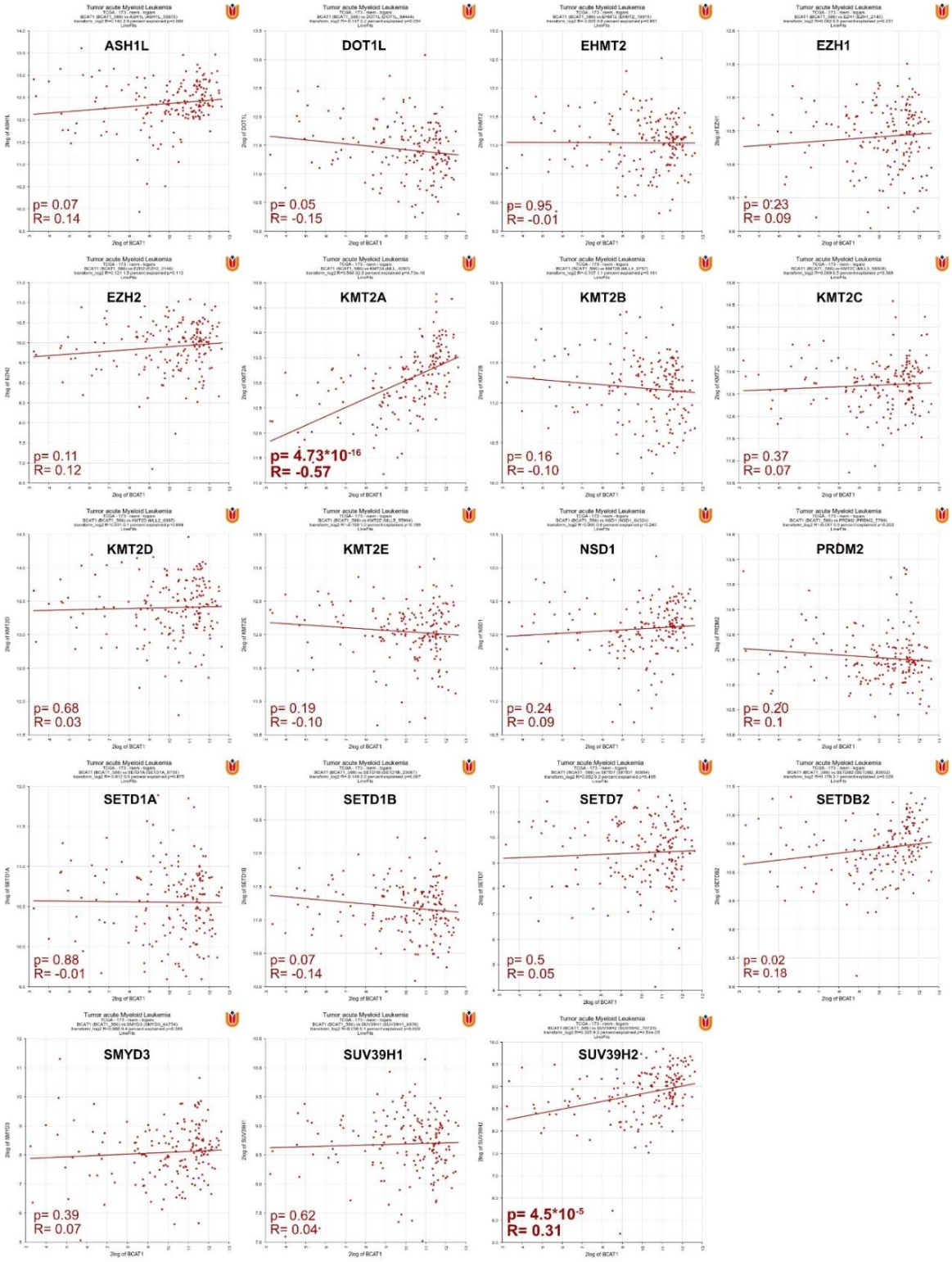

Figure S3 - Correlation of BCAT1 expression with histone methyltransferases relevant for H3K4, H3K9, and H3K27 methylation in acute myeloid leukemia.

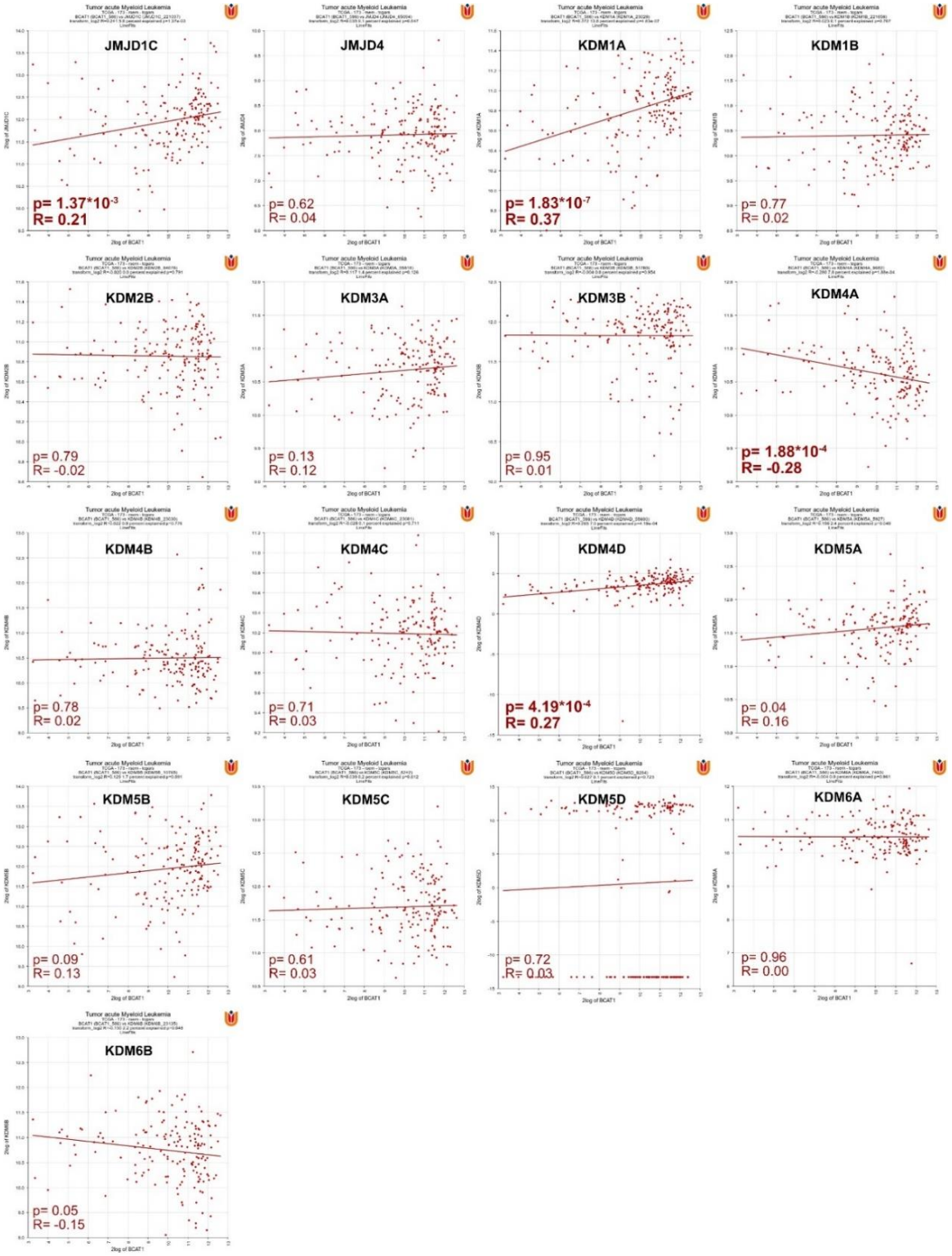

Figure S4 - Correlation of BCAT1 expression with histone demethylases relevant for H3K4, H3K9, and H3K27 methylation in acute myeloid leukemia.

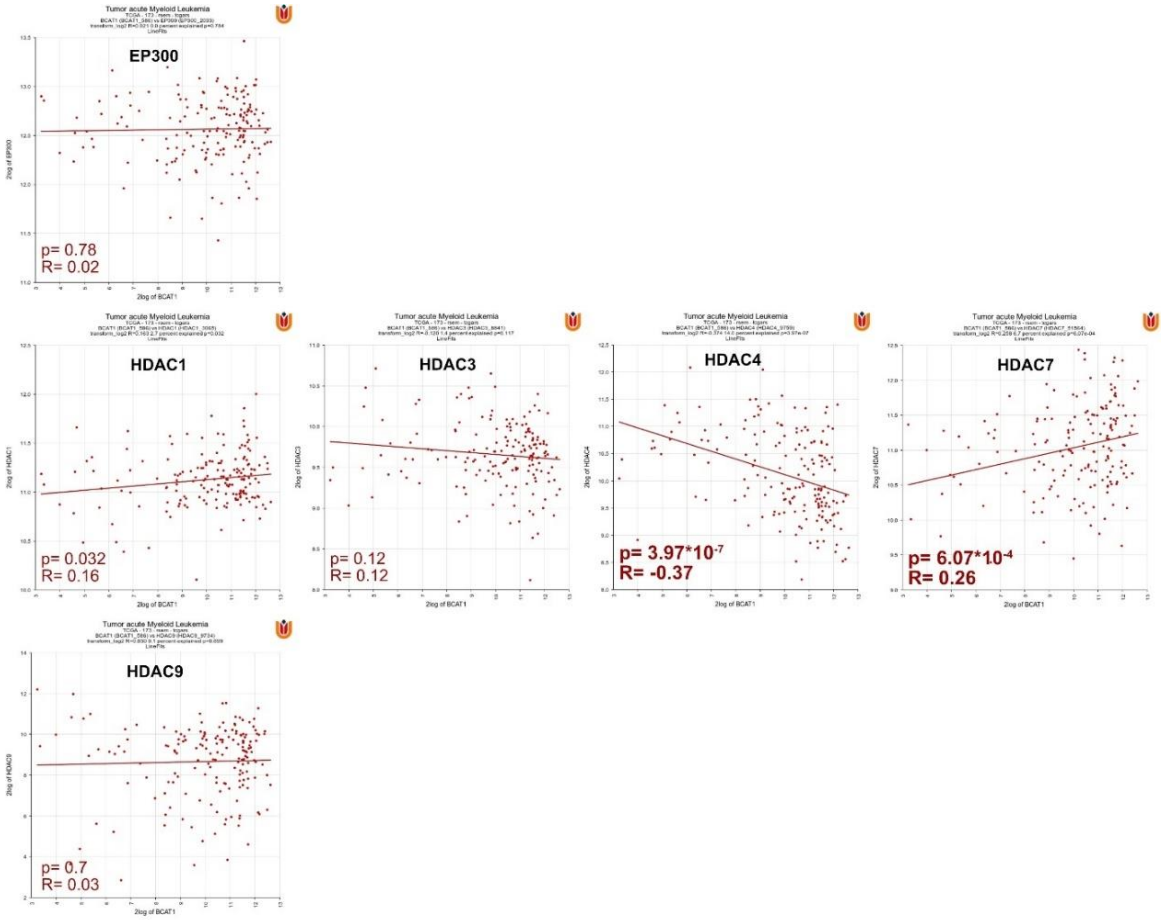

Figure S5 - Correlation of BCAT1 expression with histone acetyltransferase EP300 and deacetylases relevant for H3K27 modifications in acute myeloid leukemia

Table S1- Correlation analysis for BCAT1 and relevant chromatin modifiers in expression profiles of human AML and triple-negative breast cancer

	Acute Myeloid Leukemia TCGA LAML		**Breast Cancer GSE142102**	
	R	p-Value	R	p-Value
ASH1L	0.14	0.07	0.01	0.86
DOT1L	-0.15	0.05	0.15	0.03
EHMT2	-0.01	0.95	0.20	$2.48*10^{-3}$
EZH1	0.09	0.23	0.19	$4.09*10^{-3}$
EZH2	0.12	0.11	0.22	$1.08*10^{-3}$
KMT2A/ MLL	**0.57**	**$4.73*10^{-16}$**	**0.24**	**$2.61*10^{-4}$**
KMT2B	-0.1	0.16	0.11	0.11
KMT2C	0.07	0.37	0.14	0.04
KMT2D	0.03	0.68	0.18	$5.65*10^{-3}$
KMT2E	-0.10	0.19	0.30	$3.87*10^{-6}$

NSD1	0.24	0.09	0.05	0.44
PRDM2	-0.1	0.20	0.19	$3.75*10^{-3}$
SETD1A	-0.01	0.88	0.16	0.01
SETD1B	-0.14	0.07	0.03	0.68
SETD7	0.05	0.5	0.02	0.74
SETDB2	0.18	0.02	0.10	0.12
SMYD3	0.07	0.39	0.13	0.049
SUV39H1	0.04	0.62	0.07	0.28
SUV39H2	0.31	$4.5*10^{-5}$	0.12	0.07
JMJD1C	**0.21**	**$1.37*10^{-3}$**	**0.32**	**$7*10^{-7}$**
JMJD4	0.04	0.62	0.04	0.59
KDM1A	**0.37**	**$1.83*10^{-7}$**	**0.24**	**$3.14*10^{-4}$**
KDM2A	0.02	0.77	0.33	$3.60*10^{-7}$
KDM2B	-0.02	0.79	0.07	0.32
KDM3A	0.12	0.13	0.19	$4.57*10^{-3}$
KDM3B	0.01	0.95	0.16	0.02
KDM4A	-0.28	$1.88*10^{-4}$	0.02	0.73
KDM4B	0.78	0.02	0.08	0.26
KDM4C	0.03	0.71	0.13	0.05
KDM4D	0.27	$4.19*10^{-4}$	-0.12	0.07
KDM5A	0.16	0.04	0.14	0.04
KDM5B	0.13	0.09	0.13	0.06
KDM5C	0.03	0.61	0.09	0.19
KDM6A	0.00	0.96	0.16	0.02
KDM6B	-0.15	0.05	0.12	0.07
EP300	0.02	0.78	0.30	$3.32*10^{-6}$
HDAC1	0.16	0.032	0.21	$1.54*10^{-3}$
HDAC3	0.12	0.12	0.02	0.29
HDAC4	-0.37	$3.97*10^{-7}$	0.00	0.98
HDAC7	0.26	$6.07*10^{-4}$	0.07	0.30
HDAC9	0.03	0.7	0.177	$7.79*10^{-3}$

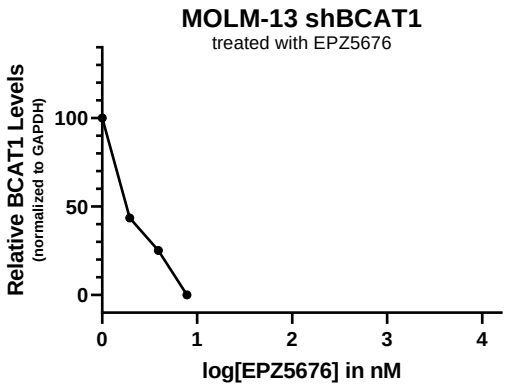

Figure S6 – DOT1L inhibition reduced BCAT1 protein even further in MLL-fusion cell line MOLM-13 with induced *shBCAT1* knockdown. Doxycycline-induced *shBCAT1* knockdown reduced BCAT1 expression immensely, however not completely. Increasing concentrations of the DOT1L inhibitor EPZ5676 were able to reduce BCAT1 even further. Here the normalization to GAPDH is shown. Higher concentrations of the inhibitor EPZ5676 resulted in minimal cell numbers and unreliable protein detection. ($N_{MOLM-13}$=1)

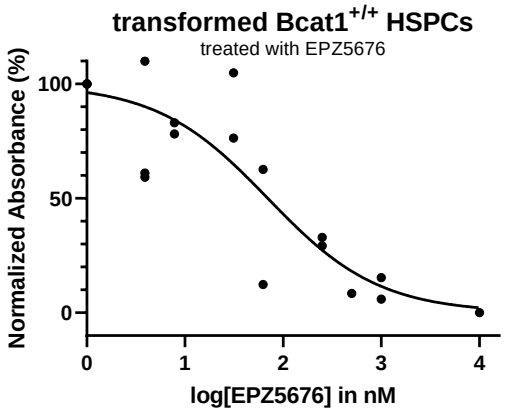

Figure S7 – Primary mouse AML cell line harboring an MLL-AF9 fusion showed a DOT1l-dependent proliferation reduction using CellTiter-Glo® assay. An inverse correlation between proliferation and increasing concentration with the DOT1L inhibitor EPZ5676 was observed after 7 days of treatment. (N=2, IC50= 70 nM)

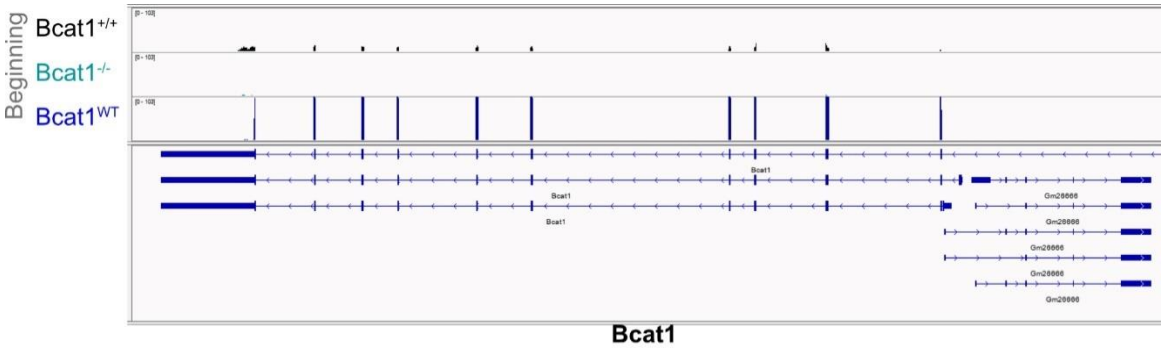

Figure S8 - Ultra-low RNA-seq data verified expression of Bcat1 in Bcat1$^{+/+}$ and Bcat1^{WT} but not in Bcat1$^{-/-}$ CFU samples. Representative IGV tracks of normalized expression profiles show expression of Bcat1 region (chr6:144,993,171-145,062,418; RefSeq genome mm10). Bcat1$^{+/+}$ and Bcat1^{WT} express Bcat1 but Bcat1$^{-/-}$ exhibits a complete knockout.

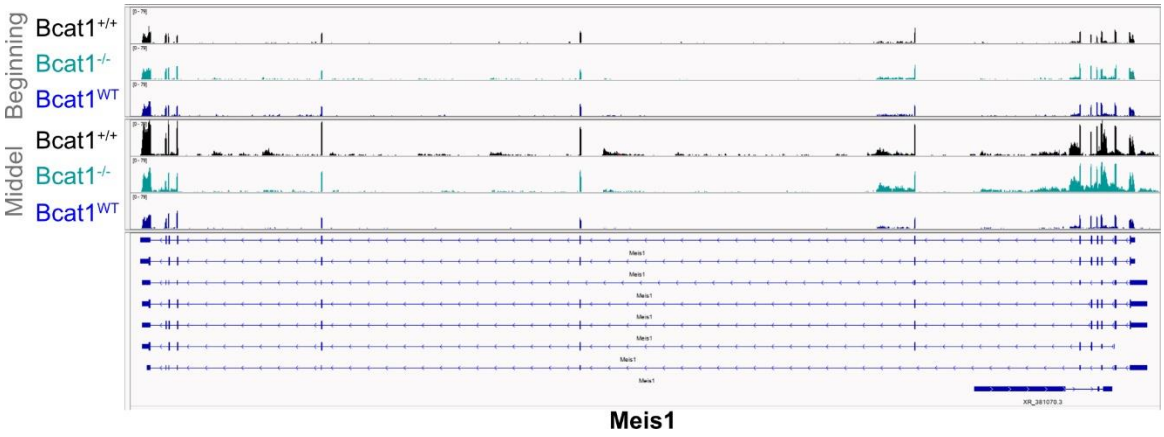

Figure S9 - Representative IGV tracks determined no expression differences of MLL-Af9 target gene Meis1 between conditions. While Meis1 expression is increased in the intermediate time point, no difference was observed between Bcat1$^{+/+}$and Bcat1$^{-/-}$ at either time. This section shows chr11:18,878,668-19,022,672 in the murine RefSeq genome mm10.

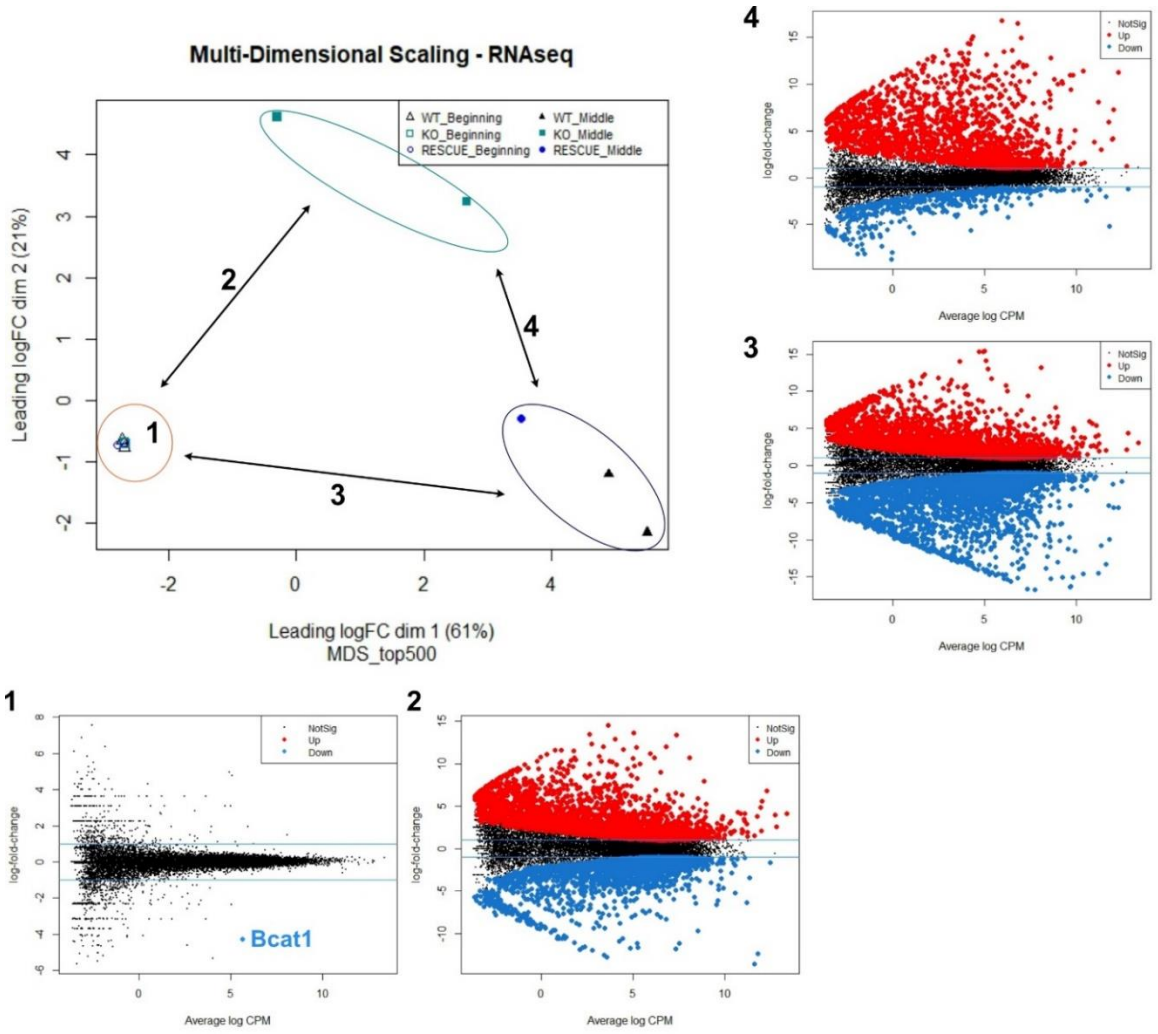

Figure S10 – Multi-Dimensional Plot highlights a multi-layered analysis approach to investigate not only differences over time but also Bcat1 status-dependent differences. MD plots show differentially expressed genes by comparing samples as indicated in the multi-dimension plot. Significantly up (red) and down (blue) regulated genes are colored, while non-significant changes are represented in black. (1: Comparison of $Bcat1^{+/+}$ and $Bcat1^{WT}$ HSPCs with $Bcat1^{-/-}$ HSPCs at early time point; 2: Comparison of $Bcat1^{-/-}$ HSPCs at the beginning with intermediate time point; 3: Comparison of $Bcat1^{+/+}$ and rescue $Bcat1^{WT}$ HSPCs at early with intermediate time point; 4. Comparison of $Bcat1^{+/+}$ and $Bcat1^{WT}$ rescue HSPC with $Bcat1^{-/-}$ HSPCs at intermediate time point)

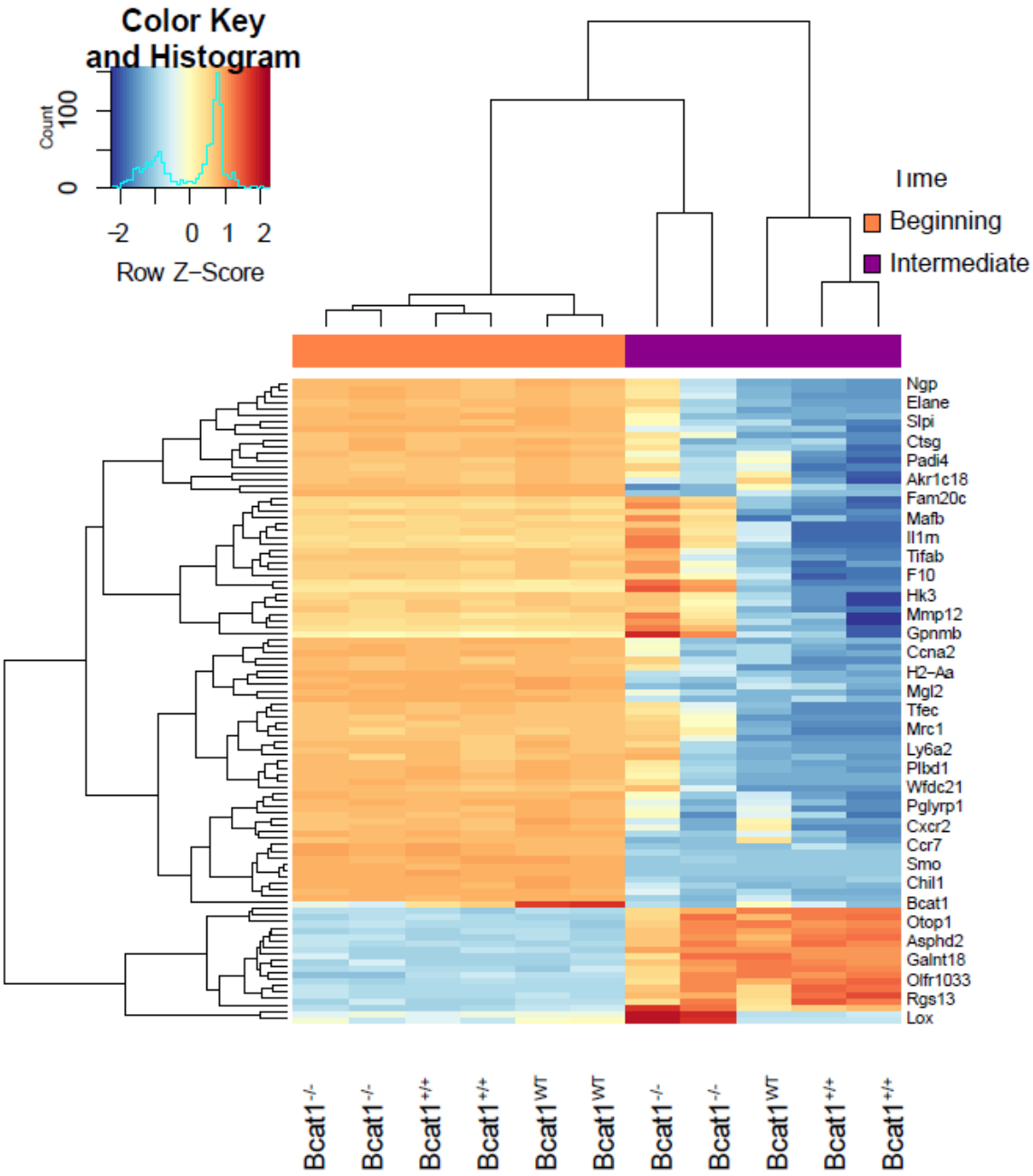

Figure S11 – Ultra-low RNA-seq of CFU samples at the beginning and after the second plating (middle) of this assay cluster by time and result in a clear hierarchical structure. Expression profiles of HSPCs at the early time point form a highly homogeneous cluster while still clustering with Bcat1 status over cell origin. Throughout the CFU, global expression changes driven by MLL-AF9 resulted in a transformed phenotype in Bcat1$^{+/+}$ and Bcat1^{WT} rescue HSPCs. This is represented in the higher variance between the different samples. Unsupervised clustering was based on the 100 most differentially expressed genes.

Table S2 – Exclusively Bcat1$^{+/+}$ and Bcat1^{WT} differential expressed genes over time. Highly significantly164 upregulated genes (red), and 402 downregulated (green) genes are shown.

Tspan13	AW046200	Hectd2	Gm16485	Olfr48	Tescl	Marchf11	4930534D22Rik
Enc1	Scara5	Gm20326	Mageh1	Adra2b	Gm5737	Calhm1	Kcnq4
Peg13	9230112J17Rik	Rgs20	Adamts9	Efcc1	Ssmem1	Lipo1	Chia1
H2bc4	Mfsd13b	Bcan	LOC665004	Skida1	Spata6l	Rln1	
H1f2	Cacnb4	4933427G23Rik	Gm9978	Kcnu1	Gm10617	Slc13a2os	
Serpinb6a	Cnrip1	Zfp711	Sox21	Gm10822	Gm10044	C230024C17Rik	
Pde1c	Ryr3	Trav4-4-dv10	Gm10690	Ccdc54	4930432E11Rik	Crp	
Frmpd1	Dmrt2	Nlrp4f	Qrfprl	Cilp	Gnat1	Samt2b	
Ctla2a	AI847159	Gm3230	Foxc2	Gm48957	Elovl4	Foxd3	
Mt2	Nap1l3	Gm16998	Exph5	Ccdc141	Olfr1509	Mdga2	
Tnfsf4	Rgs9bp	Hes7	Sult6b2	1700012I11Rik	4930547M16Rik	Gm10648	
Prrg4	Gpc6	Vwa7	Ncr1	8430423G03Rik	Spata31d1d	Gm17769	
Il15	Kazald1	Enkur	Cacng3	Irx3	Olfr49	Cpb2	
Cpt1c	Megf10	Gstm3	Grik2	Gdf6	Fhod3	Crybb3	
Gata3	Ccdc103	Hcrtr2	Lbx2	0610040F04Rik	Wscd1	2310039L15Rik	
A430035B10Rik	9130213A22Rik	Bmper	Ighv1-84	1700113H08Rik	Mrgprb3	1700021N21Rik	
Arpp21	2900041M22Rik	Chad	Emx2	Lhx3	Abcg5	Ankk1	
Tg	Dazl	Dipk1c	Gm12676	A930018P22Rik	Mtag2	Folh1	
Rundc3b	Trim10	Cyp2u1	Spag6l	1110017D15Rik	Mcidas	2810459M11Rik	
Patl2	Tdrp	Plau	Olfr1258	Scd3	1810046K07Rik	Trpc1	
Edn3	E130102H24Rik	Thsd7b	Crisp3	Tgm5	Kcna4	Capn8	
Gm6634	Ppef2	Hesx1	C330011F03Rik	Gm960	Pax9	9230019H11Rik	
Cpb1	5930430L01Rik	Slc38a11	4921528I07Rik	Hfm1	A230108P19Rik	Ldb3	
Thbs1	Slc30a4	P2ry6	Olfm4	Fancd2	Gm11545	Macroh2a2	Orm1
Ngp	Itga1	Nuf2	Cdca3	Fabp5	Cldn15	Fpr2	Glt1d1
Chil3	Timp2	Tk1	Foxm1	Tns4	Vcam1	Itga8	Tnfaip8l3
Ltf	Wfdc17	Ppic	Cdc6	Ipcef1	Gm5150	Fam169b	Cox6a2
Lcn2	Mki67	Actn1	Rin2	Chtf18	Cd302	Ifi209	Cstdc5
Elane	Ctss	Ms4a4c	Slc15a3	Cldn1	Ugt1a7c	Rasl11b	Arhgef37
F10	Chst13	Dna2	Cd86	Mcm5	Ccne2	Il1a	Shroom2
Lsp1	Glipr2	Pik3r5	Mreg	Dlgap5	Slfn1	Mob3b	Lrrc2
Gatm	Mmp9	Iqgap3	Nrg1	Mis18bp1	Gramd3	Btla	Iglc2
Ly6c2	Mmp12	Trem3	Bst1	Cd38	Kctd17	Pdlim4	Khdrbs3
Tgfbi	Rasgrp2	Rnd3	Pid1	Msantd3	Sgo2a	Sirpb1c	Chsy3
Csf3r	Bub1b	Trem1	BC035044	Flt1	Stc2	Smpdl3b	Kcnn3
Tifab	Mtus1	Gpr84	Gpr35	Lilra6	9830107B12Rik	Cd80	Stfa1
Cd177	Plbd1	Crispld2	Tmem176a	Nefh	A530064D06Rik	Bex6	9830166K06Rik
Hk3	Myof	Mefv	Pkib	Cd44	C1qa	Sncaip	Phf11b
Itgam	Sh2b2	Mertk	Irf5	Ndc80	Cacnb3	Tcf7	Tnni2
Fn1	Msr1	Sgk3	Adam19	Chdh	AW112010	Dio2	Prkaa2
Fam20c	Hrob	Il36g	Knstrn	Marchf1	Fabp4	Rapgef5	Ldhb

Dab2	Met	Mapk13	Pilra	Gapt	Tlr8	Adgrl4	Sirpb1a
Clec5a	Mcm10	Cdca2	Napsa	Ckap2l	Pdia5	Gm9733	Adcy6
Cybb	Slc7a2	Ms4a6d	Hoxa9	Pparg	4930438A08 Rik	Bmx	Pde10a
C3	Hfe	Igfbp4	Bcat1	Bcl2a1b	Nmral1	Lmo1	Mycl
Tfec	Clec4a2	Ccnb1	Prc1	Fkbp11	Ncam1	Thy1	Tmem215
Camp	Aurkb	Lrrk2	Dach1	Prdm1	Serpine2	Sirpb1b	Nr0b2
Prtn3	Cd36	Ptpro	Bcl3	Klf4	Edn1	Bcl2a1a	Sema3c
Il1rn	Plekhg1	App	Clu	Cenpi	Peli2	Layn	Chil4
Hp	Cd83	Ccne1	Septin5	2610318N02 Rik	Msx3	Dmkn	Raet1e
Abcd2	Ms4a4a	Ifi207	Dusp22	Sorl1	Ly86	Ly6g	B630019K06 Rik
Xdh	Plxnc1	Tacc3	Egr2	Itgax	Pknox2	Prr33	Sgip1
Csf1r	Mcemp1	Tmem26	Mgll	Gm14548	Tmem132a	H2-M2	Neurl1b
Clec12a	Uhrf1	Ticrr	Impa2	Slfn4	Gbx2	Ear2	Slc44a4
Nt5e	Fcnb	Dgat2	Cysltr1	Kif1a	Bcas1	Cldn11	Ffar4
Igsf6	Pxylp1	Marcks	Evl	Afap1	Tubb1	Aff2	Dclk2
Ctsh	Kif20a	Anxa3	Plppr3	Slc28a2	Sh3bp4	Galnt9	Vangl2
Dse	Ccnf	Tmem176b	Tpx2	Eme1	Gen1	Timp1	Mir99ahg
Nrp2	Arsb	Psat1	Timeless	Nlrp1a	Spsb4	9930111J21R ik1	Gm21370
Olfm1	E2f7	Crybg1	Als2cl	Slamf7	Cd300lg	Cstdc4	Smoc1
Fgr	Troap	Mogat2	Il13ra1	Kynu	Klk1b11	Cd200	Dynlt5
Cd52	Mef2c	Olr1	Cd79b	Mmp25	Slamf8	Lifr	Ugt1a6a
Mrc1	Sdc3	Fanca	Egfl7	Nme4	Arhgap24	Eya1	Echdc2
F7	Wfdc21	Ppbp	Mtfr2	Car4	Treml1	F730016J06R ik	Dcbld1
Spag5	Kif2c	Inhba	Siglece	Ankrd55	Kcnj2	Cd101	Angptl8
Ly6a2	Aurka	Pdlim1	Clec4a3	Ifi204	Oas1g	Gm15354	Gpr18
Acpp	Ms4a6c	Ccl4	Rhoj	Ifitm6	Jaml	Ppp1r26	1700071M1 6Rik
Nup210	Lbp	Prom1	Ak4	B4galt6	Oas2	Gm21188	Myo1b
Itgb2l	Clec4a1	Rab7b	Retnlg	Pram1	Cd22	Col5a1	Wtip
Ctsg	Slc25a13	Lrg1	Ceacam10	Hoxa7	Tcf7l2	Nlrp1b	Mfsd6l
Mafb	Irf8	Cdca8	Cdca5	Brip1	Mirt2	Etv4	BE692007
Clec7a	Dock1	Ltb4r1	Kif23	Polq	Serpinb10	Ksr2	Snord110
Trem2	C1qb	Fam83d	Ednrb	Inpp5j	Ass1	Slamf6	Mroh2a
						Klhl33	Ina

Table S3 - Exclusively Bcat1$^{-/-}$ differentially expressed genes over time. Highly significantly, 348 upregulated genes (red) and 92 downregulated (green) genes are shown.

Fstl1	Reps2	Lhfp	Tceal7	9130024F11 Rik	Calm5	Lrp2	Slc9a4
Lox	Klf2	Ces2c	Gm16010	Ccbe1	Nrep	Ceacam12	Sh2d6
Cdkn1c	Il7r	Cttnbp2	Serpinb1c	Nrxn1	Gm5420	Artn	Ccdc148
Fxyd2	Mkx	Prokr1	Asb11	Srgap1	Umodl1	Svep1	A430108G06 Rik
Ctsk	Pkdcc	Cd22	D030025P21 Rik	Slc47a1	Lrrc10b	Osbp2	Slc3a1
Pmp22	Cd300c2	Fmn1	Lurap1l	Mep1a	Serinc2	Ugt1a6b	Disp3
Csn2	Stac2	Dusp13	Stfa3	Zfp334	3425401B19 Rik	Spink5	Ighv1-80
Igf1	Hpse	Pira6	Igsf11	Cpne8	Pik3c2g	Gm8909	Kcnj10
Gpnmb	Gm14461	Amy1	Tmem178	Ms4a14	Slc27a6	Lrat	Dupd1

Npy	Hoxa10	Lyz1	Fbln2	Vax2	Ccdc87	Tspan12	A830009L08Rik
Apoc2	Tmem86a	Zfp618	Gm19689	Stox2	Opcml	Gpr153	Pde11a
Plpp3	Ces1d	Snta1	Wnt9b	Klra9	Scn3b	Kif5c	Zfyve28
Gpx3	Prss46	Gstt1	Hoxb7	Cbr2	Gm12185	Iglon5	1810059H22Rik
Sp9	Nos2	Jag1	Pgbd5	Ghr	Acss2os	Slc7a14	Npy5r
Gpr137b	Mmp10	Akr1b8	Clmn	Irs1	Zfp791	9530059O14Rik	Tecta
Adamts1	Tlr7	Tcaf1	C2cd4a	Etv1	Ifi44	4930579D07Rik	Adamts13
Ambp	Cd302	Adcy2	Lipn	Tmem72	Slc32a1	Glyat	Zfp811
Gstm2	Stra6l	Plekhh2	Orm3	Col19a1	Gcm2	Gm19589	Mir27b
Slc11a1	Ccl8	Boc	Epn2	Folr1	Sfrp1	Ace	Cdh4
Pdpn	Tbc1d9	Pla2g2e	Sbk2	Shc2	Zfp37	Serpinb9g	Lrrc34
Cgnl1	Fth1	Abcc8	Cybrd1	Kcnq1	Tspan10	Fzd2	Amhr2
Lrp1	Tulp4	Gm10554	Tm4sf19	Greb1	Fads2b	Fignl2	Gm10248
Wfdc17	Hoxb13	Slc9b2	Prl2c5	Tm4sf5	Pacrg	Ccdc65	Robo2
Procr	Tmem119	Gfra1	Bex1	Gsg1l	1700020N01Rik	Lrrc17	Lrrtm1
Cd14	Gdpd1	Qrfpr	Tmc3	Pdgfc	Mir23b	Gm20560	Gm13483
Saa3	Hoxa11os	Pou3f1	Rassf10	Cdr2l	Pcdhac2	Slc6a20a	Gm2011
Maoa	Ltbp2	Ifit3b	Tmem114	Dppa3	C4b	Tenm4	Tmem169
Spp1	Folr2	Ptchd1	Magi1	Ip6k3	Eya4	Sox18	Cfh
Ampd3	4931408C20Rik	Awat1	Hcn1	Cxcl14	Trim54	Selenbp2	Arntl2
Bhlhe41	Cd28	St18	Cd300e	Wdr93	Scgb1a1	Zfhx4	Kcna2
Sgk1	Pcsk9	Gprc5b	Npr1	Prl2c2	Tenm1	Bsx	Eqtn
Clmp	Spsb4	Hs3st5	Tcim	Mfsd4b3-ps	Ogdhl	Ntn1	Olfr456
Plk2	Snhg11	Plcd1	Nol4	Gstt4	Fabp3	Klhl38	Cnga3
Abcc3	Sash1	Tchhl1	Ifit1bl1	Ccser1	Elavl2	Eef1a2	1700111E14Rik
Serpinb9b	Ifit3	Tsku	Fam167b	Faim2	Zfp462	6030407O03Rik	Mir3097
Car4	Dmrta2	Naip1	Masp1	Hsd17b14	Tnni3k	Tmem30b	Prlr
Hoxa11	Heph	Frk	Sox7	Marchf4	Trpm3	Skor1	Lhx2
Tspan7	Slc39a2	Arhgap22	Kctd12b	Trim29	Mtarc1	Slc8a2	Lypd1
Mfap3l	Adamtsl5	Rasgrp3	Arhgef19	Serpinb1b	Smim38	4931408D14Rik	Gm10933
Pltp	Satb2	Amotl1	Gm19316	Astn2	Slc38a4	Gm12505	Sema3a
Mpeg1	Mak	Pappa2	Pla2g5	Rspo1	Tbx15	Pla2r1	
Fblim1	Rbp4	Clic5	Fam83f	Atp8b3	Tnnt2	Zic3	
Ctsb	Vash2	Card14	Nnmt	Cntn4	Mir1934	Steap4	
Gstm1	Sdc1	Peli3	Abhd3	Prl7a2	Gm10440	8430426J06Rik	
Itk	Tacstd2	Cd79a	Shisa8	Gcnt4	Dclk1	Ank1	Tmod2
Tnfrsf9	Garem2	Parm1	Ccdc184	2810429I04Rik	H2bc12	Fsd2	Neurl1a
Alox8	Jakmip1	Ctsw	Robo3	Gm38427	Igkv12-89	Dkk3	Akr1c21
Hdc	Sema6d	Adamtsl1	Tlr12	Ccr8	Ighv3-6	H4c2	Sod3
Klf5	Zdhhc15	Wdr86	Ighv1-11	Dach2	Dleu7	Dcaf12l1	Mei4
Ptprcap	Hbb-b1	Nlrp6	Krt18	Morc4	Chst2	C030013G03Rik	Begain
Htr7	Cnga1	Epcam	Ccn2	H2ac13	Npw	Fancd2os	Ckm
Amigo2	2700099C18Rik	H2ac20	Tmem121	Rhox5	Dlk1	Ret	Ccdc150
Hmgn2	I730030J21Rik	BC064078	Xlr	Adamts20	Col1a2	Nrap	

P2ry10	Lysmd2	Scn3a	Fcer2a	Capn13	Ybx2	Tigit
Aldh1a3	Pcbp3	Hkdc1	Slc15a1	Cryga	Trdc	Igkv8-16
Trgc1	Epb41l4b	Dmc1	Art4	Gypa	Klri2	Nccrp1

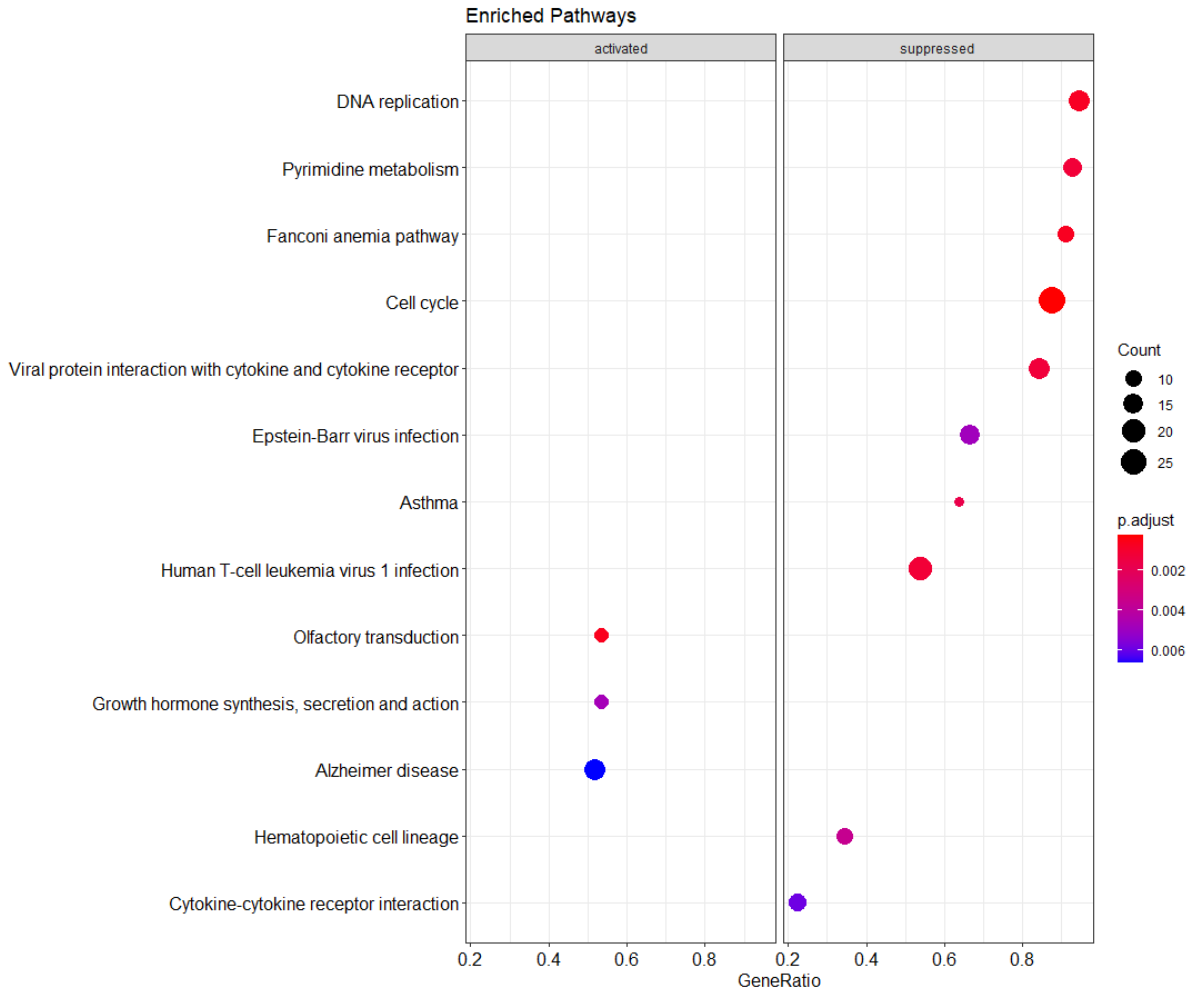

Figure S12 -KEGG pathway analysis comparing gene expression of early and intermediate Bcat1$^{-/-}$. A p-value cutoff of 0.01 and a minimum of genes was set to 10.

Table S4 – Cell cycle associated genes influenced by Bcat1$^{-/-}$ during transformation

Gene Symbol	Gene Name	Function	Expression in intermediate Bcat1$^{-/-}$
Bub1	BUB1 Mitotic Checkpoint Serine/Threonine Kinase	Essential for spindle-assembly checkpoint signaling and correct chromosome alignment.	Down
Ccna2	Cyclin A2	Promotes transition through G1/S and G2/M.	Down
Ccnb2	Cyclin B2	Cell cycle control at the transition of G2/M (mitosis)	Down
Ccnd3	Cyclin D3	Required for cell cycle G1/S transition, oncogenic properties	Down
Ccne1	Cyclin E1	Required for cell cycle G1/S transition, oncogenic properties	Down
Cdc6	Cell division cycle 6	Essential for the initiation of DNA replication	Down
Cdc7	Cell division cycle 7	Critical for the G1/S transition and DNA replication	Down
Cdc20	Cell division cycle 20	Required for two microtubule-dependent processes, nuclear movement before anaphase and chromosome separation	Down
Cdc25a	Cell division cycle 25A	Required for progression from G1 to the S phase; degraded in response to DNA damage, which inhibits the division of cells with chromosomal abnormalities	Down
Cdc25c	Cell division cycle 25c	Triggers entry into mitosis, suppresses p53-induced growth arrest, oncogene	Down
Cdc45	Cell division cycle 45	Required to the initiation of DNA replication, interacts with MCM complex	Down
Cdk1	Cyclin dependent kinase 1	Essential for G1/S and G2/M phase transitions, catalytic subunit of M-phase promoting factor (MPF), oncogenic properties	Down
Cdkn1c	Cyclin dependent kinase inhibitor 1A	Regulator of cell cycle progression at G1, plays a regulatory role in S phase DNA replication and DNA damage repair,	Up
Chek1	Checkpoint kinase 1	Reduces replication stress and activates the G2/M checkpoint	Down

Espl1	Extra spindle pole bodies Like 1, separase	Critical role in the chromosome segregation during anaphase	Down
Gadd45g	Growth arrest and DNA damage inducible gamma	Increased following stressful growth arrest conditions and DNA damage	Up
Mad2l1	Mitotic Arrest Deficient 2 Like 1	Component of the mitotic spindle assembly checkpoint	Down
Mcm2	Minichromosome maintenance complex component 2	Initiation of eukaryotic genome replication, regulate the helicase activity of the pre-replication complex	Down
Mcm3	Minichromosome maintenance complex component 3	Initiation of eukaryotic genome replication, regulate the helicase activity of the pre-replication complex	Down
Mcm4	Minichromosome maintenance complex component 4	Initiation of eukaryotic genome replication, regulate the helicase activity of the pre-replication complex	Down
Mcm5	Minichromosome maintenance complex component 5	Initiation of eukaryotic genome replication, regulate the helicase activity of the pre-replication complex	Down
Mcm7	Minichromosome maintenance complex component 7	Initiation of eukaryotic genome replication, regulate the helicase activity of the pre-replication complex	Down
Myc	Myc proto-oncogene, BHLH transcription factor	Plays a role in cell cycle progression, regulates the transcription of target genes, oncogene	Down
Orc1	Origin recognition complex subunit 1	Initiation of the DNA replication	Down
Orc6	Origin recognition complex subunit 6	Critical role in coordinating chromosome replication and segregation	Down
Pkmyt1	Protein kinase, membrane associated tyrosine/threonine 1	Negatively regulates the G2/M transition of the cell cycle	Down
Plk1	Polo like kinase 1	Several essential functions throughout M-phase of the cell cycle, supports cell proliferation and inhibits apoptosis, oncogene	Down
Rbl1	RB transcriptional corepressor like 1	Key regulator of entry into cell division, involved in	Down

		heterochromatin formation, tumor suppressor	
Tfdp1	Transcription factor Dp-1	Controls the transcriptional activity of numerous genes involved in cell cycle progression from G1 to S phase	Down
Ttk	TTK protein kinase	Essential for chromosome alignment, critical mitotic checkpoint protein	Down

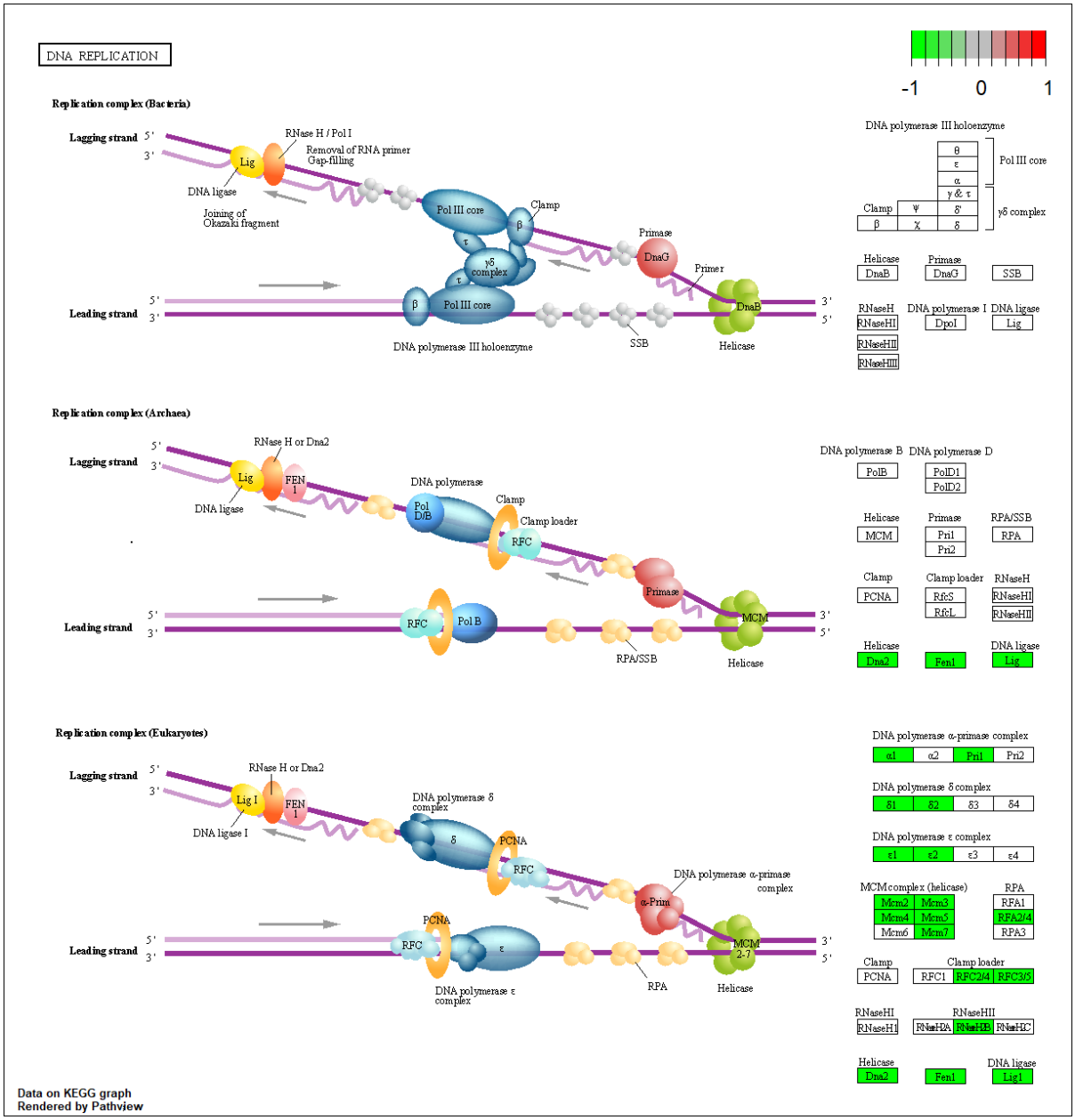

Figure S13 - Gene expression of Bcat1$^{-/-}$ over time in the KEGG pathway DNA replication (mmu03030)

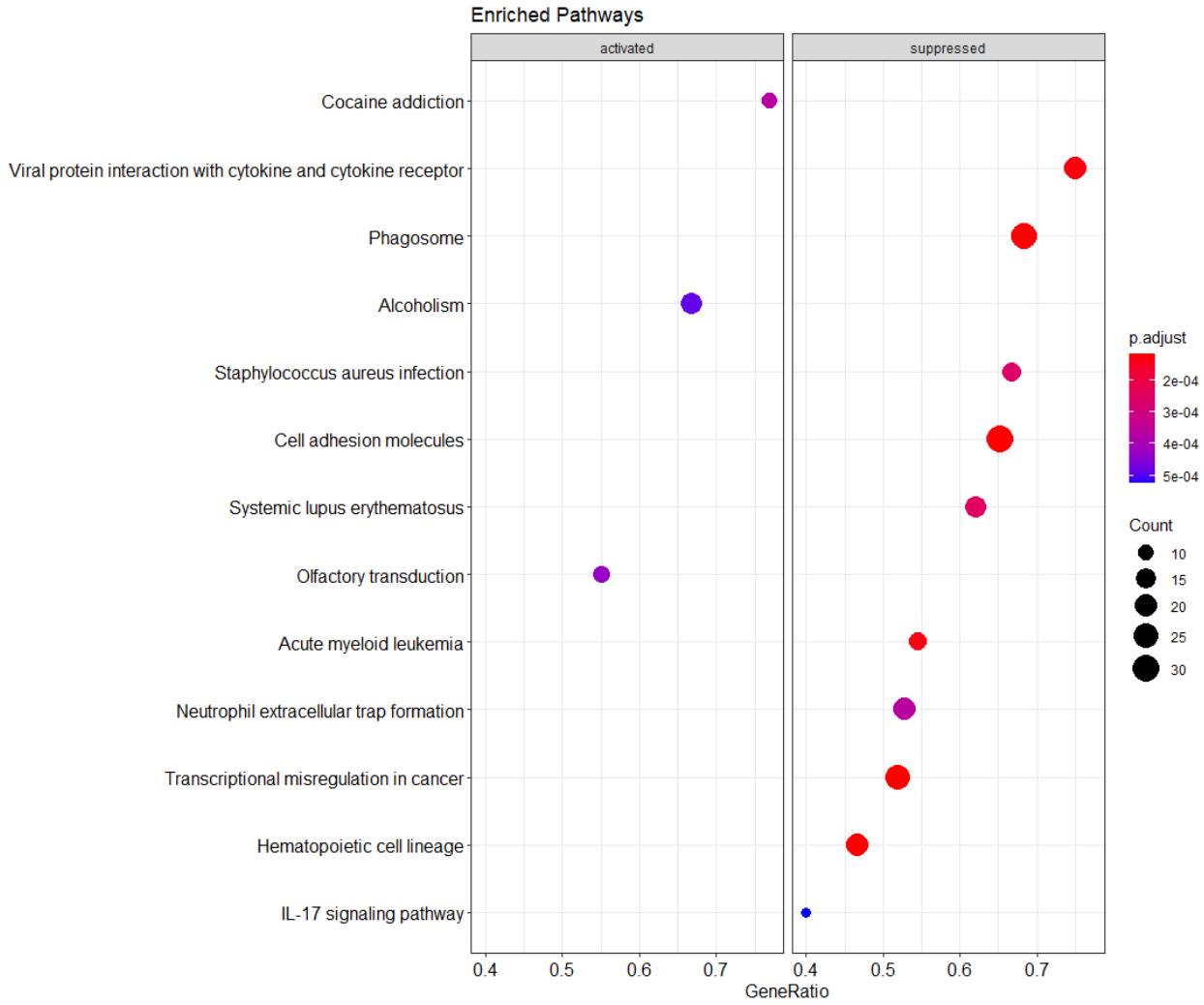

Figure S14 - KEGG pathway analysis comparing gene expression of early and intermediate Bcat1$^{+/+}$. A p-value cutoff of 0.01 and a minimum of genes was set to 10.

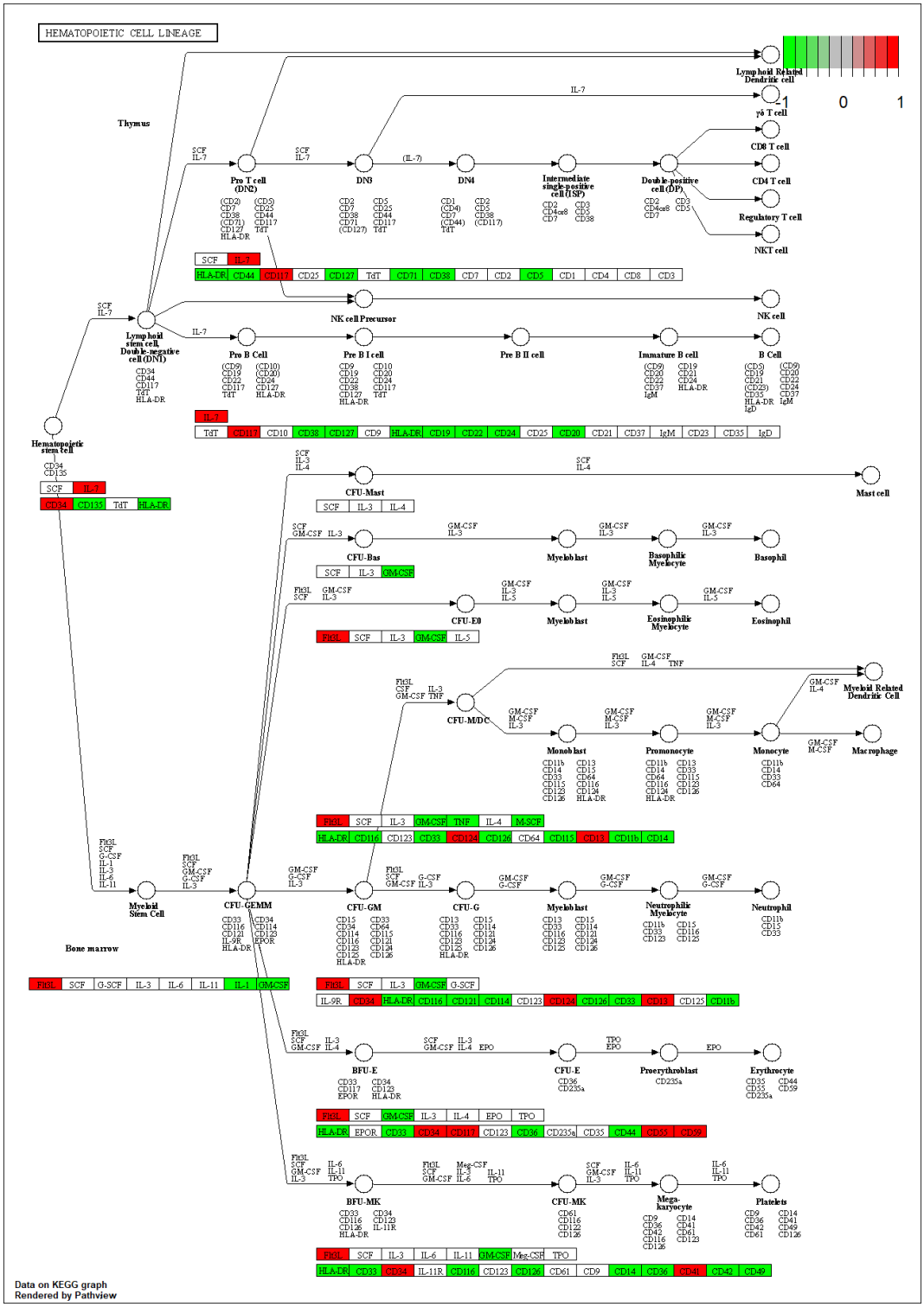

Figure S15 - Gene expression of Bcat1$^{+/+}$ over time in the KEGG pathway hematopoietic cell lineage (mmu04640)

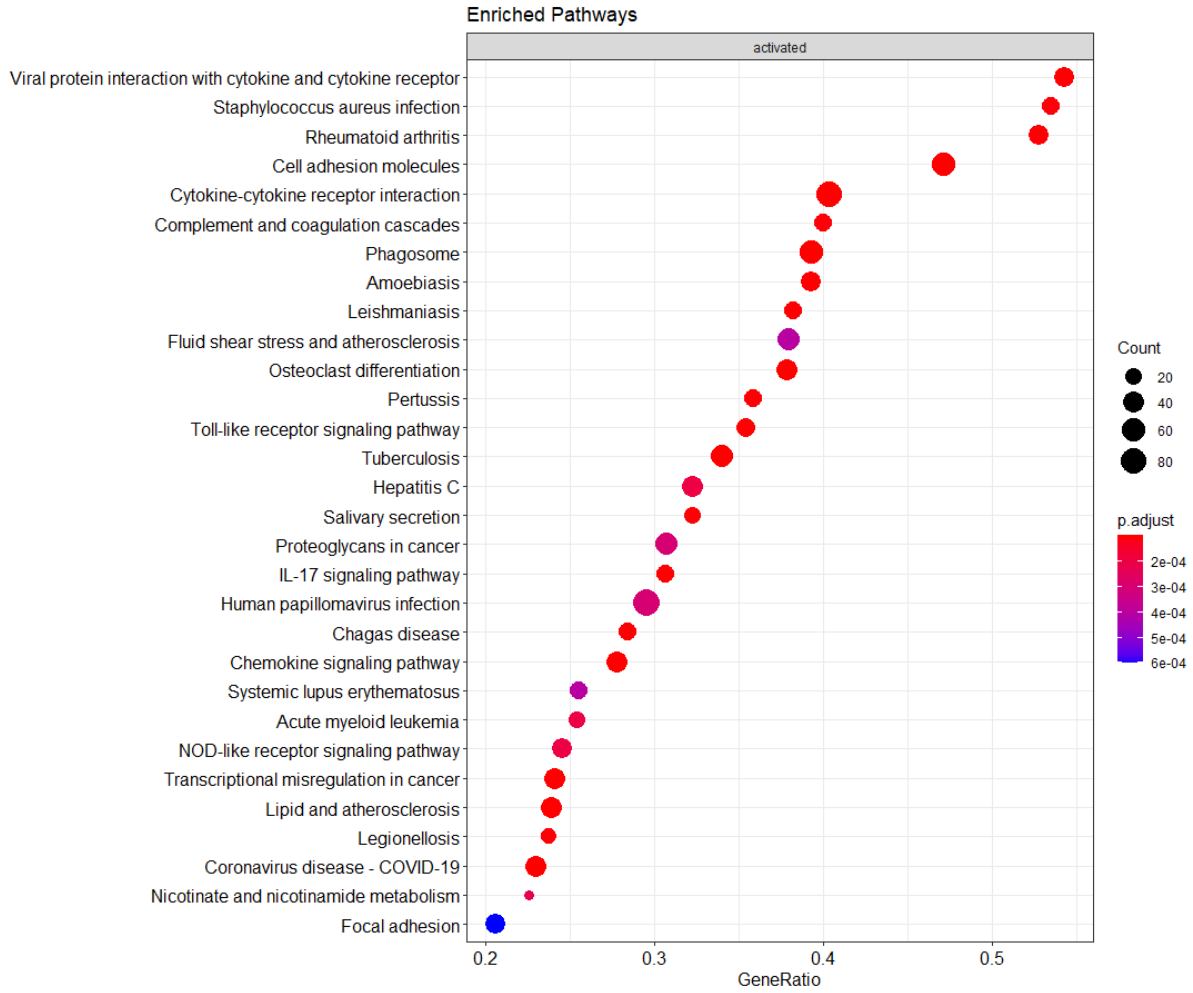

Figure S16 - KEGG pathway analysis comparing gene expression of intermediate Bcat1^{WT} and intermediate Bcat1$^{-/-}$. A p-value cutoff of 0.01 and a minimum of genes was set to 10.

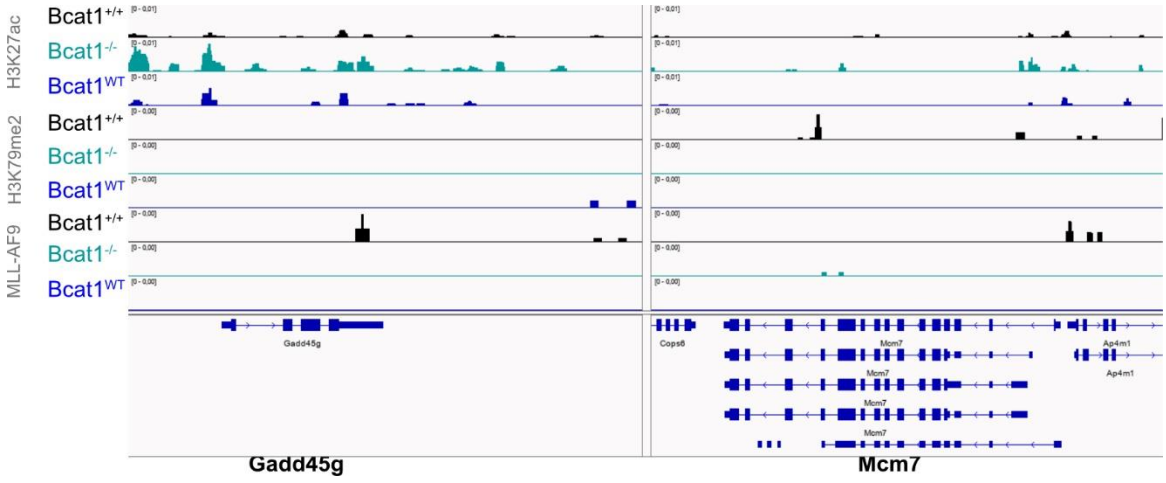

Figure S17 – Normalized IGV tracks of representative ACT-seq replicates. This image shows histone modifications H3K27ac and H3K79me2 as well as MLL-AF9 (Flag) binding at *Gadd45g* (left) and *Mcm7* (right).

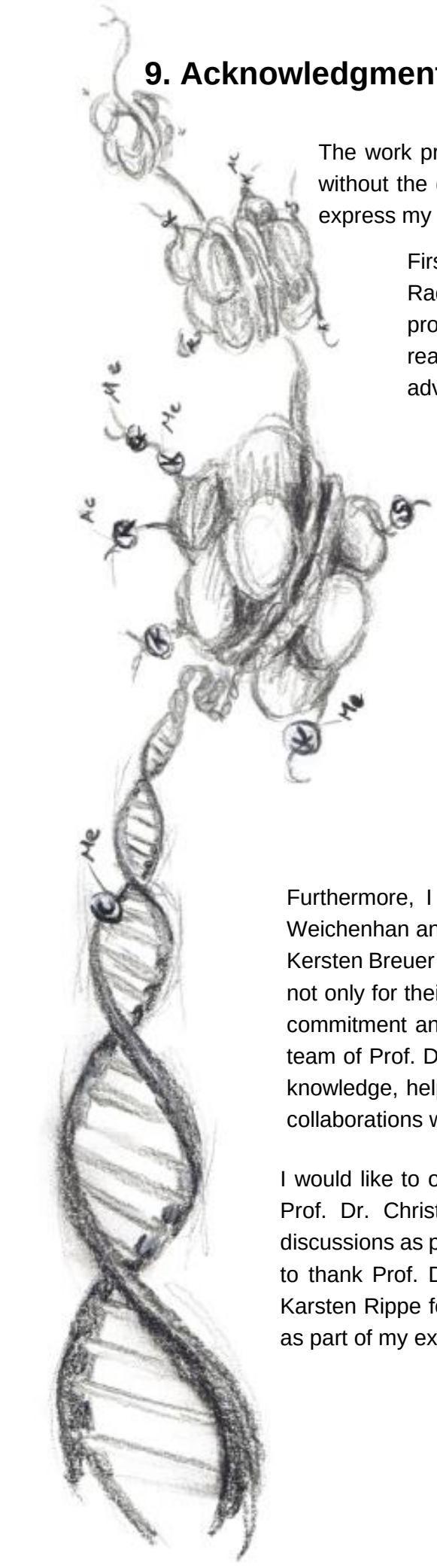

9. Acknowledgments

The work presented in this PhD thesis would not have been possible without the guidance and endless support of many people, to whom I express my gratitude:

First and foremost, I would like to thank Dr. Bernhard Radlwimmer for his supervision and support throughout this project. He provided me with all the necessary liberties to realize my own ideas while at the same time giving helpful advice and stopping me from getting lost in fruitless endeavors.

I would also like to extend my sincere thanks to Prof. Dr. Peter Lichter, for giving me the opportunity to perform my PhD work in his division and thus be part of this team of outstanding scientists. He was always willing to share scientific and strategic advice, for which I am truly thankful for.

It was a great pleasure to join forces with Dr. Liliana François Martín del Campo and later Pavle Boskovic to bring this BCAT1 project to life. I highly appreciate their enthusiastic commitment, invaluable expertise, and unwavering friendship. At the same time, I would like to thank Petra Schroeter for her patience and contributions, which were essential for the development of the project.

Furthermore, I would like to further thank our collaborators Dr. Dieter Weichenhan and Marion Bähr from the group of Prof. Dr. Christoph Plass, Kersten Breuer and Dr. Pavlo Lutsik, and the lab of Dr. Frank Westermann, not only for their willingness to share their expertise with me but also their commitment and never-ending patience. In addition, I am grateful for the team of Prof. Dr. Claudia Scholl, whose willingness to share material and knowledge, helped me greatly. It was a pleasure to establish such fruitful collaborations with all of you.

I would like to offer my special thanks to Prof. Dr. Ursula Klingmüller and Prof. Dr. Christel Herold-Mende for their valuable input and scientific discussions as part of my Thesis Advisory Committee. Likewise, I would like to thank Prof. Dr. Ursula Klingmüller, Prof. Dr. Gudrun Rappold, and Dr Karsten Rippe for their willingness to evaluate and discuss my PhD thesis as part of my examination committee.

With respect to the scientific and practical support, I would like to emphasize the contribution of Petra Schroeter, Magdalena Schlotter and Verena Kalter, who efficiently provided essential technical assistance during the course of this project. Similarly, I highly value the role of Sybille Ohl, Frauke Devens, Andrea Wittmann, Gabi Müller, and Achim Stephan for their eagerness to assist and efficiently manage the laboratory; The skillful and essential support provided by Michael Hain and Jasmin Müller was invaluable.

I would like to further thank Dr. Steffen Schmitt and Dr. Daniel Sanzio Gimenes da Cruz from the Flow Cytometry Core Facility as well as the Sequencing Core Facility and Microscopy Core Facility in providing very valuable trainings, and in maintaining such a high-standard facilities. Equally important was the role of the DKFZ Animal Facility for their relevant work in everyday care and breeding of mice.

I am very grateful to all the present and previous TMB group members Anne Jenseit, Jasmin Mangei, Dr. Lidia Silva, Dr. Liliana François Martín del Campo, Mathew Ka Hou Man, Dr. Michael Fletcher, Dr. Niclas Kneisel, Pavle Boskovic, Dr. Yonghe Wu, and Peng Yuan for their generous contributions to this work, both at the practical and theoretical level, and for their supportive and cheerful attitude all day long.

I also would like to thank all current and former members of the B060/ B062/ B06X divisions, including but not limited to Dr. Aylin Camgoz, Dr. Christian Aichmüller, Dr. Emma Phlipps, Dr. Himanshu Soni, Dr. John Wong, Karol Urbanek, Dr. Lavinia Arseni, Dr. Lena Jassowicz, Dr. Laura Llao Cid, Mariana Coelho Mendes Martines, Marie Bordas, Dr. Martina Seiffert, Michael Periscke, Milena Simovic, Dr. Patricia Benites Goncalves da Silva, Dr. Sander Lambo, Silja Schule, Tolga Lokumcu, and Umar Khalid for contributing to make every moment in the laboratory not only enlightening and of high scientific value, but also fun and memorable.

I would also like to thank my friends, Jasmin Mangei, Laura Sieber, Dr. Michael Fletcher, Mona Göttman, Dr. Natalia Voronina, Dr. Phillipp Rößner, Dr. Selcen Öztürk-Ince, and Taga Lehner, who were a source of inspiration and numerous joyful moments that made these last years a truly delightful and enriching experience.

I would like to thank my family for their love and unwavering support! You are my safe heaven, my rock and the wind under my wings. Having you by my side throughout this roller coaster means everything to me